Waves in discrete and continuous heterogeneous media : propagation, scattering, cloaking

Grégory Futhazar

ANNÉE 2014

UNIVERSITÉ DE RENNES 1

Mathématiques et ApplicationsMathématiques et Applications

THÈSE / UNIVERSITÉ DE RENNES 1
sous le sceau de l'Université Européenne de Bretagne

pour le grade de

DOCTEUR DE L'UNIVERSITÉ DE RENNES 1

Mention : Mathématiques et Applications

École doctorale Matisse

présentée par

Grégory FUTHAZAR

préparée à l'unité de recherche IRMAR – UMR6625
Institut de Recherche Mathématiques de Rennes UFR de Mathématiques

---

Ondes en milieux hétérogènes discrets et continus : propagation, diffusion, *cloaking*

Thèse soutenue à Rennes le 11 Décembre 2013

devant le jury composé de :

Pr. Samuel FOREST
Mines ParisTech / *Président*

Pr. Gérard A. MAUGIN
Université Pierre et Marie Curie / *Rapporteur*

Pr. Agnès MAUREL
ESPCI ParisTech / *Rapporteur*

Pr. Jean-Marc CONOIR
Université Pierre et Marie Curie / *Examinateur*

Pr. Lalaonirina R. RAKOTOMANANA
Université Rennes 1 / *Directeur de thèse*

Mcf. Loic LE MARREC
Université Rennes 1 / *Co-directeur de thèse*

Les chaussures sont un outil pour marcher ;
les mathématiques sont un outil pour penser.
On peut marcher sans chaussures, mais on va moins loin.
Jean-Marie Souriau

Contents

Introduction

L'étude de propagation d'ondes constitue une source intarissable de problèmes auxquels la recherche aime à se confronter, tant au niveau expérimental et numérique qu'au niveau théorique. L'équation des ondes, encore appelée équation de d'Alembert, a fait sa première apparition en 1747 dans un article de Jean le Rond d'Alembert au sujet des cordes vibrantes [d'A47]. Depuis, l'équation des ondes et sa transformée de Fourier, l'équation de Helmholtz, ont bénéficié de plusieurs siècles de recherches et le domaine de l'Analyse nous a fourni des outils puissants pour l'étude de la propagation d'onde.

Dans le domaine de la mécanique, l'équation de Navier qui gouverne la dynamique du déplacement dans un milieu élastique homogène et isotrope, nous permet d'obtenir les équations des ondes élastiques grâce à la décomposition de Helmholtz. On distingue alors les ondes longitudinales, dont la direction de propagation est colinéaire à la direction d'oscillation, des ondes transverses qui oscillent dans une direction orthogonale à la direction de propagation.

Il est usuel de travailler dans le cadre d'onde monochromatique, à fréquence fixée, et de s'intéresser ainsi à l'équation de Helmholtz. Le problème est alors exprimé dans un système de coordonnées dont le choix est motivé par la forme du domaine, afin de faciliter l'expression des conditions limites. Pour un milieu homogène muni d'une géométrie simple, l'équation de Helmholtz admet des solutions à variables séparées en accord avec le choix des coordonnées. La connaissance précise de ces solutions et de leurs propriétés nous ouvre ensuite les portes vers la résolution de problèmes plus complexes.

En multi-diffusion, ou encore *multiple scattering theory*, on s'intéresse en particulier à l'interaction d'une onde incidente avec un milieu homogène, appelé matrice, contenant des inclusions dont les propriétés mécaniques diffèrent de celui-ci. Les approches possibles sont diverses et variées [Mar06] et en particulier on peut suivre la méthode suivante. Lorsque ces inclusions, aussi appelées diffuseurs ou *scatterers*, sont sphériques ou cylindriques, on détermine le champ diffracté par une inclusion dans la matrice grâce aux conditions de continuité à l'interface inclusion/matrice, pour une forme arbitraire du champ excitant l'inclusions. Par superposition, on peut alors exprimer le champ diffracté total comme la somme des diffractions de chaque diffuseur qui interagit avec les autres. Des propriétés sont dites effectives quand elles ne dépendent pas de la position des inclusions. Dans le but de déterminer de telles propriétés, on considère une moyenne

d'ensemble du champ total sur l'ensemble des positions des inclusions. Ce faisant, on peut, en particulier, décomposer cette moyenne en une hiérarchie de moyennes conditionnelles relatives aux positions d'un sous-ensemble d'inclusions en supposant connue la position des autres. Ces méthodes dites de Foldy-Lax s'appliquent pour des ondes élastiques, acoustiques ou encore électromagnétiques. Elles sont généralement efficaces pour des longueurs d'onde λ telles que $\lambda \simeq a$ et $\lambda < d$ avec a la taille moyenne des diffuseurs et d la distance caractéristique entre deux diffuseurs voisins. Les premiers résultats furent avancés par Foldy en 1945 dans le cas d'inclusions ponctuelles et isotropes [Fol45]. Afin d'obtenir une équation de Helmholtz pour le champ effectif, il propose une hypothèse statistique de fermeture, dite de premier ordre, connue comme l'hypothèse de Foldy. Quelques années plus tard, Lax suggère d'aller un pas plus loin dans la hiérarchie et de fermer le problème au moyen de la QCA, *Quasi Crystalline Assumption* [Lax52]. Cette hypothèse, qui est aussi de nature statistique, nous conduit alors à considérer de nouvelles approximations ; en particulier, considérer une probabilité conditionnelle nous amène à nous poser la question de l'impossibilité pour deux inclusions de se superposer. C'est ce que l'on appelle la *hole correction*.

De nombreux travaux suivirent. Watermann et Truell développeront un modèle de QCA pour une *hole correction* simplifiée [WT61]. Inspirés par les travaux de Lloyd et Berry [LB67], Linton et Martin [LM06] obtiendront, dans le cas acoustique, un développement limité du nombre d'onde effectif autour du nombre d'onde incident en termes de concentration d'inclusions en considérant une *hole correction* plus appropriée pour la QCA. Conoir et Norris généraliseront la formule au cas des ondes élastiques [CN10]. Un peu en parallèle, on peut retenir le travail de Maurel et Martin [MM08] qui montre que pour des faibles contrastes, on obtient le même nombre d'onde effectif en tronquant les intégrales de Lipmann-Schwinger qui expriment la solution du problème de multiple scattering au moyen des fonctions de Green.

Ces travaux, fondés sur des équations fondamentales en milieu homogène, nous mènent alors à interpréter le comportement de milieux hétérogènes comme des milieux homogènes aux propriétés effectives lorsqu'ils sont sondés par une onde. En outre, dans un régime plus basse fréquence, les techniques d'homogénéisation permettent des interprétations similaires (voir par exemple [Mil01].

Dans une approche légèrement différente, l'agencement périodique ou quasi-périodique d'inclusions au caractère résonant, permet d'obtenir des milieux artificiels au comportement très intéressant aussi bien en électromagnétisme qu'en acoustique : ce sont les métamatériaux (*cf* [VMOS12] pour l'acoustique par exemple). Ils permettent de contrôler la propagation d'une onde incidente notamment grâce à des bandes fréquentielles interdites pour la propagation. L'association astucieuse de métamatériaux rend alors possible le *cloaking* qui consiste à créer une région indétectable lors du sondage par une onde [PSS06, LP08]. Le *cloaking* est dit passif dans le sens où nous n'interagissons pas avec l'onde incidente. Cependant, de tels phénomènes peuvent être obtenus de manière active, au moyen de sources multipolaires qui se situeraient à l'extérieur de la zone que l'on veut rendre indétectable.

À cet effet, Miller propose une méthode consistant à mesurer le mouvement des

particules à la surface que l'on veut masquer et à émettre simultanément un champ dont les amplitudes dépenderont des mesures effectuées [Mil06]. Ce faisant, la relation entre le champ émis et le champ incident n'est malheureusement pas unique pour cette méthode. Vasquez *et al.* surpasseront cette limite pour le cas de l'équation de Helmholtz 2D en formulant une équation intégrale qui exprime les amplitudes comme des fonctions linéaires du champ incident [VMO11, VMOS12, Vas]. Norris *et al.* montrèrent que cette formule intégrale pour les amplitudes des sources peut s'exprimer sous une forme explicite mettant en relation les amplitudes du champ incident et celles des sources [NAP12]. Cette dernière technique repose, elle aussi, sur la connaissance des fonctions propres de l'équation de Helmholtz en plus de la fonction de Green du milieu.

Les techniques de *multiple scattering* et *cloaking* mentionnées précédemment sont fondées sur des équations données par la théorie des milieux continus élastiques ou acoustiques. Or cette théorie atteint ses limites lorsque l'on considère, entre autres, des milieux hétérogènes ou résultant de transformations plastiques (non reversibles). Afin d'étoffer notre compréhension et d'élargir les applications, pour la propagation d'onde par exemple, il semble pertinent de requestionner le concept de *continuum* (milieu continu). Il existe pour cela plusieurs façons de généraliser le milieu continu en mécanique [Mau13a]. On en propose ici un historique non exhaustif.

En 1909 les frères Eugènes et François Cosserat introduisent un nouveau modèle de *continuum* dans leur livre intitulé "Théories des corps déformables" [CC09]. Ces milieux qui seront appelés milieux de Cosserat sont composés de points matériels auxquels sont attachés des directeurs. On dispose ainsi d'une micro-structure, c'est-à-dire une structure à l'échelle des points matériels du continuum, mais qui aura une influence sur le comportement macroscopique de celui-ci. En ce qui concerne les variables cinématiques, il nous faut alors considérer non seulement le champ de déplacement usuel, mais aussi le champ de rotation associé aux directeurs. La théorie rencontrera un succès en particulier dans la deuxième moitié du vingtième siècle. Ainsi, Mindlin [Min64] et Eringen [EC64] suggèreront la notion de milieux micromorphes qui s'avèreront propices à l'étude de la plasticité.

Cartan confiera que ses découvertes sur les connections affines [Car86], et notamment le tenseur de torsion, lui ont été inspirées par les milieux de Cosserat. Élargissant la notion de dérivée directionnelle à la dérivée covariante pour les champ tensoriels, il mettra en évidence la possibilité de défaut de transport parallèle. Il généralise ainsi les variétés riemanniennes aux variétés de Riemann-Cartan que l'on peut interpréter comme l'objet géométrique associé aux milieux de Cosserat [HO07]. Ce résultat l'incitera plus tard à prendre contact avec Einstein afin de discourir au sujet de cette connection et de son lien avec la relativité [Dev92]. La question de l'espace-temps avec torsion animera de nombreux travaux, *cf* l'aperçu historique [Ham02], dans le cadre de la théorie de jauge qui consiste à étudier un champ à travers ses groupes de symétrie locale appelés groupes de jauge. Or, le paysage mathématique de la mécanique des milieux continus est celui de la géométrie différentielle et les avancées sur le continuum espace-temps firent écho en mécanique des milieux continus. En ce sens, dans ses travaux sur les dislocations et la notion d'incompatibilité au point de vue contin-

uum, Kröner établira le lien entre le tenseur de torsion et la densité de dislocations [Kro80]. Kröner [Kro86], Edelen *et al.* [KE83, EL88] puis Lazar [Laz00], contribuèrent en introduisant la théorie des dislocations comme une théorie de jauge avec le groupe des translations comme groupe de jauge. Dans un esprit sensiblement différent, Wang et Noll [Nol67] commencèrent par définir les milieux simples et les milieux homogènes en tant que variétés différentiables soumises à des conditions d'isomorphisme matériel au sein de leurs espaces tangents. Ils en déduisirent une définition pour les milieux hétérogènes. S'inspirant des travaux de ces derniers et du circuit de Cartan, Rakotomanana montra le lien entre les discontinuités d'un champ scalaire et le tenseur de torsion, puis le lien entre les discontinuités d'un champ vectoriel et les tenseurs de torsion et courbure [Rak97]. Ces notions théoriques de géométrie différentielle ont néanmoins trouvé peu d'applications au sujet la propagation d'ondes élastiques. On retiendra principalement Lazar [Laz11] qui obtient des phénomènes de propagation de dislocations à partir des équations de champ qu'il a établies. Cependant cette propagation est consécutive au mouvement d'une ligne de dislocation qui semble être plus une perturbation plastique qu'une perturbation élastique. Le cas de la propagation d'onde dans un milieu inhomogène au sens de Noll a cependant aussi était étudié dans [TBR11].

À la lecture de cette brève introduction historique et méthodique sur l'étude des ondes et de la mécanique des milieux continus, on peut mettre en évidence les problématiques suivantes qui interviennent à différents stades du raisonnement. Dans le cadre de la multi-diffusion, la QCA est-elle la seule hypothèse de fermeture d'ordre deux ? En ce qui concerne le *cloaking* actif, comment s'applique-t-il sur une plaque, qui est un exemple particulier de milieu de Cosserat ? Revenons à la base du raisonnement en élasticité et considérons un milieu continu muni d'une structure différentielle de Riemann-Cartan causée par une densité de dislocations ; comment se comporterait la propagation d'une onde élastique ? Ce sont les trois points qui seront développés au fil de ce manuscrit.

Le chapitre 1 est consacré à une brève introduction des concepts d'élasticité, de défauts et de milieux continus généralisés. Dans le chapitre 2, on s'intéressera aux méthodes de Foldy-Lax pour la propagation d'onde suite au sondage par une source ponctuelle d'un milieu infini aléatoire. À cette occasion, on propose une hypothèse de fermeture originale comme alternative à la QCA. Certains résultats de ces travaux furent présentés au Congrès Français d'Acoustique en 2012 et un article est en cours de rédaction. Dans le chapitre 3 destiné au *cloaking* actif, on développera de manière explicite les amplitudes modales que doivent satisfaire les sources dans le cadre du *cloaking* d'onde de flexion dans une plaque de Love-Kirchhoff. Ces travaux furent menés à l'occasion d'un séjour à l'université de Manchester dans le cadre d'une collaboration avec Dr. William Parnell et Pr. Andrew Norris. Un article est en cours de rédaction. Enfin dans le dernier chapitre, nous reformulerons le problème d'élasticité dans l'esprit des milieux continus généralisés en appliquant les équations fondamentales de conservation sur une variété matérielle de Riemann-Cartan dans le but de généraliser l'équation de Navier. Avec un exemple simple, on observera comment une densité de dislocations vis peut influencer la propagation d'onde de manière non seulement quantitative mais aussi qualitative. Les résultats de ce chapitre ont été acceptés dans un *Special Issue*

de *Archives of Applied Mechanics* et ont fait l'objet de communications au GDR ondes en Mai 2012 ainsi qu'au CFM13 (Congrès Français de Mécanique) et à AfriCOMP13 (troisième conférence africaine internationale autour du thème *Computational Mechanics*) au cours de Juillet-Août 2013.

Chapter 1

Rappels théoriques

1.1 Mécanique des milieux continus

En mécanique du solide, un corps solide $\mathcal{B}$ (aussi appelé milieu ou continuum) est défini par un ensemble de particules encore appelées points matériels. Chaque point matériel M est identifié au point spatial qu'il occupe et qui est repéré par le vecteur position $\mathbf{X}$. Cette définition implique que le corps lui même est identifié par la région de l'espace qu'il occupe. Mathématiquement c'est donc un ouvert de $\mathbb{R}^3$.

Définition 1.1 *Un* corps simple *est un ouvert $\mathcal{B} \subset \mathbb{R}^3$. Une configuration de $\mathcal{B}$ est définie comme la donnée d'une application $\varphi : \mathcal{B} \to \mathbb{R}^3$. L'ensemble des configurations est noté $\mathtt{C}$. Par abus de langage, les points de $\mathcal{B}$ sont associés à leur vecteur position $\mathbf{X}$ que l'on note à l'aide de majuscules, les points de la configuration seront associés à leur vecteur position $\mathbf{x} = \varphi(\mathbf{X})$.*

Ainsi, une configuration représente un état déformé du corps solide. On peut alors définir le corps solide comme un ouvert $\mathcal{B} \subset \mathbb{R}^3$ et l'application φ n'est autre que l'inclusion via un choix de coordonnées généralement adapté à la forme du milieu. Dans cette définition particulière la structure différentielle de $\mathcal{B}$ est alors héritée de celle de $\mathbb{R}^3$. Lorsque le milieu bouge au cours du temps, on obtient alors une famille de configurations dépendantes du paramètre temps t.

Définition 1.2 *Un mouvement du corps solide $\mathcal{B}$ est une application $t \in \mathcal{U} \mapsto \varphi_t \in \mathtt{C}$, où $\mathcal{U}$ est un ouvert de $\mathbb{R}$. Pour t fixé on écrit $\varphi_t(\mathbf{X}) = \varphi(\mathbf{X}, t)$.*

Pour $t = 0$ la configuration de référence φ_0 peut être donnée, par exemple, par l'identité afin d'identifier le milieu et la région de l'espace qu'il occupe. Une configuration pour un temps $t \neq 0$ est appelée configuration actuelle. Il faut noter que pour un temps donné, l'application φ_t est une bijection entre la configuration de référence et la configuration actuelle : un point matériel ne peut pas se scinder et deux points matériels ne peuvent pas fusionner. Ainsi, un continuum est une région matérielle sur laquelle on définira les propriétés physiques comme des applications continues. Par exemple, la distribution de la masse est supposée varier continument d'un point matériel

à un autre. Dans le but de conserver le caractère continu du milieu, le mouvement doit évidemment conserver la topologie. Plus précisément, le mouvement ne doit pas créer de nouveaux trous. Afin de s'en assurer on suppose alors que pour $t \in \mathcal{U}$ fixé la configuration φ_t est un homéormorphisme (φ_t et φ_t^{-1} est $\mathcal{C}^0$ pour chaque t).
Cela dit, cette condition n'est pas suffisante pour garantir que la structure différentielle soit conservée. Des surfaces ou des courbes matérielles pourraient se plier et former des coins et/ou des arêtes matériels. Afin de conserver la structure différentielle il faut imposer que pour $t \in \mathcal{U}$ fixé, la configuration φ_t est un $\mathcal{C}^1$-difféomorphisme (φ_t et φ_t^{-1} sont $\mathcal{C}^1$ pour tout t). Par définition on remarquera que cette dernière condition implique directement celle d'homéomorphisme pour tous t.
Ainsi dans chacun des deux cas (homéomorphe ou $\mathcal{C}^1$ difféomorphe), deux points matériels sont voisins dans la configuration de référence si et seulement si ils sont voisins dans la configuration actuelle. Cette conséquence est à l'origine du concept de milieu continu. Le cadre mathématique adapté aux définitions précédentes est celui des variétés. Dans la suite de cette sous-section, on se restreint au cas idéal où φ_t est un $\mathcal{C}^1$ difféomorphisme et pour lequel la théorie est basée sur l'étude des variétés différentiables.
Afin de comparer la configuration de référence et la configuration actuelle, on définit le champ de déplacement.

Définition 1.3 *Le champ de déplacement d'un corps solide $\mathcal{B}$ est une fonction vectorielle définie sur la configuration de référence comme la différence entre la position actuelle du point matériel et sa position initiale :*

$$\mathbf{u} : (\mathbf{X}, t) \in \mathbb{R}^3 \times \mathbb{R} \to \mathbf{u}(\mathbf{X}, t) = \mathbf{x} - \mathbf{X} \in \mathbb{R}^3.$$

Nous insistons sur le fait que le changement de coordonnées du déplacement n'est pas compatible avec le changement de coordonnées de points matériels. En effet le déplacement n'est pas une quantité tensorielle.

1.1.1 Déformation

L'étude de la transformation d'un continuum $\mathcal{B}$ lors d'un mouvement φ est basée sur une analyse locale du mouvement relatif entre deux points matériels voisins $\mathbf{X}$ et $\mathbf{X} + \mathrm{d}\mathbf{X}$. On note $\mathbb{F}$ le gradient de φ_t pour t fixé :

$$\mathbb{F}(\mathbf{X}) := \nabla\varphi(\mathbf{X}, t), \quad \mathrm{d}\mathbf{x} = \mathbb{F}\mathrm{d}\mathbf{X}.$$

Exprimer le problème à l'aide du déplacement est souvent plus parlant. Puisque $\nabla\mathbf{u} = \mathbb{F} - \mathbb{I}$, on peut exprimer le tenseur de déformation de Green-Lagrange :

$$\mathbb{E} = \frac{1}{2}\big(\mathbb{F}^T\mathbb{F} - \mathbb{I}\big) = \frac{1}{2}\big(\nabla\mathbf{u} + \nabla\mathbf{u}^T + \nabla\mathbf{u}\nabla\mathbf{u}^T\big),$$

et le tenseur de déformation de Cauchy-Green $\mathbb{C}$:

$$\mathbb{C} := \mathbb{F}^T\mathbb{F}.$$

Au cours du mouvement, le changement de norme d'un vecteur infinitésimal d$\mathbf{X}$ est donné par le tenseur de Green-Lagrange :

$$||\mathrm{d}\mathbf{x}||^2 - ||\mathrm{d}\mathbf{X}||^2 = \mathrm{d}\mathbf{X}^T\big(\mathbb{F}^T\mathbb{F} - \mathbb{I}\big)\mathrm{d}\mathbf{X} = 2\mathrm{d}\mathbf{X}^T\mathbb{E}\mathrm{d}\mathbf{X}.$$

La connaissance du tenseur de Cauchy-Green est néanmoins suffisante pour exprimer non seulement la norme d'un vecteur infinitésimal dans la configuration actuelle d$\mathbf{x}$ mais aussi l'angle défini entre deux vecteurs infinitésimaux actuels d$\mathbf{x}$ and d$\mathbf{x}'$. En effet, d'un point de vue géométrique, le tenseur de Cauchy-Green est le tenseur métrique de la variété matérielle associée à la configuration actuelle.

Afin de linéariser le problème, nous pouvons faire l'hypothèse des petites perturbations (HPP) et ainsi simplifier le tenseur de Green-Lagrange. En particulier, pour des déformations infinitésimales, on définit le tenseur de déformation de Cauchy :

$$\boldsymbol{\varepsilon} := \frac{1}{2}(\nabla\mathbf{u} + \nabla\mathbf{u}^T)$$

Dans tout ce qui suivra on supposera l'HPP.

1.1.2 Lois de conservation

Dans cette sous-section nous exprimons les formulations fortes des équations de conservation. La formulation faible obtenue par le principe des puissances virtuelles sera évoquée au cours du chapitre 2 pour introduire la théorie des plaques.

Théorème 1.1 *(Conservation de la masse) La masse d'un volume élémentaire délimité par une surface fermée reste constante au cours de la transformation. La forme locale de ce principe s'énonce :*

$$\rho \det \mathbb{F} = \rho_0,$$

où ρ_0 et ρ sont respectivement la densité massique de référence et celle actuelle.

En utilisant le Principe Fondamental de la Dynamique en translation et en rotation qui exprime la conservation de la quantité de mouvement et du moment cinétique, on obtient les équations locales du mouvement :

Théorème 1.2 *(Théorème fondamental de Cauchy) On considère un continuum en mouvement en l'absence de densité de moments extérieurs. On suppose que le vecteur des contraintes appliquées à une surface de vecteur normal $\mathbf{n}$ est une fonction de ce vecteur : $\mathbf{p}_n = \mathbf{p}_n(\mathbf{n})$ (hypothèse de Cauchy). Alors le Principe Fondamental de la Dynamique est satisfait si et seulement si :*

- *Il existe un champ de tenseur $\sigma(\mathbf{x}, t)$, appelé tenseur de contraintes, tel que :*

$$\mathbf{p}_n = \sigma\mathbf{n}, \quad \sigma = \sigma^T.$$

- *Et σ satisfait :*

$$\mathrm{div}\ \sigma + \rho\mathbf{f} = \rho\mathbf{a}.$$

où $\mathbf{f}$ est la densité massique de forces extérieures et $\mathbf{a}$ le vecteur accélération.

1.1.3 Lois de comportement

Une loi de comportement exprime le lien entre les contraintes et la déformation à l'aide de principes thermo-mécaniques. Ceci nous permet alors de fermer le problème sous la forme d'une équation aux dérivées partielles que doit satisfaire le champ de déplacement. Nous nous bornons ici aux cas de milieux au comportement élastique c'est-à-dire les milieux pour lesquels l'énergie ne dépend que de la déformation considérée ($\boldsymbol{\varepsilon}$).

Théorème 1.3 *(Forme locale de la conservation d'énergie) On considère une transformation isotherme d'un continuum $\mathcal{B}$, pour lequel le flux de chaleur sur la frontière et la production volumique de chaleur sont nuls. Alors la conservation de l'énergie en $\mathbf{x}$ à l'instant t s'exprime sous la forme :*

$$\rho \frac{de}{dt}(\mathbf{x}, t) = \sigma(\mathbf{x}, t) : \dot{\boldsymbol{\varepsilon}}(\mathbf{x}, t),$$

où $\dot{\boldsymbol{\varepsilon}}(\mathbf{x}, t)$ est la dérivé temporelle de $\boldsymbol{\varepsilon}(\mathbf{x}, t)$ appelée taux de déformation.

De ce théorème on déduit que les composantes du tenseur des contraintes pour une transformation élastique sont obtenues par différentiation de l'énergie libre de Helmholtz $\psi = \rho e$:

$$\sigma = \rho \frac{\partial e}{\partial \boldsymbol{\varepsilon}} = \frac{\partial \psi}{\partial \boldsymbol{\varepsilon}}.$$

Désormais on admettra qu'un milieu élastique, c'est-à-dire qui se déforme élastiquement, est entièrement défini par son énergie libre $\psi(\boldsymbol{\varepsilon})$. Un milieu élastique est dit linéaire si son énergie libre est une fonction quadratique de la déformation :

$$\psi(\boldsymbol{\varepsilon}) = \frac{1}{2} C^{ijkl} \varepsilon_{ij} \varepsilon_{kl},$$

où les constantes mécaniques C^{ijkl} sont les composantes du tenseur d'élasticité.

Pour un milieu continu homogène linéaire et isotrope, la loi de comportement est donnée par la loi de Hooke caractérisée par deux constantes mécaniques positives :

$$\sigma = \lambda \mathrm{Tr}(\boldsymbol{\varepsilon}) \mathbf{I} + 2\mu \boldsymbol{\varepsilon},$$

où $\mathbf{I}$ est le tenseur identité. Les coefficients λ et μ sont les coefficients de Lamé.

1.1.4 Équation de Navier

En élasticité, il est souvent plus adapté d'exprimer les équations du mouvement en fonction du déplacement. En effet, le gradient du mouvement et la déformation peuvent être exprimés à partir du gradient de déplacement. Dans ce qui suit, on combine les équations de conservation et la loi de Hooke afin d'obtenir l'équation de Navier. Soit $\mathcal{B}$ un milieu isotrope, linéaire et homogène dont les coefficients de Lamé sont notés λ et

μ, on suppose qu'il est soumis à un mouvement φ_t qui est C^∞ et satisfait l'hypothèse des petites perturbations. En l'absence de contraintes extérieures, on a :

$$\rho_0 \partial_t^2 \mathbf{u} = \nabla \cdot [\lambda \mathrm{Tr}(\varepsilon)\mathbf{I} + 2\mu\, \varepsilon] .$$

Ainsi on obtient l'équation de Navier qui régit le déplacement :

$$\rho_0 \partial_t^2 \mathbf{u} = (\lambda + \mu)\nabla(\nabla \cdot \mathbf{u}) + \mu \Delta \mathbf{u}. \tag{1.1}$$

Cette équation est une équation de propagation : dérivées partielles d'ordre deux en espace en relation avec des dérivées partielles d'ordre deux en temps.

1.2 Ondes élastiques

Le point de départ est l'équation de Navier (1.1), dont il faut garder à l'esprit qu'elle est valable pour des milieux homogènes, linéaires et isotropes. On montre alors que le champ scalaire div $\mathbf{u}$ et le champ vectoriel rot $\mathbf{u}$ doivent satisfaire l'équation d'onde mais pour des vitesses de propagation différentes.

1.2.1 Équation d'onde

1.2.1.1 De Navier à d'Alembert

Ondes longitudinales (irrotationelles) : En appliquant l'opérateur de divergence à l'équation de Navier, on a :

$$\text{div } \big((\lambda + \mu)\nabla(\nabla \cdot \mathbf{u}) + \mu \Delta \mathbf{u}\big) = \text{div } \big(\rho_0 \partial_t^2 \mathbf{u}\big).$$

Par permutation des dérivées spatiales et temporelles on a :

$$\text{div } \big(\rho_0 \partial_t^2 \mathbf{u}\big) = \rho_0 \partial_t^2 \big(\text{div } \mathbf{u}\big).$$

Comme le milieu est homogène, les coefficients de Lamé sont constants et on déduit :

$$(\lambda + 2\mu)\Delta(\text{div } \mathbf{u}) = \rho_0 \partial_t^2 \big(\text{div } \mathbf{u}\big).$$

Ainsi on a obtenu l'équation d'onde pour les ondes longitudinales se propageant avec une célérité c_l :

$$\Delta(\text{div } \mathbf{u}) = \frac{1}{c_l^2} \partial_t^2 \big(\text{div } \mathbf{u}\big), \quad c_l^2 := \frac{\lambda + 2\mu}{\rho_0}.$$

Ce sont des ondes dont la polarisation, c'est-à-dire la direction du déplacement associé, est colinéaire à la direction de propagation. En particulier elles vont modifier le volume puisque la divergence d'un tel déplacement n'est pas nul. On les appelle aussi des ondes de compression.

Ondes transverses (divergence nulle) : En appliquant l'opérateur rotationel à l'équation de Navier, on a :

$$\text{rot } \big((\lambda + \mu)\nabla(\nabla \cdot \mathbf{u}) + \mu \Delta \mathbf{u}\big) = \text{rot } \big(\rho_0 \partial_t^2 \mathbf{u}\big).$$

Dans un domaine continu simplement connexe, on a rot $\big(\nabla(\text{div } \mathbf{u})\big) = 0$. De même que précédemment on obtient :

$$\mu\text{rot } (\Delta\mathbf{u}) = \mu\Delta(\text{rot } \mathbf{u}) = \rho_0\partial_t^2\text{rot } \big(\mathbf{u}\big).$$

Ceci est l'équation des ondes transverses se propageant avec une célérité c_t.

$$\mu\Delta\text{rot } (\mathbf{u}) = \frac{1}{c_t^2}\partial_t^2\text{rot } \big(\mathbf{u}\big), \quad c_t^2 := \frac{\mu}{\rho_0}.$$

Elles conservent le volume et ont une polarisation orthogonale à la direction de propagation. De plus on remarque qu'elles se déplacent plus lentement que les ondes longitudinales.

1.2.1.2 Méthode des potentiels

Méthode de Poisson

Considérons $\mathbf{u}_l$, les solutions de l'équation de Navier telles que rot $\mathbf{u}_l = \mathbf{0}$. Comme

$$\nabla(\text{div } \mathbf{u}_l) = \Delta\mathbf{u}_l + \text{rot } (\text{rot } \mathbf{u}_l) = \Delta\mathbf{u}_l,$$

l'équation de Navier (1.1) devient :

$$(\lambda + 2\mu)\Delta\mathbf{u}_l = \rho_0\partial_t^2\mathbf{u}_l.$$

Ainsi le champ de déplacement $\mathbf{u}_l$ se propage avec la même célérité que le champ div $\mathbf{u}$ des ondes longitudinales. De façon similaire, on montre que le champ de déplacement $\mathbf{u}_t$, tel que div $\mathbf{u}_t = 0$, est solution de la même équation que celle des ondes transverses :

$$\mu\Delta\mathbf{u}_t = \rho_0\partial_t^2\mathbf{u}_t.$$

La décomposition de Poisson consiste à exprimer le déplacement comme la somme des deux champs définis ci-dessus :

$$\mathbf{u} = \mathbf{u}_t + \mathbf{u}_l, \quad \text{rot } \mathbf{u}_l = 0, \quad \text{div } \mathbf{u}_t = 0.$$

On utilisera cette décomposition lors du travail sur la propagation d'onde en milieu contenant une densité constante de dislocation.

Méthode de Helmholtz

Les deux types d'ondes mis en évidence ci-dessus, suggèrent une décomposition de la forme :

$$\mathbf{u} = \nabla\Phi + \text{rot } \mathbf{\Psi},$$

dans laquelle Φ et $\mathbf{\Psi}$ sont respectivement des potentiels scalaires et vectoriels. On montre que ces deux potentiels sont solutions de l'équation d'onde respectivement pour les ondes longitudinales et les ondes transverses. Cette décomposition sera utilisée dans le chapitre sur la multi-diffusion (*multiple scattering*) dans le cadre acoustique où seules les ondes longitudinales sont définies. Il s'agira alors de travailler sur Φ plutôt que $\mathbf{u}$.

1.2.2 Équation de Helmholtz

Lorsqu'on suppose que l'onde régie par Helmholtz est monochromatique pour une fréquence angulaire ω, c'est-à-dire une dépendance en temps de la forme $\exp(-i\omega t)$, on obtient l'équation de Helmholtz :

$$\Delta \mathbf{u} + k^2 \mathbf{u} = 0, \quad k^2 = \omega^2/c^2,$$

où k est le nombre d'onde et $k^2 = \omega^2/c^2$ est la relation de dispersion pour des ondes ayant une vitesse de propagation c. On peut aussi interpréter cette équation comme la transformée de Fourier de l'équation des ondes. Dans les problèmes bidimensionels qui seront abordés par la suite, on travaille principalement en coordonnées polaires (r, θ), c'est pourquoi on choisit ici d'exposer les principaux outils qu'on utilise dans ce cas. On notera néanmoins que l'équation de Helmholtz admet des solutions à variables séparées pour d'autres systèmes de coordonnées telles que les coordonnées cartésiennes ou encore sphériques que nous avons choisies de ne pas présenter pour ne pas alourdir le propos. On précise néanmoins que la théorie des groupes de Lie permet de retrouver les systèmes de coordonnées pour lesquels il existe des solutions à variables séparées [Olv00, Mil12].

1.2.2.1 Séparation des variables (polaire)

Comme mentionné ci-dessus, on cherche des solutions à variables séparées pour les coordonnées polaires (r, θ). Par souci de simplicité, on se borne au cas d'une équation scalaire, qui pourrait être obtenue pour le potentiel Φ dans le cas acoustique. On pose donc $\Phi(r, \theta) = f(r)g(\theta)$ et, par définition du Laplacien en coordonnées polaires, on a :

$$f''(r)g(\theta) + \frac{1}{r} f'(r)g(\theta) + \frac{1}{r^2} f(r)g''(\theta) + k^2 f(r)g(\theta) = 0.$$

De plus on suppose que le champ scalaire ne s'annule jamais de sorte qu'on peut diviser par $f(r)g(\theta)$:

$$\frac{f''(r)}{f(r)} + \frac{1}{r}\frac{f'(r)}{f(r)} + \frac{1}{r^2}\frac{g''(\theta)}{g(\theta)} = -k^2.$$

Comme r et θ sont indépendants, on déduit qu'il existe une constante C telle que :

$$r^2 f''(r) + r f'(r) + \big(k^2 r^2 - C^2\big) f(r) = 0, \quad g''(\theta) + C^2 g(\theta) = 0.$$

L'équation satisfaite par g est classique et les solutions sont $\exp(\pm iC\theta)$. Par des considérations de périodicité sur g, on peut montrer que $C = n \in \mathbb{Z}$. Enfin par changement de variable $z = kr$ on conclut :

$$f''(z) + f'(z) + \big(z^2 - n^2\big) f(z) = 0, \quad g''(\theta) + n^2 g(\theta) = 0.$$

L'équation pour f est l'équation de Bessel dont les solutions sont les fonctions de Bessel $J_n(z), Y_n(z)$. En conclusion la solution générale de l'équation de Helmholtz en coordonnées polaires est :

$$\Phi(r, \theta) = \sum_{n=-\infty}^{\infty} \big(A_n J_n(kr) + B_n Y_n(kr)\big) \exp(in\theta).$$

Les coefficients A_n et B_n sont alors à déterminer à partir des conditions limites intrinsèques au problème considéré.

1.3 Un exemple de défaut

La description ci-dessus suppose que le continuum est homogène au sens de Noll-Truesdell [Nol67]. En effet, la réponse d'un continuum $\mathcal{B}$ évaluée en un point particulier $\mathbf{x} \in \mathcal{B}$ à l'instant t dépend en fait de la configuration actuelle dans laquelle se trouve le milieu à cet instant. Si seule la configuration locale $\nabla\varphi(\mathbf{X}, t)$ a une influence sur la réponse alors le milieu est dit simple en $\mathbf{X}$. Afin de définir cette notion, on rappelle quelques définitions préliminaires.
Le milieu est simple s'il est simple en tout point $\mathbf{x} \in \mathcal{B}$. Cette définition est motivée par la volonté de décrire les milieux dont les propriétés physiques telles que l'élasticité ou la viscosité par exemple, sont définies localement.
Un milieu simple est dit uniforme au sens de Noll-Truesdell si pour tous couples de points $(\mathbf{X}, \mathbf{Y})$ dans la configuration de référence, il existe un isomorphisme (dit matériel) entre un voisinage de $\mathbf{X}$ et un voisinage de $\mathbf{Y}$. Un isomorphisme matériel est en fait un isomorphisme entre deux espaces tangents et permet donc de déduire la réponse physique en $\mathbf{Y}$ pour une configuration donnée à partir de la réponse physique en $\mathbf{X}$. Ainsi un milieu avec un gradient de densité volumique est un milieu uniforme. Notons qu'un tel exemple nécessite d'avoir une densité qui dépend du gradient de la configuration afin de s'assurer qu'elle ne dépende pas du choix de coordonnées.
Un milieu est dit homogène au sens de Noll-Truesdell s'il est uniforme et s'il existe une configuration dans laquelle tous les isomorphismes matériels sont l'identité. La notion d'uniformité est relative à une configuration alors que l'homogénéité est une condition plus forte car elle décrit la capacité du milieu à être dans une configuration particulière. Reprenons l'exemple du milieu à gradient de densité ; si on peut trouver une configuration dans laquelle la densité est constante alors le milieu est homogène. Il sera pratique de considérer cette configuration comme la configuration de référence.
L'intérêt de cette définition de l'homogénéité est qu'elle nous permet de considérer des lois de comportements définies localement autour d'un point matériel. Dans ce qui suit nous ne reprendrons pas le vocabulaire introduit. Cependant ces deux définitions sont très utiles pour comprendre les limitations d'un corps simple sous-jacent à la définition du continuum comme un ouvert de $\mathbb{R}^3$ héritant de sa structure différentielle.
La géométrie différentielle est en effet la pierre angulaire de la description car toutes les quantités physiques sont définies en accord avec cette structure [Mar83]. Elle gouverne la différentiation des quantités scalaires telles que la densité de masse ou des champs de vecteurs tels que le déplacement. Ainsi, considérer le milieu comme un ouvert de $\mathbb{R}^3$ ne peut pas rendre compte d'un saut de déplacement autour d'une ligne de dislocations ni un saut de la densité de masse si on considère un milieu contenant un sous ensemble $\Omega \subset \mathcal{B}$ présentant une densité de masse différente. De tels sauts sont appelés hétérogénéités. La théorie ci-dessus nous permet de travailler sur des milieux présentant des hétérogénéités en traduisant ces sauts en termes de conditions aux

limites : une condition de saut en déplacement le long d'une ligne, une condition de continuité de la contrainte normale et du déplacement normal à une surface de discontinuité. Enfin, dans le cas de structures matérielles particulières telles que les plaques, des considérations supplémentaires sont nécessaires pour se ramener à un problème de dimension réduite (2D dans le cas des plaques) sans perdre trop d'informations sur le caractère 3D intrinsèque à la structure. Le cas de présence d'hétérogénéités dans de tels milieux sera alors aussi traduit en terme de conditions aux limites.

Cette sous-section est une revue de la notion de défaut issue d'une étude bibliographique. Elle est développée dans le cas particulier des dislocations qui sera l'exemple étudié dans le dernier chapitre. Elle nous permet entre autres de repenser le milieu continu de référence lorsqu'il présente des défauts dans sa structure. On commence par rappeller les notions de dislocations et de vecteurs de Burgers dans le contexte des réseaux cristallins. Ensuite on suivra le raisonnement de Kröner afin de développer le point de vue mécanique du continuum, et particulièrement pour les distortions plastiques que l'on définira également. Le lien avec le tenseur densité de dislocation sera lui aussi introduit excactement comme il le fût par Kröner [Kro80].

1.3.1 Dislocations

1.3.1.1 Dans un réseau cristallin

Avant toutes choses, il convient de préciser que nous employons le terme "atome" de manière générique pour décrire un élément irréductible de la structure cristalline.
Dans la nature, aucun cristal n'a de structure parfaite dans le sens où il contient toujours des défauts. La raison de la présence de tels défauts peut être de nature chimique, structurelle ou éléctrique dans lesquels des atomes étrangers à la structure peuvent intervenir. Ces défauts peuvent être classés selon leur dimension.
Le plus simple en terme de dimension est le défaut ponctuel. Sans aller plus dans le détail de sa création, on caractérise deux types de tels défauts : soit un atome est inséré dans le réseau, soit il peut en avoir été extrait. Ces deux types de défaut sont mobiles car un atome dans le voisinage du phénomène peut se mouvoir afin de combler la place libre laissée par l'atome manquant. De la même manière l'atome inséré peut prendre la place de son voisin, ce dernier prend alors le rôle de l'atome ajouté dans cette nouvelle configuration.
Si le nombre d'atomes est assez important et forme un cercle, des plans du cristal bougeront ensemble dans le but de réparer le réseau cristallin. À la fin du processus, la structure sera réparée sauf sur le bord du disque formé initiallement par les atomes manquants. Bien entendu de tels réarrangements peuvent aussi intervenir dans le cas d'extra-atomes insérés. On obtient un défaut 1D : la ligne formant le bord constitue alors la ligne du défaut. De tels défauts sont appelés dislocations.
On finit ce paragraphe par l'un des trois cas de défauts 2D : les joints de grains qui sont l'interface où se rencontrent deux sous-réseaux régulier d'orientations différentes. Ce cas particulier de défaut peut-être pensé comme une distribution de dislocations (figure 1.1).

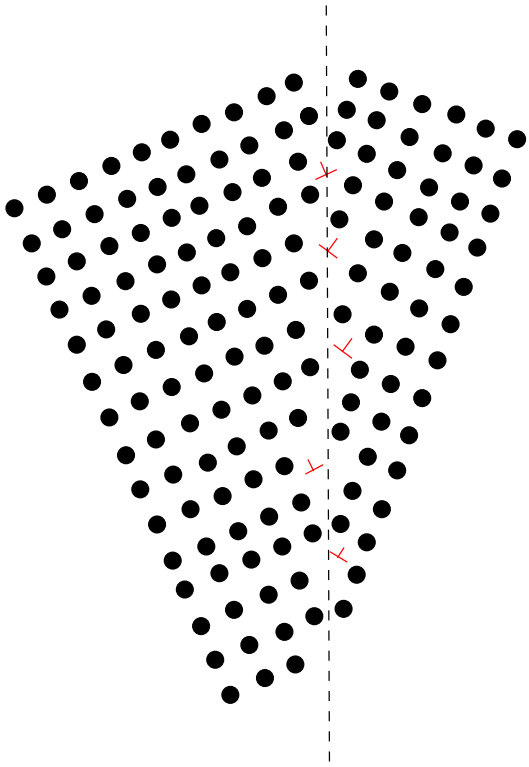

Figure 1.1: Le joint de grain est un défaut 2D obtenu à partir d'une densité de dislocation. Les symboles en rouge représentent les dislocations.

1.3.1.2 Ligne de dislocations et vecteur de Burgers

On introduit ici le vecteur de Burgers relatif à une ligne de dislocation. Soit C un chemin fermé dans un cristal idéal, on note C' son image dans le cristal comportant les dislocations. Le chemin C' est défini comme suit. À chaque pas de transitions entre un atome et son voisin dans le cristal idéal, le pas correspondant est fait dans le cristal perturbé (figure 1.2).

Alors que le chemin se ferme dans le cristal de référence, le circuit C' correspondant dans le cristal perturbé ne se ferme pas. Ce défaut de fermeture est excatement un vecteur du réseau noté $\mathbf{b}$ appelé vecteur de Burgers local [Bur39]. Il va du point de départ du chemin, au point d'arrivé. Mathématiquement, cela se traduit par :

$$\sum_{x_i \in C} \Delta\mathbf{u}(x_i) = \mathbf{b},$$

où x_i sont les atomes du cicuits et $\Delta\mathbf{u}$ est l'incrément du déplacement parcouru d'atome

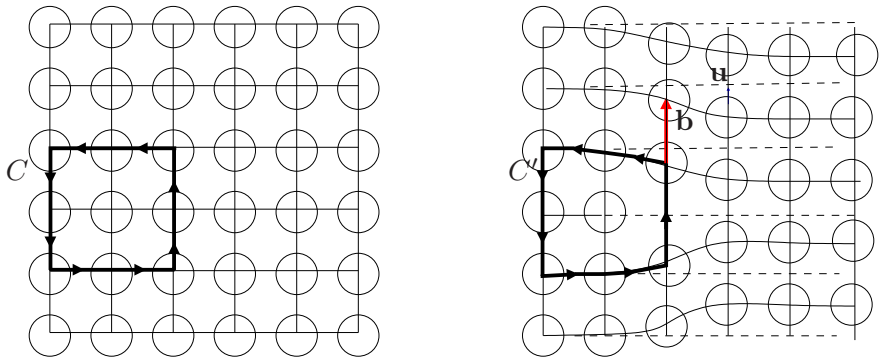

Figure 1.2: Image C' d'un circuit fermé C dans un cristal perturbé. $\mathbf{b}$ est le vecteur de Burgers et $\mathbf{u}$ représente le vecteur déplacement entre la position dans le cristal parfait et celle dans le cristal défectueux.

en atome. Par passage à la limite, on obtient pour le cas continu :

$$\int_{x \in C} \mathrm{d}\mathbf{u}(x) = \mathbf{b}.$$

Le chemin C est appelé chemin de Burgers [Bur39]. Notons que cette définition ne requiert aucune orientation de la ligne de défaut et si l'on change la direction de parcours du chemin alors le vecteur de Burger change de signe. Nous reviendrons sur le cas continu par la suite.
On distingue deux types de dislocations. Si le vecteur de Burgers est orthogonal à la ligne de défaut, on parle de dislocation coin ou encore *edge dislocation*. Si le vecteur de Burgers est colinéaire à la ligne de défaut on parle de dislocation vis ou bien *screw dislocation*.

1.3.1.3 Processus de Volterra

Ici nous introduisons le processus de Volterra qui est une expérience de pensée permettant de construire une ligne de dislocation en s'affranchissant de la structure cristalline. On commence par couper le milieu le long d'un demi-plan P de bord L destinée à être la ligne de dislocation. Ensuite on translate l'un des deux morceaux par un vecteur $\mathbf{b} \in P$ avec $\mathbf{b} \perp L$ ou $\mathbf{b} \parallel L$. Enfin on recolle à l'interface et l'état d'équilibre obtenu est une dislocation. Le vecteur de Burger est bien entendu le vecteur de translation $\mathbf{b}$. Remarquons que cette définition est valable pour un milieu continu de sorte que nous puissions parler de continuum avec une dislocation. Dans la suite nous poursuivons la discussion d'un point de vue continuum en considérant les déformations plastiques et élastiques ainsi que leurs liens avec les dislocations.

1.3.2 Déformation élastique et déformation plastique

Il s'agit ici de distinguer deux types de comportement du matériau : le comportement élastique et le comportement plastique. Ces comportements sont généralement mis en

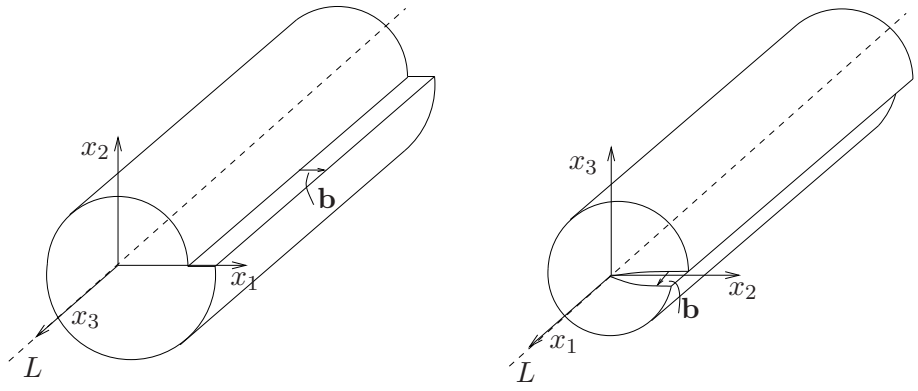

Figure 1.3: La dislocation coin (gauche) : Le vecteur de Burgers est perpendiculaire à la ligne de dislocation. La dislocation vis (droite) : Le vecteur de Burgers est parallèle à la ligne de dislocation.

évidence au cours de la déformation du milieu et donc par abus de langage on parlera de déformations élastiques et de déformations plastiques illustrées dans la figure 1.4 . La discussion qui suit est essentiellement fondée sur celle de Kröner [Kro80]. Certes, le raisonnement n'est valable que pour l'hypothèse des petites perturbations mais il est suffisant dans le cadre de notre travail.

Lorsqu'un milieu a un comportement élastique au cours d'une déformation, celle-ci sera dite élastique. On rappelle que pour ces déformations, les points voisins dans la configuration de référence restent voisins au cours du mouvement sans qu'il n'y ait eut apparition d'arêtes ou de coins dans la structure matérielle. Cela est la conséquence directe du fait que le mouvement soit un difféormorphisme et donc cela suggère aussi que la déformation soit inversible. La structure différentielle de l'élément de volume déformé est décrite par le tenseur de distortion $\boldsymbol{\beta}$ qui s'exprime dans le cas linéaire par :

$$\beta_{ij}^{\mathrm{e}} = \varepsilon_{ij}^{\mathrm{e}} + \omega_{ij}^{\mathrm{e}}.$$

On rappelle que le tenseur de déformation élastique $\boldsymbol{\varepsilon}$ décrit le changement de forme du volume élémentaire. La rotation élastique $\boldsymbol{\omega}$ décrit, quant à elle, la rotation rigide de ce volume.

Au contraire, la déformation plastique est une déformation associée à un mouvement non inversible. Plusieurs raisons peuvent être évoquées pour justifier l'existence de tels mouvements : cela peut être dû à de grandes perturbations ou encore des processus thermomécaniques qui changerait les propriétées du matériau elles-mêmes. De telles déformations impliquent généralement la création de lignes de dislocations et peuvent les faire bouger. Par exemple le pliage d'un morceau de métal à l'état solide ou encore l'écrouissage induisent des déformations plastiques. En utilisant les mêmes notations que pour la déformation élastique, on décompose la distortion plastique en deux parties, la déformation plastique et la rotation plastique :

$$\beta_{ij}^{\mathrm{P}} = \varepsilon_{ij}^{\mathrm{P}} + \omega_{ij}^{\mathrm{P}}.$$

On introduit ici la plasticité par une expérience de pensée en 2D, présentée par Kröner [Kro80] et probablement inspirée par le processus de Volterra. Le raisonnement est le suivant : on coupe l'élément de volume en collection suffisamment dense de parallélogrammes. On applique un déplacement constant sur chaque parallélogramme. On recolle alors les parallélogrammes en prenant soin d'ajouter de la matière et d'en extraire là où la différence de déplacement de chaque parallélogramme aura créé des trous ou du surplus de matière. On obtient alors un volume élémentaire compact. Le caractère non inversible d'un tel processus est dû au coupage/collage couplé à des champs de déplacement distincts.

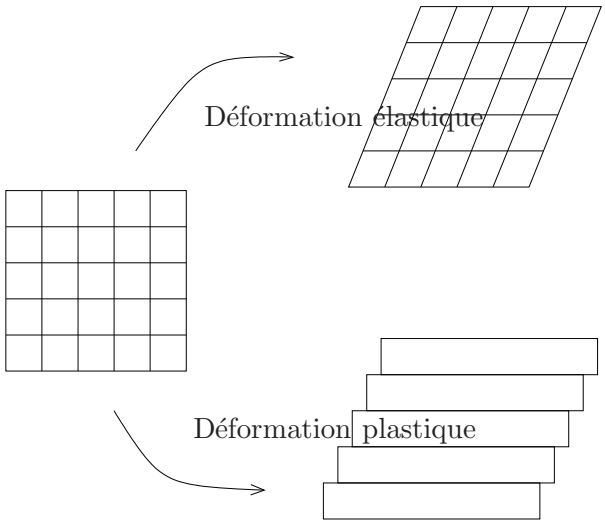

Figure 1.4: La déformation élastique est reversible. Dans la déformation plastique preésenté, on a des glissements le long d'une surface matériel : les points initialement voisins ne le sont plus.

Jusqu'ici on a donné une image qualitative des distortions plastiques et élastiques qui peut être donnée dans le cas linéaire par :

$$\beta_{ij} = \beta^{\mathrm{e}}_{ij} + \beta^{\mathrm{P}}_{ij}.$$

Si l'on suppose que la distortion (plastique ou élastique) est constante sur chaque élément de volume alors il est possible dans certain cas de définir la distortion comme le gradient d'un déplacement qui décrirait alors la manière dont les points de l'état non déformé sont transférés aux points de l'état déformé. Cependant il n'est pas nécessaire qu'une distortion donnée soit intégrable, c'est-à dire obtenue comme le gradient d'un déplacement. Ceci est connu en élasticité comme le problème de compatibilité de la déformation.

1.3.3 Compatibilité et incompatibilité : une description qualitative

Dans la sous-section précédente, on a analysé un volume élémentaire isolé. On va maintenant s'intéresser à la description de la plasticité et de l'élasticité dans le cadre

d'une configuration de référence pensée comme une collection de volumes élémentaires infinitésimaux. L'expérience de pensée nous est proposée par Kröner : on découpe le milieu en quantité suffisante de volumes élémentaires ΔV que l'on distingue en les numérotant par exemple. Sur chaque volume élémentaire on applique une déformation plastique telle que décrite précédemment. Dans le but d'étudier le phénomène macroscopiquement on suppose que les distortions plastiques varient peu d'un volume élémentaire à ces voisins. Il s'agit alors de recoller tous les volumes élémentaires. Deux cas de figures se présentent.
Dans le premier cas tous les volumes se recollent parfaitement comme autant de pièce d'un puzzle, sans nécessité d'appliquer de rotations ni de déformation. L'expérience s'arrête et l'état déformé peut être décrit sans faire appel aux processus de coupage/collage. En effet, tout se déroule comme si les contraintes appliquées avaient créé des dislocations se compensant les unes les autres pour finalement disparaître. Il n'y a pas de distortions élastiques dans le processus c'est pourquoi la distortion totale et la distortion plastique sont égales. Aucun trou n'a été créé de sorte que la déformation est compatible. Il existe alors un champ de déplacement $\mathbf{u}^{\mathrm{P}}$ bien défini en tout point, un seul vecteur associé à un seul point, et qui décrit comment les points de la configuration de référence ont été translatés pour se retrouver dans la configuration finale. En conséquence le champ de distortion est $\boldsymbol{\beta}^{\mathrm{P}} = \nabla \mathbf{u}^{\mathrm{P}}$. Cette situation idéale implique que l'état interne reste inchangé même si la forme a changé.

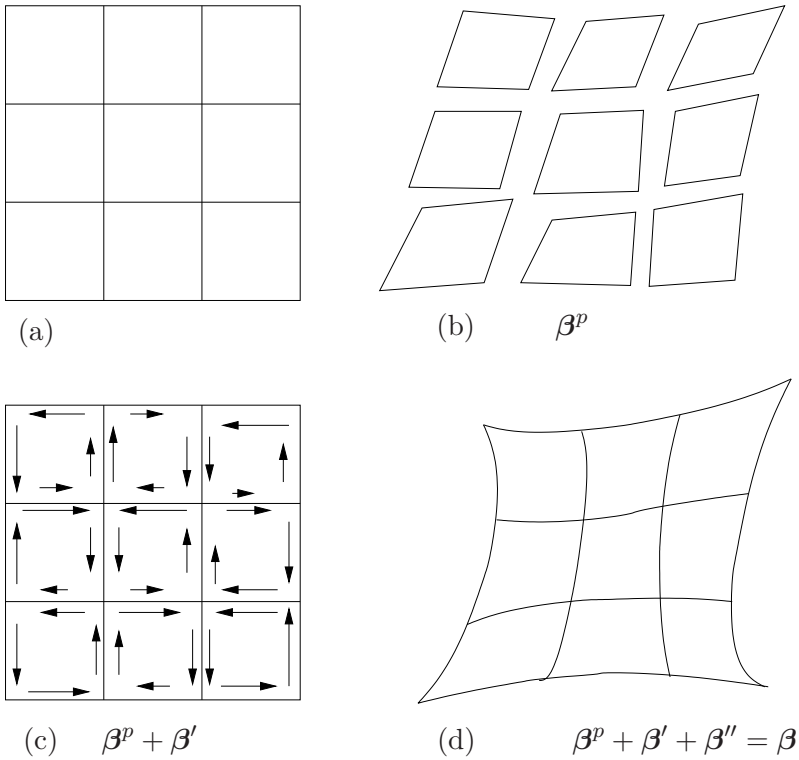

Figure 1.5: Incompatibilité des déformations élastiques et plastiques.

Dans le second cas, les volumes élémentaires ne se recollent pas. Or pour décrire une déformation du continuum, on a besoin de revenir à une configuration connexe du milieu (figure 1.5 (b)). Pour cela on applique une déformation élastique. Cette déformation n'est pas unique mais le plus simple est d'appliquer une distortion élastique $\boldsymbol{\beta}'$ qui envoie les points dans leur position initiale avant la distortion plastique (figure 1.5 (c)). On peut alors les recoller puis enlever les forces induites par le processus élastique. Enfin le milieu atteint l'état d'équilibre par une dernière distortion élastique $\boldsymbol{\beta}''$ (figure 1.5 (d)). Comme on travaille sous l'hypothèse des petites perturbations, la distortion totale est bien évidemment : $\boldsymbol{\beta} = \boldsymbol{\beta}^{\mathrm{P}} + \boldsymbol{\beta}' + \boldsymbol{\beta}''$. Notons que pour des grandes déformations, il conviendrait ici d'utiliser la décomposition de Lee, introduite pour la première fois par Bilby [BGS57].
La distortion totale peut être décrite par un déplacement total $\mathbf{u}$. En fait l'impossibilité de recoller les éléments après la distortion plastique signifie que le déplacement est discontinu aux frontières entre deux volumes. Les volumes élémentaires étant infinitésimaux, par passage à la limite on dispose d'un milieu qui présente une distribution de sauts de déplacement : le déplacement a des valeurs multiples presque partout. De manière équivalente, la distortion plastique est incompatible avec l'existence d'un champ de déplacement bien défini. Le même argument reste valable pour la déformation élastique induite par $\boldsymbol{\beta}'$ et donc la distortion élastique totale $\boldsymbol{\beta}^{\mathrm{e}} = \boldsymbol{\beta}' + \boldsymbol{\beta}''$ n'est pas non plus compatible.

Dans la sous-section suivante on donne une définition quantitative de l'incompatibilité introduisant alors les équations de compatibilité et d'incompatibilité.

1.3.4 Loi d'incompatibilité

1.3.4.1 Rappel sur les conditions d'intégrabilité

Définition 1.4 *Soit $\boldsymbol{\beta}$ un tenseur d'ordre deux, $\boldsymbol{\beta}$ est dit intégrable s'il existe un champ de vecteur $\mathbf{u}$ tel que $\boldsymbol{\beta} = \nabla\mathbf{u}$.*

Ainsi intégrabilité et compatibilité sont la même notion. On donne le théorème suivant qui nous donne une condition nécéssaire et suffisante pour la compatibilité :

Théorème 1.4 *Soit $\boldsymbol{\beta}$ un tenseur d'ordre deux défini sur un milieu simplement connexe, alors $\boldsymbol{\beta}$ est intégrable si et seulement si $\nabla \times \boldsymbol{\beta} = \mathbf{0}$.*

Il est immédiat de montrer que si $\boldsymbol{\beta}$ est intégrable alors $\nabla \times \boldsymbol{\beta} = \mathbf{0}$. Pour l'autre implication la preuve consiste à utiliser le théorème de Green pour montrer que l'intégrale de $\boldsymbol{\beta}$ ne dépend pas du chemin suivi.

1.3.4.2 Tenseur de densité de dislocations

Revenons sur l'égalité $\boldsymbol{\beta} = \boldsymbol{\beta}^{\mathrm{e}} + \boldsymbol{\beta}^{\mathrm{P}}$. Chaque point matériel du milieu possède une position initiale et une position finale auxquelles on associe un champ de vecteur

déplacement total. En posant e_{ikl}, les composantes du tenseur (anti-symétrique) de Levi-Civita, le théorème 1.4 donne :

$$\nabla \times \boldsymbol{\beta} = \mathbf{0}, \quad \text{ou de manière équivalente} \quad e_{ikl}\partial_k \beta_{lj} = 0.$$

Or $\boldsymbol{\beta}$ est la somme de ses parties élastiques et plastiques de sorte que l'on déduit :

$$\nabla \times \boldsymbol{\beta}^{\mathrm{e}} = -\nabla \times \boldsymbol{\beta}^{\mathrm{p}} := \boldsymbol{\alpha}, \quad \text{ou de manière équivalente} \quad e_{ikl}\partial_k \beta^{\mathrm{e}}_{lj} = -e_{ikl}\partial_k \beta^{\mathrm{p}}_{lj} := \alpha_{ij}.$$

Le tenseur $\boldsymbol{\alpha}$ est la densité de dislocation introduite ainsi par Kröner. L'interprétation est la suivante : puisqu'il n'y a pas eu création de trou, des dislocations ont dû être créées sur les frontières entre les volumes. Comme ces volumes élémentaires n'ont pas de sens physique, d'un point de vue macroscopique, on s'aperçoit qu'après la transformation élastoplastique, on obtient un milieu avec une distribution continue de disclocations. Une conséquence direct de la définition de $\boldsymbol{\alpha}$ est :

$$\nabla \cdot \boldsymbol{\alpha} = 0, \tag{1.2}$$

qui signifie que les lignes de dislocations ne peuvent se terminer à l'intérieur du milieu. Toutes densités de dislocations doivent vérifier cette condition.
Si on intègre sur une surface arbitraire de bord C, le théorème de Stokes donne :

$$\int\int_S \boldsymbol{\alpha} d\mathbf{S} = \int\int_S \nabla \times \boldsymbol{\beta}^{\mathrm{e}} \cdot d\mathbf{S} = \oint_C \boldsymbol{\beta}^{\mathrm{e}} d\mathbf{x}.$$

Or localement la distortion induit un déplacement donc on a $\beta^{\mathrm{e}}_{ij} dx^j = du_i$. Ainsi on obtient les composantes du vecteur de Burgers :

$$b_i = \oint_C \mathrm{d}u_i = -\int\int_S \alpha_{ij} dS^j.$$

En conclusion $\boldsymbol{\alpha}$ peut être interprété comme une densité de vecteur de Burgers locaux $\mathrm{d}\mathbf{b}$, et le vecteur de Burgers total $\mathbf{b}$ est associé à la surface considérée. Cette distincion entre vecteur de Burgers total et local sera détaillée à l'occasion d'une discussion du chapitre 4.

1.4 Milieu continu et défauts

Dans les premières sections nous sommes revenus brièvement sur les idées majeures en élasticité. Cette théorie du milieu continu est éprouvée dés que la structure du continuum présente un certain nombre de défaut. On a choisit de présenter un aperçu d'un type de défaut particulier à savoir les dislocations pour des raisons qui deviendront évidentes par la suite lorsqu'on évoquera leur lien avec la géométrie différentielle. On peut bien entendu étendre la notion de défaut, aussi appelé hétérogénéité, à l'ajout de matière à l'échelle macroscopique. Une barre de métal dans un milieu fluide constitue une hétérogénéité par exemple. En effet, à l'interface les constantes mécaniques

présentent un saut. La modélisation géométrique de ces constantes reste délicate surtout lorsque les sauts sont en quantité importante.
L'objectif général de la modélisation consiste à définir macroscopiquement le milieu comme un continuum doté de propriétés mécaniques constantes dites effectives, car elle ne dépendent pas de la position de ces défauts. Pour cela, on peut s'appuyer sur des techniques de multi-diffusion, ou sur des principes de milieux continus généralisés. Bien que nous ne nous y confrontons pas dans ce travail, les techniques d'homogénéisation peuvent aussi s'appliquer.
Dans cette section on se propose de rappeler dans un premier temps le principe de multi-diffusion, communément appelé *multiple scattering*, qui nous permet de modéliser des problèmes liés à des défauts de type inclusion. Dans un second temps, on évoque la notion de milieu continu généralisé qui peut prendre en compte la notion de défaut ou bien celle de structures matérielles particulières.

1.4.1 Multi-diffusion (*multiple scattering*)

1.4.1.1 Contexte

Lorsqu'on s'intéresse à la propagation d'onde en milieu défectueux, la théorie de multi-diffusion est une méthode puissante. En effet, on définit généralement la multi-diffusion comme l'interaction d'un champ avec deux obstacles ou plus. Ces obstacles peuvent être de différentes natures comme l'inclusion de matière par exemple, ou encore des dislocations, et sont appelés diffuseurs. La propagation du son dans un milieu comportant deux sphères rigides est un exemple typique de multi-diffusion. Le principe est plutôt simple. Le champ diffracté par un seul obstacle peut être calculé par des méthodes variées telles que la séparation des variables combinée à des conditions de continuité aux interfaces ou encore la résolution d'équations intégrales. Or dans le cas d'obstacle en quantité importante, le champ diffracté par un diffuseur fera intervenir les champs diffractés par les autres. Cette récursivité inhérente à la description du problème nous conduit à un autre point de vue de la multi-diffusion : elle consiste à calculer le champ diffracté total [Mar06]. Le régime fréquentiel aura aussi toute son influence sur ce champ total. Dans le cas des deux sphères par exemple, on peut montrer qu'à basse fréquence (longueur d'onde grande devant la taille des sphères) leur association est équivalente à un dipôle ce qui n'est pas vrai dans d'autre domaine de fréquences.
En toute première approximation, on peut supposer que le champ diffracté est la somme des champs diffractés par les diffuseurs comme s'ils étaient excités uniquement par le champ incident. C'est en fait du *single-scattering* parce que tous les effets d'interaction propres à la multi-diffusion sont négligés.

1.4.1.2 Diffraction par N diffuseurs

Supposons que l'on ait N inclusions disjointes s_j dont les propriétés sont connues : position, forme, propriétés mécaniques et conditions aux bord. Le milieu ainsi con-

stitué est sondé par une onde incidente. Le problème est donc de calculer le champ total diffracté. Mathématiquement, c'est un problème bien posé de recherche de solutions avec une condition de radiation à l'infini et des conditions aux interfaces des diffuseurs mais pour une frontière qui n'est pas simplement connexe. De fait le champ total diffracté est très sensible à la position des diffuseurs lorsque la longueur d'onde est petite devant la distance séparant deux diffuseurs. Cela peut être très compliqué à résoudre en particulier pour des interfaces non triviales. Une alternative serait de résoudre le problème directement à partir des équations intégrales mais la méthode numérique qu'on utiliserait peut s'avérer très coûteuse.

Méthode *self-consistent*

Selon Twersky [Twe67] "*it is convenient in considering multiple scattering, to assume that solutions for the component scatterers when isolated are known, and that they may be regarded as parameters on the more general problem*". Le meilleur moyen pour résoudre un problème de multi-diffusion supposant que tout est connu sur le processus de diffraction pour chaque diffuseur isolé, est d'utiliser ce qu'on appelle aussi les méthodes *self consistent*. Le principe général de cette méthode est aussi appelé méthode de Foldy-Lax et conduit à une formulation :

$$\mathbf{u} = \mathbf{u}_{\text{inc}} + \sum_{i=1}^{N} T_i \mathbf{u_i},$$

où T_i est la T-matrice, un opérateur linéaire qui modélise le lien entre le champ diffracté par s_i et le champ $\mathbf{u}_i$ agissant sur lui. Foldy utilisa un cas particulier de cette méthode pour le cas de diffuseurs isotropes ponctuels alors que Lax a développé un raisonnement plus général mais pour un T_i particulier. Dans le cas d'une géométrie relativement simple, il est souvent confortable de combiner cette méthode avec la séparation des variables de l'équation de Helmholtz que nous avons évoquée. Pour un diffuseur cylindrique, on pourra utiliser des coordonnées polaires. Les principaux outils seront alors des théorèmes d'addition tels que le théorème de Graf.

1.4.1.3 Distribution aléatoire de diffuseurs

En règle générale la position des diffuseurs n'est pas connue mais nous avons des informations sur leur distribution statistique. Dans ce cas on s'appuie sur des outils de probabilité. Considérons l'exemple de N diffuseurs identiques distribués de manière homogène dans la matrice, c'est à dire qu'on dispose d'un nombre constant de diffuseurs par unité de volume. Dans ce contexte, une configuration est la donnée de la position de l'ensemble des diffuseurs. Le principe consiste alors à faire la moyenne statistique du champ considéré pour toutes les configurations possibles afin d'obtenir un champ moyen que l'on appelera aussi champ effectif. Cette formulation peut s'exprimer par une succession hierarchisée de N intégrales de probabilités conditionnelles dont les densités sont déduites de la concentration des diffuseurs. Ces méthodes sont souvent

combinées aux méthodes *self-consistent* associées à une séparation des variables.
Composer avec cette succession de N intégrales s'avère délicat, d'autant plus que le problème devient sous-déterminé lorsque l'on veut la tronquer. Pour y remédier on doit faire appel à une hypothèse de fermeture, afin d'avoir un problème bien posé à un ordre de troncature donné. Parmi les plus connues on retient l'hypothèse de Foldy [Fol45] et la *quasi-cristalline assumption* (QCA) introduite par Lax [Lax52]. De nombreux travaux ont été menés dans cette direction et ont pour but de déterminer un nombre d'onde effectif qui gouvernerait la propagation d'une onde au sein du milieu defectueux. Ces techniques donnent des résultats intéressant à haute-fréquence c'est-à-dire pour des rapports de l'ordre de 5 entre la taille d'un diffuseur et la longueur d'onde. On retiendra par exemple Watermann et Truell [WT61] qui ont appliqué la QCA mais pour une approximation au niveau des probabilités conditionnelles pour la *hole correction* qui n'est autre que la condition mathématique pour que deux diffuseurs ne se juxtaposent pas. Plus récemment, inspiré par les travaux de Lloyd et Berry [LB67], Linton et Martin [Mar06] ont corrigé la *hole correction* et obtenu un développement limité du nombre d'onde à l'ordre deux en terme de concentration. Conoir et Norris [CN10] ont obtenu des résultats similaires pour le cas élastique. Maurel et *al* ont appliqué ces méthodes pour le problème de propagation d'onde à travers un réseau de dislocations et pour une distribution aléatoire de dislocations [MML04].

1.4.2 Milieu continu généralisé

1.4.2.1 Variété matérielle de Riemann-Cartan

Le cadre naturel de travail de la mécanique du continuum est la géométrie différentielle [Mar83]. Dans ce contexte on dispose d'une connexion affine ∇ dont les coefficients seront notés $\Gamma^{\gamma}_{\alpha\beta}$ [Car86]. Elle décrit le transport des quantités vectorielles et tensorielles sur le fibré tangent, parallèlement à la fibre. Par exemple, elle permet d'exprimer un vecteur tangent en P dans l'espace tangent en M. Plus précisément, on peut alors définir la dérivé covariante qui généralise pour les tenseurs, la notion de dérivée directionelle des fonctions. La première application de la connexion est intervenue lors d'une collaboration entre Einstein et Cartan dans le cadre de la relativité [Dev92].
Habituellement la connexion est supposée symétrique ; cela signifie que le transport parallèle d'un vecteur **u** dans la direction **v** donne le même vecteur lorsque l'on transporte parallèlement **v** dans la direction **u**. Dans ce cas la connexion est dite de Levi-Civita dont les coefficients sont les symboles de Christoffel définis uniquement par le tenseur métrique, comme c'est le cas en relativité générale.
Cependant Cartan remarqua qu'en règle générale, il n'y a aucune raison particulière pour que cette connexion soit symétrique. La partie anti-symmétrique est en fait un tenseur : le tenseur de torsion **S**. En résumé cela veut dire qu'il y a un défaut de fermeture du parallélogramme que l'on obtiendrait après le transport parallèle de **u** (resp. **v**) dans la direction **v** (resp. **u**). Ce défaut de fermeture est mesuré par l'opérateur de torsion appliqué à ces deux vecteurs. Appliquer ces deux transports parallèles est connu comme le circuit de Cartan. Lorsque la métrique ne varie pas lors d'un trans-

port parallèle, on dit que la connexion est compatible avec la métrique. Sous cette hypothèse, on peut montrer que les symboles de connexions se décomposent sous la forme [Nak96] :

$$\Gamma^{\gamma}_{\alpha\beta} = \overline{\Gamma}^{\gamma}_{\alpha\beta} + K^{\gamma}_{\alpha\beta},$$

avec $\overline{\Gamma}^{\gamma}_{\alpha\beta}$ les symboles de Christoffel et $K^{\gamma}_{\alpha\beta}$ le tenseur de contortion calculé à l'aide de la métrique et de la torsion. Une variété comportant une connexion asymétrique avec une courbure non nulle est une variété de Riemann-Cartan.
On peut aussi introduire ces variétés au moyen des *vielbein* (*triads* en 3D). Ce sont des applications locales non-holonomes. Dans le contexte de notre étude on considèrera des *triads* définis sur l'espace Euclidien $\mathbb{R}^3$ à valeur dans l'espace tangent matériel à un point M arbitraire de la connexion matérielle. La métrique et les coefficients de connexion sont alors déduits des *triads* et de leurs dérivées partielles. Cela permet de généraliser la notion de mouvement évoqué précédemment. On peut voir ces *triads* comme des transformations élastoplastiques et on met alors en évidence le lien entre les dislocations et le tenseur de torsion. Ses composantes représentent la densité surfacique de vecteur de Burgers locaux associés à une surface et une direction pour le vecteur de Burgers.

1.4.2.2 Milieux de Cosserat

Selon Cartan lui même, ses travaux furent inspirés par la théorie de nouveaux types de continuum introduits en 1909 par les frères Eugène et François Cosserat, dans leur livre intitulé "Théorie des corps déformables". Au cours du 20$^{\text{ième}}$ siècle, et plus particulièrement dans sa deuxième moitié, l'idée des frères Cosserat inspira de nombreux travaux en mécanique des milieux continus et en physique des matériaux (par exemple [Min64], [EC64]).
Le continuum imaginé par les frères Cosserats est un milieu continu muni d'une microstructure. À chaque point matériel, on associe aussi trois axes appelés directeurs. En plus du déplacement usuel $\mathbf{u}$, il faut donc considérer un champ de rotation indépendant du déplacement, attaché à chaque point de la microstructure et agissant sur les directeurs. Ce champ de rotation est mesuré par le bivecteur ω tel que $\omega_{ij} = -\omega_{ji}$.
En conséquence, la déformation du continuum doit être mesurée par la distortion $\boldsymbol{\beta}$ et la contortion $\boldsymbol{\kappa}$:

$$\beta_{ij} = \overline{\nabla}_i u_j - w_{ij},$$
$$\kappa_{ijk} = \overline{\nabla}_i \omega_{jk},$$

où $\overline{\nabla}$ est la dérivé covariante de l'espace Euclidien $\mathbb{R}^3$. En posant $\mathcal{L}$ le potentiel élastique (ou encore énergie libre de Helmholtz), il faut considérer non seulement la contrainte $\boldsymbol{\sigma} \sim \frac{\delta \mathcal{L}}{\delta \boldsymbol{\beta}}$, qui est asymétrique, mais aussi la nouvelle réponse induite par le champ de rotation : le *spin moment stress* $\boldsymbol{\tau} \sim \dfrac{\delta \mathcal{L}}{\delta \boldsymbol{\kappa}}$. Ainsi les équations d'équilibre statique satifaites par les forces et les moments sont :

$$\text{div}\ \boldsymbol{\sigma} + \boldsymbol{f} = 0,$$
$$\text{div}\ \boldsymbol{\tau} + \mathbf{m} = \overline{\boldsymbol{\sigma}},$$

où $\mathbf{f}$ et $\mathbf{m}$ sont respectivement les densités volumiques de forces et de moments alors que $\overline{\boldsymbol{\sigma}}$ est la partie symétrique du tenseur des contraintes.
La géométrie de Riemann-Cartan (RC) peut être obtenu dans les milieux de Cosserat à travers les associations :

$$\text{distortion} \longleftrightarrow \textit{triads,} \qquad \text{contortion} \longleftrightarrow \text{connexion.}$$

Cependant pour assurer l'asymétrie de la connexion, la distortion et la contortion ne doivent pas dériver respectivement d'un déplacement ni d'un champ de rotation. De tels milieux de Cosserat sont dits incompatibles parce que la contortion et la distortion ne satisfont pas les conditions de compatibilité.

1.4.2.3 Dislocations

Nous revenons rapidement sur le concept de dislocations afin de faire un rapide rappel de son histoire mais aussi afin d'établir le lien avec la géométrie (RC). Ce concept fut introduit à la fin des années 30 [Bur39], dans le but de comprendre les déformations plastiques au sein d'un solide disposant d'une structure cristalline. Lorsque l'on dispose d'un nombre conséquent de dislocations, il est pertinent de développer une théorie du continuum avec dislocations. Pour ce faire, on introduit le tenseur de densité de dislocations dont les composantes sont en relation avec l'élément de surface et la direction du vecteur de Burgers. En 1953 Nye établit la relation entre la densité de dislocations et les rotations relatives entre les plans de réseaux voisins [Nye53]. Dans sa théorie des défauts, Kröner exprime les relations entre le tenseur de Nye, défini grâce au tenseur densité de dislocations, et les conditions d'incompatibilité dans le cadre des milieux de Cosserat [Kro86, Kro60]. Dans la même période il a été montré par Kondo [Kon55], Bilby *et al* [BBS55], et Kröner que le chemin de Burgers est isomorphe au circuit de Cartan. De ces travaux on montre alors que la densité de dislocation et le tenseur de torsion sont équivalents dans une théorie géométrique du milieu continu. Cependant à ce niveau, on perd les informations sur la description cristallographique. En effet les seules caractéristiques de la torsion ne sont pas suffisantes pour déterminer de façon unique la distribution des dislocations. Une telle vision suggère une homogénéisation préalable.

1.4.2.4 Milieu faiblement continu

Partant de la structure cristalline dans les matériaux simples, Noll et Wang [Nol67] établirent le lien entre les inhomogénéités (densités de discontinuités) et les tenseurs de courbure et torsion induits par une connexion matérielle. En suivant cette approche, Rakotomanana introduisit une classe de milieu particulier : les milieux faiblements continus. Dans un milieu faiblement continu, la matière est supposée avoir une distribution continue mais des discontinuités de champ scalaires tels que la densité massique, ou encore de champ vectoriel comme la vitesse, peuvent intervenir. Ces milieux peuvent être obtenus à partir d'une configuration qui est $\mathcal{C}^1$ par morceaux. Il montre alors que les sauts induits dans les champs scalaires et/ou vectoriels peuvent être décrits au moyen des tenseurs de courbure et de torsion.

Théorème 1.5 *Soit θ un champ scalaire défini sur un continuum $\mathcal{B}$. La variation de θ d'un point à un autre dépend du chemin suivi si et seulement si le tenseur de torsion est non nul sur la variété $\mathcal{B}$. De plus la torsion caractérise le saut de θ.*

Ainsi un continuum avec des discontinuités d'un champ scalaire et une variété matérielle, dite de Weitzenbock, sans courbure mais avec une torsion non nulle, sont équivalentes.

Théorème 1.6 *Soit* $\mathbf{w}$ *un champ de vecteur défini sur un continuum $\mathcal{B}$. Si la variation de* $\mathbf{w}$ *d'un point à un autre dépend du chemin suivi alors la torsion et la courbure sont non nulles sur la variété matérielle $\mathcal{B}$ et elles caractérisent le saut de* $\mathbf{w}$*.*

L'idée de la preuve de ces théorèmes est de suivre les champs le long d'un circuit de Cartan et de prendre la limite quand celui-ci tend vers le chemin trivial. Malheureusement le raisonnement ne peut pas être appliqué pour des défauts de type inclusion présents en multi-diffusion car il n'existe pas de chemin que l'on pourrait suivre pour mettre en évidence le saut. En effet il faudrait traverser l'interface, là où le champ n'est pas continu donc *a fortiori* pas différentiable.

1.5 Contribution du travail de thèse

1.5.1 *Multiple scattering* d'ondes acoustiques en milieu aléatoire

Dans cette partie on s'intéresse à la multi-diffusion des ondes acoustiques en milieu aléatoire en suivant les méthodes dites de Foldy-Lax. En premier lieu nous énoncerons les théorèmes d'additions de Graf en introduisant une formulation algébrique originale à laquelle nous nous réfèrerons systématiquement tout au long du chapitre. Aprés avoir rappelé les résultats classiques en 2D de la diffraction d'une onde plane par un diffuseur circulaire, nous nous intéresserons plus en détails à l'exemple impliquant la diffraction par deux diffuseurs d'une onde émise par une source ponctuelle. Ce sera alors pour nous l'occasion non seulement de commenter la formulation adoptée, qui offre la possibilité d'interpréter chaque terme de couplage, mais surtout d'étudier un peu plus précisément certains termes de couplage dans l'hypothèse où les diffuseurs et la source sont tous trois éloignés les uns des autres. On notera alors la présence d'un terme de "force de diffusion" qui interroge la notion de milieu dilué et donne une idée de l'erreur induite dans les formules usuelles de *multiple scattering* qui s'appuient sur des formulations connnues pour la diffraction d'un seul diffuseur [Twe67]. Ensuite nous étudierons la formulation algébrique dans le cas général afin d'obtenir une interprétation équivalente à celle des séries de Born et des développements de Lippman-Schwinger.
Aprés avoir rappelé les notions de moyenne d'ensemble d'un champ et la hierarchie de probabilités conditionnelles qu'elles impliquent, nous les mettrons en application dans le cas de la multi-diffusion d'une onde émise par un point source au sein d'un milieu aléatoire infini. L'ordre des modèles évoqués correspond à l'ordre auquel on invoque l'hypothèse de fermeture dans la hierarchie des intégrales de probabilités.
Dans un premier temps, on commence par un modèle d'ordre 1. À cette occasion on revient rapidement sur le modèle proposé par Foldy [Fol45] que l'on appliquera à notre

problème afin d'obtenir deux équations qui permetteront d'avoir numériquement les amplitudes modales du champ effectif et le nombre d'onde effectif. Bien que le problème soit différent de celui traité par les travaux mentionnés, on retrouvera les formulations analytiques classiques au moyen d'un développement limité lorsque le nombre d'onde de l'onde incidente et le nombre d'onde effectif ont des valeurs proches l'une de l'autre. Dans un second temps, on s'inspirera de l'hypothèse de fermeture de Foldy pour introduire une méthode d'ordre 2 invoquant une hypothèse de fermeture originale qui présente l'avantage d'offrir une expression pour le champ effectif cherché et non le champ excitant un diffuseur comme c'est le cas lorsqu'on applique la QCA. Il semble alors que notre hypothèse de fermeture prenne en compte des termes de couplage supplémentaires. Ceci se traduit en particulier dans les comparaisons entre les données numériques obtenues par Chekroun *et al.* [CML$^+$09], les résultats de la QCA revisitée par Linton-Martin et nos résulats. En particulier pour des concentrations relativement élevées, notre méthode retrouve les tendances prévues par le traitement numérique (2.10).

1.5.2 *Cloaking* d'ondes de flexion dans une plaque

Les métamatériaux permettent d'éteindre un champ incident dans un domaine prédéfini, de manière passive dans le sens où cette aptitude devient intrinsèque au milieu que l'on a construit. Le but de ce chapitre est d'explorer les techniques de *cloaking* actif qui consistent à éteindre un champ incident, supposé connu, dans une région donnée, au moyen de M sources ponctuelles multipolaires. Le modèle de plaque utilisé est celui de Love-Kirchhoff requérant que l'épaisseur de la plaque soit suffisamment petite devant les autres dimensions. La question est simple : comment calibrer les M sources dont nous disposons afin d'éteindre le champ incident dans la région choisie mais sans le modifier en champ lointain?
Pour cela, on se propose de suivre le raisonnement proposé par Norris, Parnell et Amirkulova qui ont formulé de manière explicite l'expression des amplitudes modales de chaque source que l'on veut calibrer afin d'éteindre un champ incident supposé connu. Cette méthode repose en effet sur les propriétés des fonctions propres de l'équation de Helmholtz et la formulation intégrale d'une solution au moyen d'une intégrale de bord et de la fonction de Green du milieu. Or les équations d'onde de flexion dans une plaque de Love-Kirchhoff disposent de fonctions propres identiques ou similaires à celle de l'équation de Helmholtz et la formule de Rayleigh-Green offre aussi une formulation intégrale pour une onde de flexion.
Dans une première section, on commencera par un aperçu de la théorie des plaques et un rappel sur l'équation des ondes de flexion ainsi que les fonctions propres associées. Enfin on rappelera les formules de diffraction d'une onde de flexion par une inclusion cylindrique.
Dans les sections suivantes, on formule les conditions nécéssaires et suffisantes que doivent satisfaires les amplitudes modales des sources. Cela nous permettra de mener les calculs afin d'obtenir de manière explicite les expressions de ces amplitudes en fonction de celles de l'onde incidente lorsque cette dernière est soit une onde plane, soit

émise par un point source. L'idée générale est la suivante. La formule de Rayleigh-Green nous permet d'exprimer l'onde incidente en un point P repéré par $\mathbf{x}$, comme une intégrale sur le bord d'un domaine $\mathcal{D}$. Cette formulation impose en particulier que l'intégrale soit nulle si P est à l'extérieur de $\mathcal{D}$. Il suffit alors d'invoquer le théorème de Graf afin d'exprimer la fonction de Green dans des bases qui seront supposées centrées sur la position des sources. Les conditions du théorème de Graf délimiteront alors la zone de *cloaking*.
Afin d'illustrer les résultats, on se propose de montrer les simulations numériques obtenues lorsque les M sources sont disposées régulièrement sur un cercle de rayon r. Tout d'abord, ces simulations nous donneront l'occasion de discuter l'influence du nombre de sources, de la valeur de r et du nombre d'onde incident k, sur les résultats. Ainsi pour M et r fixés, la théorie est efficace pour des k relativement petits. Si on considère des k plus grands, il nous faut non seulement augmenter le nombre de source mais aussi la taille du cercle les contenant.

1.5.3 Milieux continus à gradient covariant et application à la propagation d'ondes élastiques au sein d'un milieu defectueux

Dans cette dernière partie, on étudie la propagation d'ondes élastiques au moyen de la géométrie différentielle et notamment à travers la structure de Riemann-Cartan que l'on peut supposer pour la variété matérielle associée à un continumm contenant des défauts.
On commencera par introduire les notions issues de la géométrie différentielle d'une variété RC. Plus précisément on présentera en détail comment on peut obtenir une telle structure aux moyens des *triads*, ce qui nous conduira nécessairement aux concepts de transport parallèle et de dérivées covariantes *via* la connexion ∇. Sous l'hypothèse de compatibilité avec la métrique, on peut décomposer l'opérateur ∇ en deux parties. L'une correspond à la connexion de Levi-Civita $\overline{\nabla}$ décrite par les symboles de Christoffel $\overline{\Gamma}^{\lambda}_{\alpha\beta}$ alors que l'autre est le tenseur de contortion $\mathbf{K}$ exprimé par la métrique et la torsion. On finira ces rappels par une discussion sur le lien entre la torsion et la densité de dislocation ainsi que les ordres de grandeurs qu'il nous faudra utiliser pour les exemples numériques.
Ensuite on s'intéressera à la formulation générale d'un problème d'élasticité sur une telle structure différentielle. La nature élastique du problème nous permet toujours de définir un champ de déplacement lié au mouvement considéré. L'hypothèse de petites perturbations nous autorise alors à supposer que la densité de dislocations n'est pas modifiée par le mouvement, quitte à réduire l'ordre de grandeur usuel pour les petites perturbations. En d'autres termes, le tenseur de torsion est vu comme un paramètre de notre modèle. L'idée consiste ainsi à réécrire les équations de conservation au moyen de la connexion $\nabla = \overline{\nabla} + \mathbf{K}$ dans le cas simple de la loi de Hooke. À cette occasion, on discutera de la définition de la déformation. En effet, en élasticité, le tenseur de déformation est exprimé par le gradient du déplacement et donc naturellement on peut le définir ici au moyen de la dérivée covariante issue de la connexion ∇. Une approche

différente serait de négliger les effets des défauts sur la déformation auquel cas on se restreint à exprimer la déformation par la connexion de Levi-Civita de torsion nulle. Dans un souci de questionner ces deux approches, on développera la théorie afin d'établir les équations de Navier dites généralisées pour la déformation spatiale (torsion nulle) et la matérielle qui tient compte de l'influence de la densité de dislocations.
Enfin, on se propose d'illustrer la différence entre ces deux modèles par l'étude d'un exemple plus simple construit pour une densité constante de dislocations vis toutes de même orientation. On obtient alors les relations de dispersion ainsi que la polarisation des ondes qui s'avérent quasi-transverses ou quasi-longitudinales dans chacun des deux cas. Les deux modèles impliquent des comportements anisotropes et des vitesses de propagations légèrement modifiées par rapport aux problèmes classiques d'ondes élastiques. La prise en compte d'une déformation matérielle offre des effets intéressants tels que des modes de respiration pour un déplacement uniforme, qui sont connus en particulier pour les milieux granulaires. Le deuxième effet est mis en évidence pour le régime haute fréquence dans lequel on obtient une illustration de l'escalier en spirale de Cartan [LH10] que ce dernier introduisit au début de ses travaux sur le tenseur de torsion. En effet on montre qu'il existe une onde transverse dont la polarisation effectue une rotation autour de l'axe de propagation. La période et le sens de rotation dépendent non seulement de la direction de propagation mais aussi de la densité de dislocation.

Chapter 2

Multiple scattering: acoustical wave in random media

In this chapter we focus on propagation of waves within a medium with discrete cylindrical obstacles oriented toward the same direction. For the sake of simplicity, we suppose that the ambient space and the obstacles are acoustic so that we dedicate our investigations to the acoustical potential: Only longitudinal waves propagate. We restrict the study to the case where the problem is invariant for each translation in the direction of cylinders. Therefore we consider to a infinite 2D medium Ω_0, with density ρ_0 and celerity c_0, containing N circular scatterers with radius a_i denoted s_i and $\Omega_1 = \cup_{i=1}^{i=N} s_i$. Cylinders are defects insofar as their mechanical constants ρ_i and celerity c_i are different from ρ_0 and c_0 for all $i \in \{1, \ldots, N\}$. In the following, we deal with mono-dispersive problems *i.e* every scatterers have the same mechanical and geometrical properties. The multiple scattering problem is then to model the wave propagation within this medium. We will first begin with the simple cases of $N = 1$ and $N = 2$ to finish with the case for N being arbitrary. In the second section we recall the tools of set average to model the medium as an effective one with effectivewave number during wave propagation. We will denote $\mathbf{r}$ the vector given by the cylindrical coordinates (r, θ) that is to say $\mathbf{r} = (r\cos\theta, r\sin\theta)$.

2.1 Basics on scattering

In this section we recall basics on mathematical background concerning the eigenfunctions of the Helmholtz equation and the simple example of scattering by one inclusion to introduce the formalism of our study.

2.1.1 Graf's addition theorem

Here we show different theorems that will be useful throughout our investigations on wave propagation in 2D problems. Consider two origins, say O_1 and O_2, of polar coordinates. Let P an arbitrary point whose position vectors are $\mathbf{r_i}$ respectively to O_i

for $i = 1, 2$. Let $\mathbf{r}_{21}$ the position vector of O_1 with respect to O_2 (see figure 2.1 below).

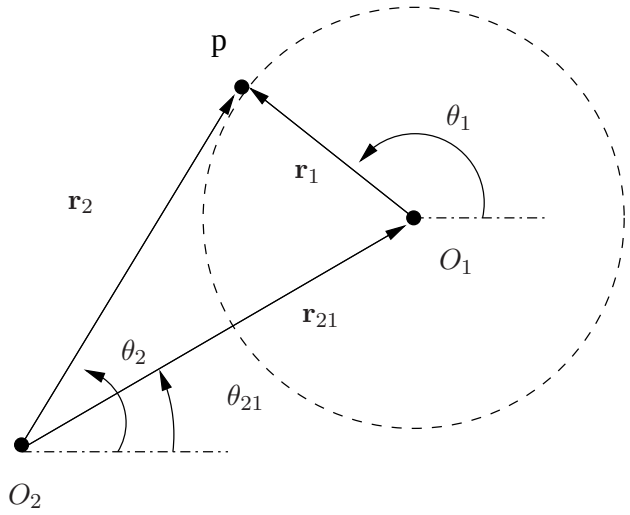

Figure 2.1: Notation of the Graff's addition theorems

Theorem 2.1.1 (Graf's addition theorem for $J_m(kr)\exp(im\theta)$) *For every $m \in \mathbb{Z}$, we have*

$$J_m(kr_2)\exp(im\theta_2) = \sum_{n=-\infty}^{\infty} (-1)^n J_n(kr_{21})\exp\big(in\theta_{21}\big) J_{m-n}(kr_1)\exp\big(i(m-n)\theta_1\big) \tag{2.1}$$

$$= \sum_{n=-\infty}^{\infty} (-1)^n J_{m-n}(kr_{21})\exp\big(i(m-n)\theta_{21}\big) J_n(kr_1)\cos\big(in\theta_1\big). \tag{2.2}$$

The proof of this theorem can be easily applied for the function $Y_m(kr)\exp(im\theta)$ and then we can deduce the following theorem for $H_m(kr)\exp(im\theta)$.

Theorem 2.1.2 (Graf's addition theorem for $H_m(kr)\exp(im\theta)$) *Let $m \in \mathbb{Z}$, if $r_1 < r_{21}$ we have*

$$H_m(kr_2)\exp(im\theta_2) = \sum_{n=-\infty}^{\infty} H_{m-n}(kr_{21})\exp\big(i(m-n)\theta_{21}\big) J_n(kr_1)\cos\big(in\theta_1\big).$$

If $r_1 > r_{21}$ we have

$$H_m(kr_2)\exp(im\theta_2) = \sum_{n=-\infty}^{\infty} J_{m-n}(kr_{21})\exp\big(i(m-n)\theta_{21}\big) H_n(kr_1)\exp\big(in\theta_1\big).$$

The singularity of the Hankel function is retrieved in the fact that there is no decomposition for $r_1 = r_{21}$. Both Graf's theorem will be fundamental in our approaches on problem involving wave propagation in 2D. As a direct application of these theorems, we introduce an algebraic formulation of multiple scattering. First we simplify the notations thanks to the following definitions.

Définition 2.1 *Let* $\mathbf{r} = (r\cos\theta, r\sin\theta)$. *The outgoing cylindrical eigenfunction* V_n *is defined by*

$$V_n(\mathbf{r}) = H_n(kr)\exp(in\theta).$$

Similarly, the regular cylindrical wavefunction U_n *is defined by*

$$U_n(\mathbf{r}) = J_n(kr)\exp(in\theta).$$

We denote U *and* V *the vector containing* U_n *and* V_n.

The wavefunction V_n is described as outgoing because it corresponds to outgoing waves at infinity: V_n satisfies the Sommerfeld radiation condition in two dimension. Indeed asymptotic expression of Hankel functions for high argument gives:

$$H_n(\mathbf{r}) \sim \sqrt{\frac{2}{\pi kr}}\exp\left(kr - \frac{n\pi}{2}) - \frac{\pi}{4}\right) \quad \text{as } r \to \infty.$$

Proposition 1 *With the same notations as above we have:*

$$U_n(\mathbf{r}) = (-1)^n U_n(-\mathbf{r}) = (-1)^n \overline{U_n(\mathbf{r})}$$

and

$$V_n(\mathbf{r}) = (-1)^n V_n(-\mathbf{r}),$$

where the $\overline{U_n(\mathbf{r})}$ *corresponds to the complex conjugate of* $U_n(\mathbf{r})$.

Now, we introduce algebraic notations which will be useful throughout this chapter. Aforementioned notations for the geometric configurations of Graf's theorems remain available. From now we denote a^i the vector containing the modal coefficients a_n^i of ϕ according to the O_i frame.

Theorem 2.1.3 *Let* ϕ *be a regular solutions of the Helmholtz equations with wavenumber* k. *Its expression in the* O_2 *frame is:*

$$\phi(P) = a^2 \cdot U(k\mathbf{r}_2).$$

In the O_1 *frame we have:*

$$\phi(P) = a^1 \cdot U(k\mathbf{r}_1) \quad , \quad \text{with } a^1 = T^{12}a^2.$$

Where the matrix T^{12} *has coefficients:*

$$(T^{12})_{nm} = U_{m-n}(k\mathbf{r}_{21}).$$

The regular function ϕ is expressed at P according to the polar coordinates centered at O_2 by:

$$\phi(P) = \phi(\mathbf{r}_2) = \sum_{n=-\infty}^{\infty} a_n^2 U_n(k\mathbf{r}_2),$$

where a_n^2 are modal coefficients. We want to express this field in the polar coordinates centered at O_1. Using the Graf's theorem 2.1.1 we thus have:

$$\phi(P) = \sum_{n=-\infty}^{\infty} \sum_{m=-\infty}^{\infty} a_n^2 U_{n-m}(k\mathbf{r}_{21} U_m(k\mathbf{r}_1).$$

Setting $\sum_{n=-\infty}^{\infty} a_n^2 U_{n-m}(k\mathbf{r}_1) = a_m^1$, we have:

$$\phi(P) = \sum_{m=-\infty}^{\infty} a_m^1 U_m(k\mathbf{r}_1),$$

which gives the wanted result. We have similar theorem for the Hankel functions.

Theorem 2.1.4 *Let $\widehat{\phi}$ be a singular solution of the Helmholtz equations with wavenumber k and satisfying the Sommerfeld radiation conditions. Its expression in the O_2 frame is:*

$$\widehat{\phi}(P) = a^2 \cdot V(k\mathbf{r}_2).$$

In the O_1 frame we have:

$$\widehat{\phi}(P) = a^1 \cdot U(k\mathbf{r}_1) \quad , \quad \text{with } a^1 = \widehat{T}^{12} a^2, \quad \text{for } r_1 < r_{21}.$$

$$\widehat{\phi}(P) = a^1 \cdot V(k\mathbf{r}_1) \quad , \quad \text{with } a^1 = T^{12} a^2, \quad \text{for } r_1 > r_{21}.$$

Where the matrix $\widehat{T}^{12}$ has coefficients:

$$(\widehat{T}^{12})_{nm} = V_{m-n}(k\mathbf{r}_{21}).$$

We emphasize that the matrix T^{12} and $\widehat{T}^{12}$ are the transpose of the separation matrix usually used in literature (*e.g.*[Mar06]). We choose to invert the upper indexes for sake of clarity: T^{12} and $\widehat{T}^{12}$ take O_2-frame coefficient and return O_1-frame. But we have to keep in mind that T^{12} and $\widehat{T}^{12}$ contains $\mathbf{r}_{21}$ and not $\mathbf{r}_{21}$.

2.1.2 Sommerfeld condition

In order to describe the scattered field in 2D, we will need a radiation condition at the infinity. This radiation condition is actually the Sommerfeld condition, which can be given as

$$\partial_{\mathbf{n}}\phi - ik\phi = o(\frac{1}{\sqrt{r}})$$

We briefly recall its physical enunciation and the consequence for the the eigenfunctions. The Sommerfeld condition tell us that the field scattered by an obstacle behaves at the infinity locally like a plane-wave :

$$\phi \sim e^{ikr}/\sqrt{r}$$

With our Fourier convention $\phi(r,t) = \phi(r)\exp -i\omega t$, we observe that this field is an outgoing field at infinity : no wave become from infinity.
Furthermore, the scattered energy has to remain the same for all spheres encircling the scatterer. This energy is related to the square of the field. It explains physically the $1/\sqrt{r}$ behaviour of the field.
For a field decomposition with cylindrical eigenfunctions, the asymptotic forms of Bessel eigenfunctions show directly that the scattered field must be decomposed with singular eigenfunction at infinity. Moreover, if the center of the polar coordinate is placed at the center of a circular inclusion, this decomposition is available in the whole external domain.

2.1.3 Scattering by one inclusion

As previously mentioned, we deal with circular defects in a 2D problem, therefore it is convenient to work with polar coordinates (r,θ) centred at the center of the scatterer. We remind also that we describe the field throughout the acoustical potential in order to restrict ourselves to scalar equations. We suppose that the medium $\Omega_0 \cup s_1$ is probed by an incoming wave with potential ϕ_{inc}, decomposed in terms of Bessel functions sequence:

$$\phi_{inc}(\mathbf{r}) = \sum_{n=-\infty}^{\infty} c_n U_n(k_0\mathbf{r}) = c \cdot U(k_0\mathbf{r}).$$

For a unitary plane wave propagating in the direction ψ, the Jacobi decomposition gives $c_n = i^n \exp(-in\psi)$. Because of the description of the problem, the field is piecewise defined and we have actually two equations. The first express the total field in the ambient space Ω_0 and the second one the transmitted field in the scatterer. Both of these fields are to be solved thanks to continuity conditions at the interface of the scatterer.

Note that in acoustic the displacement $\mathbf{u}$ and the pressure fields p of a wave are entirely expressed by the acoustical potential:

$$p = -\rho\omega^2\phi,$$
$$\mathbf{u} = \nabla\phi.$$

Therefore both fields are solutions of the Helmholtz equation.

2.1.3.1 Expression of the fields

In the ambient space
The total potential in the ambient space is:

$$\phi_0(\mathbf{r}) = \phi_{inc}(\mathbf{r}) + \phi_s(\mathbf{r}),$$

where ϕ_s is the potential scattered by s_1. This potential satisfies the Helmholtz equation in Ω_0:

$$(\Delta + k_0^2)\phi_s = 0.$$

As a consequence, we express it as a sequence of Bessel functions and because it satisfies the Sommerfeld condition we conclude that:

$$\phi_s(\mathbf{r}) = \sum_{n=-\infty}^{\infty} a_n V_n(k_0\mathbf{r}) = a \cdot V(k_0\mathbf{r}),$$

where a_n are modal amplitudes to be found. The total displacement field in Ω_0 and its pressure are denoted $\mathbf{u}_0$ and p_0.

In the scatterer
The potential relative to the transmitted field satisfies the Helmholtz equation in the medium Ω_1 and it is bounded in the whole inclusion. As the origin of the polar coordinates is centered at the center of s_1, the modal decomposition is in the form:

$$\phi_1(r,\theta) = \sum_{n=-\infty}^{\infty} b_n U_n(k_1\mathbf{r}) = b \cdot U(k_1\mathbf{r}).$$

The modal amplitudes b_n are also to be determined.

2.1.3.2 Modal amplitudes

The coefficients a_n and b_n are determined by the continuity conditions at the interface $\partial\Omega_1$. These continuity conditions are the continuity of the normal component of the displacement and the continuity of the pressure. In other words these conditions give the equations:

$$\partial_{\mathbf{n}}\phi_0(M) = \partial_{\mathbf{n}}\phi_1(M) \quad , \quad \rho_0\phi_0(M) = \rho_1\phi_1(M) \quad , \quad M \in \partial\Omega_1.$$

where $\partial_{\mathbf{n}}$ is the normal differentiation. By definition of the chosen polar coordinates, we have $\partial_{\mathbf{n}} \equiv \partial_r$ so that for $|\mathbf{r}| = a$ the continuity conditions are:

$$\begin{aligned} \sum_n (a_n \partial_r V_n(k\mathbf{r}) + c_n \partial_r U_n(k\mathbf{r})) &= \sum_n b_n \partial_r U_n(k_1\mathbf{r}), \\ \rho_0 \sum_n (a_n V_n(k\mathbf{r}) + c_n U_n(k\mathbf{r})) &= \rho_1 \sum_n b_n U_n(k_1\mathbf{r}) \end{aligned}$$

Remember that $\partial_r V_n(k\mathbf{r}) = k\ H_n'(ka)e^{in\theta}$ and $\partial_r U_n(k\mathbf{r}) = k\ J_n'(ka)e^{in\theta}$ with $|\mathbf{r}| = a$ and $\arg \mathbf{r} = \theta$. Now the functions family $(\cos(n\theta))_{n\in\mathbb{Z}}$ is orthonormal for the scalar product $< f, g >= \dfrac{1}{2\pi}\displaystyle\int_0^{2\pi} fg$. Projecting the continuity conditions on the family $(\cos(n\theta))_{n\in\mathbb{Z}}$, we thus obtain a linear system of two equations for a_n and b_n when n spans $\mathbb{Z}$.

$$\begin{aligned} a_n H_n'(ka) - \frac{k_1}{k} b_n J_n'(k_1 a) &= -c_n J_n'(ka), \\ a_n H_n(ka) - \frac{\rho_1}{\rho_0} b_n J_n(k_1 a) &= -c_n J_n(k_1 a). \end{aligned} \tag{2.3}$$

Let Δ_n denote the discriminant of this linear system:

$$\Delta_n = \frac{\rho_0 c_0}{\rho_1 c_1} H_n(ka) J_n'(k_1 a) - H_n'(ka) J_n(k_1 a),$$

we define the so called scattering and transmission coefficients w_n and z_n by:

$$z_n = -\frac{\Re(\Delta_n)}{\Delta_n} \qquad\qquad w_n = \frac{\rho_0}{\rho_1} \frac{2}{\pi i k a} \frac{1}{\Delta_n}.$$

We emphasize that these coefficients are defined for polar coordinates centered at the scatterer center.
Finally the solutions are given by:

$$a_n = z_n c_n \qquad\qquad b_n = w_n c_n,$$

Defining the diagonal matrix Z and W such that $(Z)_{nm} = z_n \delta_{nm}$ et $(W)_{nm} = w_n \delta_{nm}$ we have:

$$a = Z\ c \qquad , \qquad b = W\ c,$$

where the vectors contain the modal components a_n, b_n, and c_n for $n \in \mathbb{Z}$.

2.1.3.3 Particular cases

Impenetrable scatterer
For impenetrable scatterer there is no transmitted field ϕ_1 therefore we only need to calculate a^1. We distinguish two cases of such scatterers: rigid inclusions and void.

Rigid inclusion
The corresponding boundary condition is $\partial_{\mathbf{n}} \psi_0 = 0$. We deduce:

$$z_n = -\frac{J_n'(ka)}{H_n'(ka)}.$$

Note that this result could be obtained by taking $c_1, \rho_1 \to \infty$.

Void
In this case the boundary condition is $p_0 = -i\omega\rho_0\psi_0 = 0$. We deduce:

$$z_n = -\frac{J_n(ka)}{H_n(ka)}.$$

This result could be derived by taking $\rho_1 \to 0$.

Low frequency regime
The low frequency regime is reached when $k_i a << 1$; it means that the wavelength is large compared to the size of the scatterer. We introduce the compressibility $\chi = \rho c^2$

and after the calculation, the asymptotic expression of Bessel's functions for small argument implies [OoSU10]:

$$z_0 = \frac{i\pi}{4}\frac{\chi_0 - \chi_1}{\chi_1}(ka)^2, \qquad w_0 = \frac{\rho_0}{\rho_1},$$

$$z_1 = -\frac{i\pi}{4}\frac{\rho_0 - \rho_1}{\rho_0 + \rho_1}(ka)^2, \qquad w_1 = 2\frac{c_1}{c_0}\frac{\rho_0}{\rho_0 + \rho_1}.$$

In the case of rigid scatterer, the scattering coefficient in the low frequency regime thus gives:

$$z_0 = -\frac{i\pi}{4}(ka)^2, \qquad z_1 = \frac{i\pi}{4}(ka)^2,$$

and for void we have:

$$z_0 = \imath(ka), \qquad z_1 = -\frac{i\pi}{4}(ka)^2.$$

2.1.4 Far field pattern

Here we intend to express the far field scattered by the inclusion that is to say for $kr \gg 1$. We use the asymptotic expression of Bessel's function for high argument:

$$H_n(z) \sim \sqrt{\frac{2}{\pi z}}\exp\Big(i\big(z - n\frac{\pi}{2} - \frac{\pi}{4}\big)\Big) \sim H_0(z)\exp\Big(-in\frac{\pi}{2}\Big),$$

thus

$$V_n(k\mathbf{r}) \sim H_0(kr)\exp\Big(in\big(\theta - \frac{\pi}{2}\big)\Big).$$

Therefore we obtain the general expression for the far field scattered:

$$\phi_s \sim H_0(kr)f(\theta) \qquad \text{with} \qquad f(\theta) = \sum_n a_n \exp\Big(in\big(\theta - \frac{\pi}{2}\big)\Big)$$

Actually f depends on the incoming wave due to the relation $a = Zc$. For instance in the special case of an unitary incoming plane wave $\phi_i(M) = \exp\big(ikr\cos(\theta - \psi)\big)$ propagating in the direction ψ, the Jacobi decomposition gives

$$\phi_i(M) = \sum_n i^n \exp(-in\psi)U_n(kr) = c^1 \cdot U(k\mathbf{r}),$$

with $c_n^1 = \exp\Big(in(\frac{\pi}{2}\psi)\Big)$ and we have the general formula:

$$f(\theta, \psi) = \sum_n z_n \exp(in(\theta - \psi)) \equiv f(\theta - \psi).$$

In particular we have:

$$\begin{aligned} f(0) &= \sum_n z_n && \text{transmission: } \theta = \psi \\ f(\pi) &= \sum_n (-1)^n z_n && \text{reflection: } \theta = \psi + \pi \end{aligned}.$$

Figure (2.2) shows example of far field pattern for impenetrable inclusions and penetrable ones. Notice that the relation k_0a corresponds to the ratio between the wavelength and the radius of the inclusion. As k_0a increases we observe that the far field scattering amplitudes increase as well for each type of scatterer. For small k_0a (low frequency regime) the void case has an isotropic scattering pattern whereas the rigid inclusion scattering is weak. For high k_0a (high frequency regime) anisotropic effects are observed for each cases and the scattering amplitudes can be very large (~ 8) in direction corresponding to the incidence wave.

2.2 Scattering by two inclusions

Now we consider the problem with two inclusions s_1 and s_2 with radius a centered respectively at O_1 and O_2. We still denote M the point of observation. The position vector of M in the cylindrical base connected to a scatterer s_i will be denoted $\mathbf{r}_{i0} = (r_{i0}, \theta_{i0})$. The position vector of s_j in the cylindrical base associated to s_i is $\mathbf{r}_{ij} = \mathbf{r}_{i0} - \mathbf{r}_{j0}$ with $\mathbf{r}_{ij} = (r_{ij}, \theta_{ij})$. The inclusions do not overlap therefore $r_{12} = |\mathbf{r}_{12}| = |\mathbf{r}_{10} - \mathbf{r}_{20}| > 2a$. This configuration is illustrated in figure 2.3. The base centered on a scatterer will be called *local base*.

2.2.1 Modal decomposition

The incident field is expressed in any local base:

$$\phi_i(M) = c^1 \cdot U(k\mathbf{r}_{10}) = c^2 \cdot U(k\mathbf{r}_{20}),$$

where the upper-script of c_n^j precises the base associated to the expression. The transmitted field within s_j is naturally formulated in its own local base by:

$$\phi_t^j(M) = b^j \cdot U(k_1\mathbf{r}_{j0}) \qquad r_j < a \qquad j = 1, 2.$$

The scattered fields of s_1 and s_2 verify the Sommerfeld radiation condition and is singular at the center of the scatterer. Thus they are naturally expressed in their respective local base:

$$\phi_s^1(M) = a^1(s_1) \cdot V(k\mathbf{r}_{10}) \qquad \text{and} \qquad \phi_s^2(M) = a^2(s_2) \cdot V(k\mathbf{r}_{20}).$$

The notation should be read in the following sense: $a^i(s_j)$, $b^i(s_j)$ comprise the modal coefficient of the scatterer s_j expressed in the local base of s_i. The need of this convention will be clear later. Now the scattering of s_2 can be derived in the local basis associated to O_1 thanks to the Graf's addition theorem for Hankel functions. Indeed for $r_{10} < r_{21}$, *ie* in the vicinity of s_1:

$$\phi_s^2(M) = a^1(s_2) \cdot U(k\mathbf{r}_{10}) \qquad \text{with} \qquad a^1(s_2) = \widehat{T}^{12} a^2(s_2).$$

Hence the total scattered field can be expressed in the vicinity of s_1 respectively to its local basis by:

$$\phi_s(M) = \phi_s^1(M) + \phi_s^2(M) = a^1(s_1) \cdot V(k\mathbf{r}_{10}) + a^1(s_2) \cdot U(k\mathbf{r}_{10})$$

and for $r_{10} < r_{12}$:

$$\phi_s(M) = a^1(s_1) \cdot V(k\mathbf{r}_{10}) + a^1(s_2) \cdot U(k\mathbf{r}_{10}).$$

2.2.2 Modal system

The boundary conditions of the scatterer s_1 are:

$$\partial_{\mathbf{n}}(\phi_{inc} + \phi_s)(M) = \partial_{\mathbf{n}}\phi_t^1(M) \qquad , \qquad \rho_0\phi_{inc}(M) + \phi_s(M) = \rho_1\phi_t^1(M),$$

with M on the boundary of s_1, *ie* $r_{10} = a$. Using the expression of the fields in the local base of s_1 gives similar linear system as (2.3):

$$\begin{aligned} a_n^1(s_1)H_n'(ka) - \frac{k_1}{k}b_n^1(s_1)J_n'(k_1a) &= -\left(c_n^1 + a_n^1(s_2)\right)J_n'(ka) \\ a_n^1(s_1)H_n(ka) - \frac{\rho_1}{\rho_0}b_n^1(s_1)J_n(k_1a) &= -\left(c_n^1 + a_n^1(s_2)\right)J_n(k_1a) \end{aligned}$$

If we solve this system for the unknowns $a^1(s_1)$ and $b^1(s_1)$, we notice that s_2 acts as a secondary source throughout the base changing of its scattering coefficients:

$$a^1(s_1) = Z\left(c^1 + a^1(s_2)\right) \qquad , \qquad b^1(s_1) = W\left(c^1 + a^1(s_2)\right)$$

Following the same calculation for the boundary conditions of s_2, we obtain similar results:

$$a^2(s_2) = Z\left(c^2 + a^2(s_1)\right) \qquad , \qquad b^2(s_2) = W\left(c^2 + a^2(s_1)\right)$$

Now we complete the resolution with the relations given by the changing of basis: $a^i(s_k) = \widehat{T}^{ij}a^j(s_k)$. Hence the coefficients are solutions of the system:

$$\left\{\begin{array}{l} a^1(s_1) = Z\left(c^1 + \widehat{T}^{12}a^2(s_2)\right) \\ a^2(s_2) = Z\left(c^2 + \widehat{T}^{21}a^1(s_1)\right) \end{array}\right. , \qquad \left\{\begin{array}{l} b^1(s_1) = W\left(c^1 + \widehat{T}^{12}a^2(s_2)\right) \\ b^2(s_2) = W\left(c^2 + \widehat{T}^{21}a^1(s_1)\right) \end{array}\right.$$

We also have $c^i = T^{ij}c^j$, resulting of the Graf's theorem applied to the regular eigenfunctions. Injecting the expression of $a^2(s_2)$ in $a^1(s_1)$, we conclude that the scattering coefficients of s_1 has to satisfy the equality:

$$\left(I - Z\widehat{T}^{12}Z\widehat{T}^{21}\right)a^1(s_1) = Z\left(I + \widehat{T}^{12}ZT^{21}\right)c^1, \tag{2.4}$$

and for the transmission coefficients:

$$b^1(s_1) = WZ^{-1}a^1(s_1).$$

Of course similar results are available for the scattering and transmission coefficients of s_2. Notice that $a^j(s_j) \neq Zc^j$ unless we neglect the coupling terms between scatterers. We will go back on this in the case where each scatterer are far enough.

2.2.3 Approximation

Suppose that $\|Z\widehat{T}^{12}Z\widehat{T}^{21}\| \leq 1$, then we have the equality:

$$\left(I - Z\widehat{T}^{12}Z\widehat{T}^{21}\right)^{-1} = \sum_{n\geq 0}\left(Z\widehat{T}^{12}Z\widehat{T}^{21}\right)^{n},$$

and we deduce:

$$a^1(s_1) = \left(Z + Z\widehat{T}^{12}ZT^{21} + Z\widehat{T}^{12}Z\widehat{T}^{21}Z + Z\widehat{T}^{12}Z\widehat{T}^{21}Z\widehat{T}^{12}ZT^{21} + \dots\right)c^1,$$

where we show the coupling effect at different orders throughout the 2-scattering process. Each Z is linked to a scattering process whereas T and $\widehat{T}$ perform the base changing and gives us indications to identify which scatterer is involved in the scattering. More precisely, the first term is the scattering of the incoming waves, the second one is the scattering by s_1 of the incoming field scattered by s_2:

$$inc \to 2 \to 1 \to M,$$

where $\to$ stands for the propagating process, $i = 1, 2$ represents the scattering process of s_i and M is the observation point. Indeed it contains Z multiplied by $T^{21}c^1$. This latter corresponds to the incoming wave in the vicinity of s_2 expressed by the Graf's theorem and Z stand for the scattering process. The third term is slightly more complicated. We must keep in mind that $\widehat{T}^{21}Zc^1$ is the scattering of the incoming wave by s_1 expressed in the vicinity of s_2, then multiplied this by $Z\widehat{T}^{12}Z$ gives its order two scattering by respectively s_2 and s_1 which we can summarize by:

$$inc \to 1 \to 2 \to 1 \to M.$$

Thus this coupling term refers to a "roundtrip coupling". It is of particular interest in theories relying on ensemble average, because they always neglect it as we shall see latter.

2.2.4 Far field coupling

The total far field scattered by the system of two scatterers is $\phi_s(M) = H_0(kr_{10})\mathcal{F}_1(\theta_{10}) + H_0(kr_{20})\mathcal{F}_2(\theta_{20})$. Now, for one scatterer we have seen that the scattered field is given in the far field domain ($k_0 r_{i0} >> 1$) by:

$$\phi_{s_i}(M) = H_0(kr_{i0})\mathcal{F}_i(\theta_{i0}),$$

where $\mathcal{F}_i$ is the scattering function of the scatterer s_i:

$$\mathcal{F}_i(\theta) = \sum_n a_n^i(s_i)\exp\left(in\left(-\frac{\pi}{2} + \theta_{i0}\right)\right).$$

However the modal amplitudes now take into account the presence of the second scatterer (see Eq.(2.4). We suggest to investigate the situation corresponding to $k_0 r_{12} >> 1$. The situation is summarized in the figure 2.4.

Thus it is about estimating $a_n^i(s_i)$ given by (2.4). We perform the evaluation for each term. Observing that $\theta_{21} = \theta_{12} + \pi$, the asymptotic expressions of Hankel's function for high argument give after straightforward calculations:

$$(Z\widehat{T}^{12}\widehat{ZT^{21}})_{nm} = H_0^2(kr_{12})z_n \exp\Big(im\big(\theta_{12} - \frac{\pi}{2}\big)\Big) \exp\Big(in\big(-\frac{\pi}{2} - \theta_{12}\big)\Big) \sum_p (-1)^p z_p$$

where appears the scattering function f for reflection mode of a single scatterer probed by an unitary plane wave:

$$(Z\widehat{T}^{12}Z\widehat{T}^{21})_{nm} = z_n f(\pi) H_0^2(kr_{12}) \exp\Big(in\big(\theta_{12} - \frac{\pi}{2}\big)\Big) \exp\Big(im\big(-\frac{\pi}{2} - \theta_{12}\big)\Big).$$

In the same way:

$$(Z\widehat{T}^{12}Z)_{nm} = z_n z_m H_0(kr_{12}) \exp\Big(in\big(\theta_{12} - \frac{\pi}{2}\big)\Big) \exp\Big(im\big(\frac{\pi}{2} - \theta_{12}\big)\Big).$$

In the M frame, the point M is obviously localized by the null vector. Addition theorem of the exponential function combined with the Jacobi decomposition gives:

$$\phi_{inc}(M) = \phi_{inc}(0) = \exp(i\mathbf{k}\cdot\mathbf{r}_{0j}) \exp(i\mathbf{k}\cdot\mathbf{r}_{j0}).$$

Hence we have:

$$c_n^j = \phi_{inc}(s_j) \exp\Big(in\big(\frac{\pi}{2} - \psi\big)\Big),$$

because $\exp(i\mathbf{k}\cdot\mathbf{r}_{0j}) = \phi_{inc}(s_j)$.
Thus we deduce:

$$\begin{aligned}
\Big(Z\widehat{T}^{12}Z\widehat{T}^{21}a^1(s_1)\Big)_n &= z_n f(\pi) H_0^2(kr_{12}) \exp\Big(in\big(\theta_{12} - \frac{\pi}{2}\big)\Big) \sum_m a_m^1 \exp\Big(im\big(-\frac{\pi}{2} - \theta_{12}\big)\Big), \\
\big(Zc^1\big)_n &= z_n \exp\Big(in\big(\frac{\pi}{2} - \psi\big)\Big), \\
\Big(Z\widehat{T}^{12}Zc^2\Big)_n &= z_n H_0(kr_{12}) \exp\Big(in\big(\theta_{12} - \frac{\pi}{2}\big)\Big) \sum_m z_m \exp\Big(im\big(\pi - \theta_{12} - \psi\big)\Big).
\end{aligned}$$

After multiplying each terms of the system (2.4) by $\exp\Big(in\big(-\frac{\pi}{2} + \theta_1\big)\Big)$ and summing them over n, we obtain:

$$\begin{aligned}
\sum_n a^1(s_1)_n \exp\Big(in\big(-\frac{\pi}{2} + \theta_{10}\big)\Big) &= \mathcal{F}_1(\theta_{10}), \\
\sum_n \Big(Z\widehat{T}^{12}Z\widehat{T}^{21}a^1(s_1)\Big)_n \exp\Big(in\big(-\frac{\pi}{2} + \theta_{10}\big)\Big) &= H_0^2(kr_{12}) f(\pi) f(\theta_{10} - \theta_{21}) \mathcal{F}_1(\theta_{12}), \\
\sum_n \big(Z^1 c^1\big)_n \exp\Big(in\big(-\frac{\pi}{2} + \theta_{10}\big)\Big) &= f(\theta_{10} - \psi)\phi_{inc}(s_1), \\
\sum_n \Big(Z\widehat{T}^{12}Zc^2\Big)_n \exp\Big(in\big(-\frac{\pi}{2} + \theta_{10}\big)\Big) &= H_0(kr_{12}) f(\theta_{10} - \theta_{21}) f(\theta_{21} - \psi)\phi_{inc}(s_2).
\end{aligned}$$

Hence:

$$\mathcal{F}_1(\theta_{10}) - H_0^2(kr_{12}) f(\pi) f(\theta_{10} - \theta_{21}) \mathcal{F}_1(\theta_{12}) = f(\theta_{10} - \psi)\phi_{inc}(s_1) + H_0(kr_{12}) f(\theta_{10} - \theta_{21}) f(\theta_{21} - \psi)\phi_{inc}(s_2),$$

We emphasize that similar relation is obtained for $\mathcal{F}_2$ by interchanging indexes 1 and 2. This equation is fulfilled for every θ_{10}. In particular for $\theta_{10} = \theta_{12}$, we deduce:

$$\mathcal{F}(\theta_{12}) = \frac{f(\theta_{12} - \psi)\phi_{inc}(s_1) + H_0(kr_{12})f(\theta_1 - \theta_{21})f(\theta_{21} - \psi)\phi_{inc}(s_2)}{1 - H_0^2(kr_{12})f(\pi)f(\theta_1 - \theta_{21})}.$$

After rearranging, say for s_1, we obtain the scattering function:

$$\begin{aligned}\mathcal{F}_1(\theta_1) &= f(\theta_1 - \psi)\phi_{inc}(s_1) + \\ &H_0(kr_{12})f(\theta_1 - \theta_{21})\frac{f(\theta_{21} - \psi)\phi_{inc}(s_2) + f(\pi)H_0(kr_{12})f(\theta_{12} - \psi)\phi_{inc}(s_1)}{1 - H_0^2(kr_{12})f^2(\pi)}\end{aligned} \quad (2.5)$$

Suppose that $|f(\pi)H_0(kr_{12})| \ll 1$. As $\phi_{inc}(s_1)$ and $\phi_{inc}(s_2)$ have comparable values, the numerator reduces to $f(\theta_{21} - \psi)\phi_{inc}(s_2)$ whereas the denominator reduces to 1. Therefore we can simplify the scattering function:

$$\mathcal{F}_1(\theta) = f(\theta - \psi)\phi_i(s_1) + H_0(kr_{12})f(\theta - \theta_{21})f(\theta_{21} - \psi)\phi_i(s_2)$$

The assumption actually consists in neglecting $Z\widehat{T}^{12}Z\widehat{T}^{21}$ in the system (2.4) because this latter is the only one involving $\mathcal{O}(H_0^2(kr_{12}))$ terms (see above). The first terms correspond to the "simple scattering" of the incident field by the considered scatterer whereas the second one is more complicated. We refer to this latter as the "order 2 scattering" because it corresponds to the scheme in the form $i \to 1 \to 2$. Indeed $H_0(kr_{12})f(\theta - \theta_{21})\phi_i(s_2)$ is the scattering of ϕ_i by s_2 evaluated at s_1 according to the local base of s_2. Therefore multiply this latter by $f(\theta - \theta_{21})$ gives its scattering by s_1. We supposed that $f(\pi)H_0(kr_{12})$ could be neglected therefore $f(\pi)$ should be small enough and such formulation do not allow strong scatterer. Furthermore the hypothesis claiming k_0r_{12} being large enough suggests that it is available for the case where the distance between two scatterers is larger than the wavelength.

Let's try to understand the neglected term $Z\widehat{T}^{12}Z\widehat{T}^{21}$ namely $H_0^2(kr_{12})f(\pi)f(\theta_1 - \theta_{21})\mathcal{F}_1(\theta_{12})$. We now see that coupling term $Z\widehat{T}^{12}Z\widehat{T}^{21}$ induces not only a denominator also a third term. If we suppose that $H_0^2(kr_{12})f^2(\pi)f(\theta_1 - \theta_{21}) << 1$ with keeping $H_0^2(kr_{12})f^2(\pi)f(\theta_1 - \theta_{21})$ then the third terms has to be taken into account. With similar reasoning as previously we conclude that this latter correspond to a "roundtrip" coupling: $inc \to s_1 \to s_2 \to s_1 \to M$. If no terms can be neglected we saw that each order of scattering has to be taken into account therefore the coupling term are no more linear function of $H_0(kr_{12})f$.
Now the quantity $f(\pi)H_0(kr_{12})$ is not necessarily negligible because the back-scattering $f(\pi)$ could counterbalance $H_0(kr_{12})$ (see figure (2.2.4)). Indeed we observe that for high frequency regime and particular contrast the back-scattering could be quite strong. Of course we can always ask r_{12} to be bigger so that $f(\pi)H_0(kr_{12})$ would be negligible but it means that the notion of dilute concentration (inclusion away from each other) has a sense only for a given strength of back-scattering. Note that the back-scattering term is due to the fact that we considered two scatterers and another angle should

be involved for more. For this reason we rather speak about strength of scattering or contrast. The models developed in the literature and in this thesis do not take into account the denominator to scale the coupling because they implicitly rely on formula known for the scattering of a single inclusion.

The very simple case of problem involving two scatterers is not trivial and the description above shows the complexity of the phenomenon especially for coupling terms. This latter can be simplified under strong hypothesis such as dilute distribution according to the considered contrast. Unfortunately in practice the number of scatterers is of course more than two. As a consequence we pursue our reasoning in the general case in order to be able to model the propagation of waves within such media thanks to averaging tools.

2.3 Problem with N scatterers

Now we consider the more general case of N inclusions $(s_j), j \in \{1, \dots, N\}$ centered at $(O_j)_{j\in\{1,\dots,N\}}$. **The incoming wave ϕ_i is now emitted by a point-like source**. This choice is motivated by the fact that most of works on multiple scattering are investigated for incoming plane wave whereas point-like sources correspond to more practical problems. The principle remains the same, we want to determine scattered and transmitted waves by means of the boundary conditions. Notations and conventions introduced in the previous example with two scatterers are still available (figure 2.6). The coordinate of the observation point M in the local base of the source is now denoted by $\mathbf{r}_{s0}$ (figure 2.6).

2.3.1 Modal expression

In order to apply the boundary conditions we need to express the field in the vicinity of a scatterer, say s_1, respectively to its local coordinates. The incoming field at M is expressed in the local basis centered on the source:

$$\phi_i(M) = c^s \cdot V(k\mathbf{r}_{s0}).$$

In order to formulate this latter in the local base of s_1, we invoke the Graf's theorem:

$$\phi_i(M) = c^1 \cdot U(k\mathbf{r}_{10}), \quad \text{with } c^1 = \widehat{T}^{1s} c^s.$$

Indeed this formula is true for $r_{10} < r_{1s}$ which is satisfied for M on the boundary because the source is supposed to be outside every scatterer. The transmitted field in the inclusion s_j and its scattered field are naturally developed in its own local base:

$$\phi_t^j(M) = b^j(s_j) \cdot U(k_1\mathbf{r}_{j0}), \quad \phi_s^j = a^j(s_j) \cdot V(k\mathbf{r}_{j0}).$$

Again we use the Graf's theorem to get the scattered field of s_j in the vicinity of s_1 (for $r_{10} < r_{1j}$) respectively to the local base of s_1 and we have:

$$\phi_s^j(M) = a^1(s_j) \cdot U(k\mathbf{r}_1) \qquad \text{with} \qquad a^1(s_j) = \widehat{T}^{1j} a^j(s_j)$$

Hence the total scattered field expressed in the local base of s_1 is obtained by summation:

$$\phi_s(M) = \sum_j \phi_s^j(M) = a^1(s_1)\cdot V(k\mathbf{r}_1) + \sum_{1\neq j} a^1(s_j)\cdot U(k\mathbf{r}_1) \qquad \text{for} \qquad r_1 < \min_{j\neq 1}(r_{1j})$$

The right-hand sum corresponds to the contribution of all scatterers except s_1.

2.3.2 Modal system

Now the projected boundary conditions for s_1 give us a system equivalent to (2.3):

$$\begin{aligned} a_n^1(s_1)H_n'(ka) - \frac{k_1}{k} b_n^1(s_1)J_n'(k_1 a) &= \left(-c_n^1 + \sum_{1\neq j} a_n^1(s_j)\right) J_n'(ka) \\ a_n^1(s_1)H_n(ka) - \frac{\rho_1}{\rho_0} b_n^1(s_1)J_n(k_1 a) &= \left(-c_n^1 + \sum_{1\neq j} a_n^1(s_j)\right) J_n(k_1 a) \end{aligned}$$

For convenience we express the modal amplitudes of each scatterer s_j in its own local coordinates with the formula: $a^1(s_j) = \widehat{T}^{1j} a^j(s_j)$. After solving the previous system for unknowns $a_n^1(s_1)$ and $b_n^1(s_1)$, we thus deduce that the modal amplitudes of transmitted and scattered field for the inclusion s_1 fulfill equations which are similar to those obtained for a single inclusion probed by a source containing the incident field and scattered fields of other inclusions:

$$a^1(s_1) = Z\left(c^1 + \sum_{1\neq j} \widehat{T}^{1j} a^j(s_j)\right) \qquad , \qquad b^1(s_1) = W\left(c^1 + \sum_{1\neq j} \widehat{T}^{1j} a^j(s_j)\right), \tag{2.6}$$

Those expressions are still available for other scatterers provided that we change the index 1 by the corresponding one. In the case of a plane wave incidence, we would obtain the same formulation but we emphasize the difference hidden in the terms c_n^i which are now given by $c^1 = \widehat{T}^{1s} c^s$. Here the quantity $e^1 = c^1 + \sum_{1\neq j} \widehat{T}^{1j} a^j(s_j)$ is the keystone because knowing e^1 is sufficient to know the modal coefficient a^1 and b^1. We take time to gives its signification. Let denote ϕ_{ex}^i the field exciting the scatterer s_1, it is defined as the sum of the incident field and the total wave scattered by all inclusions except s_1:

$$\phi_{ex}^1(M) = \phi_i(M) + \sum_{1\neq j} \phi_s^j(M) = c^s \cdot V(k_0\mathbf{r}_{s0}) + \sum_{1\neq j} a^j \cdot V(k_0\mathbf{r}_{j0}).$$

In the local frame of s_1 and for M in the vicinity of s_1, the Graf's theorem gives:

$$\phi_{ex}^1(M) = \left(\widehat{T}^{1s} c^s + \sum_{1\neq j} \widehat{T}^{1j} a^j\right) \cdot V(k_0\mathbf{r}_{10}).$$

Hence e^1 is the vector containing the modal coefficients of the exciting field of s_1 evaluated in its vicinity.

2.3.3 Explicit expression for a scatterer in term of the incoming field

Here we want to obtain an explicit solution for the scatterer s_1. We use the previous expressions of $a^j(s_j)$ to obtain for s_1:

$$a^1(s_1) = Z\left(c^1 + \sum_{j\neq 1} \widehat{T}^{1j} Z\left(c^j + \widehat{T}^{j1}a^1(s_1) + \sum_{i\neq(j,1)} \widehat{T}^{ji}a^i(s_i)\right)\right).$$

After rearranging:

$$\left(1 - \sum_{j\neq 1} Z\widehat{T}^{1j}Z\widehat{T}^{j1}\right) a^1(s_1) = Z\left(I + \sum_{j\neq 1} \widehat{T}^{1j}Z\widehat{T}^{j1}\right) c^1 + \sum_{1\neq j\neq i\neq 1} Z\widehat{T}^{1j}Z\widehat{T}^{ji}a^i(s_i)$$

Again we can take into account:

$$a^i(s_i) = Z\left(c^i + \widehat{T}^{i1}a^1(s_1) + \widehat{T}^{ij}a^j(s_j) + \sum_{j\neq k\neq 1} \widehat{T}^{ik}a^k(s_k)\right) \qquad , \qquad \forall j = 1,\dots,N,$$

and injecting this latter gives:

$$\Big(1-\sum_{1\neq j} Z\widehat{T}^{1j}Z\widehat{T}^{j1} - \sum_{1\neq j\neq i\neq 1} Z\widehat{T}^{1j}Z\widehat{T}^{ji}\widehat{T}^{i1}\Big)a^1(s_1) = Z\Big(1+\sum_{1\neq j} \widehat{T}^{1j}Z\widehat{T}^{j1} + \sum_{1\neq j\neq i\neq i} \widehat{T}^{1j}Z\widehat{T}^{ji}\widehat{T}^{i1}\Big)c^1$$
$$+ \sum_{1\neq j\neq i\neq k\neq 1} Z\widehat{T}^{1j}Z\widehat{T}^{ji}Z\widehat{T}^{ik}a^k(s_k). \quad (2.7)$$

We pursue this iteration N times to obtain the exact solution under the form:

$$\left(I - \sum_{i\neq 1} Q^{1i}Z\widehat{T}^{i1}\right) a^1(s_1) = Z\left(I + \sum_{i\neq 1} Q^{1i}Z\widehat{T}^{i1}\right) c^1$$

$$Q^{1i} = \widehat{T}^{1i} + \sum_{j\neq i} \widehat{T}^{1j}Z\widehat{T}^{ji} + \sum_{j\neq k\neq i} \widehat{T}^{1j}Z\widehat{T}^{jk}Z\widehat{T}^{ki} + \dots \qquad (i,j,k,\dots) > 1$$

This formula has no practical utility but it gives an exact idea of what are the process of scattering in terms of coupling between the inclusions and their order. Indeed each $Z\widehat{T}$ stands for the scattering by one inclusion. Hence this formulation of the exact solution in our theory is the equivalent of the expansion in Born series or the Lippmann-Schwinger expansion using the Green function [MM08].

2.4 Ensemble average

Previously we saw how to set the problem of multiple scattering and the way to solve it provided that the positions of the scatterers are given. However the solutions are

too complicated to deal with and moreover, there is no reason to know those positions in experiment or in practical problems such as non destructive testing. Therefore we choose to apply some probabilistic tools to simulate the response of medium containing scatterers as if it was an homogeneous one: The coherent part of the total field is derived by averaging the value of the field at a fixed point, M, over all possible configuration of scatterers. The notations and conventions introduced previously remains available: the vectors localizing M in the O_j-frame would be denoted $\mathbf{r}_{j0}$ and therefore $\mathbf{r}_{0j}$ is the position of s_j in the M-frame. Because M is supposed to be known, the positions of inclusions will always be given in the M-frame.

A configuration is defined by the set of all positions of inclusions $\Lambda_N = \{\mathbf{r}_{01}, \mathbf{r}_{02}, \ldots, \mathbf{r}_{0N}\}$ and is weighted by its density of probability $p(\Lambda_N)$. Ensemble average of any field ϕ is defined by:

$$\langle\phi\rangle = \int\!\!\ldots\!\!\int \phi \; p(\Lambda_N) \; d\mathbf{r}_{0N} \ldots d\mathbf{r}_{02} d\mathbf{r}_{01} \tag{2.8}$$

where the field ϕ is measured at the fixed point. Hence, $\langle\phi\rangle$ is a spatial-dependent statistical quantity. Strictly speaking, the term *coherent signal* is more rigorous than *coherent field* which supposes implicitly that $\langle\phi\rangle$ behaves spatially as a *wave* whereas it is not necessarily the case. In the context of our multiple scattering problem, we will apply the ensemble average to the total field. Then, supposing that the coherent signal $\langle\phi\rangle$ is actually an *effective wave*, we will look for the *effective wavenumber* k_e such as $\langle\phi\rangle$ is solution of $(\Delta + k_e^2)\langle\phi\rangle = f_e$ where f_e is an eventual effective source term.
In Eq.2.8 the integration domains must be chosen in order to respect two restrictions:

1. The inclusions do not overlap, which means $r_{ij} \geq b$ with $b > 2a$.

2. The integration domains must be limited to domains where ϕ have sense.

The first restriction will be taken into account throughout the conditional probability density as we will see in the following. The second restriction is not always emphasized but it has to be checked [Mar] as illustrated in the following two examples. First, if $\phi \equiv \phi_s$, each integration must be performed in $\mathbb{R}^2$ except in a circular circle $\mathcal{C}_0$ of radius a centered at M because inside $\mathcal{C}_0$ we have only the internal field. Second, in the present model the incident field ϕ_i is produced by a source S in the ambient space Ω_0 at $\mathbf{r}_{0s}$. Hence $\phi_i(M) = c^s \cdot V(k_0\mathbf{r}_s)$ is not relevant if an inclusion overlaps the source, therefore we have the condition $r_{sj} > a$ for $j = 1, \ldots N$ integration Eq.2.8 must be performed out of the circle $\mathcal{C}_S$ of radius a and center S. This condition must be satisfied for any quantity ϕ.
As presented by [LM06], the probability density of the whole configurations $p(\Lambda_N)$ can be cast into a successive hierarchy of conditional probability density:

$$p(\Lambda_N) = p(\mathbf{r}_{01}) \; p(\mathbf{r}_{02}|\mathbf{r}_{01}) \; p(\mathbf{r}_{03}|\mathbf{r}_{02}, \mathbf{r}_{01}) \ldots p(\mathbf{r}_{0N}|\mathbf{r}_{0(N-1)}, \ldots, \mathbf{r}_{01}) \tag{2.9}$$

where $p(\mathbf{r}_{0(j+1)}|\mathbf{r}_{0j}, \ldots \mathbf{r}_{01})$ is the density governing the probability to find s_{j+1} centered at $\mathbf{r}_{0(j+1)}$ the position of s_j, $s_{j-1}, \ldots s_1$ being given. The last terms of Eq.2.9 can be

synthesized as follows:

$$p(\Lambda_N) = p(\mathbf{r}_{01})\ p(\mathbf{r}_{02}|\mathbf{r}_{01}) \\ p(\mathbf{r}_{03}\dots\mathbf{r}_{0N}|\mathbf{r}_{02},\mathbf{r}_{01}) \quad (2.10)$$

The ensemble average follows the same hierarchy:

$$\langle\phi\rangle = \int \langle\phi\rangle_1\, p(\mathbf{r}_{01}) d\mathbf{r}_{01}, \quad \langle\phi\rangle_1 = \int \langle\phi\rangle_{12}\, p(\mathbf{r}_{02}|\mathbf{r}_{01}) d\mathbf{r}_{02}, \langle\phi\rangle_{12} = \int\!\!\dots\!\!\int \phi\, p(\mathbf{r}_{03}\dots\mathbf{r}_{0N}|\mathbf{r}_{01},\mathbf{r}_{02}) d\mathbf{r}_{03}\dots d\mathbf{r}_N \quad (2.11)$$

where the j^{th}-order ensemble average $\langle\phi\rangle_{1\dots j}$ corresponds to average obtained over all position of inclusions except s_1, $s_2, \dots s_j$ for which the positions are known.
The more simple forms of the conditional probability densities are the uniform distribution:

$$p(\mathbf{r}_1) \approx \frac{1}{A}\ , \qquad p(\mathbf{r}_{0(j+1)}|\mathbf{r}_{0j},\dots\mathbf{r}_{01}) \approx \frac{1}{A_{j+1}} \prod_{k=1}^{j} \mathcal{H}(r_{(j+1)k} - b) \quad (2.12)$$

where $\mathcal{H}$ is the Heaviside step function and $b \geq 2a$ is the minimum distance between two inclusions. A_{j+1} is the area of the surface whose indicator function is $\prod_{k=1}^{j} \mathcal{H}(r_{(j+1)k} - b)$. For dilute media, each circle defined by $\mathcal{H}(r_{(j+1)k} - b)$ do not overlap and the surface can be defined as:

$$A_{j+1} = A - j\pi b^2$$

where A is the area of the domain of $\mathbb{R}^2$ containing the N inclusions. Of course the validity of the second approximation decreases as j and concentration increases. For dense medium and large j: $0 < A_{j+1} < A - j\pi b^2$. For an infinitely large domain a more abrupt approximation can be used for small j:

$$p(\mathbf{r}_{0(j+1)}|\mathbf{r}_{0j},\dots\mathbf{r}_{01}) \approx \frac{1}{A} \prod_{k=1}^{j} \mathcal{H}(r_{(j+1)k} - b) \quad (2.13)$$

that corresponds to the so-called hole correction for the pair correlation function:

$$p(\mathbf{r}_{02}|\mathbf{r}_{01}) \approx \frac{1}{A}\mathcal{H}(r_{12} - b) = p(r_{12})$$

These densities are given without constraints on M. However we emphasize that in the multiple scattering problem, the field is piecewisely defined inside and outside the inclusions. Consequently this fact should be taken into account in the averaging process. For example let M be overlapped by an inclusion, say s_1, it means that we focus on configurations with the condition that M is in the circle $\mathcal{C}_1$ centred at O_1 with radius a. M has probability to be anywhere in $\mathcal{C}_1$, s_1 being fixed, and the others inclusions are randomly distributed in the matrix. The formulation does not change but the density $p(\mathbf{r}_{01})$ has to be replaced by:

$$p(\mathbf{r}_{01}) = \frac{1}{\pi a^2}\ ,$$

and the other conditional probabilities are unchanged.
Actually, for a surface concentration φ of scatterers, the mean field at a fixed point M is $\langle\phi\rangle = \varphi\langle\phi_1\rangle + (1-\varphi)\langle\phi_0\rangle$ where $\langle\phi_0\rangle$ and $\langle\phi_1\rangle$ are the mean of external and internal field.
The total scattered field is $\phi_s = \sum_j \phi_s^j$. After ensemble average and because the scatterers have same mechanical and geometrical properties, the contributions of an inclusion is indistinguishable from the others which means $\langle\phi_s^1\rangle = \left\langle\phi_s^{j\neq 1}\right\rangle$ and $\langle\phi_s\rangle = N\langle\phi_s^1\rangle$. Let s_1 be chosen as a representative inclusion. In particular for uniform probability density, if the scatterers do not overlap the source (what is always supposed in the following) we have:

$$\langle\phi_s\rangle = n_0\int\langle\phi_s^1\rangle_1\ d\mathbf{r}_{01}, \quad \text{and} \qquad \langle\phi_0\rangle = \phi_i + \langle\phi_s\rangle = \phi_i + n_0\int\langle\phi_s^1\rangle_1\ d\mathbf{r}_{01} \tag{2.14}$$

where $n_0 = N/A = \varphi/\pi a^2$ is the number of inclusions per unit area (or density of inclusions). Note that $\langle\phi_s^1\rangle_1 \neq \left\langle\phi_s^{j\neq 1}\right\rangle_1$ but the contribution of other scattered fields for fixed s_1 are still indistinguishable $\langle\phi_s^2\rangle_1 = \left\langle\phi_s^{j\neq 1}\right\rangle_1$ at this order of ensemble average. For an averaged internal field:

$$\langle\phi_1\rangle = \frac{1}{\pi a^2}\int\langle\phi_t^1\rangle_1\ d\mathbf{r}_{01}. \tag{2.15}$$

The quantities $\langle\phi_s^1\rangle_1$ and $\langle\phi_t^1\rangle_1$ are calculated accordingly to ϕ_i and the scattering from $N-1$ other inclusions. The contribution of these $N-1$ inclusions in $\langle\phi_t^1\rangle_1$ and $\langle\phi_i^1\rangle_1$ are indistinguishable.

2.5 First order theory

2.5.1 Foldy's model

In the Foldy model [Fol45], the case of unitary plane wave incident field is investigated for isotropic point scatterers. In practice, considering such scatterers is equivalent to a low frequency situation with no contrast for mass densities ($\rho_1 \sim \rho_0$). Because scatterers are point-like in this example, there are no condition on the integral's domain for the averages. The observation point M is localized by $\mathbf{r}$ and the scatterers are at $\mathbf{r}_i$. Therefore the effective field $\langle\psi\rangle$ is calculated from the previous formula 2.14 of $\langle\phi_0\rangle$:

$$\langle\phi\rangle = \phi_i + \langle\phi_s\rangle = \phi_i + n_0\int\langle\phi_s^1\rangle_1\ d\mathbf{r_1}. \tag{2.16}$$

All the effects are hidden in the term $\langle\phi_s^1\rangle_1$ which need to be evaluated. As the scatterers are point-like and isotropic, ϕ_s^1 must be proportional to $H_0(|\mathbf{r}-\mathbf{r}_1|)$. Moreover this field is also proportional to the scattering coefficient and to a quantity interpreted as the value of an excitation at the position of the inclusion. Thus ϕ_s^1 is in the form:

$$\phi_s^1(\mathbf{r}) = Z\phi_{ex,1}^1(\mathbf{r_1})H_0(k_0|\mathbf{r}-\mathbf{r}_1|),$$

where Z is a constant corresponding to the "strength" of the scatterer and $\phi^1_{ex,1}(\mathbf{r_1})$ is the value at $\mathbf{r}_1$ of the field exciting s_1. This latter is unknown and hard to define rigorously. To deal with this issue, we use the Foldy's closure assumption which consists in setting:

$$\langle\phi(\mathbf{r})\rangle_1 = \langle\phi^1_{ex,1}(\mathbf{r})\rangle_1, \quad \text{for } \mathbf{r} \text{ in the vicinity of } \mathbf{r}_1. \tag{2.17}$$

This assumption is purely statistic and does not rely on the characteristic of the scatterers. Actually it consists in considering that the exciting field in the vicinity of s_1 is basically the total field as if s_1 was not present. This latter field is thus obtained for $N-1$ scatterer and does not differ a lot from the total field with N scatterers. Hence the effective field is solution of the Foldy's integral equation:

$$\langle\phi(\mathbf{r})\rangle = \phi_i(\mathbf{r}) + n_0 Z \int \langle\phi(\mathbf{r}_1)\rangle\, H_0(k_0|\mathbf{r}-\mathbf{r}_1|)\, d\mathbf{r_1}.$$

Now we notice that $H_0(k_0|\mathbf{r}-\mathbf{r}_1|) = 4iG(\mathbf{r},\mathbf{r}_1)$ where G is the 2D Green function solution of the Helmholtz equation $(\Delta + k_0^2)G(\mathbf{r},\mathbf{r_1}) = \delta(\mathbf{r}-\mathbf{r}_1)$, with δ the Dirac distribution. Applying $(\Delta + k_0^2)$ we obtain:

$$(\Delta + k_0^2)\,\langle\phi(\mathbf{r})\rangle = Z n_0 \int \langle\phi(\mathbf{r}_1)\rangle\,(\Delta + k_0^2) H_0(k_0|\mathbf{r}-\mathbf{r}_1|)\, d\mathbf{r}_1,$$

so that:

$$(\Delta + k_0^2)\,\langle\phi(\mathbf{r})\rangle = 4inZn_0 \int \langle\phi(\mathbf{r}_1)\rangle\,\delta(|\mathbf{r}-\mathbf{r}_1|)\, d\mathbf{r}_1 = 4in_0 Z\,\langle\phi(\mathbf{r})\rangle\,.$$

All the previous hypothesis permit us to conclude that the effective field is solution of the Helmholtz equation:

$$(\Delta + k_e^2)\,\langle\phi\rangle = 0, \qquad \text{with } k_e^2 = k_0^2 - 4in_0 Z. \tag{2.18}$$

Thus it shows that the effective field does propagate as a wave, at least under the considered assumptions. Furthermore this result is a definion of the wavenumber k_e and was first obtained by Foldy in the case of unitary incident plane wave probing a medium containing a random distributions of N isotropic point-like scatterers. Actually the Foldy closure assumption (2.17) can be used in a more general case. For example [LM05] solved the scattering of unitary plane wave by a semi-infinite medium with random distributions of penetrable scatterers.

2.5.2 Foldy closure assumption

In the following we aim to use our formulation to derive the effective wavenumber k_e in the case of incident wave emitted by a point-like source in an infinite domain.
Our reasoning follows the same way as previous work in that sense: k_e will be evaluated at the first order in the formula (2.11), namely we cut this latter at $\langle\phi\rangle_1$. The

investigations will be performed thanks to the Foldy's closure assumption (2.17) transposed on the modal coefficients. It gives same formula for k_e as in previous works with the difference that it is for point-like source. Hence the type of source does not really matter what seems reasonable.

$\langle \phi_s^1 \rangle_1$ is singular at the center of s_1 and is supposed to satisfy the Sommerfeld radiation condition in the infinite homogeneous matrix. Thus it is expanded with singular eigenfunctions:

$$\langle \phi_s^1 \rangle_1 = \langle a^1 \rangle_1 \cdot V(k\mathbf{r}_{10})$$

The averaged external field $\langle \phi \rangle$, what would be defined as the effective field in the following is supposed to behaves as the incoming wave but propagates in an effective medium with k_e wave numbers: $\langle \phi \rangle = d^s \cdot V(k_e \mathbf{r}_s)$ where d^s and k_e have to be defined. Of course $\langle \phi \rangle$ is regular in the vicinity of all inclusion as it is proved by Graf's theorem for $r_{10} < r_{1s}$:

$$\langle \phi \rangle = d^s \cdot V(k_e \mathbf{r}_s) = d^1 \cdot U(k_e \mathbf{r}_{10}), \qquad d^1 = \widehat{T}_e^{1s} d^s. \tag{2.19}$$

The subscript e on $\widehat{T}_e^{1s}$ means that the matrix is calculated with the wavenumber k_e. Applying the Foldy's closure assumption, the wave exciting s_1 is supposed to be the effective field $\langle \phi \rangle$:

$$\langle a^1 \rangle_1 = Z d^1$$

Thus the Foldy's problem is expressed in the form:

$$\langle \phi \rangle = \phi_i + n_0 \int \langle \phi_s^1 \rangle_1 \, d\mathbf{r}_{01}, \quad \text{with} \qquad \langle \phi_s^1 \rangle_1 = (Z d^1) \cdot V(k\mathbf{r}_{10}) \tag{2.20}$$

To compute the integral in Eq.2.20, the terms depending on the position of s_1 are regrouped. Use transpose matrix $\widehat{S}_e^{1s} = (\widehat{T}_e^{1s})^T$ to have:

$$\langle \phi_s^1 \rangle_1 = d^s \cdot \widehat{S}_e^{1s} Z V(k\mathbf{r}_{10})$$

and then

$$\int \langle \phi_s^1 \rangle_1 \, d\mathbf{r_{01}} = d^s \cdot \Phi, \quad \text{with} \quad \Phi = \int \widehat{T}^{s1} Z V(k\mathbf{r}_1) d\mathbf{r}_{01}$$

The integration is performed on $\mathcal{B} = \mathbb{R}^2 - \{\mathcal{C}_0 \cap \mathcal{C}_S\}$.

2.5.3 Derivation of the effective field

The main task is now to compute each components of Φ:

$$\Phi_n = \sum_m z_m \int V_{n-m}(k_e \mathbf{r}_{s1}) V_m(k\mathbf{r}_{10}) \; d\mathbf{r}_{01}$$

The integral can be evaluated with the Green theorem as proposed by [LM06]-Eq.(67) for an incoming plane wave probing a semi-infinite heterogeneous domain. As our problem is slightly different, point source and infinite domain, we give the details of the calculus in the following.

First, we remark that along the integration domain no singularities are possible for

$V(k_e\mathbf{r}_{10})$ and for $V(k_e\mathbf{r}_{s1})$ because s_1 do not overlap the source neither M ($r_{10} > a$ and $r_{s1} > a$). Hence the terms in the integral are finite and there is no source in the domain. Thus, in the integration domain, the eigenfunction are solutions of:

$$\begin{aligned} \left(\Delta + k_e^2\right) V_{n-m}(k_e\mathbf{r}_{s1}) &= 0 \quad (2.21) \\ \left(\Delta + k^2\right) V_m(k\mathbf{r}_{10}) &= 0 \quad (2.22) \end{aligned}$$

Multiply Eq.2.21 by $V_m(k\mathbf{r}_{10})$ and Eq.2.22 by $V_{n-m}(k_e\mathbf{r}_{s1})$ and subtract both of them, we formulate the terms in the integrals defining Φ_n by means of the equality:

$$\left(k_e^2 - k^2\right) V_{n-m}(k_e\mathbf{r}_{s1}) V_m(k\mathbf{r}_{10}) = V_{n-m}(k_e\mathbf{r}_{s1})\Delta V_m(k\mathbf{r}_{10}) - V_m(k\mathbf{r}_{10})\Delta V_{n-m}(k_e\mathbf{r}_{s1}). \quad (2.23)$$

The surface integral on $\mathcal{B}$ is replaced by a contour integral according to the Green theorem:

$$\begin{aligned} \int_{\mathcal{B}} V_{n-m}(k_e\mathbf{r}_{s1})\Delta V_m(k\mathbf{r}_{10}) - V_m(k\mathbf{r}_{10})\Delta V_{n-m}(k_e\mathbf{r}_{s1})\ d\mathbf{r}_{01} \ = \\ \int_{\partial\mathcal{B}} V_{n-m}(k_e\mathbf{r}_{s1})\partial_{\mathbf{n}} V_m(k\mathbf{r}_{10}) - V_m(k\mathbf{r}_{10})\partial_{\mathbf{n}} V_{n-m}(k_e\mathbf{r}_{s1})\ d\mathbf{r}_{01} \end{aligned} . \quad (2.24)$$

The boundary $\partial\mathcal{B}$ is decomposed into three contours: $\mathcal{C}_0$, $\mathcal{C}_S$ and $\mathcal{C}_\infty$ the circle centered at M with radius $R \to \infty$: the physical boundary of $\mathcal{B}$. We can suppose without particular attention that these contours do not overlap.

Contribution of $\mathcal{C}_0$:
For $\mathcal{C}_0$ the Graf's addition theorem is used to expand $V_{n-m}(k_e\mathbf{r}_{s1})$ in the M-frame because we must integrate over $\mathbf{r}_{01}$. Observing that $r_{01} = a$ along $\mathcal{C}_0$, we have $r_{01} < r_{1s}$:

$$V_{n-m}(k_e\mathbf{r}_{s1}) = \sum_p V_{n-m-p}(k_e\mathbf{r}_s) U_p(k_e\mathbf{r}_1)$$

In M-frame the external normal is $b\vec{n} = -\mathbf{e}_r$ and $\partial_{\mathbf{n}} U_p(k_e\mathbf{r}_{01}) = -k_e J'_p(k_e a)\exp(ip\theta_{01}$ and $\partial_{\mathbf{n}} V_m(k\mathbf{r}_{10}) = (-1)^m \partial_{\mathbf{n}} V_m(k\mathbf{r}_{01}) = -(-1)^m k H'_m(ka)\exp(im\theta_{01})$. The integration along $\mathcal{C}_0$ is now:

$$\begin{aligned} (-1)^m \int_{\partial\mathcal{C}_0} V_{n-m}(k_e\mathbf{r}_{s1})\partial_{\mathbf{n}} V_m(k\mathbf{r}_{01}) - V_m(k\mathbf{r}_{01})\partial_{\vec{n}} V_{n-m}(k_e\mathbf{r}_{s1})\ d\mathbf{r}_{01} = \\ -(-1)^m \sum_p V_{n-m-p}(k_e\mathbf{r}_{s0}) \left(kH'_m(ka)J_p(k_e a) - k_e J'_p(k_e a)H_m(ka)\right) a \int_0^{2\pi} \exp(i(m+p)\theta_{01} d\theta_{01} \end{aligned}$$

Apply the orthogonality relation of $\exp(im\theta)$ to obtain:

$$\begin{aligned} \int_{\partial\mathcal{C}_0} V_{n-m}(k_e\mathbf{r}_{s1})\partial_{\mathbf{n}} V_m(k\mathbf{r}_{10}) - V_m(k_e\mathbf{r}_{10})\partial_{\mathbf{n}} V_{n-m}(k\mathbf{r}_{s1})\ d\mathbf{r}_{01} = 2\pi V_n(k_e\mathbf{r}_{s0})\mathcal{N}_m(k_e, k) \\ \text{with } \mathcal{N}_m(k_e, k) = k_e a J'_m(k_e a)H_m(ka) - kaJ_m(k_e a)H'_m(ka) \end{aligned}$$

Contribution of $\mathcal{C}_\infty$:
The calculations are the same except that the Graf's theorem is performed for $r_{01} = R$ with $R > r_{s0}$. Therefore the contribution of $\mathcal{C}_\infty$ is:

$$2\pi U_n(k_e\mathbf{r}_{s0})R\Big(k_eH'_m(k_eR)H_m(kR) - kH_m(k_eR)H'_m(kR)\Big),$$

for $R \to \infty$. As the wavenumber k_e is complex, the asymptotic forms of $H_n(k_eR)$, $H_n(kR)$ for $R \to \infty$ gives directly:

$$\int_{\mathcal{C}_\infty} V_{n-m}(k_e\mathbf{r}_{s1})\partial_{\mathbf{n}}V_m(k\mathbf{r}_{10}) - V_m(k\mathbf{r}_{10})\partial_{\mathbf{n}}V_{n-m}(k_e\mathbf{r}_{s1})\ d\mathbf{r}_1 = 0$$

Contribution of $\mathcal{C}_S$:
The same procedure is performed for $\mathcal{C}_S$. On this boundary we reasonably have $r_{s0} > r_{1s}$, because $r_{1s} = a$ and the Graf's theorem gives:

$$V_m(k\mathbf{r}_{10}) = \sum_p U_{m-p}(k\mathbf{r}_{1s})V_p(k\mathbf{r}_{s0}),$$

and integration along $\mathcal{C}_S$ gives:

$$-(-1)^{m-p}\sum_p V_p(k\mathbf{r}_{s0})\left(kJ'_{m-p}(ka)H_{n-m}(k_ea) - k_eH'_{n-m}(k_ea)J_{m-p}(ka)\right)a\int_0^{2\pi}\exp(i(n-p)\theta_{s1})d\theta_{s1}$$

what becomes after using orthogonality:

$$\int_{\partial\mathcal{C}_S} V_{n-m}(k_e\mathbf{r}_{s1})\partial_{\mathbf{n}}V_m(k\mathbf{r}_{10}) - V_m(k_e\mathbf{r}_{10})\partial_{\mathbf{n}}V_{n-m}(k\mathbf{r}_{s1})\ d\mathbf{r}_{01} = -2\pi\ V_n(k\mathbf{r}_{s0})\mathcal{N}_{n-m}(k,k_e)$$

Analytic expression of Φ_n:
Combining each result and using $\mathcal{N}_{-p} = \mathcal{N}_p$, we have

$$\Phi_n = \frac{2\pi}{k_e^2 - k^2}\ \left(V_n(k_e\mathbf{r}_{s0})\sum_m z_m\mathcal{N}_m(k_e,k) - V_n(k\mathbf{r}_{s0})\sum_m z_m\mathcal{N}_{m-n}(k,k_e)\right) \quad (2.25)$$

2.5.4 Analytic expressions

According to Eq.2.25 and Eq.2.20, we observe that the Foldy hypothesis implies:

$$d^s\cdot V(k_e\mathbf{r}_{s0}) = c^s\cdot V(k\mathbf{r}_{s0}) + \frac{2\pi n_0}{k_e^2-k^2}\ \Big(d^s\cdot V(k_e\mathbf{r}_{s0})\sum_m z_m\mathcal{N}_m(k_e,k) - \sum_n d_n^s V_n(k\mathbf{r}_{s0})\sum_m z_m\mathcal{N}_{n-m}(k,k_e)\Big) \quad (2.26)$$

In this formula, terms propagating with wavenumber k and k_e can be separated to obtain a system of two equations:

$$\begin{aligned} 1 &= n_0 \frac{2\pi}{k_e^2 - k^2} \sum_m z_m \mathcal{N}_m(k_e, k) \\ \frac{c_n^s}{d_n^s} &= n_0 \frac{2\pi}{k_e^2 - k^2} \sum_m z_m \mathcal{N}_{m-n}(k, k_e) \qquad n \in \mathbb{Z} \end{aligned} \tag{2.27}$$

The first equation determines implicitly the effective wavenumber. The second system of equation (extinction principle) gives the modal amplitudes of the exciting field [LM06], we rather refer to it as the extinction principle. However the complexity of this equations, especially the first one, is an obstacle to their analytic treatment. In practice, we computationally solve the first one by looking for k_e that satisfies the equation. Several values of k_e could be found, nevertheless the numerical tools shows that it is not the case. The second equation becomes trivial provided that we know k_e.

Taylor expansion:
Let know suppose that $k_e a = ka + \epsilon$ with $|\epsilon| \ll 1$ first order Taylor expansion of Bessel functions gives:

$$\mathcal{N}_n(k_e, k) = -\frac{2i}{\pi} + \epsilon\, \mathcal{M}_n(k) \quad , \quad \text{and} \qquad \mathcal{N}_n(k, k_e) = -\frac{2i}{\pi} - \epsilon\, \mathcal{M}_n(k)$$
$$\text{with} \qquad \mathcal{M}_n(k) = ka \left((\frac{n^2}{(ka)^2} - 1) J_n(ka) H_n(ka) - J_n'(ka) H_n'(ka) \right) + \mathcal{O}(\epsilon^2)$$

If ka and $k_e a$ are closed enough to suppose $\mathcal{N}_n(k, k_e) \approx -\frac{2i}{\pi}$ the effective wavenumber is the classical

$$k_e^2 = k^2 - 4in_0 \sum_m z_m \tag{2.28}$$

and the modal amplitudes of $\langle \phi \rangle$ and ϕ_i are the same according to the extinction principle. Hence we generalized the Foldy formula (2.18) to the waves emitted by a point-like source. In order to investigate the validity domain of this approximation let's observe that $k_e a = ka + \epsilon$ implies $k_e^2 = k^2 + 2\epsilon k/a + \mathcal{O}(\epsilon^2)$. The assumption $|\epsilon| \ll 1$ can be formulated in terms of surface concentration $\varphi = n_0 \pi a^2$:

$$\varphi\, \chi \ll 1, \quad \text{with} \qquad \chi = \frac{2}{\pi ka} |\sum_n z_n|$$

Keeping in mind that $\varphi < 1$ (*e.g.*), we restrict ourselves to dependency of χ on the contrast between the scatterers and the matrix. In Fig.2.7, χ is presented for various adimensional frequency ka for impenetrable and penetrable inclusions.

As ka decreases we observe that the criterion on χ seems more reliable to ensure the validity of (2.28) for every contrasts except void inclusion. Indeed, this latter appears as a critical case for using formula (2.28). The concentration φ should be taken into account to balance χ if we deal with this kind of scatterers. For rigid inclusion the criterion is fulfilled only for low frequencies $ka \approx 0.1$. Concerning the penetrable

scatterers, high frequencies $ka \approx 10$ do not allow us to apply (2.28). However it becomes remarkably consistent for contrasts around the unitary value. In conclusion, we emphasize that it seems sensitive to only rely only on the concentration to use the Foldy formula. It confirms the conclusion concerning the far field coupling investigated in section 2.2. For the aforementioned cases which do not fulfill the criterion, we recommend to solve the first equation of 2.27.

2.6 Second order

2.6.1 Second order closure assumption

In order to improve the multiple scattering problem, $\left\langle \phi_s^1 \right\rangle_{12}$ the second order ensemble average must be explicitly taken into account in order to evaluate $\left\langle \phi_s^1 \right\rangle_1$:

$$\left\langle \phi_s^1 \right\rangle_1 = \int \left\langle \phi_s^1 \right\rangle_{12} p(r_{12}) \mathrm{d}\mathbf{r}_{02} \quad \text{with} \qquad \left\langle \phi_s^1 \right\rangle_{12} \neq \left\langle \phi_s^1 \right\rangle_1$$

$$\langle \psi_s \rangle = n_0 \int \left\langle \psi_s^1 \right\rangle_1 \mathrm{d}\vec{r}_{01} = n_0 \iint \left\langle \psi_s^1 \right\rangle_{12} p(r_{12}) \mathrm{d}\vec{r}_{02} \mathrm{d}\vec{r}_{01} \quad \text{with}$$

The goal of the following is to calculate $\left\langle \phi_s^1 \right\rangle_1$ then we will be able to deduce $\langle \phi \rangle$ by averaging on $\mathbf{r}_{01}$. First of all we need to evaluate $\left\langle \phi_s^1 \right\rangle_{12}$: the field scattered by s_1 if the position of s_2 is known. Remind that, at this level, s_2 represents the $N-1$ scatterers. Sommerfeld radiation condition still implies $\left\langle \phi_s^1 \right\rangle_{12} = \left\langle a^1 \right\rangle_{12} \cdot V(k\mathbf{r}_{10})$. However, we emphasize that interactions between s_1 and the representative scatterer s_2 are hidden behind the term $\left\langle a^1 \right\rangle_{12}$ as we have seen in section 2.3.
Because the scatterers are indistinguishable, after averaging the left-hand side of Eq.(2.6) over $\mathbf{r}_{0i}$ with $i \neq 1, 2$, we deduce:

$$\left\langle a^1 \right\rangle_{12} = Zc^1 + (N-1)Z\, \widehat{T}^{12} \left\langle a^2 \right\rangle_{12} \tag{2.29}$$

To sum up, the problem is an equation comprising two unknowns: the effective modal amplitudes $\left\langle a^1 \right\rangle_{12}$ and $\left\langle a^2 \right\rangle_{12}$, the scattering amplitude of s_2 knowing the position of s_1. At this level we need to invoke a closure assumption on $\left\langle a^2 \right\rangle_{12}$ to obtain a well-posed problem. This assumption should concern the representative scatterer s_2. As in the Foldy case, it seems natural to suppose that this latter is excited by the effective field and its scattering amplitude should be proportional to the effective amplitude:

$$\left\langle a^2 \right\rangle_{12} = Zd^2$$

Notice that the Z proportional coefficient is inspired by the scattering of a single inclusion but it is questionable. Under our closure assumption Eq.2.29 becomes:

$$\left\langle a^1 \right\rangle_{12} = Zc^1 + (N-1)Z\widehat{T}^{12}Zd^2. \tag{2.30}$$

The modal amplitudes d^2 are obtained for local decomposition around s_2 thanks to the Graf's theorem with $r_{s2} > r_{20}$:

$$d^2 = \hat{T}_e^{2s} d^s \quad , \quad \text{with} \quad (\hat{T}_e^{2s})_{nm} = V_{m-n}(k_e \mathbf{r}_{s2}).$$

Once more,$\widehat{T}_e$ is defined with wavenumbers k_e. As $N-1 \approx N$, we finally obtain

$$\left\langle a^1 \right\rangle_{12} = Zc^1 + N\ Z\widehat{T}^{12} Z\widehat{T}_e^{2s} d^s \tag{2.31}$$

Because $V_n(k\mathbf{r}_1)$ is independent of the position of s_2, we have:

$$\left\langle \phi_s^1 \right\rangle_1 = \int \left\langle a^1 \right\rangle_{12} p(r_{12}) d\mathbf{r}_{02} \cdot V(k\mathbf{r}_{10}) \quad \text{or} \qquad \left\langle a^1 \right\rangle_1 = \int \left\langle a^1 \right\rangle_{12} p(r_{12}) d\mathbf{r}_{02} \tag{2.32}$$

2.6.2 Derivation of the effective field

First we need to calculate $\left\langle \phi_s^1 \right\rangle_1$ and it reduces to calculate its modal coefficients $\left\langle a^1 \right\rangle_1$. They are given by the right-hand side of Eq.2.32 combined with 2.31:

$$\begin{aligned} \left\langle a^1 \right\rangle_1 &= Zc^1 + NZ \int \widehat{T}^{12} Z\widehat{T}_e^{2s}\ p(\mathbf{r}_{02}|\mathbf{r}_{01}) d\mathbf{r}_{02}\ d^s \\ &= Zc^1 + n_0\ ZD^{1s} d^s \end{aligned} \quad , \quad D^{1s} = \int \widehat{T}^{12} Z\widehat{T}_e^{2s}\ d\mathbf{r}_{02}.$$

Let us take a break in order to discuss the integration's domain that we should to derive D^{1s}. The first scatterer s_1 is supposed to be fixed at a known position therefore the hole correction imposes that the representative s_2 verifies $r_{12} \geq b$ to ensure that both s_1 and s_2 do not overlap. The hole correction should also be applied to forbid overlapping between the source S and s_2: $r_{s2} \geq a$. We could define an hole correction to avoid the observation point M to be inside the representative scatterer s_2. However, we suggest to begin with neglecting this effect as it was previously done in many works concerning ensemble average at order 1 or 2. Consequently the integration's domain is the infinite domain without the disks centered on S and s_1 with convenient radius.
The evaluation of each components of the matrix D^{1s}:

$$(D^{1s})_{nm} = \sum_p z_p \int V_{p-n}(k\mathbf{r}_{21}) V_{m-p}(k_e\mathbf{r}_{s2})\ d\mathbf{r}_{12} \tag{2.33}$$

is performed with the method used in the previous section which transforms the integral over the volume into an integral over the boundary of this volume. Rigorously speaking this boundary comprises three connected components. Both contours are introduced by the hole corrections: the circles $\mathcal{C}_S$ and $\mathcal{C}_1$, respectively centered at S and O_1 with radius a and b. The third one is $\mathcal{C}_\infty$ introduced in the first order theory. The calculation for this latter is the same as previously and it shows that the contribution of this integral is zero.

Contribution of $\mathcal{C}_S$
If s_2 is on $\mathcal{C}_S$, we suppose $r_{1s} > r_{2s}$ what is true in most of cases. Therefore applying the Graf's addition theorem gives a convenient expression to perform the integral over $\mathbf{r}_{s2}$:

$$V_{p-n}(k\mathbf{r}_{21}) = \sum_q U_{p-n-q}(k\mathbf{r}_{2s}) V_q(k\mathbf{r}_{s1})$$

After calculation the contribution from $\mathcal{C}_S$ is:

$$(C_S)_{nm} = \frac{2\pi}{k^2 - k_e^2} \sum_p z_p V_{m-n}(k\mathbf{r}_{s1}) \mathcal{N}_{m-p}(k, k_e). \tag{2.34}$$

Contribution of $\mathcal{C}_1$
Along $\mathcal{C}_1$, we have in general $r_{12} < r_{1s}$ with $r_{12} = b$:

$$V_{m-p}(k_e\mathbf{r}_{s2}) = \sum_q V_{m-p-q}(k_e\mathbf{r}_{s1}) U_q(k_e\mathbf{r}_{12})$$

and the contribution from $\mathcal{C}_1$ is:

$$(C_1)_{nm} = -\frac{2\pi}{k^2 - k_e^2} \sum_p z_p V_{m-n}(k_e\mathbf{r}_{s1}) \mathcal{N}^b_{n-p}(k_e, k) \tag{2.35}$$

where the suffix ^{b} is used to remind that $\mathcal{N}^b$ is the same as $\mathcal{N}$ but with b replacing a.

Expression of (D^{1s})
According to our previous considerations, we have $(D^{1s})_{nm} = (C_S)_{nm} + (C_1)_{nm}$. Consequently the n-component of the vector $D^{1s}d^s$ is:

$$\begin{aligned}(D^{1s}d^s)_n &= \sum_m \frac{2\pi}{k^2 - k_e^2} \sum_p z_p \left(V_{m-n}(k\mathbf{r}_{s1}) \mathcal{N}_{m-p}(k, k_e) - V_{m-n}(k_e\mathbf{r}_{s1}) \mathcal{N}^b_{n-p}(k_e, k) \right) d^s_m \\ &= \frac{2\pi}{k^2 - k_e^2} \sum_p z_p \left(\sum_m V_{m-n}(k\mathbf{r}_{s1}) \mathcal{N}_{m-p}(k, k_e) d^s_m - \mathcal{N}^b_{n-p}(k_e, k) d^1_n \right)\end{aligned}$$

because $\sum_m V_{m-n}(k_e\mathbf{r}_{s1}) d^s_m = d^1_n$. Finally we have the following equality:

$$\left\langle a^1_n \right\rangle_1 = z_n c^1_n + \frac{2\pi n_0}{k^2 - k_e^2} z_n \left(\sum_m V_{m-n}(k\mathbf{r}_{s1}) d^s_m \sum_p z_p \mathcal{N}_{m-p}(k, k_e) - d^1_n \sum_p z_p \mathcal{N}^b_{n-p}(k_e, k) \right). \tag{2.36}$$

At his level, it is tempting to go straight to the calculation of $\langle\phi\rangle$ by integrating over the positions of s_1. However we suggest to approximate the $\left\langle a^1_n \right\rangle_1$. First we suppose that this term is of order of $V_n(k_e\mathbf{r}_{s1})$ that is to say the averaged exciting field in the vicinity of s_1 is supposed to be emitted from S and propagates with k_e. A comparable assumption was made by *e.g.* [LM06] to express the exciting field in an other coordinates system. Let us integrate (2.36) over θ_{s_1}. After straightforward calculations orthogonality conditions give:

$$\mathcal{O}(H_0(k_e r_{s1})) \simeq c^s_n H_0(k r_{s1}) + \frac{2\pi n_0}{k^2 - k_e^2} z_n \left(H_0(k r_{s1}) d^s_n \sum_p z_p \mathcal{N}_{m-p}(k, k_e) - d^s_n H_0(k_e r_{s1}) \sum_p z_p \mathcal{N}^b_{n-p}(k_e,$$

Noting that k_e is complex, we divide the equations by $H_0(kr_{s1})$ and take the limit when kr_{s1} goes to the infinity. Thus we have:

$$0 \simeq c^s_n + \frac{2\pi n_0}{k^2 - k_e^2} z_n d^s_n \sum_p z_p \mathcal{N}_{m-p}(k, k_e). \tag{2.37}$$

Hence we can neglect $c_n^s + \dfrac{2\pi n_0}{k^2 - k_e^2} z_n d_n^s \sum_p z_p \mathcal{N}_{m-p}(k, k_e)$.

We can then suppose:

$$\begin{aligned} \left\langle a_n^1 \right\rangle_1 &= z_n d_n^1 \frac{2\pi n_0}{k_e^2 - k^2} \sum_p z_p \mathcal{N}_{n-p}^b(k_e, k) \\ 0 &= c_n^s + \frac{2\pi n_0}{k^2 - k_e^2} z_n d_n^s \sum_p z_p \mathcal{N}_{m-p}(k, k_e). \end{aligned} \tag{2.38}$$

We should keep in mind that $=$ is actually an approximation. Concerning the first equation of 2.38, we notice that it can be re-formulated by introducing a modified scattering coefficient ζ_n such as:

$$\left\langle a_n^1 \right\rangle_1 = \zeta_n d_n^1 \quad , \qquad \zeta_n = z_n \frac{2\pi n_0}{k_e^2 - k^2} \sum_p z_p \mathcal{N}_{n-p}^b(k_e, k)$$

Hence, the last step consist in calculating:

$$\langle \phi \rangle = \phi_i + n_0 \int \left\langle \phi_s^1 \right\rangle_1 d\mathbf{r}_{01}, \quad \text{with} \qquad \left\langle \phi_s^1 \right\rangle_1 = (\zeta d^1) \cdot V(k\mathbf{r}_{10}) \tag{2.39}$$

Now, we observe that it is exactly the same formulation as the first order problem (2.20) with identification $\zeta \leftrightarrow Z$. Without further consideration, it suffices to use the previously obtained equations (2.27) with $\zeta \leftrightarrow Z$:

$$1 = \frac{2\pi n_0}{k_e^2 - k^2} \sum_n \zeta_n \mathcal{N}_n(k_e, k) = \left(\frac{2\pi n_0}{k_e^2 - k^2} \right)^2 \sum_n z_n \mathcal{N}_n(k_e, k) \sum_p z_p \mathcal{N}_{n-p}^b(k_e, k) \tag{2.40}$$

At this step the extinction principle gives an other equation for the d_n^s:

$$\frac{c_n^s}{d_n^s} = n_0 \frac{2\pi}{k_e^2 - k^2} \sum_m \zeta_m \mathcal{N}_{m-n}(k, k_e). \tag{2.41}$$

Finally we obtain two formula for the amplitudes d_n, namely (2.37) and (2.41). It is not necessarily a contradiction because both of this equations are actually approximation, nevertheless it suggests that our model can not determine the modal amplitude of the effective wave. Injecting (2.37) in (2.41) leads to an equation involving z_n and ka. Further investigations on these conditions could help to give a limit of our model in term of contrast, *via* z_n or in term of ka.

From now we focus on the equation (2.40) giving an approximation of k_e. Our aim is to compare our model with others and numerical simulations. However these latter concern unitary incident planewave in a semi-infinite medium. It means that we have to adjust our theory in the case of unitary plane incidence. Actually we do not expect the approximated effective wavenumber being different as we have seen in the first order theory. For the first integration, the calculation will remain the same except that there is no hole correction due to the source . The extinction principle

will actually change because the medium is semi-infinite, the calculations for this term is given by the method of [LM06]. The most important thing to observe is that the (2.40) remains available because it is given by the hole correction in the vicinity of s_1. Thus we can compare the wavenumber given by (2.40) with those given by numerical simulations and other models.

2.6.3 Comparison with numerical simulations

2.6.3.1 Numerical setup

Numerical simulations are computed with velocity-pressure formulation of a ADER-4 finite difference scheme. The problem is meshed on a uniform Cartesian grid with $\Delta x = \Delta y = 10^{-4}\ m$. A priori these schemes are not adapted to simulate the propagation through a large number of circular interfaces: (ı) the geometrical description of interfaces is poor, (ıı) the jump conditions are not enforced numerically and (ıı) non-smoothness of the solution across interfaces decreases the accuracy of the scheme. To remove these drawbacks, we use an immersed interface method [LP04, Lom10] improving the jump conditions at the interface up to the third order. Doing so ensures the efficiency of Cartesian grid methods and the accuracy of an interface meshing. The immersed interface method imposes an exclusion distance between two inclusion's centers: $b = 2a + 2.5\Delta x$.
The numerical configuration is presented in Fig.2.8. An incoming plane wave probes with normal incidence a semi infinite random domain where acquisition lines are placed along the direction of propagation. The plane wave is a Ricker with central frequency 250 kHz. The random media is made of circular inclusions ($\rho = 2610\,\mathrm{kg.m^{-3}}$, $c = 2470\ \mathrm{m.s^{-1}}$) with radius $a = 6$ mm randomly embedded in the matrix ($\rho = 2050\,\mathrm{kg.m^{-3}}$, $c = 2250\ \mathrm{m.s^{-1}}$). Note that the acoustical contrast between matrix and scatterer is particularly low. The acquisition lines are composed of 400 recorders with 0.001 m spacing. The first receiver is placed at the boundary of the random media. For each simulation 100 acquisition lines are regularly placed with 0.072 m spacing. 4 simulations are performed for each of the following concentration $\varphi = 24\%,\ 36\%, 48\%$ and 60%.
A typical seismogram obtained from a single acquisition line is provided in Fig.2.9. The coherent field is evaluated by averaging the signals recorded along the 4×100 receivers lines. The coherent part behaves as a dispersive field affected by spacial attenuation. Attenuation is estimated from the spacial decrease of the coherent amplitude spectrum $A(y, \omega)$ along the y-propagation. More precisely $\alpha(\omega) := \Im m(k_e)$ is determined by the slope of a least-square linear fit of $\ln(A(y, \omega))$. The phase velocity $c_e(\omega) := \Re e(k_e)$ is computed by applying a $\mathfrak{p}$–ω transform to the space-time coherent field, where $\mathfrak{p} = 1\,/\,c$ is the slowness of the waves. The general method is presented in [MY81, MHR88] and adapted presentation of these signal processing can be found in [CML$^+$09, CMA$^+$09]. Reliable estimations of c_e and α_e are obtained only if a sufficiently large amount of independent lines are averaged. Unfortunately, this number depends on frequency, concentration and acoustic contrast. To define a trusty frequency range, estimations

with coherent field obtained from the average of 3×100 acquisition lines are compared with the estimations obtained from the full data (Fig.2.9-right). In the frequency range $0.2 \leq ka \leq 7.5$ the discrepancy between each estimation of c_e is lower than 2 m/s whereas the discrepancy is lower than 0.5 Np/m for α_e for all concentrations.

2.6.3.2 Comparision

Estimation obtained from numerical simulation and signal processing are compared with results from the present model (Eq.2.40) and Linton-Martin model. For this latter, the implicit equation [LM05]-Eq.71 has been chosen rather than the well-known formulas [LM05]-Eq.7 or [LM05]-Eq.81 which are approximations for dilute media and low frequency range.
These two models and simulation are different in terms of geometry and source-type. Semi-infinite heterogenous domain is considered in the simulation as in Linton-Martin paper. Consequently, there is a risk to observe boundary effects in the effective wavenumber. Nevertheless [LM05]-Eq.71 was obtained in such a way that boundary effects were negligible. This is equivalent to be in an infinite domain like in the presented model. Previous comparison [CMLP12] between Linton-Martin's adaptation to the elastic case [CN10] and simulations performed in the same configuration have shown good agreement between simulation and model up to 24% what may induced that boundary do not affect the effective wavenumber's estimation from simulation (this may be due to the relatively long acquisition lines). Lastly, we suppose that the effective wavenumber must be equivalent for plane wave or point-like source. According to these remarks, all the previously mentioned differences do not forbid comparison.
The limits of the model can be presented in term of concentration and frequency (Fig.2.10). At low concentration ($\varphi = 24\%$) the two models give similar predictions what confirms that the source and geometrical configuration do not affect so much the comparison. At large frequency ($ka > 1$) the presented model is able to predict the behavior of the effective phase velocity in a larger frequency range than the Linton-Martin's model if the concentration increases. Moreover in the low-frequency limit Linton-Martin's prediction of c_e looks clearly better than the presented model. For the two models the more critical frequency domain is around resonance $ka \approx 1$. In term of attenuation, again the presented model give a more accurate prediction as the frequency and the attenuation increase. For dense medium, Linton-Martin predicts a negative attenuation around $ka \approx 0.5$ and at high frequency. This is not observed with the presented model even if its prediction is not accurate around $ka \approx 0.5$ for $\varphi > 48\%$.

2.7 Conclusion

The QCA was introduced by Lax in 1952 [Lax52] and formulated by:

$$\left\langle \phi^2(M) \right\rangle_{12} = \left\langle \phi^2(M) \right\rangle_2 . \tag{2.42}$$

This approximation is actually a statistical assumption inspired by crystalline structure according to the Lax's own words [Lax52]:

"Equation (2.42) may be referred to as the quasi-crystalline approximation since it is strictly valid in the crystalline case. The quasi-crystalline assumption is equivalent to neglect of the fluctuation of the effective field as s_2 due to a deviation of a particle s_1 from its average position. The success of this assumption is based on the approximate validity of the cellular liquids. Certainly further investigation of this assumption is necessary."

The exact validity of the QCA in the crystalline case may be understood thanks to the following argument. In the crystalline structure, all configurations maybe obtained from an arbitrary one by performing permutations between the positions of the N scatterers. Thus knowing the position of one scatterer is equivalent to knowing the position of two scatterers.
The QCA was used in a lot of works *e.g.* Wattermann-Truell [WT61], LLoyd-Bery [LB67], Linton-Martin [LM06], Conoir-Norris [CN10]. In general using the QCA involves additional assumption in order to fully close the problem. We aim at discussing the consequence of this latter. For convenience we choose to illustrate our comparison thanks to the works of Linton-Martin without recalling the equation in order to avoid interference between notations. We emphasize that A^i is the modal coefficient of the exciting fields whereas our a^i are the scattering coefficient.
In their article, the formula (54) gives a relation between averaged modal coefficients of **exciting fields** $\langle A^1 \rangle_1$ and $\langle A^2 \rangle_{12}$ which is then replaced by $\langle A^2 \rangle_2$ thanks to the QCA. At this level the problem is not completely closed because we have only one equation for two unknowns: $\langle A^1 \rangle_1$ and $\langle A^2 \rangle_2$. Thus we need the following assumption: *the averaged exciting field for a fixed scatter is the effective field.* Hence the effective field is modeled by the $\langle A^1 \rangle_1$ for arbitrarily fixed s_1. This allows us to express the coefficient $\langle A^2 \rangle_2$ in term of $\langle A^1 \rangle_1$ thanks to addition theorems involving the effective wavenumber k_e. Consequently we obtain an eigenvalue problem which permits us to deduce $\langle A^1 \rangle_1$ and k_e.

In our approach, the spirit is not so different: we do consider the effective field as the average exciting field. Nevertheless the local feature of the exciting field leads us to do this analogy only for the scatterer s_2. Inspired by the formula obtained for a single scatterer, we assume that the modal scattering amplitudes for the scatterer s_2 are $a^2 = Zd^2$ where d^2 is the modal amplitude vector for the effective field. This assumption gives an expression for an averaged modal scattering amplitude for s_1, this latter being at a position supposed to be known. Now the effective field is originally defined as the average of the field scattered by s_1 over its positions. At the end of our reasoning two averaging are performed to obtain an equation leading to the calculation of k_e and the modal amplitudes of the effective field d^s. Focusing on the formula (2.30), we see that two order of scattering occurs in the closed problem because two Z matrix act on the effective modal coefficients d. More precisely the scattering chain $i \to 2 \to 1$ is explicitly taken into account in our process involving two successive averages. In that sense it seems that such coupling are taken into account. Nevertheless we saw in

the case of far field-coupling between two scatterers formula (2.5) that such coupling is modulated by:

$$\frac{1}{1 - f^2(\pi) H_0^2(kr_{12})}.$$

This coefficient is absent in the formula (2.30). Furthermore our closure assumption implies a problem in which all approximations and their errors are confined in the terms d of the effective field. Nevertheless this modal amplitude can not be exactly determined, it is the price to pay for considering that s_2 is excited by the effective field, namely $a^2 = Zd^2$. Both expressions for d^s induced conditions on the z_n (*i.e.* on the contrast as well) and on ka. These conditions need further investigations.

The proposed formulation of the multiple scattering problem is consistent with the Foldy approximation. At higher order this formulation induces a reformulation of the closure assumption. So far it seems reliable as an alternative to the QCA as an order 2 theory.

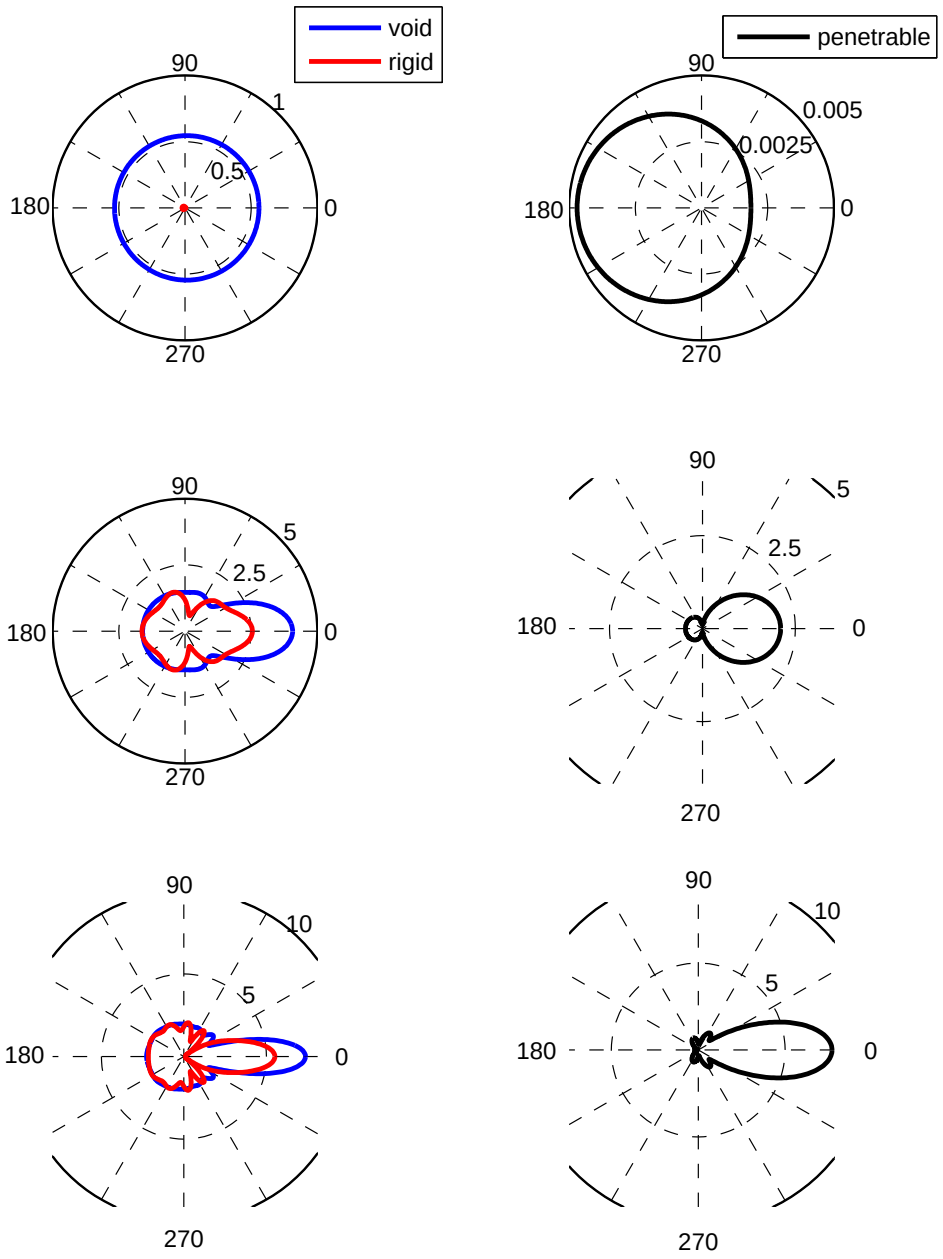

Figure 2.2: Far field pattern for impenetrable scatterers (on the left) and penetrable scatterer (on the right) obtained for small contrast ($c_1 = 1.2c_0$,$\rho_1 = 1.2\rho_0$). $k_0 a$ spans $\{0.1, \pi, 10\}$ corresponding to lines 1, 2 and 3.

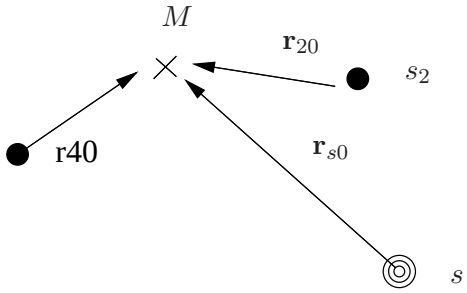

Figure 2.3: Conventions for coordinates for two scatterers

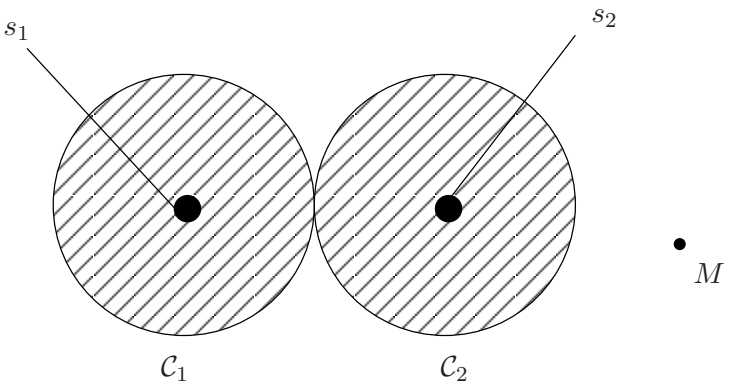

Figure 2.4: The investigations are performed for $k_0 r_{12} >> 1$, $k_0 r_{01} >> 1$, $k_0 r_{02} >> 1$ namely M outside $\mathcal{C}_1 \cup \mathcal{C}_2$ and s_j outside $\mathcal{C}_i$ for $i \neq j$.

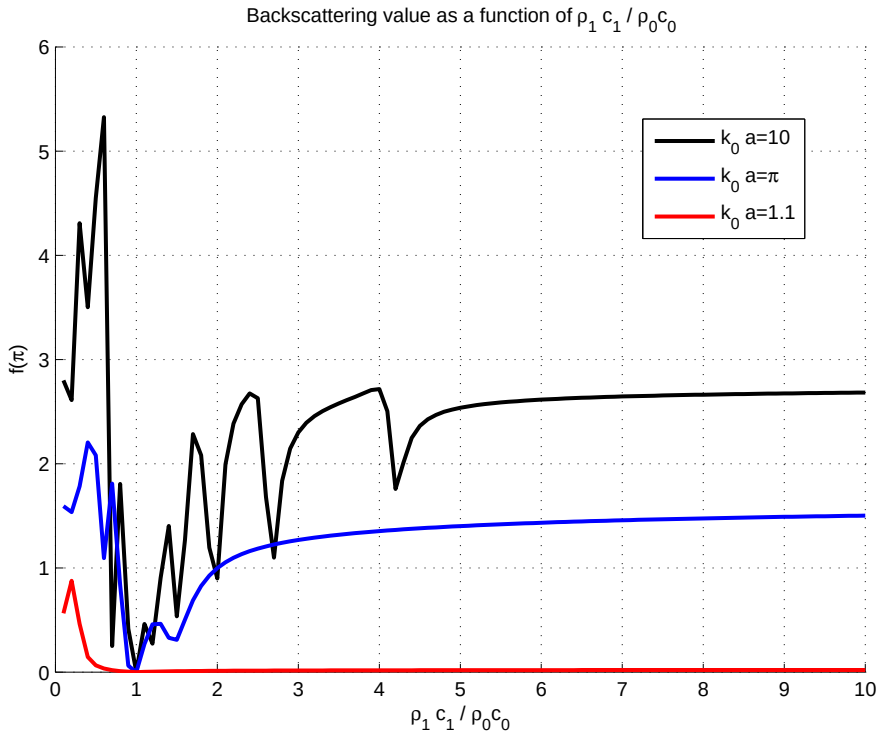

Figure 2.5: The value of the back-scattering for different $k_0 a$. The contrast $\frac{\rho_1 c1}{\rho_0 c0}$ spans $[0, 10]$.

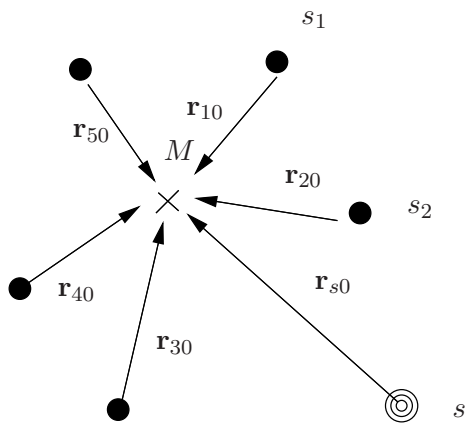

Figure 2.6: Conventions for coordinates

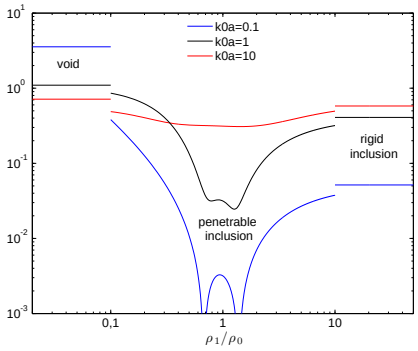

Figure 2.7: χ for $ka = 0.1,\ 1$, and 10. The horizontal lines give results for void (left side) and rigid inclusion (right side). In the center, the case of penetrable inclusion is given for $c_1/c_0 = 1 + 3/100$ and ρ_1/ρ_0 varying from 1/10 to 10.

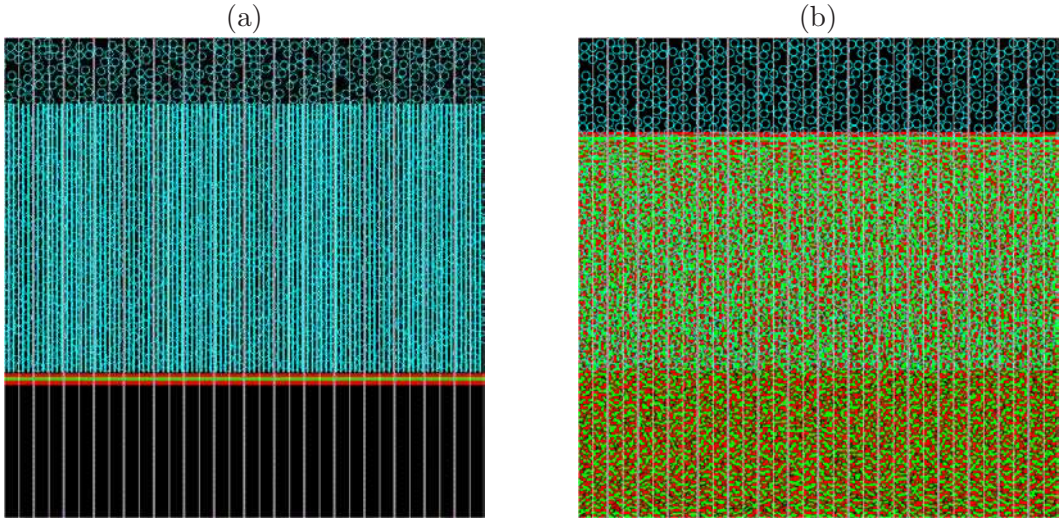

Figure 2.8: Concentration $\varphi = 48\%$, initial instant (a) and after 4000 time steps (b). The vertical columns in (a) denote the positions of receivers. Each vertical slice in (a) and (b) corresponds to a parallelized subdomain during the simulation.

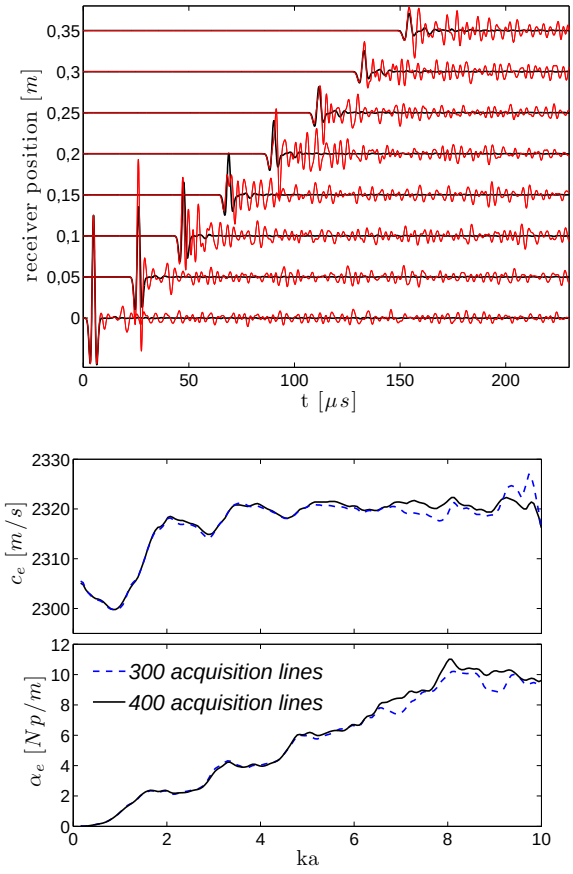

Figure 2.9: Left: signal along a single receiver line (thin red) and coherent average (thick black). Right: estimation of the phase velocity (top) and attenuation (bottom) obtained after ensemble average over 300 and 400 acquisition lines. $\varphi = 36\%$ case.

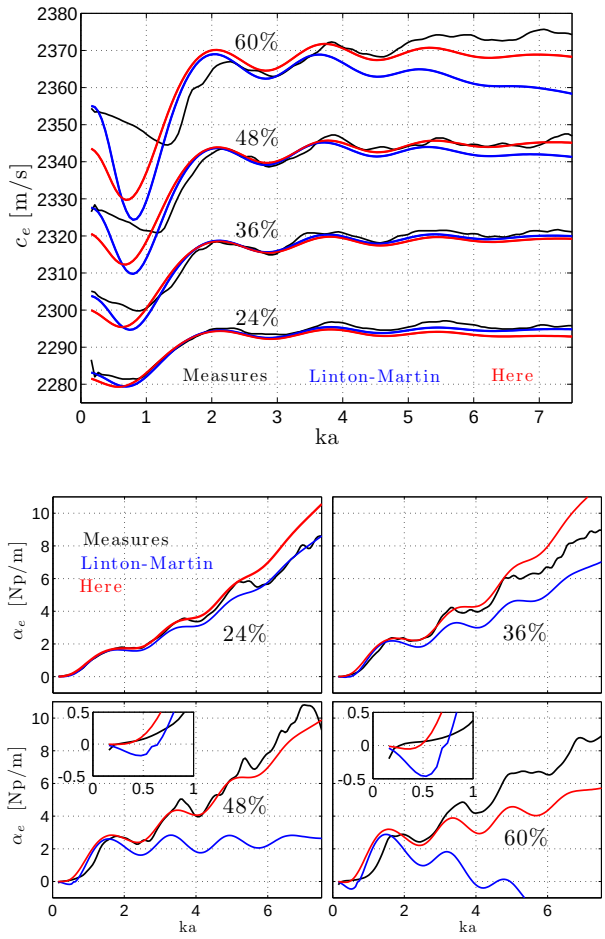

Figure 2.10: Effective phase velocity (left) and attenuation (right) obtained from simulation (black), Linton-Martin (blue) and present (red) models at various concentrations. Right: the axe's ranges are the same for all figures and the inserts is a low frequency zoom.

Chapter 3

Cloaking of bending waves in Kirchhoff-Love thin plates

3.1 Introduction

Controlling and limiting the vibration of thin plates has a multitude of applications in structural acoustics and vibration. It is a subject that has received great attention in the literature where a variety of techniques have been proposed to reduce the overall structural noise. A related topic is that of *cloaking* a region of space, so that objects within this region are not seen or affected by incoming waves. Both passive [PSS06, LP08] and active [VMO11, VMOS12, Vas] methods have been proposed. The former requires complex metamaterials in order to guide waves around the region whereas the latter requires knowledge of the incident wave in order to activate wave sources in order to nullify the total field in a given region. Importantly the sources must be non-radiating. Recently explicit forms for the required source coefficients were given by Norris *et al.* in the contexts of scalar Helmholtz [NS11] in the two dimensional scenario. Another important case in terms of applications is that of thin plates. Here we consider this problem in the context of the Kirchhoff plate theory, an approximate theory requiring that the plate thickness h is small compared to other characteristic length scales, but not so thin that the lateral deflection of the plate is comparable to h. We assume a plate of uniform thickness h. Kirchhoff theory is notable in that shear energy is neglected and there is uncoupled membrane-bending action. Improvements to the theory such as Mindlin-Reissner model, could be considered but the theory is extremely accurate in many physical applications in structural acoustics.

3.2 Basics on thin plate theory

We choose to define thin plates from the definition of the "surfaces déformables" introduced by the Cosserat brothers.

Définition 3.1 *A deformable surface is a continuous 2D manifold $\mathcal{S}$. Let* (x_1, x_2)

denote the curvilinear coordinates, the points $M(x_1, x_2)$ endowed with 3 vectors called the directors $\Big(\mathbf{d_1}(x_1, x_2), \mathbf{d_2}(x_1, x_2), \mathbf{d_3}(x_1, x_2)\Big)$

As a consequence of this definition the transformations of a deformable surface include not only the displacement of the points $M \in \mathcal{S}$ but also the rotation of each rigid trihedral $\Big(\mathbf{d_1}, \mathbf{d_2}, \mathbf{d_3}\Big)$ as seen in the general introduction. Below the definition of thin plate follows.

Définition 3.2 *A thin plate is a 3D continuum with initial configuration limited by two parallel plans so that the distance h between the latter is supposed to be small compared to other characteristic lengths:*

$$\mathcal{P} : \Big\{(X_1, X_2, X_3) \in \mathbb{R}^3, -\frac{h}{2} \leq X_3 \leq \frac{h}{2}\Big\},$$

where X_i are the curvilinear coordinates of the initial configuration. The plane $\mathcal{S}$ defined by $X_3 = 0$ is the mean plane.

The mean plane of the plate is identified with a connected domain of $\mathbb{R}^2$. In the previous definition, the mean plane corresponds exactly to geometrical one because we suppose that the mass density is uniform for the sake of simplicity. If it is not the case, then the mean plane is defined as the set of the mass centers.

The theory generally take into account the particular geometry of the plates thanks to the theory of differentiable manifold. Hence the derivatives shall be replaced by the covariant derivatives defined by the Christoffel symbols given by the metric associated to the particular shape of the plate. We will go back on theses notions in the latter chapter. For the sake of simplicity we restrict our overview in the case where the initial configuration is flat therefore the coordinates will be the Cartesian or the polar ones.

The purpose of this section is to establish the wave equation for bending waves in such a structure. For such waves, the inertial terms induced by rotation are neglected. In the following, we remind the expression of the strain tensor and the static equilibrium equations in the general case of Mindlin-Reissner plate under the small strain assumption. Then we deduce the equations for Love-Kirchhoff thin plates which gives the same static equations except for boundary conditions and we recall the elasticity for such a plate. Finally, we establish the wave equation for bending waves after calculation of the inertial terms and we recall the associated separated eigenfunction for polar coordinates.

3.2.1 Strain of thin plates

Here we recall the strain tensor as a function of the displacement $\overline{\mathbf{u}}$ of the mean plane and of the rotation θ of the directors.

3.2.1.1 Displacement and hypotheses

According to our restriction to flat initial configuration, we decompose the transformation in a local basis of $\mathbb{R}^3$ denoted $(\mathbf{e_1}, \mathbf{e_2}, \mathbf{e_3})$:

$$\varphi(X_1, X_2, X_3) = x_i(X_1, X_2, X_3)\mathbf{e_i}.$$

Hence the components of the displacement are:

$$u_i(X_1, X_2, X_3) = x_i(X_1, X_2, X_3) - X_i.$$

These components are supposed to fulfill the following hypothesis.

Hypothesis 3.2.1 *Let M be an arbitrary point of the plates, then the displacement field at M is decomposed into two parts:*

- *the displacement $\overline{\mathbf{u}}$ of M' (projection of M on the mean plane)*
- *a rotation $\boldsymbol{\theta}$ around M.*

In other words, the displacement $\mathbf{u}$ is written under the form:

$$\mathbf{u} = \begin{pmatrix} u_1 = \overline{u}_1(X_1, X_2) + X_3\theta_1(X_1, X_2) \\ u_2 = \overline{u}_2(X_1, X_2) - X_3\theta_2(X_1, X_2) \\ u_3 \end{pmatrix}$$

This assumption means that the tangent basis of any layer are all identical to the tangent basis of the mean plane.
The vector $\mathbf{e_3}$ is the normal vector of the mean plane and we will denote it by $\mathbf{n}$ for sake of clarity. In order to distinguish the operation in the mean plane from those according to $\mathbf{n}$, we introduce the following notation that we will use in this chapter:

$$\nabla\mathbf{u} = \nabla_\beta u_\alpha \mathbf{e}_\alpha \otimes \mathbf{e}_\beta + \nabla_\beta u_3 \mathbf{e}_3 \otimes \mathbf{e}_\beta + \nabla_3 u_\alpha \mathbf{e}_\alpha \otimes \mathbf{e}_3 + \nabla_\beta u_3 \mathbf{e}_3 \otimes \mathbf{e}_3,$$

for $\alpha, \beta \in \{1, 2\}$ and the Einstein convention for summation.

3.2.1.2 Strain tensor of a thin plate

Even if the thickness of a thin plate is supposed to be small, the plate remains a 3D continuum therefore its Cauchy small strain tensor is expressed by:

$$\boldsymbol{\varepsilon} = \frac{1}{2}(\nabla\mathbf{u} + \nabla\mathbf{u}^t).$$

In general the component u_3 can be approximated by $\overline{u}_3$ in the calculation of $\varepsilon_{\alpha 3}$. Basically this approximation is justified provided that the variation of u_3 in the direction orthogonal to the mean-plan is almost zero. The calculation of ε_{33} will be performed

under the assumption of in-plane stress (see below). Applying the assumption for the displacement field, we have:

$$\begin{array}{rcl} \varepsilon_{\alpha\beta} & = & \frac{1}{2}(\nabla_\beta \overline{u}_\alpha + \nabla_\alpha \overline{u}_\beta) + \frac{1}{2}(\nabla_\beta \theta_\alpha + \nabla_\alpha \theta_\beta) \\ \varepsilon_{\alpha 3} & = & \varepsilon_{3\alpha} = \frac{1}{2}(\theta_\alpha + \nabla_\alpha \overline{u}_3) \\ \varepsilon_{33} & = & \nabla_3 u_3 = \nabla_3 \overline{u}_3(X_1, X_2). \end{array}$$

Hence we distinguish two main contributions in the strain tensor. The first one is the in-plane strain of the mean plane which we shall denote $\overline{\boldsymbol{\varepsilon}}$. The second one corresponds to the strain $\overline{\boldsymbol{\kappa}}$ resulting from the bending of the mean plane and corresponding to a modification of its curvature. Accordingly to this remark we give the definition of each terms:

$$\overline{\varepsilon}_{\alpha\beta} := \frac{1}{2}(\nabla_\beta \overline{u}_\alpha + \nabla_\alpha \overline{u}_\beta), \qquad \overline{\kappa}_{\alpha\beta} := \frac{1}{2}(\nabla_\beta \theta_\alpha + \nabla_\alpha \theta_\beta), \qquad \varepsilon_{\alpha\beta} = \overline{\varepsilon}_{\alpha\beta} + \overline{\kappa}_{\alpha\beta} X_3.$$

3.2.2 Equilibrium equations

3.2.2.1 Kirchhoff assumption

In a 3D continuum we can decompose the stress into two parts, the in-plane stresses and the out-of-plane stresses:

$$\boldsymbol{\sigma} = \begin{pmatrix} \sigma_{11} & \sigma_{12} & 0 \\ \sigma_{21} & \sigma_{22} & 0 \\ 0 & 0 & 0 \end{pmatrix} + \begin{pmatrix} 0 & 0 & \sigma_{13} \\ 0 & 0 & \sigma_{23} \\ \sigma_{31} & \sigma_{32} & \sigma_{33} \end{pmatrix}$$

With our convention for the plate, we have $\sigma_{33} = 0$ on the surfaces defined by $X^3 = \pm h$. The thickness of the plates suggest us to assume the following hypothesis.

Hypothesis 3.2.2 *The Kirchhoff assumption affirms that each layer of the plate with infinitesimal thickness are in a in-plane stress state.*

This assumption is not necessarily verified for a given thin plate and the theory could be developed without it. However it simplifies the formulation of the problem and especially the virtual powers. Henceforth every results will be formulated accordingly to Kirchhoff assumption.

3.2.2.2 Thickness averaged forces

While deriving the virtual powers acting on layer with infinitesimal thickness, we do not need to consider the normal stresses σ_{33} due to the Kirchhoff assumption. These virtual powers are expressed by means of the (thickness averaged) moment, shear and

laminar components of the forces. They are defined by:

$$M_{\alpha\beta}(\mathbf{X}) = \int_{-h/2}^{h/2} X_3 \sigma_{\alpha\beta}(\mathbf{X}, X_3) dX_3, \qquad \text{(bending moment)} \tag{3.1}$$

$$Q_{\alpha}(\mathbf{X}) = \int_{-h/2}^{h/2} \sigma_{\alpha 3}(\mathbf{X}, X_3) dX_3, \qquad \text{(shear force)} \tag{3.2}$$

$$N_{\alpha\beta}(\mathbf{X}) = \int_{-h/2}^{h/2} \sigma_{\alpha\beta}(\mathbf{X}, X_3) dX_3 \qquad \text{(laminar force)}, \tag{3.3}$$

where $\mathbf{X} = (X_1, X_2)$ The mechanical interpretations of the components of this tensors are found in the literature (*e.g.* [Rak09]).

3.2.2.3 Equilibrium equations

Virtual Power Principle (VPP)
Let denote $\mathbf{p}$, $\mathbf{m}$ and q respectively the laminar surface force, the laminar surface moment and the normal surface force acting on the mean plane $\mathcal{S}$. On the boundary of the mean plane $\partial\mathcal{S}$ we denote $\overline{\mathbf{p}}$, $\overline{\boldsymbol{\tau}}$ and $\overline{q}$ respectively the laminar force, the tangent moment and the transverse force per unit length. Let $\partial\mathcal{S}_u$, $\partial\mathcal{S}_\theta$ and $\partial\mathcal{S}_3$ be three subset of the boundary of the mean plane on which the displacement $\overline{\mathbf{u}}$, the rotation field $\boldsymbol{\theta}$ and the component u_3 are respectively supposed to be fixed.
We define the following function spaces:

$$\begin{aligned}
H^1(\mathcal{S}) &:= \Big\{ f \in \mathcal{L}^2(\mathcal{S}), f' \in \mathcal{L}^2(\mathcal{S}) \Big\} \\
V_u &:= \Big\{ \mathbf{v} \in \mathbb{R}^2, v_\alpha \in H^1(\mathcal{S}), \mathbf{v} = 0 \text{ on } \partial\mathcal{S}_u \Big\} \\
V_\theta &:= \Big\{ \boldsymbol{\theta} \in \mathbb{R}^2, \theta_\alpha \in H^1(\mathcal{S}), \boldsymbol{\theta} = 0 \text{ on } \partial\mathcal{S}_\theta \Big\} \\
V_3 &:= \Big\{ v \in \mathbb{R}, v \in H^1(\mathcal{S}), v = 0 \text{ on } \partial\mathcal{S}_3 \Big\}
\end{aligned}$$

We state the principle without going further into the details and into the mathematical definitions.

Theorem 3.2.1 *For all virtual velocity field, the sum of the virtual powers of the internal deformation and the virtual powers of the inertial forces are equal to the virtual power of the external forces. We can show that it gives:*

$$\begin{aligned}
&\int_{\mathcal{S}} \hat{\overline{\mathbf{u}}} \cdot \Big(\text{div } \mathbf{N} + \mathbf{p} - \rho h \frac{\partial^2 \overline{\mathbf{u}}}{\partial t^2} \Big) d\mathcal{S} + \int_{\mathcal{S}} \hat{\boldsymbol{\theta}} \cdot \Big(\text{div } \mathbf{M} - \mathbf{Q} + \mathbf{m} - \frac{\rho h^3}{12} \frac{\partial^2 \overline{\boldsymbol{\theta}}}{\partial t^2} \Big) d\mathcal{S} + \int_{\mathcal{S}} \hat{\overline{u}}_3 (\text{div } \mathbf{Q} + q) d\mathcal{S} \\
&\quad + \int_{\partial\mathcal{S}} \hat{\overline{\mathbf{u}}} \cdot \big(\overline{\mathbf{p}} - \mathbf{N}(\mathbf{n}) \big) dl + \int_{\partial\mathcal{S}} \hat{\boldsymbol{\theta}} \cdot \big(\overline{\boldsymbol{\tau}} - \mathbf{M}(\mathbf{n}) \big) dl + \int_{\partial\mathcal{S}} \hat{\overline{u}}_3 \big(\overline{q} - \mathbf{Q}(\mathbf{n}) \big) dl = 0
\end{aligned} \tag{3.4}$$

for every $(\hat{\overline{\mathbf{u}}}, \hat{\boldsymbol{\theta}}, \hat{\overline{u}}_3) \in V_u \times V_\theta \times V_3$. *The operator divergence* div *is defined for coordinates on to the mean plane, in other words it contains partial derivatives of* X_α.

The equation (3.4) correspond to the equation for the Mindlin-Reissner thin plates. As we do not investigate the active cloaking in this context, we do not go further. We will use them only deduce the equation for the Love-Kirchhoff thin plates.

3.2.3 Elastic Love-Kirchhoff thin plates

3.2.3.1 Equilibrium equations

We begin with the definition of the Love-Kirchhoff thin plate.

Définition 3.3 *A Love-Kirchhoff thin plate corresponds to a thin plate on which we suppose the conservation of the normal* $\mathbf{n}$ *during the transformation. In other word,* $\mathbf{n}$ *remains orthogonal to the mean plan in the deformed state.*
In that case the transverse shift is zero:

$$\varepsilon_{\alpha 3} = 0 \Longrightarrow \theta_\alpha = -\nabla_\alpha \overline{u}_3. \tag{3.5}$$

Hence the shear stress $\mathbf{Q}$ has no effect.
The number of degree of freedom is decreased compared to the general case. Indeed the equation (3.5) means that the rotation $\boldsymbol{\theta}$ and the displacement $\overline{\mathbf{u}}$ are no more independent. Injecting this relations in the VPP, the equation (3.4) take the following form:

$$\int_{\mathcal{S}} \hat{\overline{\mathbf{u}}}\cdot\Big(\text{div } \mathbf{N}+\mathbf{p}-\rho h\frac{\partial^2\overline{\mathbf{u}}}{\partial t^2}\Big)d\mathcal{S}+\int_{\mathcal{S}} \nabla\hat{\overline{u}}_3\cdot\Big(\text{div } \mathbf{M}-\mathbf{Q}+\mathbf{m}-\frac{\rho h^3}{12}\frac{\partial^2\overline{\boldsymbol{\theta}}}{\partial t^2}\Big)d\mathcal{S}+\int_{\mathcal{S}} \hat{\overline{u}}_3(div\ \mathbf{Q}+q)d\mathcal{S}$$
$$+\int_{\partial\mathcal{S}} \overline{\mathbf{u}}\cdot\big(\overline{\mathbf{p}}-\mathbf{N}(\mathbf{n})\big)dl-\int_{\partial\mathcal{S}} \nabla_\alpha\overline{u}_3\cdot\big(\overline{\boldsymbol{\tau}}-\mathbf{M}(\mathbf{n})\big)dl+\int_{\partial\mathcal{S}} \overline{u}_3\big(\overline{q}-\mathbf{Q}(\mathbf{n})\big)dl=0, \tag{3.6}$$

for every $(\overline{\mathbf{u}},\boldsymbol{\theta},\overline{u}_3)\in V_u\times V_\theta\times V_3$.
Only the fourth term is modified by the Love-Kirchhoff model therefore the local equations remains unchanged.

3.2.4 Elasticity for Love-Kirchhoff thin plates

The purpose of this paragraph is to recall basics on the constitutive law for the plates. According to the definition of the Love-Kirchhoff thin plate, the shear force has no effect. The energy conservation laws of thermomechanic ensure that the internal stress such as the laminar force $\mathbf{N}$ and the bending moment $\mathbf{M}$ are both obtained by differentiating the elastic density potential ψ per unit surface in the following sense:

$$N_{\alpha\beta}=\frac{\partial\psi}{\partial\overline{\varepsilon}_{\alpha\beta}}(\overline{\varepsilon}_{\alpha\beta},\overline{\kappa}_{\alpha\beta}),\qquad M_{\alpha\beta}=\frac{\partial\psi}{\partial\overline{\kappa}_{\alpha\beta}}(\overline{\varepsilon}_{\alpha\beta},\overline{\kappa}_{\alpha\beta})$$

The shear force $\mathbf{Q}$ have no effect therefore it can not be determined thanks to a constitutive law but shall be deduced from the local equations and the boundary conditions

whenever we find $\mathbf{M}$.
The most simple case occurs for a quadratic potential energy:

$$\psi(\overline{\varepsilon}_{\alpha\beta}, \overline{\kappa}_{\alpha\beta}) = \frac{1}{2}\Big(A^{\alpha\beta\gamma\eta}\overline{\varepsilon}_{\alpha\beta}\overline{\varepsilon}_{\gamma\eta} + 2C^{\alpha\beta\gamma\eta}\overline{\varepsilon}_{\alpha\beta}\overline{\kappa}_{\gamma\eta} + D^{\alpha\beta\gamma\eta}\overline{\kappa}_{\alpha\beta}\overline{\kappa}_{\gamma\eta}\Big),$$

which induces linear constitutive laws:

$$N_{\alpha\beta} = A^{\alpha\beta\gamma\eta}\overline{\varepsilon}_{\gamma\eta} + C^{\alpha\beta\gamma\eta}\overline{\kappa}_{\gamma\eta}, \qquad M_{\alpha\beta} = C^{\alpha\beta\gamma\eta}\overline{\varepsilon}_{\gamma\eta} + D^{\alpha\beta\gamma\eta}\overline{\kappa}_{\gamma\eta}. \tag{3.7}$$

The coefficients $A^{\alpha\beta\gamma\eta}, C^{\alpha\beta\gamma\eta}$ and $D^{\alpha\beta\gamma\eta}$ are directly calculated from the Hooke's law of three-dimensional continuum and the relations (3.1) and (3.3). Hence we have:

$$N_{\alpha\beta} = h\overline{E}^{\alpha\beta\gamma\eta}\overline{\varepsilon}_{\gamma\eta}, \qquad M_{\alpha\beta} = \frac{h^3}{12}\overline{E}^{\alpha\beta\gamma\eta}\overline{\kappa}_{\gamma\eta}. \tag{3.8}$$

The coefficients $\overline{E}^{\alpha\beta\gamma\eta}$ are defined thanks to the Young modulus E and the Poisson ratio ν:

$$\overline{E}^{\alpha\beta\gamma\eta} = \frac{E}{1-\nu^2}\Big[\nu g^{\alpha\beta}g^{\gamma\eta} + \frac{1-\nu}{2}\big(g^{\alpha\gamma}g^{\beta\eta} + g^{\alpha\eta}\delta^{\beta\gamma}\big)\Big],$$

with $g^{\alpha\beta}$ is the metric of the coordinates basis of the mean plane. If the mean plane is actually planar, then the metric reduces to the identity matrix. Thus for $\alpha \neq \beta$, the components reduces to:

$$\begin{aligned} \overline{E}^{\alpha\alpha\beta\beta} &= \frac{E\nu}{1-\nu^2}, \\ \overline{E}^{\alpha\beta\alpha\beta} &= \overline{E}^{\alpha\beta\beta\alpha} = \frac{E}{2(1+\nu)}, \\ \overline{E}^{\alpha\alpha\alpha\alpha} &= \frac{E}{1-\nu^2}. \end{aligned} \tag{3.9}$$

3.2.5 Bending waves in thin plates

3.2.5.1 Harmonic wave equation

From now we detail the bending wave equation for the plate as we did for the Helmholtz equation in the general introduction.
Consider an unbounded flat thin plate of thickness h in the context of the Kirchhoff theory. The axes x_1 and x_2 of the Cartesian reference system $(\mathbf{O}, x_1, x_2, x_3)$ lie on the middle plane of the plate whereas x_3 is the out-of-plane (normal) coordinate. It is also helpful to define $\mathbf{x} = (x_1, x_2, 0)$ and we denote the out-of-plane displacement as $W(\mathbf{x}, t)$. The differential operators now act only on $\mathbf{x}$ so that there are no more confusions and we use the Latin indexes. In the Love-Kirchhoff plates the inertial terms of the rotation $\boldsymbol{\theta}$ are negligible. Furthermore, we suppose that no external forces act on the plate, therefore the VPP (3.6) gives:

$$\frac{h^3}{12}\int_{\mathcal{S}} \overline{E}^{\alpha\beta\lambda\mu}\nabla_\mu\left(\nabla_\lambda W\right)\nabla_\beta\left(\nabla_\alpha\hat{W}\right)d\mathcal{S} + h\int_{\mathcal{S}}\rho\frac{\partial^2 W}{\partial t^2}\hat{W}d\mathcal{S} = 0. \tag{3.10}$$

Then we integrate by part twice the first term. As the mean plane is supposed to be plan, the formulae (3.9) are available and (3.11) reduces to:

$$\frac{Eh^3}{12(1-\nu^2)}\int_{\mathcal{S}}\hat{W}\nabla^2\nabla^2 W d\mathcal{S}+h\int_{\mathcal{S}}\rho\frac{\partial^2 W}{\partial t^2}\hat{W}d\mathcal{S}=0 \tag{3.11}$$

The constant $D=Eh^3/(12(1-\nu^2))$ is the flexural rigidity of the plates. The equation (3.11) is fulfilled for every $\hat{W}$ therefore we obtain the local equations for the plate:

$$D\nabla^2\nabla^2 W=\rho h\frac{\partial^2 W}{\partial t^2}$$

Let us now assume time harmonic behavior, $W(\mathbf{x},t)=\Re\{w(x_1,x_2)e^{-i\omega t}\}$ so that

$$(\nabla^2\nabla^2-k^4)w=(\nabla^2+k^2)(\nabla^2-k^2)w=0 \tag{3.12}$$

where the wavenumber k is defined via the dispersion relation $k^4=\omega^2\rho h/D$.

3.2.5.2 Eigenfunction and properties

In polar coordinates $\mathbf{r}=r(\cos\theta\mathbf{e}_1+\sin\theta\mathbf{e}_1)$ and after separtation of variables, the eigenfunction of the harmonic wave equation (3.12) are defined for $n\in\mathbb{Z}$:

$$U_n^{\pm}(\mathbf{r})=J_n(kr)e^{\pm in\theta}, \qquad \mathcal{U}_n^{\pm}(\mathbf{r})=I_n(kr)e^{\pm in\theta}, \tag{3.13}$$

$$V_n^{\pm}(\mathbf{r})=H_n^{(1)}(kr)e^{\pm in\theta}, \qquad \mathcal{V}_n^{\pm}(\mathbf{r})=\frac{2i}{\pi}K_n(kr)e^{\pm in\theta} \tag{3.14}$$

where $H_n^{(1)}(kr)=J_n(kr)+iY_n(kr)$ is the Hankel function of the first kind and n^{th} order, $I_n(kr)=i^{-n}J_n(ikr)$ and $2K_n(kr)=\pi i^{n+1}H_n^{(1)}(ikr)$. The factor used in the $\mathcal{V}_n^{\pm}$ is for convenience. We denote the following derivative functions as

$$U_n^{\pm\prime}(\mathbf{z})=J_n'(k|\mathbf{z}|)e^{\pm in\arg\mathbf{z}}, \qquad \mathcal{U}_n^{\pm\prime}(\mathbf{z})=I_n'(k|\mathbf{z}|)e^{\pm in\arg\mathbf{z}} \tag{3.15}$$

and note that the properties

$$U_n^{\pm}(-\mathbf{z})=(-1)^nU_n^{\pm}(\mathbf{z}), \qquad \mathcal{U}_n^{\pm}(-\mathbf{z})=(-1)^n\mathcal{U}_n^{\pm}(\mathbf{z}), \tag{3.16}$$

$$V_n^{\pm}(-\mathbf{z})=(-1)^nV_n^{\pm}(\mathbf{z}), \qquad \mathcal{V}_n^{\pm}(-\mathbf{z})=(-1)^n\mathcal{V}_n^{\pm}(\mathbf{z}), \tag{3.17}$$

The functions $\mathcal{U}_n^{\pm}$ and $\mathcal{V}_n^{\pm}$ describe evanescent solutions whereas $U_n^{\pm}$ and $V_n^{\pm}$ does propagates. We emphasize that all of these functions satisfy the Graf's theorem introduced in chapter 1:

First introduce Graf's addition theorems in the form:

$$V_l^{+}(\mathbf{x}-\mathbf{y})=\sum_{n=-\infty}^{\infty}\begin{cases}V_n^{+}(\mathbf{x})U_{n-l}^{-}(\mathbf{y}), & |\mathbf{x}|>|\mathbf{y}|,\\ U_n^{+}(\mathbf{x})V_{n-l}^{-}(\mathbf{y}), & |\mathbf{x}|<|\mathbf{y}|,\end{cases} \tag{3.18}$$

and

$$\mathcal{V}_l^{+}(\mathbf{x}-\mathbf{y})=\sum_{n=-\infty}^{\infty}\begin{cases}\mathcal{V}_n^{+}(\mathbf{x})\mathcal{U}_{n-l}^{-}(\mathbf{y}), & |\mathbf{x}|>|\mathbf{y}|,\\ \mathcal{U}_n^{+}(\mathbf{x})\mathcal{V}_{n-l}^{-}(\mathbf{y}), & |\mathbf{x}|<|\mathbf{y}|,\end{cases} \tag{3.19}$$

The form is slightly different from the first chapter because it is expressed for a difference of a vector, that is why the upperscript can be the minus sign.

3.2.6 Scattering by cylindrical inhomogeneity

We consider a circular region of inhomogeneity with radius a perfectly included in an infinite plate. The exterior and the interior will be respectively denoted by 0 and 1 so that the properties in each region are D_i, ρ_i, ν_i and h_i for $i = 0, 1$. Furthermore we restrict our study to time harmonic motion and the wavenumbers will be denoted by k_0 and k_1. For the sake of simplicity that the inhomogeneity is located at the center of the polar coordinates (r, θ). The incoming waves is supposed to be regular so that:

$$w_{inc}(\mathbf{x}) = \sum_{n=-\infty}^{\infty} \mathcal{A}_n^U U_n^+(k_0\mathbf{x}) + \mathcal{A}_n^{\mathcal{U}} \mathcal{U}_n^+(k_0\mathbf{x}).$$

For example if w_{inc} is an unitary plane wave propagating in the direction ψ, $w_{inc}(\mathbf{x}) = \exp\Big(ikr\cos(\theta - \psi)\Big)$, then the Jacobi identity gives:

$$\mathcal{A}_n^U = i^n \exp(-in\psi) \quad \text{and} \quad \mathcal{A}_n^{\mathcal{U}} = 0.$$

The scattered field w_0 (fulfilling Sommerfeld condition) and the (regular) field inside the inhomogeneity w_1 are:

$$w_0(\mathbf{x}) = \sum_{n=-\infty}^{\infty} A_n V_n^+(k_0\mathbf{x}) + B_n \mathcal{V}_n^+(k_0\mathbf{x}), \quad |\mathbf{x}| \geq a$$
$$w_1(\mathbf{x}) = \sum_{n=-\infty}^{\infty} C_n U_n^+(k_1\mathbf{x}) + E_n \mathcal{U}_n^+(k_1\mathbf{x}), \quad |\mathbf{x}| \leq a.$$

As in the chapter on the multiple scattering, we wish to determine the coefficients A_n, B_n, C_n and E_n thanks to the given $\mathcal{A}_n^U$ and $\mathcal{A}_n^{\mathcal{U}}$ using the continuity conditions at the interface $|\mathbf{x}| = a$. According to Kirchhoff theory, these conditions are those of continuity of the displacement field w, its normal derivatives $\dfrac{\partial w}{\partial r}$, the normal components M_r^i and Q_r^i of the bending moment $\mathbf{M}^i$ and the shear force $\mathbf{Q}^i$ of each region. The latter two quantities are expressed in polar coordinates by:

$$M_r^i = -D_i\Big[\frac{\partial^2 w}{\partial r^2} + \nu_i\Big(\frac{1}{r}\frac{\partial w}{\partial r} + \frac{1}{r^2}\frac{\partial^2 w}{\partial \theta^2}\Big)\Big],$$

$$Q_r^i = -D_i\frac{\partial}{\partial r}\Delta w - D_i(1-\nu_i)\frac{1}{r^2}\frac{\partial^2}{\partial\theta^2}\Big(\frac{\partial w}{\partial r} - \frac{w}{r}\Big).$$

Applying the orthogonality conditions leads to the system of equations $\mathbf{FY} = \mathbf{GA}$ where:

$$\mathbf{F} = \begin{pmatrix} H_n(\alpha_0) & K_n(\alpha_0) & -J_n(\alpha_1) & -I_n(\alpha_1) \\ H_n'(\alpha_0) & K_n'(\alpha_0) & -\kappa J_n'(\alpha_1) & -\kappa I_n'(\alpha_1) \\ S_{H_n}^0 & S_{K_n}^0 & -DS_{J_n}^1 & -DS_{I_n}^1 \\ T_{H_n}^0 & T_{K_n}^0 & -DT_{J_n}^1 & -DT_{I_n}^1 \end{pmatrix},$$

and

$$\mathbf{Y} = \begin{pmatrix} A_n \\ B_n \\ C_n \\ E_n \end{pmatrix}, \quad \mathbf{G} = - \begin{pmatrix} J_n(\alpha_0) & I_n(\alpha_0) \\ J_n'(\alpha_0) & I_n'(\alpha_0) \\ S^0_{J_n} & S^0_{I_n} \\ T^0_{J_n} & T^0_{I_n} \end{pmatrix}, \quad \mathbf{A} = \begin{pmatrix} \mathcal{A}_n^U \\ \mathcal{A}_n^{\mathcal{U}} \end{pmatrix}.$$

The prime denotes differentiation with respect to the argument of the considered function, and we have defined $\kappa = k_1/k_0$, $\alpha_i = k_i a$, $D = D_1/D_0$. We have used the following notation [WJP11]:

$$\begin{aligned} S^i_{X_n} &= \Big[n^2(1-\nu_i) \mp \alpha_i^2\Big] X_n(\alpha_i) - (1-\nu_i)\alpha_i X_n'(\alpha_i), \\ T^i_{X_n} &= n^2(1-\nu_i) X_n(\alpha_i) - \Big[n^2(1-\nu_i) \pm \alpha_i^2\Big] \alpha_i X_n(\alpha_i), \end{aligned}$$

in which the upper sign is taken for $X_n = J_n$ or H_n and the lower sign for the others.

3.3 Active cloaking

3.3.1 Problem overview

We consider an infinite thin plate as in the previous section for which the notations remain valid. Furthermore we suppose that an incoming wave $\tilde{w}$ is propagating in the plate and we investigate the active cloaking we could perform by mean of M source fields. For that we have to suppose that we know exactly all the features of the field $\tilde{w}$. The active cloaking system considered here consists of array of M point-like multipole sources located at position $\mathbf{x}_m \in \mathbb{R}^2$ for $m \in \{1, \ldots, M\}$. The active sources are in the exterior region with respect to the cloaked region C and this type of cloaking may be called 'active exterior cloaking'. By virtue of destructive interference between the source fields and the incoming field, the total wave amplitude vanishes in the cloaked region $\mathcal{C}$ therefore defects in this region do not scatter and are undetectable by the incoming wave. The advantage of this cloaking device are:

- the cloaked region is not completely surrounded by a single cloaking device;
- only a small number of active sources are needed;
- the procedure works for broadband input sources;
- the cloaking effect is independent of the location of the scatterer in the cloaking region.

A disadvantage of this approach is that the source field may become uncontrollably large in the vicinity of the sources positions. Realistically these would be replaced by regions of finite extent and thus their magnitude would be reduced. An other inconvenient is that the incident field has to be known. Nevertheless we emphasize that the expressions require only the expansion of the incident field in the basis of eigenfunctions (3.13) and (3.14).

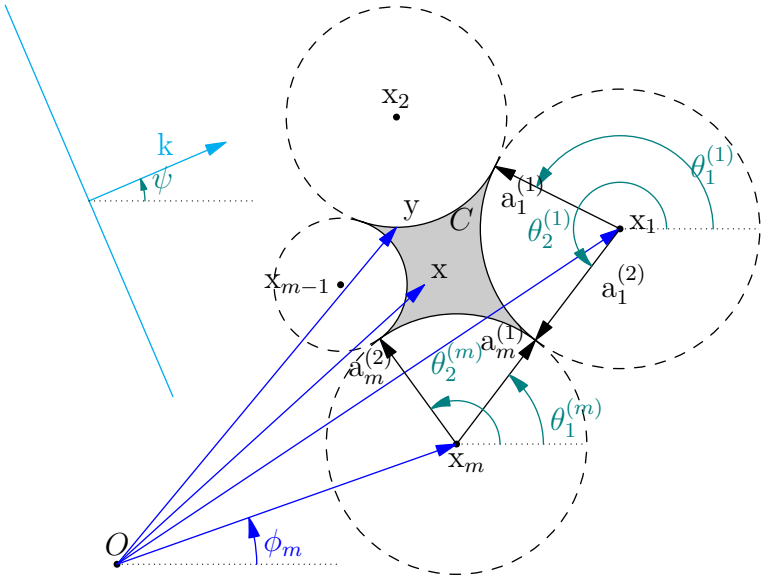

Figure 3.1: Insonification of the actively cloaked region $\mathcal{C}$ generated by M active sources at $\mathbf{x}_m$, $m \in \{1, \ldots, M\}$. The region $\mathcal{R}$ is defined as the exterior of the dashed circular arcs. The incident field in this case is a plane wave vector $\mathbf{k}$ in the direction ψ.

The shaded region in figure 3.1 is the cloaked zone $\mathcal{C}$ generated by the M sources. The boundary of $\mathcal{C}$ is the closed union of the circular arcs $\{a^{(m)}, \theta_1^{(m)}, \theta_2^{(m)}\}$ related to the source $\mathbf{x}_m$. Note that this circular arcs will be involved because of the Graf's addition theorem. In the general case $a^{(m)}, \theta_1^{(m)}$ and $\theta_2^{(m)}$ are distinct for different values of m. The figure 3.1 shows the problem for incident plane waves but the solution will be derived for arbitrary incident fields. We thus wish to determine the active source field w_d which will nullify the incident wave within some region $\mathcal{C}$ and will itself be zero outside some finite region, i.e. be non-radiating.
The total field is in the form of the incident wave and the active source field:

$$w(\mathbf{x}) = \tilde{w}(\mathbf{x}) + w_d(\mathbf{x}).$$

The reason for the notation $\tilde{w}$ for the incident field rather that the more obvious w_{inc} will become clear later. The incoming wave is well-defined everywhere and the source field has singularity at every source positions $\mathbf{x}_m$ therefore we can assume a general form of the incident and source wave fields in the forms:

$$\tilde{w}(\mathbf{x}) = \sum_{n=-\infty}^{\infty} A_n U_n^+(\mathbf{x}) + \mathcal{A}_n \mathcal{U}_n^+(\mathbf{x}),$$

$$w_d(\mathbf{x}) = \sum_{m=1}^{M} \sum_{n=-\infty}^{\infty} B_{m,n} V_n^+(\mathbf{x} - \mathbf{x}_m) + \mathcal{B}_{m,n} \mathcal{V}_n^+(\mathbf{x} - \mathbf{x}_m).$$

The active source problem is now to find the coefficients $B_{m,n}$ and $\mathcal{B}_{m,n}$ such that w vanishes in some region $\mathcal{C}$, and to define the region $\mathcal{C}$.

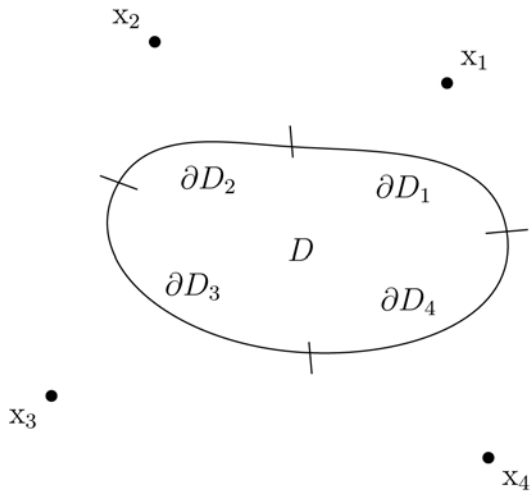

Figure 3.2: A configuration of $M = 4$ sources and a region $\mathcal{D}$ in which the integral identity 3.24 holds.

3.3.2 Integral equation

All tensors arising in the following are defined with respect to the Cartesian basis introduced above. It turns out to be useful in the following to define the (thickness averaged) moment and shear components of the forces in terms of the stress tensor σ_{ij} as

$$m_{ij}(\mathbf{x}) = \int_{-h/2}^{h/2} \sigma_{ij}(\mathbf{x}, x_3) dx_3 = -C_{ijkl} w_{,kl}(\mathbf{x}) = -D[(1-\nu) w_{,ij} + \nu \delta_{ij} \nabla^2 w], \quad (3.20)$$

$$q_i(\mathbf{x}) = \int_{-h/2}^{h/2} \sigma_{i3}(\mathbf{x}, x_3) dx_3 = -D \nabla^2 w_{,i}. \quad (3.21)$$

where $f_{,j}$ denotes the derivative of f with respect to x_j.

We define the Green's function of the equation (3.12) , according to

$$(\nabla^2 \nabla^2 - k^4) G(\mathbf{x}, \mathbf{y}) = \frac{1}{D} \delta(\mathbf{x} - \mathbf{y}) \quad (3.22)$$

and so the Green's function is

$$G(\mathbf{x} - \mathbf{y}) = \frac{i}{8k^2 D} \left(V_0(\mathbf{x} - \mathbf{y}) + \mathcal{V}_0(\mathbf{x} - \mathbf{y}) \right) \quad (3.23)$$

Consider a region $\mathcal{D}$ such that depicted in figure 3.2 chosen so that it does not contain any sources. We will determine the explicit form for the active source amplitudes together with the form of $\mathcal{D}$ that ensures cloaking. The latter, already introduced as $\mathcal{C}$, is the region depicted in figure 3.1. By assumptions W satisfies (3.12) in $\mathcal{D}$ therefore

we can write the Rayleigh-Green theorem [Kit85]:

$$w(\mathbf{x}) = \int_{\partial\mathcal{D}} q(\mathbf{y})G(\mathbf{y}-\mathbf{x}) - Q(\mathbf{y})w(\mathbf{y})\ dS \\ + \int_{\partial\mathcal{D}} w_{,i}(\mathbf{y})M_{ij}(\mathbf{y}-\mathbf{x}) - G_{,i}(\mathbf{y}-\mathbf{x})m_{ij}(\mathbf{y})\ dS \quad (3.24)$$

where $\partial\mathcal{D}$ is the boundary of $\mathcal{D}$ depicted in figure 3.2 as the union of the arcs $\partial\mathcal{D}_m$. The vector $\mathbf{n}$ is the normal exterior to $\partial\mathcal{D}$ and $q = q_i n_i$. The derivatives on the terms associated with the Green's function are derivatives associated with $\mathbf{y}$. We have also defined the associated moment and shear forces associated with the Green's function,

$$M_{ij}(\mathbf{y}-\mathbf{x}) = -D[(1-\nu)G_{,ij}(\mathbf{y}-\mathbf{x}) + \nu\delta_{ij}\nabla_y^2 G(\mathbf{y}-\mathbf{x})], \quad (3.25)$$
$$Q_i(\mathbf{y}-\mathbf{x}) = -D\nabla_y^2 G_{,i}(\mathbf{y}-\mathbf{x}) \quad (3.26)$$

derivatives here being also defined with respect to $\mathbf{y}$. Finally we note that $\mathbf{Q} = Q_i n_i$. We introduce the following identities

$$w_{,i}M_{ij}n_j = \phi_N M_N + \phi_T M_T, \quad (3.27)$$
$$G_{,i}m_{ij}n_j = \Phi_N m_N + \Phi_T m_T \quad (3.28)$$

where $m_N = m_{ij}n_i n_j, M_N = M_{ij}n_i n_j$ are the normal moments, $m_T = m_{ij}n_i t_j, M_T = M_{ij}n_i t_j$ are the twisting moments (t_j is the jth component of the tangent $\mathbf{t}$ to $\partial\mathcal{D}$), $\phi_N = w_{,i}n_i, \Phi_N = G_{,i}n_i$ and $\phi_T = w_{,i}t_i, \Phi_T = G_{,i}t_i$. These allow us to simplify the integral equation (3.24) into the form

$$w(\mathbf{x}) = \int_{\partial\mathcal{D}} q(\mathbf{y})G(\mathbf{y}-\mathbf{x}) - Q(\mathbf{y}-\mathbf{x})w(\mathbf{y})\ dS \\ + \int_{\partial\mathcal{D}} \phi_T(\mathbf{y})M_T(\mathbf{y}-\mathbf{x}) - \Phi_T(\mathbf{y}-\mathbf{x})m_T(\mathbf{y})\ dS \\ + \int_{\partial\mathcal{D}} \phi_N(\mathbf{y})M_N(\mathbf{y}-\mathbf{x}) - \Phi_N(\mathbf{y}-\mathbf{x})m_N(\mathbf{y})\ dS \quad (3.29)$$

We want to determine the cloaked region $\mathcal{C} \subset \mathcal{D}$ in which the total field w vanishes $w = \tilde{w} + w_d = 0$ so that

$$w_d(\mathbf{x}) = -\tilde{w}(\mathbf{x}) = -\int_{\partial\mathcal{C}} \tilde{q}(\mathbf{y})G(\mathbf{y}-\mathbf{x}) - Q(\mathbf{y})\tilde{w}(\mathbf{y})\ dS \\ - \int_{\partial\mathcal{C}} \tilde{\phi}_T(\mathbf{y})M_T(\mathbf{y}-\mathbf{x}) - \Phi_T(\mathbf{y}-\mathbf{x})\tilde{m}_T(\mathbf{y})\ dS \\ - \int_{\partial\mathcal{C}} \tilde{\phi}_N(\mathbf{y})M_N(\mathbf{y}-\mathbf{x}) - \Phi_N(\mathbf{y}-\mathbf{x})\tilde{m}_N(\mathbf{y})\ dS. \quad (3.30)$$

Therefore we have

$$w_d(\mathbf{x}) + \int_{\partial\mathcal{C}} \tilde{q}(\mathbf{y})G(\mathbf{y}-\mathbf{x}) - Q(\mathbf{y}-\mathbf{x})\tilde{w}(\mathbf{y})\, dS + \int_{\partial\mathcal{C}} \tilde{\phi}_T(\mathbf{y})M_T(\mathbf{y}-\mathbf{x}) - \Phi_T(\mathbf{y}-\mathbf{x})\tilde{m}_T(\mathbf{y})\, dS + \int_{\partial\mathcal{C}} \tilde{\phi}_N(\mathbf{y})M_N(\mathbf{y}-\mathbf{x}) - \Phi_N(\mathbf{y}-\mathbf{x})\tilde{m}_N(\mathbf{y})\, dS = 0 \quad (3.31)$$

which we shall write as

$$w_d(\mathbf{x}) + I_S(\mathbf{x}) + I_T(\mathbf{x}) + I_N(\mathbf{x}) = 0 \quad (3.32)$$

Recall the form of w_d,

$$w_d(\mathbf{x}) = \sum_{m=1}^{M}\sum_{n=-\infty}^{\infty} B_{m,n}V^+((\mathbf{x}-\mathbf{x}_m)) + \mathcal{B}_{m,n}\mathcal{V}^+((\mathbf{x}-\mathbf{x}_m)), \quad (3.33)$$

and let us write,

$$B_{m,n} = B^S_{m,n} + B^T_{m,n} + B^N_{m,n}, \quad (3.34)$$

$$\mathcal{B}_{m,n} = \mathcal{B}^S_{m,n} + \mathcal{B}^T_{m,n} + \mathcal{B}^N_{m,n}, \quad (3.35)$$

where the superscripts S, T and N correspond to the contributions from the separate integral terms in (3.31) associated with shear, twisting moment and normal moment respectively.

In order to evaluate the integrals in convenient form, write the Green's function, for $|\mathbf{y}-\mathbf{x}_m| < |\mathbf{x}-\mathbf{x}_m|$ as

$$G(\mathbf{y}-\mathbf{x}) = \frac{i}{8k^2D}\sum_{n=-\infty}^{\infty} U_n^-(\mathbf{y}-\mathbf{x}_m)V_n^+(\mathbf{x}-\mathbf{x}_m) + \mathcal{U}_n^-(\mathbf{y}-\mathbf{x}_m)\mathcal{V}_n^+(\mathbf{x}-\mathbf{x}_m). \quad (3.36)$$

Using this form of the Green's function, it may be shown that we can write the integrals in the forms

$$\{I_S, I_T, I_N\}(\mathbf{x}) = -\sum_{m=1}^{M}\sum_{n=-\infty}^{\infty} \{B^S_{m,n}, B^T_{m,n}, B^N_{m,n}\}V_n^+(\mathbf{x}-\mathbf{x}_m) + \{\mathcal{B}^S_{m,n}, \mathcal{B}^T_{m,n}, \mathcal{B}^N_{m,n}\}\mathcal{V}_n^+(\mathbf{x}-\mathbf{x}_m) \quad (3.37)$$

where upon defining $\gamma = i/(8k^2D)$, the coefficients associated with the shear term are

$$\{B^S_{m,n}, \mathcal{B}^S_{m,n}\} = \gamma\int_{\partial C_m} \tilde{q}(\mathbf{y})\{U_n^-, \mathcal{U}_n^-\}(\mathbf{y}-\mathbf{x}_m) + Dk^2\tilde{w}(\mathbf{y})\mathbf{n}\cdot\nabla_y\{-U_n^-, \mathcal{U}_n^-\}(\mathbf{y}-\mathbf{x}_m)dS_y \quad (3.38)$$

the change in sign in the latter term arising from the use of $\nabla_y^2 U_n^- = -k^2 U_n^-$ and $\nabla_y^2 \mathcal{U}_n^- = k^2 \mathcal{U}_n^-$ therein.

Next, using the fact that $\mathbf{t} \cdot \mathbf{n} = 0$, we obtain

$$\{B_{m,n}^T, \mathcal{B}_{m,n}^T\} = -\gamma \int_{\partial C_m} D(1-\nu)\tilde{\phi}_T(\mathbf{y}) \left[\mathbf{n} \cdot \nabla_y (\mathbf{t} \cdot \nabla_y \{U_n^-, \mathcal{U}_n^-\}(\mathbf{y} - \mathbf{x}_m))\right] + \tilde{m}_T(\mathbf{y}) \left[\mathbf{t} \cdot \nabla_y \{U_n^-, \mathcal{U}_n^-\}(\mathbf{y} - \mathbf{x}_m)\right] dS_y, \quad (3.39)$$

and finally the normal moment contribution, using $\mathbf{n} \cdot \mathbf{n} = 1$,

$$\begin{aligned}\{B_{m,n}^N, \mathcal{B}_{m,n}^N\} = &-\gamma \int_{\partial C_m} \tilde{m}_N(\mathbf{y}) \mathbf{n} \cdot \nabla_y \{U_n^-, \mathcal{U}_n^-\}(\mathbf{y} - \mathbf{x}_m) dS_y \\ &- \gamma \int_{\partial C_m} \tilde{\phi}_N(\mathbf{y}) D(1-\nu) \mathbf{n} \cdot \nabla_y (\mathbf{n} \cdot \nabla_y \{U_n^-, \mathcal{U}_n^-\}(\mathbf{y} - \mathbf{x}_m)) dS_y \\ &- \gamma \int_{\partial C_m} \tilde{\phi}_N(\mathbf{y}) \nu D k^2 \{-U_n^-, \mathcal{U}_n^-\}(\mathbf{y} - \mathbf{x}_m) dS_y \quad (3.40)\end{aligned}$$

where again the change in sign in the middle term arises from the use of the governing equations. Note that for this to be true simultaneously for all m, the contours $\partial \mathcal{C}_m$ must be circular arcs as depicted in figure 3.2. Therefore $\mathcal{C}$ is the region with boundary as the closed concave union of circular arcs defined by $\{a_m, \theta_1^{(m)}, \theta_2^{(m)}\}$ and denoted as $\mathcal{C}_m$, see figure 3.4.1. Actually the cloaked region $\mathcal{C}$ is exactly the subdomain of $\mathcal{D}$ in which the Graf's theorem can be simultaneously invoked for all of the M active sources. From now each integral over $\mathcal{C}_m$ will be performed accordingly to circular coordinates centred at $\mathbf{x}_m$ the position of the source m. By doing this we have to multiply the integral by -1. Indeed the counter-clockwise with respect to $\mathbf{x}_m$ is opposite to the counter-clockwise traversal of $\partial \mathcal{C}$ with respect to some origin inside $\mathcal{C}$. Introducing the notation $\alpha^{(m)} = k a_m$, we can evaluate the shear coefficients as

$$\begin{aligned}\{B_{m,n}^S, \mathcal{B}_{m,n}^S\} = &\gamma k^2 D \{J_n(\alpha^{(m)}), I_n(\alpha^{(m)})\} \int_{\theta_1^{(m)}}^{\theta_2^{(m)}} \mathbf{n} \cdot \nabla_y \tilde{w}(\mathbf{y}) e^{-in\theta}\, a^{(m)} d\theta \\ &+ \gamma k^2 D \alpha^{(m)} \{-J_n'(\alpha^{(m)}), I_n'(\alpha^{(m)})\} \int_{\theta_1^{(m)}}^{\theta_2^{(m)}} \tilde{w}(\mathbf{y}) e^{-in\theta}\, d\theta. \quad (3.41)\end{aligned}$$

The twisting and normal moments terms are

$$\begin{aligned}\{B_{m,n}^T, \mathcal{B}_{m,n}^T\} = in\gamma \Big(&\{J_n(\alpha^{(m)}), I_n(\alpha^{(m)})\} \int_{\theta_1^{(m)}}^{\theta_2^{(m)}} \tilde{m}_T(\mathbf{y}) e^{-in\theta}\, d\theta \\ + D(1-\nu) k \{&J_n'(\alpha^{(m)}) - \frac{1}{\alpha^{(m)}} J_n(\alpha^{(m)}), I_n'(\alpha^{(m)}) - \frac{1}{\alpha^{(m)}} I_n(\alpha^{(m)})\} \int_{\theta_1^{(m)}}^{\theta_2^{(m)}} \tilde{\phi}_T(\mathbf{y}) e^{-in\theta}\, d\theta \Big). \quad (3.42)\end{aligned}$$

and

$$\{B^N_{m,n}, \mathcal{B}^N_{m,n}\} = -\gamma\alpha^{(m)}\Big(\{J'_n(\alpha^{(m)}), I'_n(\alpha^{(m)})\}\int_{\theta_1^{(m)}}^{\theta_2^{(m)}} \tilde{m}_N(\mathbf{y})e^{-in\theta}\,d\theta$$
$$+ Dk\Big[(1-\nu)\{J''_n(\alpha^{(m)}), I''_n(\alpha^{(m)})\} + \nu\{-J_n(\alpha^{(m)}), I_n(\alpha^{(m)})\}\Big]\int_{\theta_1^{(m)}}^{\theta_2^{(m)}} \tilde{\phi}_N(\mathbf{y})e^{-in\theta}\,d\theta\Big) \tag{3.43}$$

3.3.3 Plane wave incidence

Consider an incident plane-wave of unit amplitude, i.e.

$$\tilde{w}(\mathbf{x}) = w_\psi(\mathbf{x}) = e^{ik\hat{\mathbf{e}}(\psi)\cdot\mathbf{x}} \tag{3.44}$$

where $\hat{\mathbf{e}}(\psi) = (\cos\psi, \sin\psi)$ is a unit direction vector. We note that with this definition we can write, for $\mathbf{y} \in \partial C_m$, $\tilde{w}(\mathbf{y}) = \tilde{w}(\mathbf{x}_m)\tilde{w}(\mathbf{a})$ where we have defined $\mathbf{a} = a_m\hat{\mathbf{e}}(\theta)$. Let us also define

$$L^{ij}_n(\alpha^{(m)}) = \int_{\theta_1^{(m)}-\psi}^{\theta_2^{(m)}-\psi} \sin^i\Theta\cos^j\Theta e^{i\alpha^{(m)}\cos\Theta - in\Theta}\,d\Theta. \tag{3.45}$$

In order to remain as clear as possible, we do not develop here the calculations. For the exact expressions of the L^{ij}'s and the details of derivations for the integrals in 3.41, 3.42 and 3.43 we suggest to read the annex. To summarize, the analytic expressions are expressed by.

$$\int_{\theta_1^{(m)}}^{\theta_2^{(m)}} \tilde{w}(\mathbf{y})e^{-in\theta}d\theta = \tilde{w}(\mathbf{x}_m)e^{-in\psi}L^{00}_n(\alpha^{(m)}),$$

$$\int_{\theta_1^{(m)}}^{\theta_2^{(m)}} \tilde{\phi}_N(\mathbf{y})e^{-in\theta}d\theta = ik\tilde{w}(\mathbf{x}_m)e^{-in\psi}L^{01}_n(\alpha^{(m)}),$$

$$\int_{\theta_1^{(m)}}^{\theta_2^{(m)}} \tilde{\phi}_T(\mathbf{y})e^{-in\theta}d\theta = -ik\tilde{w}(\mathbf{x}_m)e^{-in\psi}L^{10}_n(\alpha^{(m)}),$$

$$\int_{\theta_1^{(m)}}^{\theta_2^{(m)}} \tilde{m}_N(\mathbf{y})e^{-in\theta}d\theta = Dk^2\tilde{w}(\mathbf{x}_m)e^{-in\psi}((1-\nu)L^{02}_n(\alpha^{(m)}) + \nu L^{00}_n(\alpha^{(m)})),$$

$$\int_{\theta_1^{(m)}}^{\theta_2^{(m)}} \tilde{m}_T(\mathbf{y})e^{-in\theta}d\theta = -Dk^2(1-\nu)\tilde{w}(\mathbf{x}_m)\sin(\theta-\psi)\cos(\theta-\psi)e^{i\alpha^{(m)}\cos(\theta-\psi)}.$$

The modal amplitudes for an unitary incoming plane wave are thus given by injecting the previous formulae in the equations 3.41, 3.42, and 3.43.

Finally we have to check that the active source field vanish far enough from the cloaked area. The Rayleigh-Green theorem is available for every $\mathbf{x}$. However we had to use the Graf's addition theorem therefore, rigorously speaking, the given expressions are available for $\mathbf{x}$ in the region $\mathbb{R}^2/\cup_{i=1..n} C_i$ with $C_i = \{\mathbf{x} \in \mathbb{R}^2, |\mathbf{x} - \mathbf{x_i}|\}$. This latter includes not only the cloaking region $\mathcal{C}$ but also the region $\mathcal{R}$ defined in figure 3.1. Nevertheless we suggested to take the values defined by (3.41), (3.42), and (3.43) as the modal amplitudes. As we first observed for $\mathbf{x} \in \mathcal{C}$, the result cancels the incoming waves due to the Rayleigh-Green theorem (3.24). If $\mathbf{x}$ is in $\mathcal{R}$ then $\mathbf{x}$ is not in the domain delimited by $\partial\mathcal{C}$ corresponding to the integration domain and the Rayleigh-Green theorem ensure that the integral (3.24) is zero. Therefore the active source field is zero in the far field region $\mathcal{R}$. However we have no clue about the field near to a source, we will attempt to discuss it further.

3.3.4 Punctual source field incidence

Let us assume that the source generating incident waves, localized at S, is sufficiently far away. Therefore any contribution to the incident field from the evanescent terms is negligible. I.e. we take $\mathcal{A}_n = 0$ for all n. The incident field has now singularity at the position $\mathbf{x}_s$ of the source point and thus it is under the form

$$\tilde{w}(\mathbf{y}) = \sum_{l=-\infty}^{\infty} A_l V_l^+(\mathbf{y} - \mathbf{x}_s). \tag{3.46}$$

Furthermore we suppose that S is in the region $\mathcal{R}$ defined above so that for every $m \in \{1 \dots M\}$ we have $a^{(m)} < |\mathbf{x}_m - \mathbf{x}_s|$. Therefore we can apply the Graf's theorem and we deduce:

$$\tilde{w}(\mathbf{y}) = \sum_{l=-\infty}^{\infty} \tilde{A}_l U_l^+(\mathbf{a}^{(m)}) \quad \text{with} \quad \tilde{A}_l = \sum_{p=-\infty}^{\infty} A_p V_{p-l}(\mathbf{x}_m - \mathbf{x}_s).$$

Defining $G_l(\theta_1,\theta_2)=e^{il\theta_2}-e^{il\theta_1}$, similar calculations gives:

$$\int_{\theta_1^{(m)}}^{\theta_2^{(m)}}\tilde{w}(\mathbf{y})e^{-in\theta}d\theta=\sum_{l=-\infty}^{\infty}\tilde{A}_lJ_l(\alpha^{(m)})\frac{1}{i(l-n)}G_{l-n}(\theta_1^{(m)},\theta_2^{(m)}),$$

$$\int_{\theta_1^{(m)}}^{\theta_2^{(m)}}\tilde{\phi}_N(\mathbf{y})e^{-in\theta}d\theta=k\sum_{l=-\infty}^{\infty}\tilde{A}_lJ_l'(\alpha^{(m)})\frac{1}{i(l-n)}G_{l-n}(\theta_1^{(m)},\theta_2^{(m)}),$$

$$\int_{\theta_1^{(m)}}^{\theta_2^{(m)}}\tilde{\phi}_T(\mathbf{y})e^{-in\theta}d\theta=\frac{1}{a^{(m)}}\sum_{l=-\infty}^{\infty}\tilde{A}_lJ_l(\alpha^{(m)})\frac{1}{(l-n)}G_{l-n}(\theta_1^{(m)},\theta_2^{(m)}),$$

$$\int_{\theta_1^{(m)}}^{\theta_2^{(m)}}\tilde{m}_N(\mathbf{y})e^{-in\theta}d\theta=-Dk^2\sum_{l=-\infty}^{\infty}\tilde{A}_l\Big((1-\nu)J_l''(\alpha^{(m)})-\nu J_l(\alpha^{(m)})\Big)\frac{G_{l-n}(\theta_1^{(m)},\theta_2^{(m)})}{i(l-n)},$$

$$\int_{\theta_1^{(m)}}^{\theta_2^{(m)}}\tilde{m}_T(\mathbf{y})e^{-in\theta}d\theta=-\frac{D(1-\nu)}{(a^{(m)})^2}\sum_{l=-\infty}^{\infty}\tilde{A}_l\Big(\alpha^{(m)}J_l'(\alpha^{(m)})-J_l(\alpha^{(m)})\Big)\frac{lG_{l-n}(\theta_1^{(m)},\theta_2^{(m)})}{(l-n)}.$$

Injecting these formula in the equations (3.41),(3.42) and (3.43), we then deduce the coefficient for an incident field defined by (3.46). Of course the field radiated by the active sources will be zero in the region $\mathcal{R}$ for the same reasons as in the previous case because it relies on the application of the Rayleigh-Green theorem 3.24 and the Graf's theorem for the Green function 3.36.

It is important to notice that the formulae obtained in this subsection remain available for an incident field under the form:

$$\tilde{w}(\mathbf{y})=\sum_{l=-\infty}^{\infty}A_lU_l^+(\mathbf{y}-\mathbf{x}_s),\tag{3.47}$$

with the condition of redefining $\tilde{A}_l$ by $\tilde{A}_l=\sum_{p=-\infty}^{\infty}A_pU_{p-l}(\mathbf{x}_m-\mathbf{x}_s)$ because of the Graf's theorem. Furthermore their would be no conditions on the position of the punctual source thanks to the addition theorem for regular Bessel functions.

3.3.5 Necessary and sufficient conditions

"Near field" will refer to the field inside the cloaked region whereas "far field" will refer to the field outside the cloaked region. Without loss of generality we suppose that the origin of the coordinates is inside the cloaked region and of course $a^(m)<x_m$. We have the following theorem which the equivalent of the theorem of [NAP12]:

Theorem 3.3.1 *The necessary and sufficient conditions on the cloaking device for non*

radiating are:

$$\forall n \in \mathbb{Z}: \qquad \sum_{m=1}^{M} \sum_{l=-\infty}^{\infty} \begin{cases} B_{m,l} U_{n-l}^{-}(\mathbf{x}_m) & = 0, \\ \mathcal{B}_{m,l} \mathcal{U}_{n-l}^{-}(\mathbf{x}_m) & = 0 \end{cases} \tag{3.48}$$

If $\mathbf{x}$ is in the far field domain, we have $x > |x_m + a^{(m)}|$ for $m = 1..M$. Thus we can apply the first cases of the Graf's theorems 3.18 and 3.19 with $\mathbf{y} = \mathbf{x}_m$:

$$w_d(\mathbf{x}) = \sum_{n=-\infty}^{\infty} F_n V_n^{+}(\mathbf{x}) + \mathcal{F}_n \mathcal{V}_n^{+}(\mathbf{x}) \tag{3.49}$$

where

$$F_n = \sum_{m=1}^{M} \sum_{l=-\infty}^{\infty} B_{m,l} U_{n-l}^{-}(\mathbf{x}_m), \qquad \mathcal{F}_n = \sum_{m=1}^{M} \sum_{l=-\infty}^{\infty} \mathcal{B}_{m,l} \mathcal{U}_{n-l}^{-}(\mathbf{x}_m) \tag{3.50}$$

With $\theta = \arg\mathbf{x}$, the far field amplitude functions $f(\theta)$ and $g(\theta)$ such as:

$$w_d(\mathbf{x}) = f(\theta) H_0(kx) + g(\theta) H_0^{(2)}(kx),$$

are given by the expansion of the Hankel functions for high arguments:

$$\begin{array}{ll} f(\theta) = \sum_n f_n e^{in\theta}, & f_n = i^{-n-\frac{1}{2}} \\ g(\theta) = \sum_n g_n e^{in\theta}, & g_n = i^{n+\frac{1}{2}}. \end{array}$$

Now a nondimensional total power radiated by the sources is given by the non-negative far field flux parameters:

$$\Phi = \int_0^{2\pi} |f(\theta)|^2 = 4 \sum_n |F_n|^2 \quad \text{and} \quad \Psi = \int_0^{2\pi} |g(\theta)|^2 = 4 |\mathcal{F}_n|^2.$$

As both components of w_d do not radiates energy into the far field, for $n \in \mathbb{Z}$, F_n and $\mathcal{F}_n$ must vanish. Thus we showed the necessity. If $\sum_{m=1}^{M} \sum_{l=-\infty}^{\infty} B_{m,l} U_{n-l}^{-}(\mathbf{x}_m) = 0$ and $\sum_{m=1}^{M} \sum_{l=-\infty}^{\infty} \mathcal{B}_{m,l} \mathcal{U}_{n-l}^{-}(\mathbf{x}_m) = 0$ then it is straightforward to see that $w_d(\mathbf{x}) = 0$ in the far field domain after using Graf's addition theorem.

Concerning the cancellation of the incoming wave in the near field, we have only the following sufficient conditions:

Theorem 3.3.2 *If we have:*

$$\forall n \in \mathbb{Z}: \qquad \sum_{m=1}^{M} \sum_{l=-\infty}^{\infty} \begin{cases} B_{m,l} V_{n-l}^{-}(\mathbf{x}_m) & = -A_n, \\ \mathcal{B}_{m,l} \mathcal{V}_{n-l}^{-}(\mathbf{x}_m) & = -\mathcal{A}_n \end{cases} \tag{3.51}$$

then the incoming wave is canceled in the near field domain.

If $\mathbf{x}$ is in the near field domain, we have $x < |x_m + a^{(m)}|$ for $m = 1..M$. Thus we can apply the second cases of the Graf's theorems 3.18 and 3.19 with $\mathbf{y} = \mathbf{x}_m$:

$$w_d(\mathbf{x}) = \sum_{n=-\infty}^{\infty} E_n U_n^+(\mathbf{x}) + \mathcal{E}_n \mathcal{U}_n^+(\mathbf{x}), \tag{3.52}$$

where

$$E_n = \sum_{m=1}^{M} \sum_{l=-\infty}^{\infty} B_{m,l} V_{n-l}^-(\mathbf{x}_m), \qquad \mathcal{E}_n = \sum_{m=1}^{M} \sum_{l=-\infty}^{\infty} \mathcal{B}_{m,l} \mathcal{V}_{n-l}^-(\mathbf{x}_m). \tag{3.53}$$

Under the assumptions 3.51, we have $A_n + E_n = 0$. Therefore the incoming field is canceled.

Discussion on the necessity: Although it is claimed in the paper [NAP12], it seems that the sufficient conditions are not necessary ones. Indeed requiring that the field is canceled in the vicinity of the origin is not sufficient to ensure $A_n + E_n = 0$ and $\mathcal{A}_n + \mathcal{E}_n = 0$. As we will see in the numerical treatments their value might be high whereas they are scaled by U_n^+ and $\mathcal{U}_n^+$ so that the incoming wave will actually be canceled. If we want to show the necessity, we need an argument on the norm we should use to evaluate $w_d + w_{inc}$ in the near field domain, as we did with the energy for the far field.

3.4 Numerical examples

3.4.1 Active source configuration

We illustrate the result for a plane wave incidence on configurations of the type shown in the figure 3.3. The M sources are symmetrically located on a circle. Thus for $m \in \{1, \dots M\}$ we have:

$$a^{(m)} = a, \quad |\mathbf{x}_m| = r, \quad \phi_m = (m-1)\theta_0, \quad \text{with } \theta_0 = \tfrac{2\pi}{M},$$

and by necessity $a = r \sin(\frac{\pi}{M})$. By symmetry the circular arcs all have the same angular extent whose angles are defined by:

$$\theta_{1,2}^{(m)} = \pi + \theta_m \mp |\frac{\pi}{2} - \frac{\pi}{M}|. \tag{3.54}$$

Note that the cloaked region $\mathcal{C}$ can be formed by a minimum of three sources. A configuration with $M = 8$ is shown in figure(3.3). All calculations were performed for plane wave incidence on this configuration with varying number of sources, $M \geq 3$.

3.4.2 Total field

The total field for unit amplitude plane wave incidence with angle $\psi = \frac{\pi}{8}$ on configurations of active sources of type described in subsection 3.4.1is illustrated through several examples.

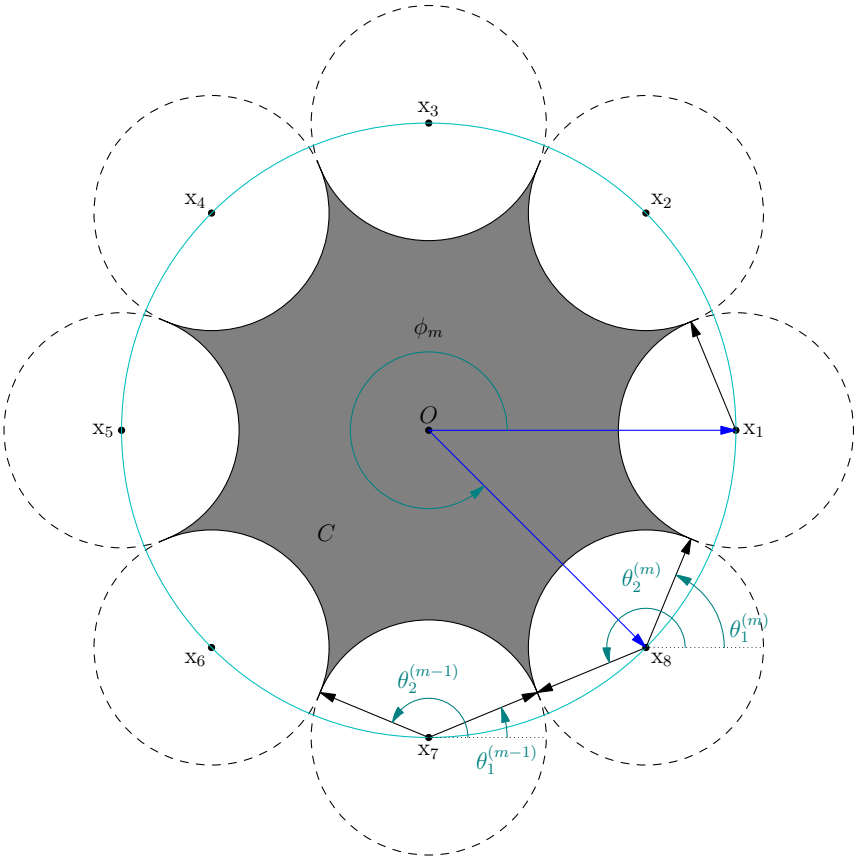

Figure 3.3: numerical configuration for 8 sources

Figure 3.4 shows the absolute value of the total field for four active sources: The subplot provide different view in order to indicate that the field is canceled in the cloaked area $\mathcal{C}$, and that the radiated field w_d is essentially zero outside the region $\mathcal{Z} = \cup_{i=1..n} C_i$ with $C_i = \{\mathbf{x} \in \mathbb{R}^2, |\mathbf{x} - \mathbf{x_i}\}$. The principal variation in the source field, and thus in the total field, is located inside the circular regions centered on the the active sources. Indeed we found very large value of source field inside this region due to the fact that the modal amplitudes were initially derived with the Graf's addition theorem. In the following we just truncate the values at an arbitrary one (2) in order to make the figure clear.

Figure 3.5 correspond to the same configuration with $M = 4$ but for higher frequency with $k = 10$. Here the plots show the real part of the total field, and we clearly retrieve the incoming plane wave in $\mathcal{Z}$ whereas the cloaked region appears to be larger than $\mathcal{C}$. The number of mode considered in the multipole decomposition of this example is quite high ($N = 50$). It seems more interesting to investigate the effects of fewer modes. For N on the order of kr, the cloaking remains efficient as illustrated in figure 3.6. We notice that the footprints of the active sources, are smaller than in the previous example, indicating that the higher orders tend to fill the area where the total source

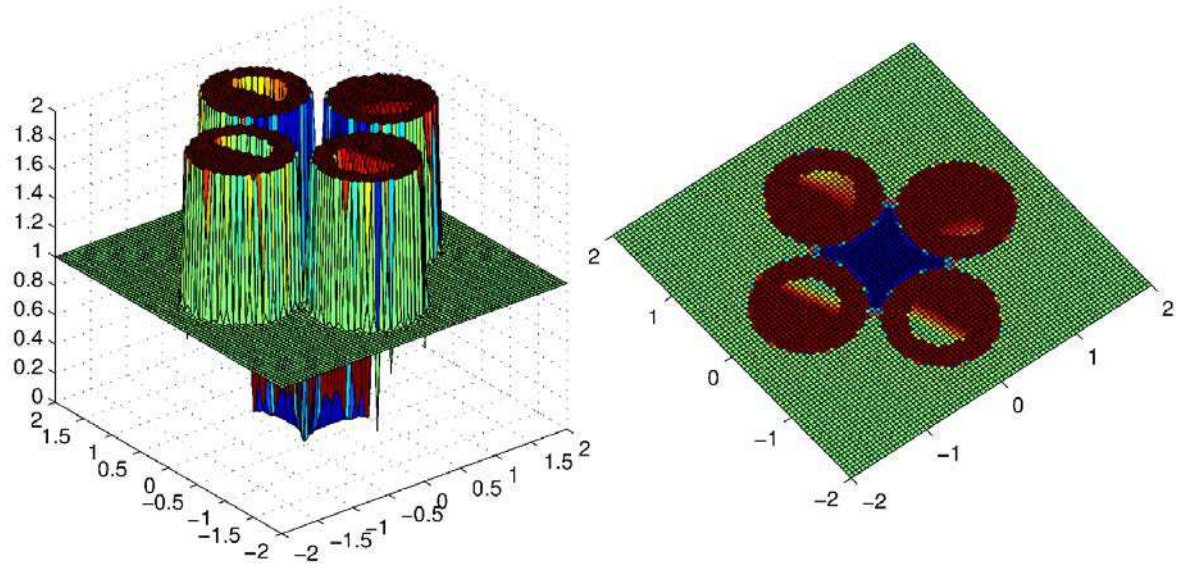

Figure 3.4: Absolute value of the total field with 4 active sources, $r = 1$, angle of incidence $\psi = \frac{\pi}{8}$, wavenumber $k = 5$ and $N = 50$. Values above 2 in magnitude are clipped to make the figure visible.

field w_d is highly variable. Furthermore the shape of the footprint does not seem as a circle any more and the effect of each considered modes is directly observable. Only $N = 5$ modes are used in the figure 3.7 and we observe that the cloaking effects is deteriorated due to an inadequate number of multipoles. The incoming plane wave is almost observable in the region that we aim to cloak, nevertheless the radiated field do not perturb the far field. Again we notice that the footprints of the active sources are smaller than in figures 3.5 and 3.6 and we observe clearly the footprint of each considered modes.

Finally in figure 3.8 we investigate the effect of larger number of actives sources for small number of modes. Comparison of figures 3.8 and 3.7 confirms the tendency previously observed: more active sources improves the accuracy of the cloaking effect.

3.4.3 Near and far field modal amplitudes

In the previous figures from 3.6 to 3.8, we observed that the conditions for the cloaking, namely non radiating sources and canceled field in $\mathcal{C}$, are more or less fulfilled from a case to an other. Here we suggest to discuss the efficiency of the cloaking device by focusing on the far field and near field coefficient.

If all terms in the infinite sums in equations (3.55) are available then the farfield is exactly zero and the incident wave is fully canceled by the sources. In practice we truncate this sums at order N so that the near fields and the far fields are approximated

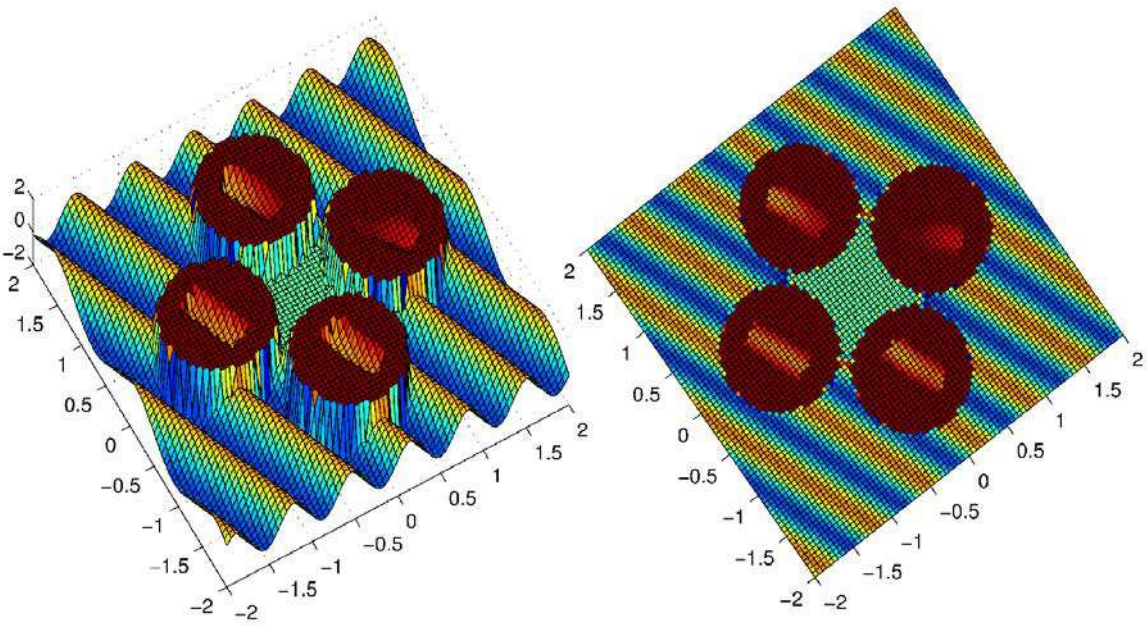

Figure 3.5: Real part of the total field with 4 active sources, $r = 1$, angle of incidence $\psi = \frac{\pi}{8}$, wavenumber $k = 10$ and $N = 50$. Values above 2 in magnitude are clipped to make the plots visible.

by:

$$\forall n \in \mathbb{Z}: \qquad \sum_{m=1}^{M} \sum_{l=-N}^{N} \begin{cases} B_{m,l} U_{n-l}^{-}(\mathbf{x}_m) & = F_n^{\text{app}}, \\ \mathcal{B}_{m,l} \mathcal{U}_{n-l}^{-}(\mathbf{x}_m) & = \mathcal{F}_n^{\text{app}} \\ B_{m,l} V_{n-l}^{-}(\mathbf{x}_m) & = E_n^{\text{app}}, \\ \mathcal{B}_{m,l} \mathcal{V}_{n-l}^{-}(\mathbf{x}_m) & = \mathcal{E}_n^{\text{app}} \end{cases}. \tag{3.55}$$

This truncation of the sum is equivalent to limiting the order of the active multipole sources. If we examine the formulae giving the modal sources, we note that it depends on ka, M and the angles between each sources. However, for the considered configuration of sources, the angles are uniquely defined by M (3.54). Thus the adimensional parameters relative to the model are , ka, M and the truncation order N. Now $a = \sin(\frac{\pi}{M})$ for $r = 1$ thus fixing M imposes the value of a and modifying ka is equivalent to modify k. Consequently the cloaking strategy relies on independent parameters: k, M and the truncation order N. In order to assess the efficiency of the cloaking we examine the farfields and the nearfields as functions of theses parameters.

The farfield determine the radiated field outside the cloaking area and must necessarily be small whereas the nearfield is defined in the cloaked region and must cancel

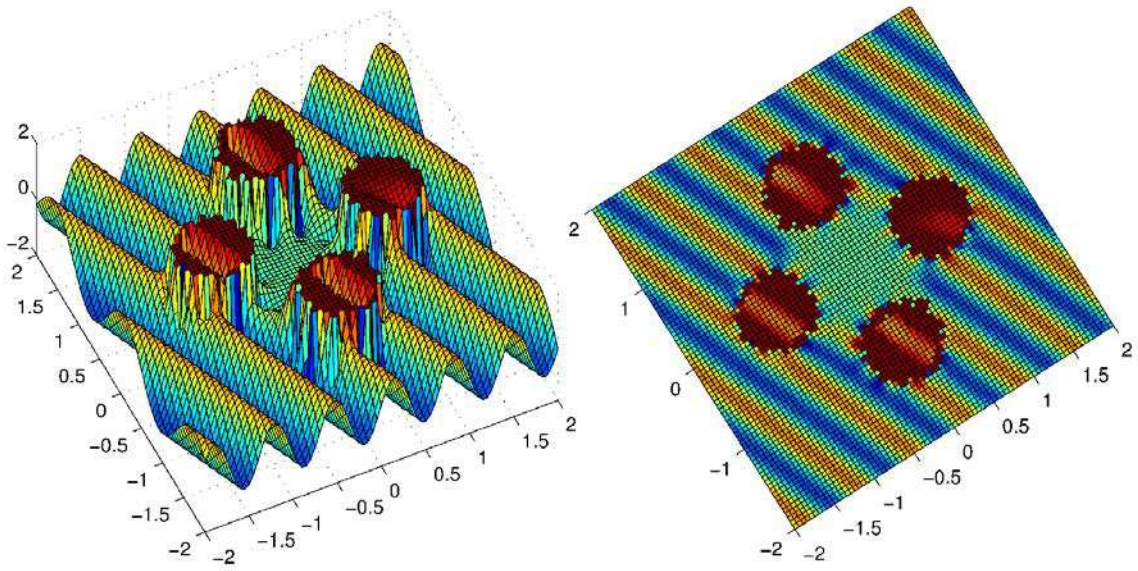

Figure 3.6: Real part of the total field with 4 active sources, $r = 1$, angle of incidence $\psi = \frac{\pi}{8}$, wavenumber $k = 10$ and $N = 10$. Values above 2 in magnitude are clipped to make the plots visible.

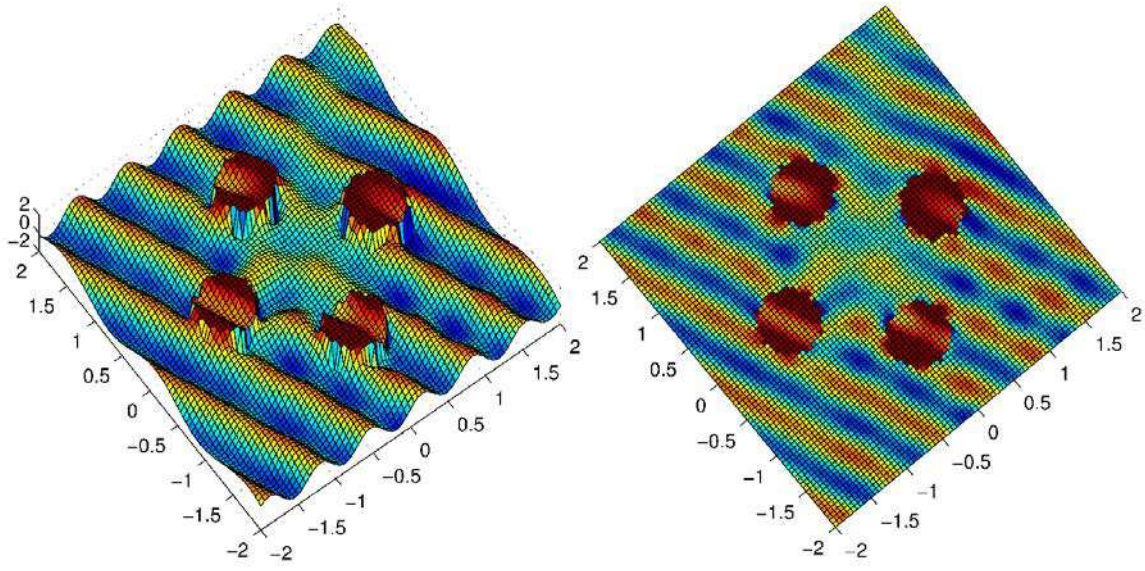

Figure 3.7: Same as in figure 3.6 except now $N = 5$.

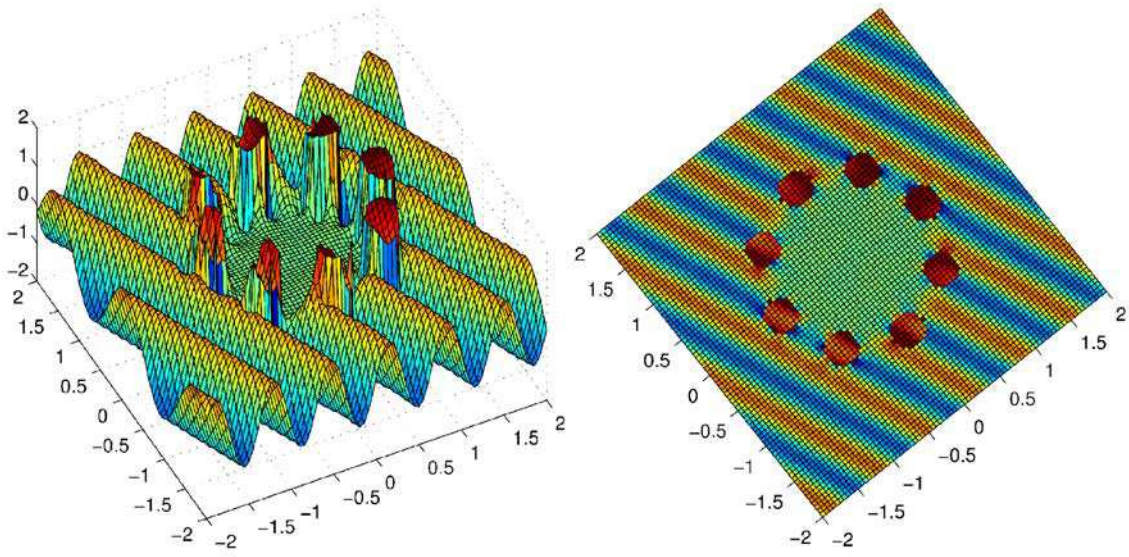

Figure 3.8: Same as in figure 3.7 except now $M = 8$.

the incident field. Both conditions correspond respectively to $F_n^{\text{app}}, E_n^{\text{app}} + A_n, \mathcal{F}_n^{\text{app}}$ and $\mathcal{E}_n^{\text{app}} + \mathcal{A}_n$ taking small values. In this subsection we investigate the influence of the parameters k, N and M on these quantities. The sources are located on the unit circle, $r = 1$, and we aim to cloak an incident plane waves with $\psi = \frac{\pi}{8}$.

The far field amplitudes coefficient $|F_n^{\text{app}}|$ and $|\mathcal{F}_n^{\text{app}}|$ for $n \in \{-10, \ldots, 10\}$ are shown in figure 3.9 for various values of the wavenumber k, the number of sources M and the truncation order N. The farfield decreases as N increases, M increases and k decreases. The convergence of the farfield coefficients is quite fast as function of N for k and M fixed.

The near field amplitudes $|E_n^{\text{app}} + A_n|$ and $|\mathcal{E}_n^{\text{app}} + \mathcal{A}_n|$ are shown in figure 3.10 to 3.12. In opposition to the farfields coefficients, we have to take large order enough or the truncation to achieve small nearfield coefficients. Indeed figure 3.10 shows that accuracy comparable to the farfields coefficients is performed for N on the order 60 or more. Furthermore, we notice that the nearfields coefficients increase in magnitude with $|n| \leq N$ which is not the case for the farfields coefficients. However the relative high value of $|E_n^{\text{app}} + A_n|$ and $|\mathcal{E}_n^{\text{app}} + \mathcal{A}_n|$ do not mean that the incoming waves is not cancelled nor that the total field is divergent for high value of N. In fact we have to keep in mind that the coefficients $|E_n^{\text{app}} + A_n|$ and $|\mathcal{E}_n^{\text{app}} + \mathcal{A}_n|$ are respectively multiplied by $J_n(k|\mathbf{x}|)$ and $I_n(k|\mathbf{x}|)$ for $\mathbf{x} \in C$ thus for small $k|\mathbf{x}|$ and n fixed the limiting forms $\{J_n(k|\mathbf{x}|), I_n(k|\mathbf{x}|)\} \sim \frac{1}{n!}\Big(\frac{k|\mathbf{x}|}{2}\Big)^n$ can balance the high values of $|E_n^{\text{app}} + A_n|$ and $|\mathcal{E}_n^{\text{app}} + \mathcal{A}_n|$. This confirms the fact that the condition 3.51 is sufficient but not necessary.

We show the dependency of the nearfield coefficient on the number of sources M in

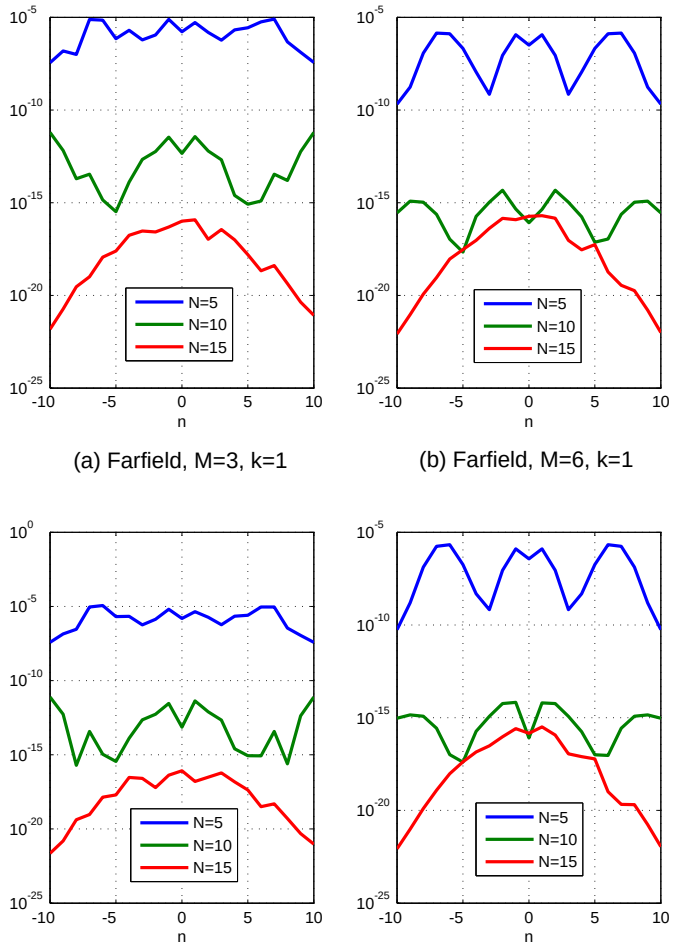

Figure 3.9: Dependence of the farfield coefficient amplitudes $|F_n^{(app)}|$ (upper part) and $|\mathcal{F}_n^{(app)}|$ (lower part) on the order n of the modal sums for different value of N and different number of sources M. The incident wavenumber is $k = 1$.

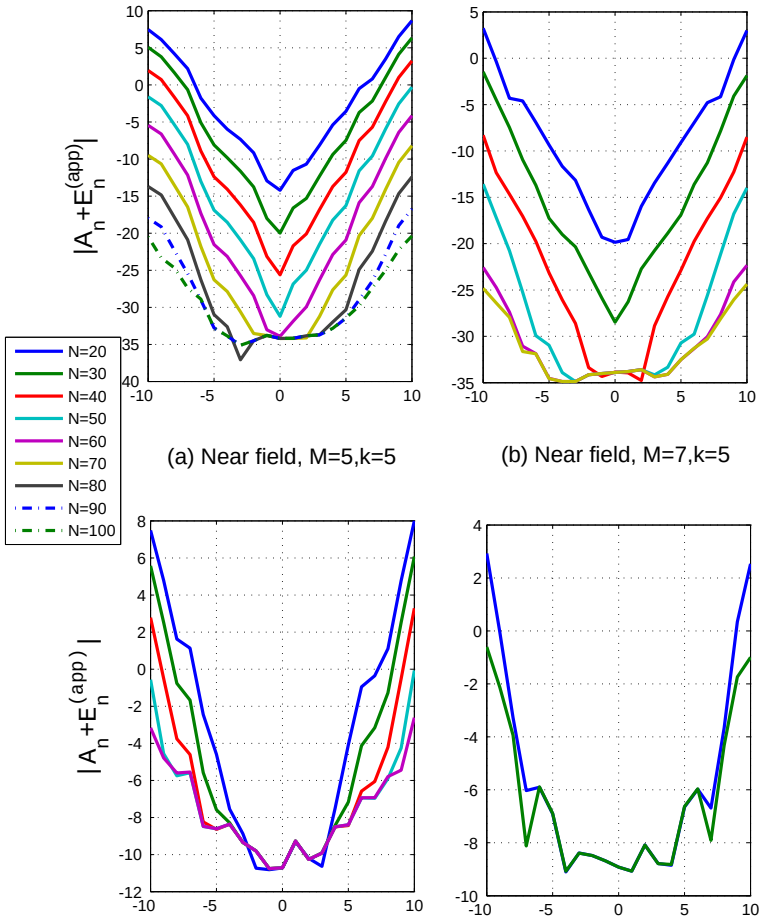

Figure 3.10: Dependence of the nearfield coefficient amplitudes $|A_n + E_n^{(app)}|$ (upper part) and $|\mathcal{A}_n + \mathcal{E}_n^{(app)}|$ (lower part) on the order n of the modal sums for different value of N and different number of sources M. The incident wavenumber is $k = 1$.

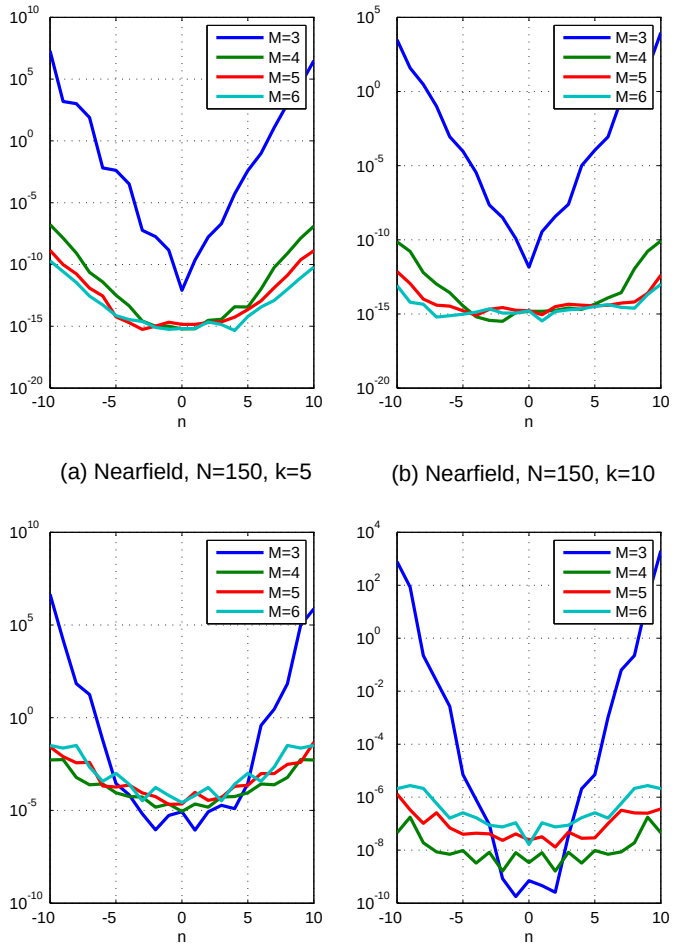

Figure 3.11: Dependence of the nearfield coefficient amplitudes $|A_n + E_n^{(app)}|$ (upper part) and $|\mathcal{A}_n + \mathcal{E}_n^{(app)}|$ (lower part) on the order n of the modes for different value of k and different number of sources M. The truncation order is $N = 150$.

figure 3.11. Generally, as with the farfield coefficients, increasing the number of sources improves the efficiency of the cloaking. Among the proposed examples, we notice that the case of minimum of sources, $M = 3$, is radically different from the other $M \geq 4$. Adding at least one more source and taking $M = 4$ importantly reduces the error of $|A_n + E_n^{(app)}|$ from $\sim 10^{-4}$ to 10^{-15} for $k = 5, 10$, $n = \pm 5$. Concerning the coefficient corresponding to the evanescent part $|\mathcal{A}_n + \mathcal{E}_n^{(app)}|$, the difference between $M = 3$ and the $M \geq 3$ is less significant for $n \in \{-5, \ldots, 5\}$.

Finally, figure 3.12 shows the influence of k on the nearfield coefficients, taking $k \in \{5, 10, 15, 20\}$. Unlike the farfield case, the accuracy of the cloaking improves with increasing k. Nevertheless we should keep in mind that theses coefficients are multiplied by $J_n(k|\mathbf{x}|)$ and $I_n(k|\mathbf{x}|)$ which increase in magnitude for increasing k and fixed $|\mathbf{x}|$.

The numerical results of the investigations in figures 3.10 through 3.12 show that greater accuracy is achieved for more sources. In the case $M = 3$, the minimum number of sources required, the nearfield coefficient could be large enough to significantly perturb the cloaking effect. This suggest taking $M = 4$ at least. Nevertheless we expect M being larger to fit more precisely, like a necklace, an arbitrary shape of cloaking area. Furthermore it allows us to use monopoles or dipoles which could be easier to deal with for experimental investigations.

3.5 Conclusion

The active cloaking strategy can be viewed as an inverse problem: we have to find the source amplitudes associated to a given incident field in order to cancel this latter in some finite region. The results given here provide solutions for this inverse problem for arbitrary incident wave. We only require the entire expansion of the incident field into cylindrical waves but we can evaluate the source fields to any degree of accuracy by increasing the order of truncation N associated to the number of modes of the sources. Simultaneously the active field is non radiating because it has been shown that it vanishes identically outside a region $\mathcal{R}$.
The error associated to an order of truncation has been studied in some specific scenario. For the far-field amplitude we showed that the error decreases as N increases, M increases and k decreases. In this case, small error is attained for moderate N, $N \sim 10$. On the other hand small errors for the near-field are obtained for relatively large values of N. Furthermore at least $M = 4$ sources are required. In contrast to the far-field, errors decrease for increasing k. The question of practicability remains open. We attempt to give the limitations that we should deal with. First the sources are supposed to be invisible for the incoming waves. We have no idea of how it could be obtained. Then the model of the plates induces that the displacement field should not vary brutally, therefore we have to pay attention on the vicinity of the sources. Finally the convergence requires high modal decomposition and it can be very sensitive to calibrate them. A first response to the last two issues might be proposed by the choice of large number of sources. Indeed this would allow us to use only monopole or dipole sources which are easier to calibrate. Furthermore, the more sources we use, the

smaller are the circles in the vicinity of the sources. Therefore high value of M reduces the region where the displacement is uncontrollable. For sufficiently large M it could become so tiny that it would approximately correspond to the singularity of the source. Further discussions with experimenters are required to enriches the possible responses and surely the practical limitations. Unfortunately this aspect was not investigated in this thesis.

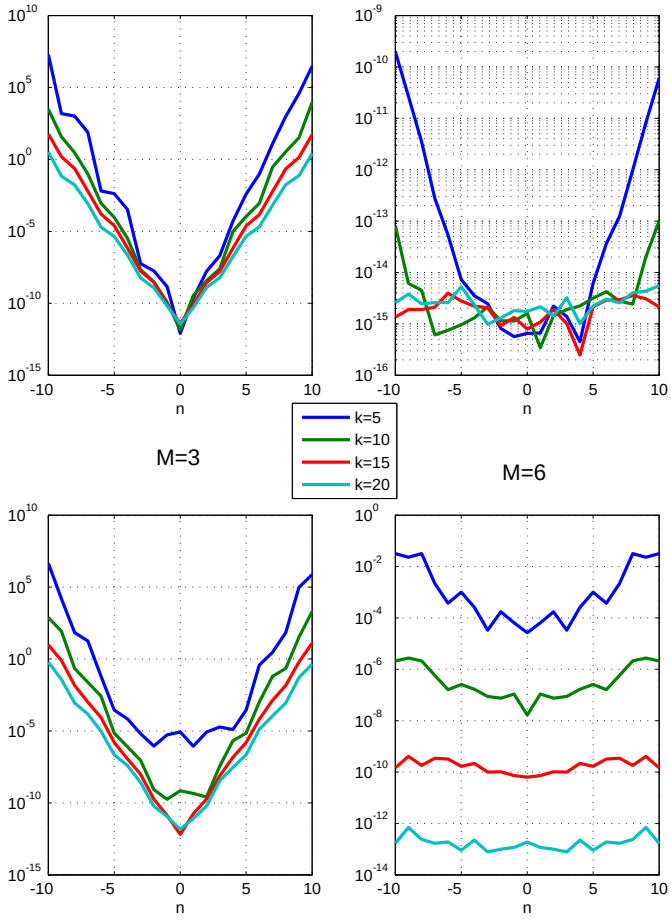

Figure 3.12: Dependence of the nearfield coefficient amplitudes $|A_n + E_n^{(app)}|$ (upper part) and $|\mathcal{A}_n + \mathcal{E}_n^{(app)}|$ (lower part) on the order n of the modes for different number of sources M and different value of k. The truncation order is $N = 150$.

Chapter 4

Elastic waves in covariant gradient continua

4.1 Introduction

Dispersion and attenuation of waves during its propagation are well-known phenomena corroborated by experimental measurements and numerical simulations. Analysis of elastic waves within complex media is an active research field. Moreover, the general terminology of complex media includes various subclasses such as, for example, heterogeneous media, fractured media or media with perturbed microscopic lattice. In order to improve the propagation modelling, rigorous underlying concepts are needed to describe each type of complex medium. For instance in heterogeneous media, multiple scattering models focus on the scattering relations between disconnected scatterers according to their concentration whereas homogenization deals with smooth variations of material properties *e.g.* [MML04].
This paper focus on media for which vector fields (such as displacement) or scalar fields (such as matter density) are not continuous. It can be observed on lattice undergoing dislocations or disclinations [Ana07]. Description of such microscopical defect involves discrete models. The diffraction of a single dislocation line embedded in a perfect elastic medium has been already addressed in *e.g.* [Mur63, Lun88, MML]. In materials such as metals, the density of structural defects is very large. Obtaining a macroscopic result implies spatial averaged techniques [MML04]. To avoid difficulties induced by the superposition of two successive models we propose a full mesoscopic model. We assume a smooth continuous density of structural defect in order to use the tools of Riemann-Cartan differential geometry *e.g.* [Rak97]. Indeed, the defect modifies the material geometry for this model.
The role played by geometry in physics is commonly acknowledged. In 1909, the Cosserat brothers introduced a model of continuum involving an independent field of rotation in addition to the displacement. This model was the first step for the study of larger classes of continua. For example a non-homogeneous continuum can be modelled by an homogeneous Cosserat continuum. Cartan was inspired by this approach and has

developed continuum models based on Riemann-Cartan (RC) manifold, endowed with not only the metric (measuring the shape change) but also an affine connection ∇ which replaces the classical gradient operator $\overline{\nabla}$ [Car86]. The affine connection is enriched by the torsion tensor and gives rise to the curvature tensor. If one of these tensors is non-zero, the geometrical equivalence between the Euclidean space and the continuum is lost. This loss corresponds to a non-holonomic deformation of the continuum inducing an incompatible state [Kro80]. Bilby and Smith [BBS55], Kondo [Kon55] and Kröner [Kro80] highlight that the method of the Cartan's circuit brings new perspectives for modelling a continuous distribution of dislocations and disclinations in the continuum, and a link with the incompatibility of strain is introduced. This approach gave similar results as the classical studies of some statical problems with one dislocation. Noll gave a new definition of "homogeneity" and, as consequence, of "non-homogeneity" for simple materials: a continuum is said to be homogeneous if there exists a state of deformation of the material manifold in which the mass density is uniform [Nol67]. Following this approach, one of the authors proposes a class of non-homogeneity allowing discontinuities of scalar fields and vector fields described by torsion and curvature [Rak97]. The application to wave propagation in non-homogeneous continuum is developed in [TBR11] under the hypothesis of covariant spatial strain for continuum. The aforementioned works broaden the concept of generalized continua [Mau13b] which is originally intended in the sense of Germain [Ger73].
We first recall the geometric concepts needed to describe the continuum. Then we introduce the continuum with defects through non-holonomic deformation of a perfect material and we recall the relation between non-holonomic deformation, torsion tensor and Burgers vector of dislocations. The torsion represents indeed the density of Burgers vectors. The RC geometry is then used to derive the mechanical conservation laws. However, a fundamental discussion arises concerning the choice of covariant derivative defining the strain. We could neglect or not the defect's influence on the deformation, that is to say using the symmetric connection $\overline{\nabla}$ or the full connection ∇ to define the strain. In order to address this question both models are developed and compared at each step of the present paper.
For a linear constitutive law we obtain a 3D propagation equation which extends the Navier equation on an arbitrary RC manifold with an uniform and stationary torsion density. We develop an example of a continuum with uniform density of screw dislocations. We present both analytic and numerical dispersion relations for various directions of propagation, frequencies and densities of dislocation. These dispersion equations are related to one quasi-longitudinal wave and two quasi-transversal waves. The dynamical results suggest that the spatial strain defined with $\overline{\nabla}$ does not capture some physical phenomena such as the breathing of dislocations. For the material strain defined with ∇ the wave has a chiral behaviour which would be observed over large propagation distances.

4.2 Geometric approach

4.2.1 A mesoscopic model for complex media

In the following we introduce a model of continuum with defects in the framework of differential geometry. Physically, material and structural defects can be continuously distributed or localized within matter. In order to preserve the advantages of the approach of the continuum mechanic, the representative volume of the material is supposed to encompass a wide number of (possibly discrete) defects. Hence, we consider a mesoscopic model where the lattice structure of the material is not directly observable. Moreover a modification of the classical differential tools may be seen as being the mesoscopic illustration of the microstructural defects. These geometrical tools are described in [Nak96].

4.2.2 Differential tools and Riemann-Cartan geometry

It is tricky to give a recall on differential geometry which would be brief but also self-consistent, because a lot of notions need to be developed. Therefore we made our best to suggest an heuristic approach, based on concepts of continuum mechanics, to summarize the Riemann-Cartan geometry on the material manifold. Only knowledges on tensor calculus are needed but some details found in [Nak96] would be helpful.

To the Euclidean space $\mathbb{E}$ are associated local coordinates $(X^i)_{i=1...3}$ and the metric g_{ij}. The metric is an order 2 tensor which defines an inner product between vector fields. As the Cauchy-Green strain tensor, it is related to the norm of a vector and to the angle between two vectors. A transformation is applied on $\mathbb{E}$ and defines a new configuration $\mathbb{M}$ of the continuum with local coordinates $(x^\mu)_{\mu=1...3}$ inducing the new metric $g_{\mu\nu}$ (Fig.4.1). The $\mathbb{M}$-state models the material manifold. Greek indices are used to express the coordinates in the material manifold whereas the Latin ones refer to the Euclidean space so that $\mathbf{e_i}$ (resp. $\mathbf{e}_\mu$) are the basis vectors of the tangent space of $\mathbb{E}$ (resp. $\mathbb{M}$). The transition between both states is performed by the triads e_i^μ which is related to the local transformations (not reduced to be only plastic) of the $\mathbb{E}$-state into the $\mathbb{M}$-state: $\mathrm{d}x^\mu = e_i^\mu \, \mathrm{d}X^i$, in particular in classical continuum mechanics we have $e_i^\mu = \partial x^\mu / \partial X^i = \partial_i x^\mu$. The material metric $g_{\mu\nu}$ and the reciprocal triads e_μ^i are related by: $g_{\mu\nu} = e_\mu^i e_\nu^j g_{ij}$, with $e_i^\mu e_\mu^j = \delta_i^j$, and where δ_i^j is the Kronecker symbol. The manifolds $\mathbb{E}$ and $\mathbb{M}$ are interpreted as two different states of the same body. The $\mathbb{E}$-state is considered as an homogeneous continuum whereas the $\mathbb{M}$-state includes structural defects engendered by non-holonomic deformations [Nol67]. Indeed, the differential structure of $\mathbb{M}$ is not necessarily Euclidean (Fig.4.1). In this framework, the covariant derivative generalizes the notion of the directional derivative of vector fields and tensor fields. In the material coordinates, the covariant derivative of a basis vector $\mathbf{e}_\beta$ along the direction $\mathbf{e}_\alpha$ is obtained by the affine connection ∇ [Nak96] and defined by $\nabla_\alpha \mathbf{e}_\beta := \Gamma_{\alpha\beta}^\gamma \mathbf{e}_\gamma$, with its connection's coefficients expressed in terms of the triads: $\Gamma_{\alpha\beta}^\gamma = e_i^\gamma \partial_\alpha e_\beta^i = -e_\beta^i \partial_\alpha e_i^\gamma$. The connection of the material manifold is assumed to be metric compatible $\nabla g = 0$

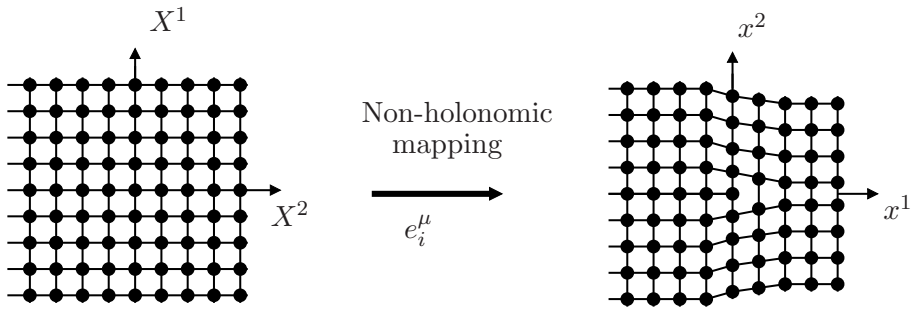

Figure 4.1: The local coordinates x^α on the material manifold define a new geometry on it. This geometry might be non Euclidean. The triads define a new metric, the torsion and the curvature are not necessarily zero.

e.g. [Nak96]. In this context the torsion tensor is defined by:

$$S^\gamma_{\alpha\beta} = \frac{1}{2}\big(\Gamma^\gamma_{\alpha\beta} - \Gamma^\gamma_{\beta\alpha}\big) = \frac{1}{2}e^\gamma_i\big(\partial_\alpha e^i_\beta - \partial_\beta e^i_\alpha\big), \quad \text{then} \quad S^\gamma_{\alpha\beta} = -S^\gamma_{\beta\alpha}\ .$$

The relation $\partial_\alpha e^i_\beta - \partial_\beta e^i_\alpha = 0$ expresses the Schwarz integrability condition for the triads. In other words, a non integrable (or non-holonomic) transformation corresponds to a non-zero torsion. This torsion tensor measures the failure of the closure of the parallelogram made by the small displacement vectors and their parallel transports (cf figure4.2).

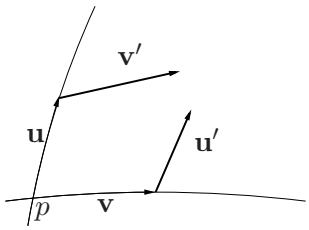

Figure 4.2: The vector $\mathbf{v}$ (resp. $\mathbf{u}$) is transported along the line tangent to the vector $\mathbf{u}$ (resp. $\mathbf{v}$) becoming $\mathbf{v}'$ (resp. $\mathbf{u}'$). The presence of the torsion is illustrated by the non closure of the parallelogram.

If the integrability condition is verified then the material manifold is said Riemannian. In this case the connection is the Levi-Civita's connection $\overline{\nabla}$. It is uniquely defined by the metric with the condition of metric compatibility [Nak96]. The connection coefficients are the Christoffel symbols $\overline{\Gamma}^\gamma_{\alpha\beta}$ defined by:

$$\overline{\Gamma}^\gamma_{\alpha\beta} = \frac{1}{2}g^{\gamma\lambda}(\partial_\alpha g_{\beta\lambda} + \partial_\beta g_{\lambda\alpha} - \partial_\lambda g_{\alpha\beta})\ .$$

The curvature tensor is expressed by mean of the connection's coefficients *e.g.* [Nak96]:

$$R^{\cdot\lambda}_{\alpha\cdot\beta\gamma} = \partial_\beta\Gamma^\lambda_{\gamma\alpha} - \partial_\gamma\Gamma^\lambda_{\beta\alpha} + \Gamma^\lambda_{\beta\kappa}\Gamma^\kappa_{\gamma\alpha} - \Gamma^\lambda_{\gamma\kappa}\Gamma^\kappa_{\beta\alpha}, \quad \text{then} \quad R^{\cdot\lambda}_{\alpha\cdot\beta\gamma} = -R^{\cdot\lambda}_{\alpha\cdot\gamma\beta}\ .$$

A manifold endowed with both curvature and torsion is a Riemann-Cartan manifold. We can decompose the connection's coefficient into two parts:

$$\Gamma^{\gamma}_{\alpha\beta} = \overline{\Gamma}^{\gamma}_{\alpha\beta} + K^{\gamma}_{\alpha\beta} \ , \tag{4.1}$$

with the contortion tensor $\mathbf{K}$:

$$K^{\gamma}_{\alpha\beta} = \frac{1}{2}\left(S^{\gamma}_{\alpha\beta} + g^{\gamma\lambda} S^{\kappa}_{\lambda\beta} g_{\kappa\alpha} + g^{\gamma\lambda} S^{\kappa}_{\lambda\alpha} g_{\kappa\beta} \right) \ . \tag{4.2}$$

In this case we can also express the curvature by:

$$R^{\cdot\lambda}_{\alpha\cdot\beta\gamma} = \overline{R}^{\cdot\lambda}_{\alpha\cdot\beta\gamma} + \overline{\nabla}_{\beta} K^{\lambda}_{\gamma\alpha} - \overline{\nabla}_{\gamma} K^{\lambda}_{\beta\alpha} + K^{\lambda}_{\beta\kappa} K^{\kappa}_{\gamma\alpha} - K^{\lambda}_{\gamma\kappa} K^{\kappa}_{\beta\alpha} \ , \tag{4.3}$$

where $\overline{R}^{\cdot\lambda}_{\alpha\cdot\beta\gamma}$ are the components of the curvature associated to the Levi-Civita's connection, and depend only on the metric tensor's components. This decomposition shows the contribution of the contortion (then the torsion) in the curvature. For instance we may have a metric such it does not involve curvature whereas torsion does. This will be illustrated by the example treated in section 4.4.1. For a given set of metric and connection, the Bianchi's identities are satisfied [Nak96]. We conclude with an important remark. We have interpreted the $\mathbb{E}$-space as a reference state and the $\mathbb{M}$-space as the material one. The local coordinates attached to the matter express the fields as if we live in the $\mathbb{M}$-space. Moreover, for an external observer (out of the $\mathbb{M}$-space) the tensor fields are generally still expressed in the coordinates of the ambient space which is Euclidean. We can always express the tensors in the Euclidean coordinates by using the triads and reciprocal triads. For example, for a vector we have: $\mathbf{u} = u^{\alpha}\mathbf{e}_{\alpha} = u^{i}\mathbf{e_i}$, with $u^{i} = e^{i}_{\alpha} u^{\alpha}$.

4.2.3 Physical meaning

Special case of defects : the dislocations We focus on the dislocations (discontinuities of the displacement field) which are line-like defects characterized by the Burgers vector $\mathbf{b}$. The simplest examples of dislocations are shown in the figure (4.3). The principle is the following: one cuts a half-plane whose boundary is the dislocation line L. Then the upper part of the continuum is translated by the vector $\mathbf{b}$ which can be parallel to the dislocation line (screw dislocation) or be perpendicular to it (edge dislocation), $\mathbf{b}$ being included in the cut plane. $\mathbf{b}$ is not necessarily constant along L. After gluing, the continuum comes to the equilibrium state.

Relation Torsion tensor and Burgers vector In the case where the dislocations are associated to a single line, Burgers [Bur39] introduces $b^{i} = \oint_{C} du^{i}(x)$ to define the singularity of the displacement $\mathbf{u}$ along a curve C surrounding the dislocation line. Here, the Burgers vector $\mathbf{b} = b^{i}\mathbf{e_i}$ does not depend on the curve as long as it surrounds the dislocation line. We define the screw dislocations for $\mathbf{b}$ being collinear to the line and the edge dislocations for $\mathbf{b}$ being orthogonal to the line. In the theory of continuum mechanics, the chosen scale suggests us to deal with density of dislocations rather than

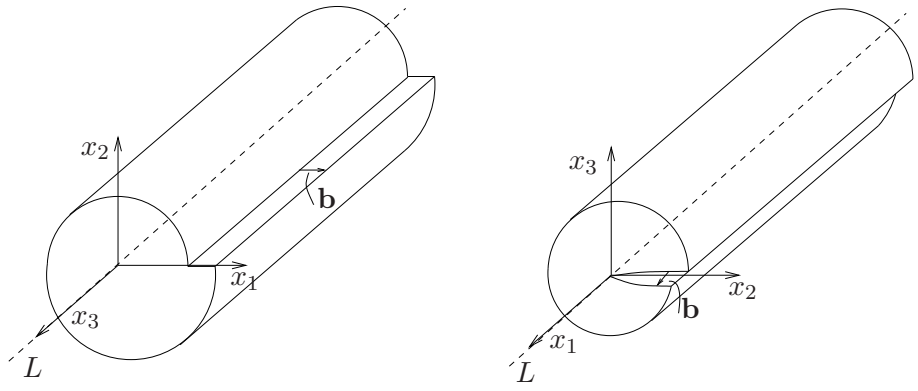

Figure 4.3: The edge dislocation (left): the Burgers vector is perpendicular to the dislocation line. The screw dislocation (right): the Burgers vector is parallel to the dislocation line.

dislocation's lines because we can not surround a single line: the representative volume element includes more than one defect. The failure of the closure is a vector (still denoted $\mathbf{b}$) which may be expressed in the material or spatial (Euclidean) coordinates. Let C being an arbitrary closed curve, the Euclidean components b^i of the failure of the closure is given by: $b^i = \oint_C dx^\alpha \partial_\alpha X^i(x) = \oint_C dx^\alpha e^i_\alpha$. This is the integral form of the incompatibility law introduced by Kröner [Kro80]. It can be expressed through the integral over a surface Σ having contour C as boundary:

$$b^i = \int_\Sigma dx^\alpha \wedge dx^\beta (\partial_\alpha e^i_\beta - \partial_\beta e^i_\alpha), \quad \text{where } dx^\alpha \wedge dx^\beta \text{ is the surface element.}$$

Hence

$$b^i = \int_\Sigma dx^\alpha \wedge dx^\beta e^i_\gamma S^\gamma_{\alpha\beta} = \int_\Sigma dx^\alpha \wedge dx^\beta S^i_{\alpha\beta} \tag{4.4}$$

shows that the torsion tensor may be interpreted as the density of Burgers vector. Here $\mathbf{b}$ shall be thought as the total Burgers vector resulting from all dislocation lines going through the surface Σ. The upper index of $S^i_{\alpha\beta}$ corresponds to the component of the associated total Burgers vector and the lower indices correspond to the material coordinates of the plane containing the surface Σ. Eq.4.4 gives the components of $\mathbf{b}$ in the Euclidean space for convenience but the surface is clearly expressed in the material space. Because a body with continuous dislocations density may be modelled by a material manifold with non-zero torsion *e.g.* [LS96], we suggest to describe the defects with the torsion tensor rather than using the Burgers vectors as usually. Moreover the Burgers vector is not a topological invariant [YDH98] and the type of defect (screw or edge) is not invariant [Kro80]-p241. Since the torsion contains some informations about the defects without precisely determining the crystallographic structure, we avoid specifying lines and types of defects in this section. Note that this continuum approach may introduce some shortcomings because it neglects the possible interaction of defects accruing from the microscopic scale, see [Kro01] for details. Similar remarks can be done

for the curvature tensor and the Franck vector defined for disclinations [Kle08, KV92]. Because the torsion may induce a curvature according to Eq.4.3, the dislocations are in fact interrelated with the disclinations.

Order of magnitude The experimental quantitative estimations of **S**'s components has not been found after a detailed bibliography where no quasi-static nor ultrasonic experimental protocols are devoted to the evaluation of this geometrical quantity. In the classical literature on plasticity theory, the Burgers vector has the same order of magnitude than the lattice size: $b \sim 10^{-10}\ m$. Therefore it is tempting to conclude $S_{ij}^k \sim b/\ell^2 \sim 10^4\ m^{-1}$ for a typical distance between dislocations $\ell \sim 10^{-7}\ m$. According to [FH97] this overestimates the individual effect of the lattice's dislocation. Strain gradient methods use a larger length scale $\hat{\ell} \sim 1 - 10\ \mu m$ for which the microscopic effects can be related to a macroscopic strain gradient effect [GHNH99]. If this latter typical dimension is used we obtain $S_{ij}^k \sim b/\hat{\ell}^2 \sim 1\ m^{-1}$.

4.3 Generalized Navier equation in a Riemann-Cartan manifold

4.3.1 Constitutive laws

In the previous section, we saw how non-holonomic transformation changes the intrinsic geometry of matter. This new geometry is interpreted as a material manifold with defects. In elastoplasticity based on a gauge theory, the equations describe the fields evolution with respect to a reference state without defect as in the first section [Laz02, Kro80]. In such a method, triads (or equivalently torsion and metric) are unknown functions that we have to determine in order to entirely describe the motion of matter: it cannot be related to the displacement field. Hence the tensor fields attached to the matter vary during the transformation, they do depend on time variable. Our approach is slightly different. We focus on a superimposed evolution of a continuum with defects assuming small elastic perturbations. The continuum is considered to be at the equilibrium in the defective state. Consequently our reference state is modelled by a RC manifold in order to take into account the presence of defects. Furthermore the superimposed elastic perturbation is a diffeomorphism therefore it does not create new defects. Basically the connection (and by the way the contortion) is a fixed parameter in the Lagrangian function (and so the free energy) so that we do not consider its variation during the superimposed transformation. Adopting a generalized continuum method, we consider the same conservation equations as in classical elasticity but we need to define the differential operators by means of the material connection attached to the (defective) reference state. It captures the influence of the defects during the superimposed motion. Let $\mathbf{u}$, ε and σ be respectively the superimposed displacement field, the small-strain tensor and the (symmetric) stress tensor. Then the conservation laws are *e.g.* [Rak97] : (1) for the mass conservation $\rho = \rho_0 \det(e_i^\alpha)$; and (2) for the momentum conservation without external force : $\rho_0 \partial_t^2 \mathbf{u} = \nabla \cdot \sigma$. We assume a linear

Hooke's constitutive law for an homogeneous isotropic elastic medium with constant Lamé coefficients λ and μ: $\sigma = \lambda \mathrm{Tr}(\varepsilon)\mathbf{I} + 2\mu\varepsilon$ where $\mathbf{I}$ is the identity tensor. We obtain the equation of propagation for the displacement:

$$\rho_0 \, \partial_t^2 \mathbf{u} = \nabla \cdot [\lambda \mathrm{Tr}(\varepsilon)\mathbf{I} + 2\mu \, \varepsilon] \, . \tag{4.5}$$

At this step the definition of the strain tensor is questionable because two points of view can be adopted. According to the RC geometry of the reference state, as a first point of view, it seems more rigorous to use the covariant derivative ∇ to calculate the gradient of the displacement. Indeed the strain tensor describes how the continuum is locally modified (*i.e.* the matter's motion with respect to its vicinity). In this case, the gradient should use the material connection which, in addition to the metric, characterizes the geometrical structure of the material manifold *e.g.* [Nol67]. From another slightly different but second point of view, we could suppose that the superimposed deformation is only sensitive to the metric, hence the influence of the defects on the definition of the strain would be neglected: each infinitesimal volume is deformed without further restriction due to the defected arrangement within matter. Adopting this second hypothesis, we can calculate the strain (as the symmetric part of the displacement gradient) with the help of the Levi-Civita's connection $\overline{\nabla}$. Hereafter we derive Eq.4.5 for each hypothesis.

4.3.2 Spatial strain

In this framework the strain is defined as in classical continuum theory:

$$\varepsilon = \frac{1}{2} \left[\overline{\nabla}\mathbf{u} + (\overline{\nabla}\mathbf{u})^t \right] , \tag{4.6}$$

where $\overline{\nabla}$ is the Levi-Civita connection whose coefficients are the Christoffel's symbols associated to the metric of the $\mathbb{M}$-space: $\overline{\nabla}\mathbf{u} = \left(\partial_j u^i + \overline{\Gamma}^i_{jk} u^k\right) \mathbf{e_i} \otimes \mathbf{e^j}$. The strain is obtained without taking into account the torsion and the curvature of the continuum. Here ε is a mixed tensor. A full contravariant or covariant tensor can be obtained by using the metric tensor: $\varepsilon_{ij} = g_{ik}\varepsilon^k_j$ and $\varepsilon^{ij} = g^{jk}\varepsilon^i_k$. The stress tensor is expressed with Levi-Civita's connection as well:

$$\sigma = \lambda \left(\overline{\nabla} \cdot \mathbf{u} \right) \mathbf{I} + \mu \left(\overline{\nabla}\mathbf{u} + (\overline{\nabla}\mathbf{u})^t \right) \, . \tag{4.7}$$

However, we have to remind that in the conservation laws Eq.4.5, the material divergence is applied. Now the divergence of a full contravariant tensor is:

$$\nabla \cdot \sigma = \left(\partial_i \sigma^{ji} + \Gamma^i_{ik}\sigma^{jk} + \Gamma^j_{ik}\sigma^{ki} \right) \mathbf{e_j} \, , \tag{4.8}$$

what would be synthesized by using the decomposition Eq.4.1 and with the following notation: $\nabla \cdot \sigma = \overline{\nabla} \cdot \sigma + K \cdot \sigma$. Note that the convention $K \cdot \sigma$ must not be confused with the classical tensor contraction. The material divergence acting on each term of the stress Eq.4.7 gives:

$$\nabla \cdot \left[(\overline{\nabla} \cdot \mathbf{u})\mathbf{I} \right] = \overline{\nabla}\big(\overline{\nabla} \cdot \mathbf{u}\big) + (\overline{\nabla} \cdot \mathbf{u})\big(K \cdot \mathbf{I}\big) \, ,$$

$$\nabla \cdot \left[\overline{\nabla}\mathbf{u} \right] = \overline{\nabla} \cdot \big(\overline{\nabla}\mathbf{u}\big) + K \cdot (\overline{\nabla}\mathbf{u}), \qquad \nabla \cdot \left[(\overline{\nabla}\mathbf{u})^t \right] = \overline{\nabla} \cdot (\overline{\nabla}\mathbf{u})^t + K \cdot (\overline{\nabla}\mathbf{u})^t \, .$$

We recall the classical identities: $\overline{\nabla}\cdot(\overline{\nabla}\mathbf{u}) = \overline{\Delta}\mathbf{u}$ and $\overline{\nabla}\cdot(\overline{\nabla}\mathbf{u})^t = \overline{\nabla}(\overline{\nabla}\cdot\mathbf{u})$. Finally the equation of propagation becomes:

$$\rho_0\partial_t^2\mathbf{u} = (\lambda+\mu)\overline{\nabla}\big(\overline{\nabla}\cdot\mathbf{u}\big) + \mu\overline{\Delta}\mathbf{u} + \mathbf{f}^{\mathrm{sp}}, \tag{4.9}$$

where $\mathbf{f}^{\mathrm{sp}}$ is the additional force terms due to the presence of the defects, for spatial strain, depending on the torsion tensor $\mathbf{S}$:

$$\mathbf{f}^{\mathrm{sp}}(\overline{\nabla}\mathbf{u},\mathbf{S}) = \lambda(\overline{\nabla}\cdot\mathbf{u})\big(K\cdot\mathbf{I}\big) + \mu\ K\cdot\big(\overline{\nabla}\mathbf{u} + (\overline{\nabla}\mathbf{u})^t\big)$$

Equation (4.9) is compatible with a linear elastic continuum with a given state of pre-stress described by an internal energy proportional not only to the square of the gradient of displacement but also to a linear part of it. Further investigations are needed to highlight the relation of dislocations density and such a pre-stress (*e.g.* [Ies]). In the case of a reference state without defects ($\mathbf{S}=0$), $\mathbf{f}^{\mathrm{sp}}$ vanishes and Eq.4.9 reduces to the classical Navier equation. The additional internal force $\mathbf{f}^{\mathrm{sp}}$ contains only first order derivatives of the displacement components and invokes linear contribution of contortion component. In particular, even in the case where torsion gives rise to curvature, the latter does not affect the wave propagation.

4.3.3 Material strain

Here the small-strain tensor is defined by means of material covariant derivative:

$$\varepsilon = \frac{1}{2}\left[\nabla\mathbf{u} + (\nabla\mathbf{u})^t\right], \tag{4.10}$$

and is now designated as material strain. It obviously introduces additional terms compared to the Levi-Civita connection as we can observe in the following. In the same way, some authors have explicitly considered some compensating gauge fields, assimilated to rotation angles, in the strain definition *e.g.* [SG05]. This allows us to have gauge covariant derivatives. Because $\mathrm{Tr}(\varepsilon) = \nabla\cdot\mathbf{u}$, the stress tensor is:

$$\sigma = \lambda\,(\nabla\cdot\mathbf{u})\,\mathbf{I} + \mu\left(\nabla\mathbf{u} + (\nabla\mathbf{u})^t\right)\ . \tag{4.11}$$

Let define the convention: $\nabla\mathbf{u} = \overline{\nabla}\mathbf{u} + K\mathbf{u}$, with $K\mathbf{u} = K^i_{jk}u^k\mathbf{e_i}\otimes\mathbf{e^j}$, and $\nabla\cdot\mathbf{u} = \overline{\nabla}\cdot\mathbf{u} + K\cdot\mathbf{u}$ with $K\cdot\mathbf{u} = K^i_{ik}u^k$. The divergence of each part of Eq.4.11 is uniformly written in terms of elementary operations involving $\overline{\nabla}$ and K:

$$\begin{aligned}
\nabla\cdot[(\nabla\cdot\mathbf{u})\mathbf{I}] &= \overline{\nabla}\big(\overline{\nabla}\cdot\mathbf{u}\big) + (\overline{\nabla}\cdot\mathbf{u})\big(K\cdot\mathbf{I}\big) + \overline{\nabla}\big(K\cdot\mathbf{u}\big) + (K\cdot\mathbf{u})\big(K\cdot\mathbf{I}\big)\ ,\\
\nabla\cdot[\nabla\mathbf{u}] &= \overline{\nabla}\cdot\big(\overline{\nabla}\mathbf{u}\big) + K\cdot(\overline{\nabla}\mathbf{u}) + \overline{\nabla}\cdot\big(K\mathbf{u}\big) + K\cdot(K\mathbf{u})\ ,\\
\nabla\cdot\big[(\nabla\mathbf{u})^t\big] &= \overline{\nabla}\cdot(\overline{\nabla}\mathbf{u})^t + K\cdot(\overline{\nabla}\mathbf{u})^t + \overline{\nabla}\cdot(K\mathbf{u})^t + K\cdot(K\mathbf{u})^t\ .
\end{aligned}$$

We see that the first two terms in these three expressions correspond to the case with spatial strain. Hence the internal force terms added to the classical Navier equation are here:

$$\begin{aligned}
\mathbf{f}^{\mathrm{mat}} &= \mathbf{f}^{\mathrm{sp}} + \lambda\Big(\overline{\nabla}\big(K\cdot\mathbf{u}\big) + (K\cdot\mathbf{u})\big(K\cdot\mathbf{I}\big)\Big) + \mu\Big(\overline{\nabla}\cdot\big(K\mathbf{u} + (K\mathbf{u})^t\big) + K\cdot\big(K\mathbf{u} + (K\mathbf{u})^t\big)\Big)\\
&= \mathbf{f}^{\mathrm{sp}} + \lambda\,\nabla\big(K\cdot\mathbf{u}\big) + \mu\,\nabla\cdot\big(K\mathbf{u} + (K\mathbf{u})^t\big)\ .
\end{aligned}$$

Hence the wave equation is:

$$\rho_0 \partial_t^2 \mathbf{u} = (\lambda + \mu)\overline{\nabla}(\overline{\nabla} \cdot \mathbf{u}) + \mu \overline{\Delta}\mathbf{u} + \mathbf{f}^{\text{mat}} \ . \tag{4.12}$$

Again, we find the classical Navier equation if $\mathbf{S} = 0$. The influence of the defects is much more complicated. Actually, in addition to the extra force $\mathbf{f}^{\text{sp}}$, we have covariant derivatives acting on the defect which induces a $\mathcal{O}(K^2)$-dependence on contortion. Moreover, this extra term contains $\mathcal{O}(K)$-terms too: $\mathbf{f}^{\text{sp}}$ is not a first order approximation of $\mathbf{f}^{\text{mat}}$. Hence, a spatial strain can not be chosen as a first approximation of the full material model for low density of defects. Another formulation (detailed in Appendix) gives:

$$\begin{aligned} \rho_0 \partial_t^2 \mathbf{u} &= (\lambda + \mu)\nabla(\nabla \cdot \mathbf{u}) + \mu \Delta \mathbf{u} + \mathbf{t}^{\text{mat}}, \quad \text{with:} \\ \mathbf{t}^{\text{mat}} &= \lambda \left(\nabla \cdot \mathbf{u}\right)(K \cdot \mathbf{I}) + \mu g^{kj} \left(R_{lk} u^l - S^l_{ik} \nabla_l u^i\right) \mathbf{e_j}. \end{aligned} \tag{4.13}$$

The presence of $\mathbf{t}^{\text{mat}}$ in this second formulation shows that the substitutions $\overline{\nabla} \to \nabla$ and $\overline{\Delta} \to \Delta$ are not sufficient to derive an exact equation in a distorted media. $\mathbf{t}^{\text{mat}}$ contains $\mathcal{O}(K)$-terms, hence this substitution is even wrong at the first approximation for a low defect density. Here $R_{lk} = R^{\cdot j}_{l \cdot jk}$ is the Ricci's tensor measuring the change of the volume form along a geodesic. In three dimensional geometry the curvature tensor is totally expressed by the Ricci's tensor [Nak96]. This second formulation also shows that the Ricci's curvature directly contributes in the wave equation. $\mathbf{f}^{\text{sp}}$ and $\mathbf{f}^{\text{mat}}$ are configurational forces, like Peach-Koehler forces *e.g.* [Mau10]. It's not the case for $\mathbf{t}^{\text{mat}}$.

4.4 Illustration and discussion for a simple torsion density

4.4.1 Simple form of defect density

As equations Eq.4.9 and Eq.4.12 are general, they are too complicated to build a simple illustration of both models. Indeed it is tricky to study an example for which $\mathbf{S}$ varies because the material term $\mathbf{f}^{\text{mat}}$ contains partial derivatives of K implying derivatives of S^i_{jk} terms. This is not the case for the spatial case but the partial differential equations could be hard to deal with. Moreover it is tempting to choose $\mathbf{S}$ (and so K) as a Dirac δ-function which would correspond to a unique dislocation. This choice involves some terms containing the jumps of the displacement components and of their derivatives (*cf* the terms proportional to K) along the dislocation line for both material and spatial case. Nevertheless for the material case we would have also the jumps of components of the torsion tensor, this latter being due to the derivatives of K.

Let us first observe that as for classical elasticity, the deformation between the (defected) reference state and the deformed one remains a diffeomorphism therefore we can suppose that the torsion is not modified. For the sake of simplicity the Cartesian coordinates are used so that the metric is trivial ($g_{ij} = \delta_{ij}$). Therefore we do not need to distinguish between upper and lower positions of indices and the Christoffel's

symbols are zero. Hence we focus on a simple geometry with non-zero torsion and $\overline{R} = 0$ where $\overline{R}$ is the curvature induced by the Levi-Civita's connection. We consider a simple example made of an infinite continuum with a uniform (and constant in time) density of screw dislocations associated to a Burgers vector $\mathbf{b}$ oriented along $\mathbf{e_1}$. Under these hypotheses, we have $S^i_{jk} = 0$ except for $S^1_{23} = -S^1_{32} := S$. It means that the density of the defects (and not the Burgers vector as it is usually supposed) is constant: indeed the larger is the surface of integration in Eq.4.4, the larger is the norm of the total Burgers vector. Using Eq.4.2, all the components of the contortion are zero except: $K^1_{23} = K^2_{13} = K^2_{31} = S/2$, $K^1_{32} = K^3_{12} = K^3_{21} = -S/2$, in particular $K^j_{ki} + K^i_{kj} = 0$ and $K^i_{ij} = K^i_{ji} = K^j_{ii} = 0$. Introducing this contortion in Eq.4.3 shows that the components of the Ricci tensor reduces to: $R_{ij} = -K^k_{jl}K^l_{ki}$. After the calculations, we obtain $R_{ij} = 0$ except for $R_{11} = S^2/2$. The curvature is caused by the defects density and not by the metric tensor. Here we have first defined the torsion and the metric so that the Bianchi identities are directly satisfied. We emphasize that for a finite body, we should probably formulate suitable boundary conditions so that particular boundary layers might appear.

4.4.2 Dynamical equations

The simple form chosen for the torsion is now injected in the equation of propagation. Some details are given in appendix. For the spatial strain Eq.4.6, the propagation equation Eq.4.9 gives:

$$\begin{aligned}
\rho_0\partial_t^2 u_1 &= (\lambda+\mu)\partial_1\partial_i u_i + \mu\partial_i\partial_i u_1, \\
\rho_0\partial_t^2 u_2 &= (\lambda+\mu)\partial_2\partial_i u_i + \mu\partial_i\partial_i u_2 + \mu S\left(\partial_1 u_3 + \partial_3 u_1\right), \\
\rho_0\partial_t^2 u_3 &= (\lambda+\mu)\partial_3\partial_i u_i + \mu\partial_i\partial_i u_3 - \mu S\left(\partial_1 u_2 + \partial_2 u_1\right).
\end{aligned} \tag{4.14}$$

For the material strain tensor Eq.4.10 the propagation equation Eq.4.13 reduces to:

$$\begin{aligned}
\rho_0\partial_t^2 u_1 &= (\lambda+\mu)\partial_1\partial_i u_i + \mu\partial_i\partial_i u_1 + \mu S\left(\partial_2 u_3 - \partial_3 u_2\right), \\
\rho_0\partial_t^2 u_2 &= (\lambda+\mu)\partial_2\partial_i u_i + \mu\partial_i\partial_i u_2 + \mu S\left(\partial_3 u_1 + 2\partial_1 u_3 - S u_2\right), \\
\rho_0\partial_t^2 u_3 &= (\lambda+\mu)\partial_3\partial_i u_i + \mu\partial_i\partial_i u_3 - \mu S\left(2\partial_1 u_2 + \partial_2 u_1 + S u_3\right).
\end{aligned} \tag{4.15}$$

4.4.3 Analysis of some particular solutions

For the material strain, oscillations can be observed for a spatially uniform displacement $\mathbf{u}$. It induces $u_1 = const$ and $(\partial_t^2 + (c_t S)^2)u_i = 0$ for $i = 2, 3$ where $c_t = \sqrt{\mu/\rho_0}$ is the celerity of the shear waves in a perfect medium. The associated time harmonic solutions are:

$$u_2 = U_2 e^{i\varpi t}, \qquad u_3 = U_3 e^{i\varpi t}, \qquad \text{with} \qquad \varpi = c_t S.$$

This vibration with infinite wavelength is sometimes called breathing. In some case, these vibrations can be observed as a temporal modulation of the static solution $\mathbf{u^e}(\mathbf{x})$

of the classical Navier equation in a perfect elastic medium (no defects):

$$\mathbf{0} = (\lambda + \mu)\overline{\nabla}(\overline{\nabla} \cdot \mathbf{u^e}) + \mu\overline{\Delta}\mathbf{u^e}.$$

As an example, let us consider an irrotationnal solution of the plane strain elastic problem in the $(\mathbf{e_2}, \mathbf{e_3})$-direction (perpendicular to the defects). In such a case $\mathbf{u^e}(\mathbf{x}) = \overline{\nabla}(\psi(x_2, x_3))$ where ψ is a potential defined by the boundary conditions. If this solution is injected into the modified Navier equation Eq.4.15 the static solution can be enriched by a time-oscillating behaviour: $\mathbf{u}(\mathbf{x}, t) = \mathbf{u^e}(\mathbf{x})e^{\pm i\varpi t}$. In other words, the spatial dependence is governed by the macroscopic geometry (and boundary conditions) whereas the frequency is induced by the microstructure. Contrary to the classical modes, the eigen-frequency seems to be independent of the size of the specimen and all the domain oscillates in phase (at least in this typical example). Of course some boundary conditions can cancel this phenomenon. This breathing-mode is not damped and occurs in the low frequency range: $\varpi/(2\pi) \sim 515\ Hz$ for steel ($c_t \sim 3240\ m/s$) if $S = 1$. Similar effects has been observed in the granular media or in the dynamics of a lattice using various methods [MMW63]. This breathing is not observed if the spatial strain is used.

4.4.4 Plane-wave eigenfunctions

We are interested in the wave solutions of these dynamical equations. We assume eigenfunctions with plane-wave form $\mathbf{u}(\mathbf{x}, t) = \mathbf{U}e^{i(\mathbf{k}\cdot\mathbf{x}-\omega t)}$. Here $\mathbf{U}$ is the polarization of the wave describing the direction of the displacement. In absence of source and boundaries, its amplitude has no signification. For plane-wave this vector has neither spatial nor temporal dependence. $\mathbf{k} = k\mathbf{n}$ is the wavevector where $\mathbf{n}$ denotes the direction of propagation ($\|\mathbf{n}\| = 1$). The wavenumber k is related to the frequency ω through a dispersion equation. Anisotropic propagation is characterized by dependence of k on the direction of propagation. Spatial attenuation (or amplification) occurs if k is complex. Let us define the polar angle ϕ as the angle between $\mathbf{k}$ and the direction of the defects line $\mathbf{e_1}$ and let us introduce an azimutal angle θ measured from $\mathbf{e_2}$ ($0 \leq \phi \leq \pi$ and $0 \leq \theta < 2\pi$). With this convention, a plane-wave is given by:

$$\mathbf{u} = \mathbf{U}e^{ik\mathbf{n}\cdot\mathbf{x}-i\omega t}, \quad \text{with} \quad \mathbf{n}\cdot\mathbf{x} = \cos\phi\, x_1 + \sin\phi\cos\theta\, x_2 + \sin\phi\sin\theta\, x_3\ .$$

Injecting this form into the equations of propagation (Eq.4.9 or Eq.4.13) gives:

$$(-k^2M + ikN + D)\mathbf{U} = -\omega^2\mathbf{U}, \tag{4.16}$$

where M is the classical matrix found in elasticity without defect: $M = c_t^2\mathbf{I} + (c_l^2 - c_t^2)\mathbf{n}\otimes\mathbf{n}$ and $c_l = \sqrt{(\lambda + 2\mu)/\rho_0}$ is the celerity of the longitudinal waves in a perfect medium. N and D are additional matrix terms induced by the torsion. They can respectively be interpreted as an attenuation and additional stiffness operators. Their forms differ according to the model used for the strain. If the spatial strain is chosen:

$$N^{sp} = c_t^2 S \begin{pmatrix} 0 & 0 & 0 \\ \sin\phi\sin\theta & 0 & \cos\phi \\ -\sin\phi\cos\theta & -\cos\phi & 0 \end{pmatrix}, \qquad D^{sp} = 0.$$

For the material definition of strain the matrices are:

$$N^{mat} = c_t^2 S \begin{pmatrix} 0 & -\sin\phi\sin\theta & \sin\phi\cos\theta \\ \sin\phi\sin\theta & 0 & 2\cos\phi \\ -\sin\phi\cos\theta & -2\cos\phi & 0 \end{pmatrix} , \quad D^{mat} = -c_t^2 S^2 \begin{pmatrix} 0 & 0 & 0 \\ 0 & 1 & 0 \\ 0 & 0 & 1 \end{pmatrix} .$$

For the material strain, the matrix $-k^2M + ikN + D$ is Hermitian: all eigenvalues are real and the eigenvectors form an orthogonal basis of $\mathbb{C}^3$. It's not the case for the spatial strain where $-k^2M + ikN + D$ can be non-diagonalizable: in such a case the problem may be no more considered as hyperbolic. That will be emphasized in section 4.4.8.

4.4.5 Dispersion relation

The eigenfunctions are defined as being the non-trivial solutions of the linear system Eq.4.16. The dispersion relation is then given by:

$$\det(-k^2M + ikN + D + \omega^2\mathbf{I}) = 0 \ .$$

For the spatial strain this expression can be rewritten as:

$$\left(k^2 - \frac{\omega^2}{c_l^2}\right)\left(k^2 - \frac{\omega^2}{c_t^2}\right)^2 - k^2S^2\cos^2(\phi)\left(k^2\big(\gamma + (1-\gamma)\cos(2\phi)\big) - \frac{\omega^2}{c_l^2}\right) = 0 \, , \quad \gamma = \left(\frac{c_t}{c_l}\right)^2 . \tag{4.17}$$

The dispersion relation is more complicated for the material strain and is put into a polynomial form:

$$\begin{aligned} & k^6 + a_2k^4 + a_1k^2 + a_0 = 0 \ , \qquad \text{with} \\ a_2 &= \left(\frac{\varpi^2}{c_t^2}\frac{(\cos(\phi))^2(5 - 9\cos(2\phi))}{2} - 2\frac{\omega^2}{c_t^2}\right) - \left(\frac{\omega^2}{c_l^2} + \frac{\varpi^2}{c_l^2}\frac{(\sin(\phi))^2(7 + 9\cos(2\phi))}{2}\right), \\ a_1 &= \frac{\omega^2 - \varpi^2}{c_t^2}\frac{\omega^2 - \varpi^2(\cos\phi)^2}{c_t^2} + 2\frac{\omega^2}{c_l^2}\frac{\omega^2 + \varpi^2\cos(2\phi)}{c_t^2}, \\ a_0 &= -\frac{\omega^2}{c_l^2}\left(\frac{\omega^2 - \varpi^2}{c_t^2}\right)^2 . \end{aligned} \tag{4.18}$$

For both models, the traditional form of the dispersion relation in an unperturbed medium is found for $S \to 0$. Both equations are independent of θ and invariant by the transformation $\phi \to \pi - \phi$. It is consistent with the geometry of the problem which is invariant by any rotations around $\mathbf{e_1}$ and symmetric to the $(\mathbf{e_2}, \mathbf{e_3})$-plane. In the following, the problem will be analysed for $\theta = 0$ and $0 \le \phi \le \pi/2$. For a propagation perpendicular to the defect line $\cos\phi = 0$ in Eq.4.17, we obtain the classical shear $k = \omega/c_t := k_t$ and longitudinal $k = \omega/c_l := k_l$ wavenumbers. The defect does not perturb the propagation. This phenomenon is not observed if the material strain is used.

4.4.6 Wavenumbers

The dispersion relations Eq.4.17 and Eq.4.18 are cubic functions of k^2 with real coefficients. We have three roots for k^2 and then 6 roots for k: $\pm k_1, \pm k_2$, and $\pm k_3$ which may be complex. For various directions of propagation, the evolution of the three roots k_1, k_2 and k_3 with frequency ω are computed for the typical values of steel and $S = 1\ m^{-1}$ (obtaining $-k_1$, $-k_2$ and $-k_3$ is straightforward).
Fig.4.4 shows the behaviour of the real part of the roots obtained with spatial strain. The classical roots for $\phi = \pi/2$ are not presented. The dependence of Eq.4.17 on the direction of propagation ϕ means an anisotropic dispersion relation. This effect is observed both in the low and high frequency regime. In high frequency regime, two wavenumbers have a quasi-shear solution ($k \sim k_t$) and one is closely related to the longitudinal solution k_l. The quasi-shear solutions are more affected by the torsion than the longitudinal one. For $\omega = 0$, a non-zero root is given by $k = S\cos(\phi)\sqrt{\gamma + (1-\gamma)\cos(2\phi)}$, which can be purely real or imaginary according to ϕ.
In the case of the material strain, the roots can be analytically found for $\phi = 0$ and $\phi = \pi/2$. We have the following set of roots:

$$\phi = 0\ , \qquad k = \left\{ k_l\ ,\quad k_t\left(1 - \frac{\varpi}{\omega}\right)\ ,\quad k_t\left(1 + \frac{\varpi}{\omega}\right) \right\},$$

$$\phi = \frac{\pi}{2}\ , \qquad k = \left\{ k_l\sqrt{1 - \frac{\varpi^2}{\omega^2}}\ ,\quad k_t\sqrt{1 - \frac{\varpi}{\omega}}\ ,\quad k_t\sqrt{1 + \frac{\varpi}{\omega}} \right\}.$$

The real parts of the roots obtained with the material strain are given in Fig.4.5 for various directions of propagation ϕ. In the intermediate frequency regime their behaviour is strongly dependent on the direction of propagation. As for the spatial strain, the high frequency regime highlights one quasi-longitudinal and two quasi-shear modes.
The phase velocities $c_\varphi = \Re e(\omega/k)$ of each mode are given in Fig.4.6 for three frequencies. The results are given for both (spatial and material) strains and mainly in a high frequency regime where the phase velocity has more sense. For both models, the anisotropy decreases as the frequency increases. If the spatial strain is chosen, the dispersion concerns mainly the shear waves propagating in a direction close to the defect line $\mathbf{e_1}$. For the material strain, the anisotropy is observable in all directions and is more pronounced. The domain of variation of the phase velocity is remarkably large for $\omega = 7\ 10^3$ rad/s, where two waves have a phase velocity close to c_l around $\phi = 0$. This effect is observed in the first picture in Fig.4.5 where two branches of the dispersion curves cross-over.
The imaginary part of the wavenumbers has some physical interest too because it is related to an attenuation ($\Im m(k) > 0$) or an amplification ($\Im m(k) < 0$) of the wave during its propagation. For the spatial strain, the wavenumbers are purely real for $\phi = 0,\ \pi/6$ and $\Im m(k)$ is given only for $\phi = \pi/3$ in Fig.4.7 (with the same label and color convention as Fig.4.4). Both quasi-shear wavenumbers are complex exhibiting an attenuation for one root and an amplification for the other. At high frequency attenuation/amplification is asymptotically constant. The behaviour of $\Im m(k_1)$ with

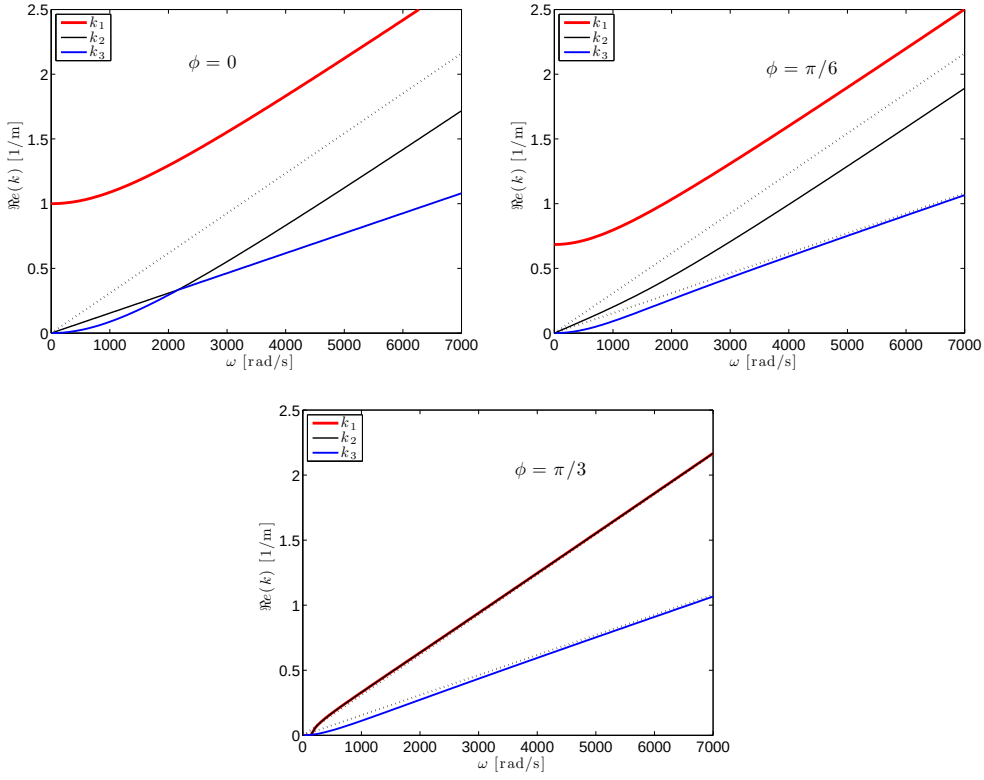

Figure 4.4: Dispersion curves $\Re e\big(k(\omega)\big)$ with spatial strain for a propagation direction $\phi = 0,\ \pi/6$ and $\pi/3$. Roots are labeled arbitrarily k_i, $i = 1, 2, 3$. Doted lines are the dispersion curves in a perfect medium (and for $\phi = \pi/2$ too): $k_l = \omega/c_l$ and $k_t = \omega/c_t$. Simulation is performed for $S = 1\ m^{-1}$ and typical steel values: $\rho_0 = 7500\ kg.m^{-3}$, Young modulus $E = 210\ GPa$ and Poisson ratio $\nu = 1/3$.

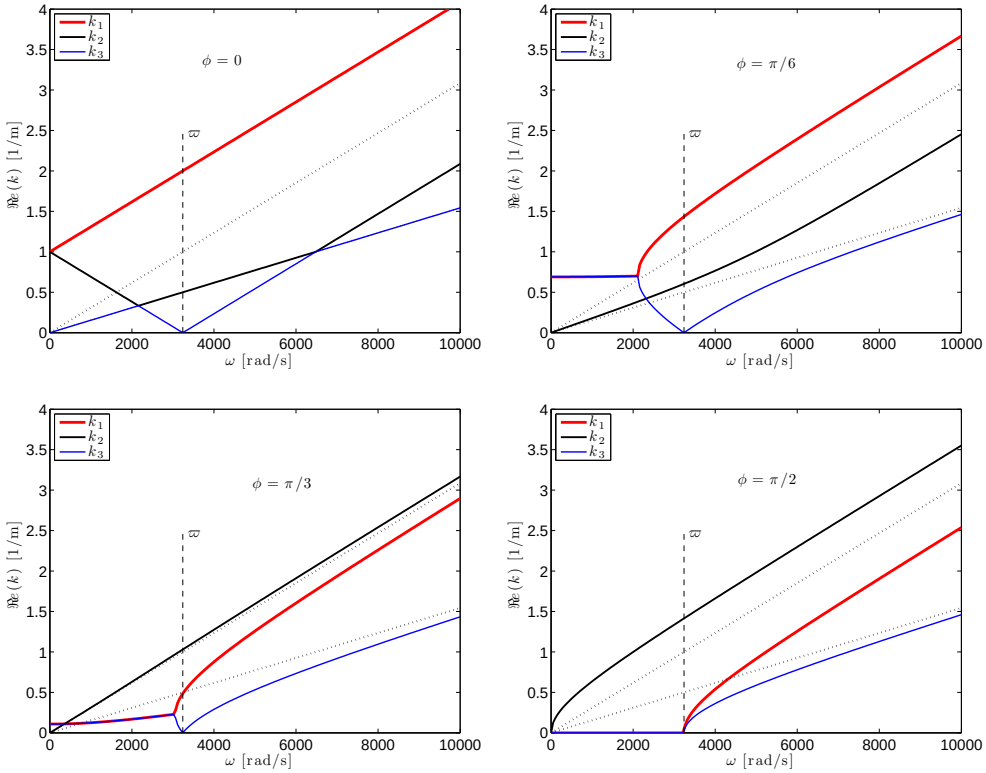

Figure 4.5: Dispersion curves $\Re e\big(k(\omega)\big)$ with material strain at $\phi = 0,\ \pi/6,\ \pi/3$ and $\pi/2$. The vertical line localizes ϖ. Same numerical values as Fig.4.4.

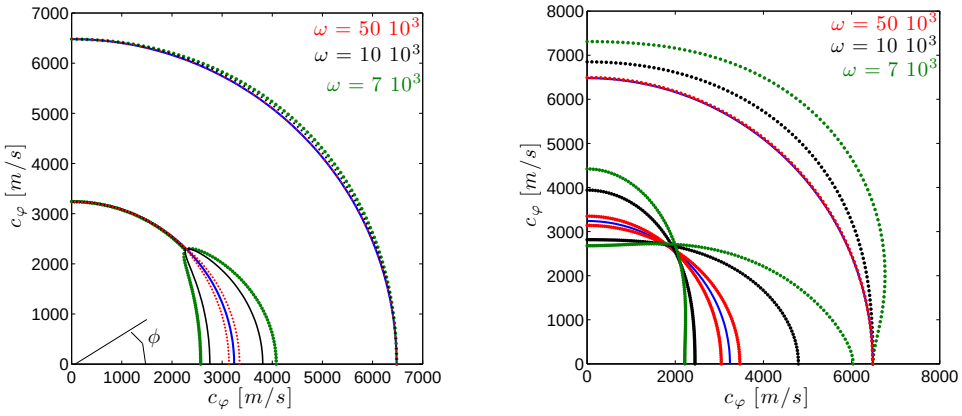

Figure 4.6: Phase velocity $c_\varphi(\phi)$ for three frequencies. Spatial (left) and material (right) strain's model. The blue lines indicate $c_l = 6480\ m/s$ and $c_t = 3240\ m/s$. Same values as Fig.4.4.

direction of propagation ϕ is given for three frequencies on Fig.4.7. In an infinite domain, $\Im m(k) < 0$ has no physical significance because the solution explodes at infinity. If the material strain is used k is always real for $\omega \geq \varpi$. The attenuation/amplification concerns mainly the low-frequency domain, which may imply boundary layers different from those obtained by a second gradient model where long-range interactions at the microscopic level are activated in a high-frequency regime [dMP12]. Bellow the cut-off frequency ϖ, only one root is purely real: only one mode can propagate in an infinite domain. Contrary to usual experimental measurement within heterogeneous media, the attenuation is not an increasing function of frequency. Such result has already been observed with discrete dislocation models [MML, MML04] . This confirms Kröner's prediction on limitation induced by models where torsion density is the mean value of the representative ensemble element [Kro01]. In [MML04] Maurel *et al* show that the traditional behaviour of the attenuation versus frequency can be recovered if a spatial average over the distribution of the dislocation lines is performed. Hence, in our approach where torsion is uniform, the results obtained for attenuation with the material strain looks more in conformity with the literature than the results obtained with the spatial strain. Further experimental investigations focusing on waves within continuum with dislocations would be helpful to understand these results.

4.4.7 High frequency regime

The roots k of Eq.4.17 or Eq.4.18 can be symbolically expressed with the Cardano's method. In the high frequency regime, a first-order Taylor expansion is used around $\varpi/\omega = 0$ to give an asymptotic form of k_i (indexes related to Fig.4.4 and Fig.4.5). For both spatial and material strains one obtains the general form:

$$k_1 = k_t + \kappa \ , \qquad k_2 = k_t - \kappa \ , \qquad k_3 = k_l \ ,$$

but the perturbation κ varies with the model used for strain:

$$\begin{aligned} \kappa &= \frac{S}{2}\cos\phi\sqrt{\cos 2\phi} && \text{spatial strain,} \\ \kappa &= \frac{S}{4}(1+3\cos 2\phi) && \text{material strain.} \end{aligned}$$

For the spatial strain, κ is imaginary for $\pi/4 < \phi < \pi/2$ in concordance with observation in Fig.4.4 and Fig.4.7. The eigenfunction in the high-frequency regime are of the form:

$$\mathbf{u^1} = \mathbf{U^1} e^{i\boldsymbol{\kappa}\cdot\mathbf{x}} e^{i(\mathbf{k_t}\cdot\mathbf{x}-\omega t)}, \qquad \mathbf{u^2} = \mathbf{U^2} e^{-i\boldsymbol{\kappa}\cdot\mathbf{x}} e^{i(\mathbf{k_t}\cdot\mathbf{x}-\omega t)}, \qquad \mathbf{u^3} = \mathbf{U^3} e^{i(\mathbf{k_l}\cdot\mathbf{x}-\omega t)},$$

with $\boldsymbol{\kappa} = \kappa\mathbf{n}$. The expressions of the eigenvectors $\mathbf{U^i}$ can be obtained too. Without structural defects, the polarization of the waves are generally related to longitudinal, shear-horizontal and shear-transversal modes: with a cylindrical basis $\mathbf{U^3} = \mathbf{e_r}$, $\mathbf{U^2} = \mathbf{e}_\theta$, $\mathbf{U^3} = \mathbf{e_z}$ respectively.
In presence of defects and using the spatial strain, the eigenvectors associated to each root are in first approximation (neglecting $\mathcal{O}(S)$ terms):

$$\mathbf{U^1} = \mathbf{e}_\theta + i\frac{\sqrt{\cos 2\phi}}{\cos\phi}\mathbf{e_z} \ , \qquad \mathbf{U^2} = \mathbf{e}_\theta - i\frac{\sqrt{\cos 2\phi}}{\cos\phi}\mathbf{e_z} \ , \qquad \mathbf{U^3} = \mathbf{e_r} \ ,$$

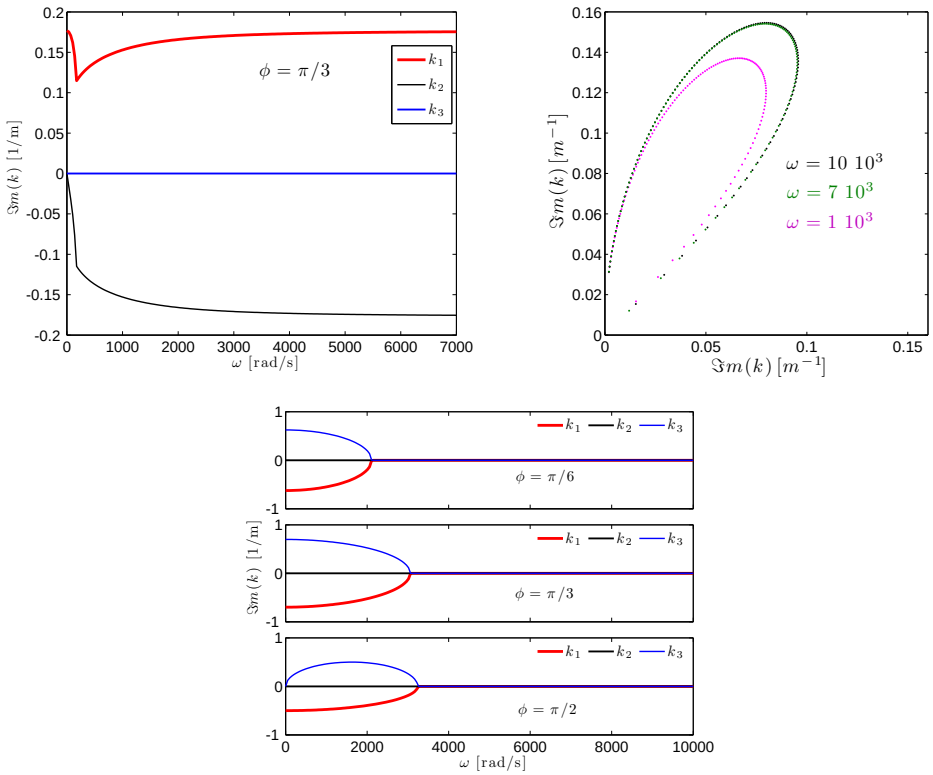

Figure 4.7: Top: behavior of $\Im m(k)$ with spatial strain. Left: $\Im m\big(k(\omega)\big)$ for $\phi = \pi/3$ only (zero for all k_i at $\phi = 0,\ \pi/6$). Right: $\Im m\big(k_1(\phi)\big)$ for three frequencies. Bottom: $\Im m(k)$ with material strain for $\phi = \pi/6,\ \pi/3,\ \pi/2$ ($\Im m(k) = 0$ for $\phi = 0$). Same values as Fig.4.4.

for $\phi \neq \pi/2$. The problem for $\phi = \pi/2$ is particular because the system has only two eigenvectors $\mathbf{e_r}$ and $\mathbf{e_z}$ and it will be studied later in detail (see section 4.4.8). Without loss of generality, the two last wave-functions can be linearly associated to form a new couple of eigenfunctions:

$$\mathbf{v^1} = \frac{\mathbf{u^1} + \mathbf{u^2}}{2} \ , \qquad \mathbf{v^2} = \frac{\mathbf{u^1} - \mathbf{u^2}}{2i} \ .$$

For $0 \leq \phi < \pi/2$:

$$\begin{aligned} \mathbf{v^1} &= \left(\cos\left(\boldsymbol{\kappa} \cdot \mathbf{x}\right) \mathbf{e}_\theta - \frac{\sqrt{\cos 2\phi}}{\cos\phi} \sin\left(\boldsymbol{\kappa} \cdot \mathbf{x}\right) \mathbf{e_z} \right) e^{i(\mathbf{k_t} \cdot \mathbf{x} - \omega t)} \ , \\ \mathbf{v^2} &= \left(\sin\left(\boldsymbol{\kappa} \cdot \mathbf{x}\right) \mathbf{e}_\theta + \frac{\sqrt{\cos 2\phi}}{\cos\phi} \cos\left(\boldsymbol{\kappa} \cdot \mathbf{x}\right) \mathbf{e_z} \right) e^{i(\mathbf{k_t} \cdot \mathbf{x} - \omega t)} . \end{aligned}$$

For the material strain's model the same process is used to obtain:

$$\mathbf{U^1} = \mathbf{e}_\theta + i\mathbf{e_z} \ , \qquad \mathbf{U^2} = \mathbf{e}_\theta - i\mathbf{e_z} \ , \qquad \mathbf{U^3} = \mathbf{e_r} \ ,$$

and

$$\begin{aligned} \mathbf{v^1} &= \left(\cos\left(\boldsymbol{\kappa} \cdot \mathbf{x}\right) \mathbf{e}_\theta - \sin\left(\boldsymbol{\kappa} \cdot \mathbf{x}\right) \mathbf{e_z} \right) e^{i(\mathbf{k_t} \cdot \mathbf{x} - \omega t)} := \mathbf{V_1}(\mathbf{x}) e^{i(\mathbf{k_t} \cdot \mathbf{x} - \omega t)} \ , \\ \mathbf{v^2} &= \left(\sin\left(\boldsymbol{\kappa} \cdot \mathbf{x}\right) \mathbf{e}_\theta + \cos\left(\boldsymbol{\kappa} \cdot \mathbf{x}\right) \mathbf{e_z} \right) e^{i(\mathbf{k_t} \cdot \mathbf{x} - \omega t)} := \mathbf{V_2}(\mathbf{x}) e^{i(\mathbf{k_t} \cdot \mathbf{x} - \omega t)} . \end{aligned}$$

With the material strain, the interpretation is clear: as a shear-wave propagates, its polarization ($\mathbf{V_1}$ or $\mathbf{V_2}$) regularly turns around the propagation's axis. The shear-wave's polarization follows the Cartan's spiral staircase [LH10]. Note that κ, and then the speed of rotation, is a function of the direction of propagation ϕ. For a propagation in the direction of the defects $\kappa = S$ whereas $\kappa = -S/2$ for a propagation in $(\mathbf{e_2}, \mathbf{e_3})$-plane. The sign of κ changes at $\phi = \phi_c \sim 54.7°$: a clockwise rotation governs the polarization for $0 \leq \phi \leq \phi_c$ whereas it's a counter-clockwise for $\phi_c \leq \phi \leq \pi/2$ (first picture in Fig.4.8). The second picture in Fig.4.8 shows the propagation of a shear-wave with $\mathbf{e_3}$ polarization at origin. Due to the rotation of the polarization the in-plane component (plotted in this figure) is no more zero. The initial polarity is recovered after a distance $L = 2\pi/\kappa$. This must be compared to the small wavelength of shear-waves (in Fig.4.8, $\lambda = 2\pi/k_t \sim 0.2\ m$). Hence, the chiral structure of the wave induces a spatial modulation of a fixed component of the wave over a large distance L. From a practical point of view, these considerations suggest that the structural defects may be observed in the high-frequency range for a propagation over a long distance. Remark that in many experimental devices, the ultrasonic characterization of dislocation is performed on small specimen [MCE+12, LHD+13]. Close to the direction of the defects, the displacement obtained with spatial strain behaves like for the material case. Moreover the eigen-vectors have an elliptical polarity for $0 < \phi < \pi/4$. For $\pi/4 \leq \phi < \pi/2$ the analysis based on the eigenfunction $\mathbf{v^1}$ and $\mathbf{v^2}$ does not offer any advantage because the wave is spatially attenuated (κ is complex).

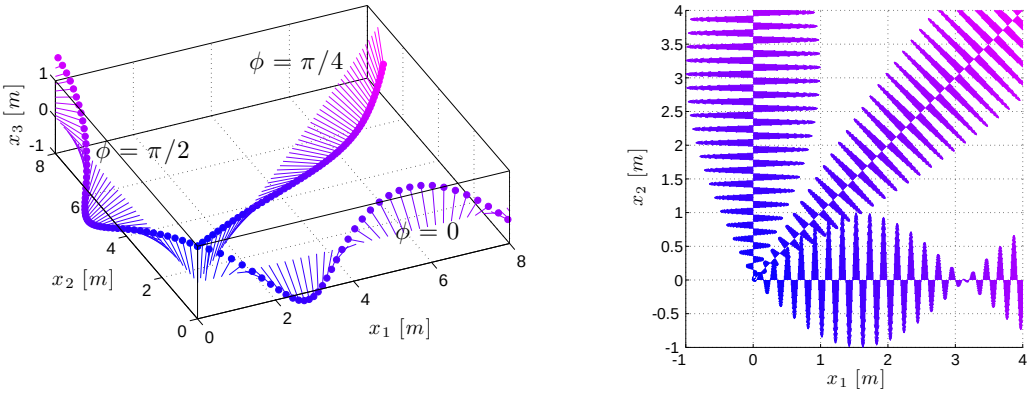

Figure 4.8: Left: polarization $\mathbf{V_1}$ of $\mathbf{v^1}$-wave function during the propagation, for three directions of propagation. The polarization is adjusted to be $\mathbf{e_3}$ at the origin. Right: real part of the in-plane component of $\mathbf{v^1}$ with the same convention. Same numerical values than Fig.4.4 and $\omega = 10^5$ rad/s.

4.4.8 In-plane component for spatial strain

4.4.8.1 Existence of plane solution

If the spatial model is used for the strain, only two eigenvectors have been found for propagation along $\mathbf{e_2}$. In order to focus on this point, we address the problem Eq.4.14 for an harmonic displacement in the form $\mathbf{u}(x_2)e^{-i\omega t}$. This solution refers to a in-plane solution as it varies only with a single Cartesian coordinate. We have:

$$\begin{aligned} -k_t^2 u_1 &= \partial_2^2 u_1 \ , \\ -k_l^2 u_2 &= \partial_2^2 u_2 \ , \\ -k_t^2 u_3 &= \partial_2^2 u_3 - S\partial_2 u_1 \ . \end{aligned}$$

We recognize the Helmholtz equation for the component u_1 and u_2. Therefore we have:

$$u_1(x_2) = U_1^{\pm} e^{\pm i k_t x_2} \ , \qquad u_2(x_2) = U_2^{\pm} e^{\pm i k_l x_2},$$

which are eigenfunctions found in the previous problem for $\phi = \pi/2$. $U_1^{\pm}$ and $U_2^{\pm}$ are defined by the boundary conditions. The projection onto $\mathbf{e_3}$ gives:

$$\partial_2^2 u_3 + k_t^2 u_3 = \pm i k_t S U_1^{\pm} e^{\pm i k_t x_2},$$

which is a second order linear equation with source term. Its solutions are:

$$u_3 = \left(\left(x_2 \pm \frac{i}{2k_t} \right) S U_1^{\pm} + U_3^{\pm} \right) \frac{e^{\pm i k_t x_2}}{2} \ .$$

It is difficult to give a particular meaning to these solutions in a general frame. Moreover the amplification imposed by the x_2 linear dependence is not compatible with the small

perturbation hypothesis in an infinite domain. In a large domain $x_2 S U_1^{\pm} \ll 1$ may be not satisfied if $U_1 \neq 0$. For a plane solution, the $\mathbf{e_1}$-shear polarization is not allowed in an infinite domain.

4.4.8.2 Existence of cylindrical solution

Of course the previous result is due to the restriction of the problem to in-plane solution. The symmetry of the problem suggests that the cylindrical coordinates can be used. Let us consider a cylindrical solution in the form: $\mathbf{u}(r)e^{-i\omega t}$ with $r^2 = x_1^2 + x_2^2$. Eq.4.14 can be put in a general form:

$$-\rho_0\omega^2\mathbf{u} = (\lambda+\mu)\overline{\nabla}(\overline{\nabla}\cdot\mathbf{u}) + \mu\overline{\Delta}\mathbf{u} + S\mu\overline{\nabla}\times\mathbf{w} \ , \tag{4.19}$$

where $\mathbf{w} = \mathbf{u} - u_1\mathbf{e_1}$ is the displacement perpendicular to the defects. Along $\mathbf{e_1}$ the problem is:

$$-k_t^2 u_1 = \frac{1}{r}\partial_r\left(r\partial_r u_1\right) \ ,$$

for which the regular solution is the classical Bessel function of zero order $u_1(r) = U_1 J_0(k_t r)$, where U_1 is defined by the boundary conditions. We decompose $\mathbf{w}$ onto cylindrical base: $\mathbf{w} = u_r\mathbf{e_r} + u_\theta\mathbf{e}_\theta$. The projections of Eq.4.19 onto $\mathbf{e_r}$ and $\mathbf{e}_\theta$ are respectively:

$$\begin{aligned} -k_l^2 u_r &= \frac{1}{r}\partial_r\left(r\partial_r u_r\right) \ , \\ -k_t^2 u_\theta &= \frac{1}{r}\partial_r\left(r\partial_r u_\theta\right) - S\partial_r u_1 \ . \end{aligned}$$

The radial component is $u_r(r) = U_r J_0(k_t r)$. Moreover the azimuthal component is a solution of a non-homogeneous Bessel differential equation where anti-plane and azimuthal components are coupled:

$$\frac{1}{r}\partial_r\left(r\partial_r u_\theta\right) + k_t^2 u_\theta = k_t S U_1 J_0'(k_t r) \ ,$$

which gives:

$$u_\theta(r) = U_\theta J_0(k_t r) - \frac{\varpi}{\omega}U_1 J_1(k_t r) \ .$$

For $\varpi \ll \omega$ the solution of the classical elasticity is found. Even if the spatial strain does not accept the $\mathbf{e_1}$-polarization in an infinite domain, all cylindrical polarizations are possible. More complicated forms can be obtained if azimuthal dependence is introduced: $\mathbf{u}(r,\theta)$.

4.5 Conclusion

In this paper we have established a model inspired by non Riemaniann geometric methods used in mechanics of generalized continuum. Defects are modelled with intrinsic differential operators taking into account torsion, metric and curvature. In this framework the definition of the strain tensor seems quite sensitive because we could express

it in term of either spatial connection or material one. *A priori*, the material connection is more rigorous because it takes into account the geometric structure of the material manifold (defected reference state) on the strain. We showed that it includes disclination effects through the Ricci tensor's contribution. To illustrate the difference between both definitions we deal with a simple case of constant density of screw dislocations in an infinite continuum. We obtained then a generalized Navier equation for both definitions of strain (Eq.4.5 and Eq.4.12). The added term in the Navier equation $\mathbf{f}^{\mathrm{sp}}$ is not an approximation of $\mathbf{f}^{\mathrm{mat}}$ where $\mathcal{O}(S^2)$ would be neglected. Therefore the effects caught in the material are not due to large density of defects which is not an argument to neglect their influence on the strain. Furthermore both definitions imply anisotropy for the wave propagation however the dispersion and the attenuation are radically different. In the considered case with homogeneous density of defect, material strain model shows no attenuation for high frequency which has been observed with discrete model of dislocation. The material case is the only one to show chirality effect which could be observed along a large distance and be used to measure the density of defects in a continuum. Moreover the material strain induces curvature in term of dislocation density so that it introduces a stiffness operator which may induce a breathing mode of vibration for the continuum. In the spatial strain's case, the transition between perfect continuum and continuum with dislocations shows a drastic change on the form of solutions as for example the sudden non existence of certain polarization of plane-wave solutions whenever the dislocation density is non zero. However we showed that cylindrical solutions are not affected by this sudden change because all polarization are possible in this case.
Recent works ([dMP12, PRGM13, RMG13]) investigated the reflexion and the transmission of planes waves at surfaces carrying discontinuities or material properties in a second-gradient materials by means of suitable boundary conditions describing exactly the jumps across the given surface. The problem seems very close to ours but it makes sense to relate both theories. Indeed the torsion tensor captures the jumps along a closed path encircling the dislocation lines and not across a surface. However, we emphasize that particular configurations of dislocations produce surfaces of discontinuities: *the grain boundaries*. These latter might be related with the type of surface studied in the mentioned works. Furthermore an interface between a dislocated continuum and an homogeneous one may imply some kind of boundary layers observed throughout transmission/reflection coefficients provided that we consider suitable boundary conditions. Such examples would be very close to the aforementioned papers, the microstructure parameter being S. Comparisons with other models of waves propagation through medium with dislocations remain sensitive because most of recent works are discrete models with single dislocations that oscillate [MML], whereas we deal with continuous (and time-constant) density which is not modify by the superimposed displacement. Discussion could be enriched by considering a full perturbation of the connection: strain and defect density.

Conclusion

L'étude de la propagation d'onde en milieux hétérogènes nous a conduit sur trois sujets *a priori* bien distincts dont nous rappelons respectivement les principaux éléments de conclusion et quelques perspectives. Ensuite nous nous efforcerons de conclure sur des perspectives plus générales en ce qui concerne la modélisation des milieux hétérogènes.

Conclusion générale

Le chapitre 2 a fait l'objet d'une étude des méthodes de Foldy-Lax dans le cadre de la propagation d'onde acoustique suite au sondage par une source ponctuelle d'un milieu aléatoire infini. Au cours de cette étude, nous avons développé une formulation algébrique du problème au travers de laquelle nous retrouvons les interprétations déjà connues en *multiple scattering theory*. A l'occasion d'une étude plus poussée de l'exemple de multi-diffusion pour deux inclusions, nous avons discuté des phénomènes de couplages faibles. On a ainsi mis en évidence l'importance du contraste matrice/inclusion dans la notion de milieu dilué. En développant la méthode à l'ordre 1, nous avons généralisé les résultats connus au cas d'une incidence émise par une source ponctuelle en milieu infini. De plus, l'amplitude du champ effectif semble bien défini. Quant à l'ordre 2, il a été développé dans le but d'apporter une alternative à la QCA en appliquant une hypothèse de fermeture de type Foldy qui nécessite alors deux moyennes d'ensemble. La formulation qui en résulte semble plus appropriée car elle concerne le champ effectif et non le champ excitant comme c'est le cas dans la littérature. Les simulations numériques confirment cette tendance. Cependant, le principe d'extinction (2.38) implique une incertitude sur les amplitudes modales effectives. Afin de mesurer l'importance de cette incertitude, la suite directe de l'étude pourrait être une étude analytique des différents paramètres, combinée à la comparaison des résultats avec les données numériques.
Il faut néanmoins préciser que le contraste n'est pas explicitement pris en compte dans notre modèle alors qu'il gouverne les phénomènes d'interactions. Il faut donc faire preuve de précaution : l'ordre 2 du modèle statistique ne signifie pas qu'on a pris en compte les termes de couplages, du moins pas dans l'entièreté de leurs effets. Or l'étude de la situation à deux corps donne une petite idée de ce que l'on néglige lorsqu'on extrapole les formules que l'on connait pour la diffraction par un seul diffuseur. On peut donc imaginer qu'une étude plus approfondie de ce problème par d'autres méthodes, puisse nous orienter vers une meilleure compréhension des interactions qu'il peut y

avoir pour des forts contrastes. C'est à la lumière de ces recherches qu'on pourra tenter d'améliorer la méthode. Dans une optique plus pratique, il serait intéressant de développer le modèle dans le cas élastique tridimensionel qui s'avére moins délicat à réaliser d'un point de vue expérimental. En outre, l'efficacité théorique des modèles d'ordre 2 (le notre comme la QCA) encourage l'ouverture à d'autres problèmes tels que des milieux qui présentent des diffuseurs sur un domaine borné. Enfin, de manière plus générale, il faut savoir rester critique. La résolution proposée dans ce manuscrit révèle ses limites : elle résulte de nombreuses hypothèses et autres approximations qu'il est parfois délicat de manipuler et souvent difficile d'interpréter. La raison est simple : la formulation est fondée sur l'expression de conditions aux limites pour un bord qui présente un nombre important de composantes connexes. Nous préférons envisager le problème autrement : le milieu est avant tout un *continuum* donc il nous faut faire un effort pour le considérer comme tel et en déduire sa structure différentielle. En ce sens les méthodes proches de celle du chapitre 4 sont aussi des perspectives que nous envisageons.

Le chapitre 3 était consacré au *cloaking* actif pour les ondes de flexion dans une plaque de Love-Kirchhoff. Nous avons ainsi exprimé les amplitudes modales des sources en fonction de celle du champ incident lorsque celui ci est une onde plane unitaire ou une onde émise par un point source (hors de la zone de *cloaking*). Ce dernier cas s'applique en particulier dans le cas d'une onde diffractée par un défaut. Les conditions d'efficacité du *cloaking* ont été définies comme une condition de non-radiation du champ total émis par les sources, combinée à l'extinction du champ incident dans la zone de *cloaking*. En ce qui concerne la condition de non-rayonnement, nous l'avons traduite comme une condition nécessaire et suffisante sur les amplitudes modales (3.55). Par contre nous sommes restés plus nuancés que [NAP12] au sujet de la condition d'annulation que nous traduisons par une condition suffisante sur les amplitudes modales (3.51). Au terme des simulations numériques, nous avons tenté d'identifier la validité de ces conditions en fonction de différents paramètres : le nombre d'onde k, le nombre de sources M et l'ordre N de la décomposition modale pour les sources. L'efficacité générale de la méthode est similaire aux résultats obtenus en acoustique.
Quant à la faisabilité au niveau expérimental, les limites sont multiples. Tout d'abord, il faut s'assurer que les sources ne diffractent pas le champ incident. Ensuite, les phénomènes au voisinage d'une source s'avèrent problématiques. En effet le modèle de plaque n'autorise pas des variations brutales pour le champ de déplacement. Enfin, techniquement, il peut être délicat de calibrer autant d'amplitudes pour les sources. Néanmoins, des perspectives de recherche se dessinent afin de palier à ces deux dernières difficultés. En effet, nous suggèrons de s'intéresser plus particulièrement au cas de nombreuses sources. On peut alors se restreindre à des sources monopolaires ou dipolaires. En outres, la zone de *cloaking* se rapprochera du cercle contenant les sources ; la zone non contrôlée s'en trouvera réduite en taille et tendra à coïncider avec la singularité de la source. Ce travail est avant tout de nature experimentale étant donné ces premiers éléments de problématiques. Cela dit, il n'est pas à exclure que la théorie soit remise en question notamment pour des phénomènes de bords qu'il faudrait modéliser.

On retiendra tout de même que le *cloaking* actif permettrait peut-être d'établir des protocoles mettant en valeur les phénomènes de couplages en filtrant l'excitation au voisinage d'une inclusion.

Le chapitre 4 est une contribution au projet ambitieux d'établir une théorie d'élasticité élargie à des continuums défectueux. En particulier nous nous sommes intéressés aux dislocations car elles permettent de modéliser le *continua* par une variété matérielle munie d'une structure de Riemann-Cartan. On a quelque peu élargi l'étude proposée par Tamarasselvame [TBR11] en considérant un milieu 3D, généralisant ainsi les équations de Navier. De plus, nous avons soulevé la question du choix de définition du tenseur de déformation en fonction de l'influence des dislocations sur celle-ci. On a ainsi distingué la déformation covariante dite matérielle et celle dite spatiale qui utilise la connexion de Levi-Civita. Les équations de Navier ont été généralisées pour ces deux cas. Enfin on a effectué une première étude qualitative à partir d'un exemple simple de milieu comportant une densité constante de dislocations vis toutes de même orientation. Il apparaît alors clairement que la déformation spatiale n'est pas un cas dégénéré de la déformation matérielle pour laquelle on aurait négligé les termes quadratiques de la densité de dislocation. En outre le cas matériel présente des phénomènes intéréssants tels que des (*i*) modes de respiration pour un champ de déplacement uniforme dont la période temporelle dépend de la densité de dislocations ; (*ii*) ou encore l'existence d'une solution dont la polarisation suit l'escalier en spirale de Cartan pour des hautes fréquences. Ce dernier effet nous suggère de poursuivre le travail en considérant la déformation matérielle car on montre clairement l'influence de la structure différentielle sur la polarisation des ondes ; ceci ne se retrouve pas avec la déformation spatiale.
L'étape suivante pourrait être la poursuite de l'étude qualitative en suivant le raisonnement pour une densité uniforme de dislocations coin. Il est à noter que, dans ce cas, l'équation sera légèrement plus compliquée. Il serait aussi intéressant d'envisager le problème en milieu fini. Quelques difficultés se présentent presque directement. Tout d'abord, il faudra requestionner la pertinence d'une densité uniforme de dislocations au regard des conditions géométriques au bord. En effet, l'interface entre le milieu de Riemann-Cartan et son extérieur, qui est euclidien, implique une discontinuité de la géométrie qui est délicate à imaginer. Pour cela on envisage d'étudier plus en détails les équations de Bianchi, qui donnent des conditions nécessaires que doivent vérifier torsion et courbure. Ensuite, les conditions cinématiques aux bords pourront être aussi le sujet d'une modification en vue d'aboutir à une formulation cohérente qui tient compte d'un saut dans la géométrie. Au delà de ces éventualités, la théorie requiert des ajustements et des précisions que nous détaillons dans les perspectives.

Perspectives

Les applications possibles du *cloaking* actif nécessitent des recherches expérimentales que nous avons tentées de cerner. Quant aux techniques de diffusion multiple abordées,

leur étude nous a révélé la complexité d'un raisonnement parfois obscurci par une multitude d'hypothèses et d'approximations. Dans ce cas, comme nous l'évoquions, nous suggérons de porter une attention toute particulière au contraste et son influence sur les interactions. Mais il semble plus pertinent de poursuivre l'élaboration de l'approche du chapitre 4 car elle nous permet de s'affranchir des conditions de bords, qui sont souvent lourdes à manipuler. Dans le cadre général de l'étude des ondes en milieux hétérogènes, nous envisageons donc essentiellement des perspectives dont le but est d'affiner cette approche. Notons qu'il est possible d'étudier le cas d'obstacles sphériques en 3D en introduisant un autre ingrédient, le tenseur de non-métricité de Weyl, qui semble être un bon candidat pour "géométriser" des défauts ponctuels. Cela dit, des étapes intermédiaires sont essentielles avant de compliquer autant le problème. Nous en proposons ici une liste non exhaustive tout en gardant à l'esprit la difficulté sous-jacente à chaque question.

Tout d'abord, le modèle suggère qu'il y ait eut une homogénéisation qui nous permette d'obtenir la géométrie à partir d'une description discrète des défauts. Ce point est essentiel dans la compréhension du modèle afin de pouvoir faire le lien avec le caractère discret que l'on associe souvent à la notion de défaut. Il y a donc un effort à faire à ce niveau du raisonnement. Une étude bibliographique est requise avant de pouvoir affirmer quelle méthode doit être envisagée. Néanmoins on peut imaginer qu'une homogénéisation des équations d'incompatibilités, voire des équations de Bianchi, soit une piste sérieuse. Cela permettrait d'introduire une échelle caractéristique dont il faudra tenir compte pour préciser le domaine fréquentiel de validité du *continuum* considéré.

Enfin, dans notre approche, la géométrie est supposée donnée *a priori*. Cela nous permet ainsi d'y superposer un petit déplacement élastique dont on suppose qu'il ne perturbe pas la densité de dislocations. Or ceci n'est absolument pas évident et constitue une hypothèse qu'il est important de comprendre : est-ce une approximation? Un début de réponse peut se dessiner *via* la théorie de jauge des dislocations. En effet elle permet d'obtenir des équations de champs qui définiront l'évolution de la géométrie. Ainsi Lazar [Laz11] a pu déterminer des solutions pour les distortions élastiques et plastiques suite au mouvemement d'une ligne de dislocation. On suggère donc de compléter l'étude en tentant de résoudre le problème en supposant un mouvement élastique afin de savoir quelle évolution est induite pour la densité de dislocations. À la lumière de cette étude, il faudra alors requestionner notre approche.

Appendix A

Modal amplitudes for plane wave incidence

Consider an incident plane-wave of unit amplitude, i.e.

$$\tilde{w}(\mathbf{x}) = w_\psi(\mathbf{x}) = e^{ik\hat{\mathbf{e}}(\psi)\cdot\mathbf{x}} \tag{A.1}$$

where $\hat{\mathbf{e}}(\psi) = (\cos\psi, \sin\psi)$ is a unit direction vector. We note that with this definition we can write, for $\mathbf{y} \in \partial C_m$, $\tilde{w}(\mathbf{y}) = \tilde{w}(\mathbf{x}_m)\tilde{w}(\mathbf{a})$ where we have defined $\mathbf{a} = a_m\hat{\mathbf{e}}(\theta)$. Let us also define

$$L_n^{ij}(\alpha^{(m)}) = \int_{\theta_1^{(m)}-\psi}^{\theta_2^{(m)}-\psi} \sin^i\Theta\cos^j\Theta e^{i\alpha^{(m)}\cos\Theta - in\Theta}\, d\Theta. \tag{A.2}$$

Therefore, given (A.1), we find that

$$\mathbf{n}\cdot\nabla_y\tilde{w}(\mathbf{y}) = ik\tilde{w}(\mathbf{x}_m)\cos(\theta-\psi)e^{i\alpha^{(m)}\cos(\theta-\psi)} \tag{A.3}$$

and so we can show that

$$\int_{\theta_1^{(m)}}^{\theta_2^{(m)}} \mathbf{n}\cdot\nabla_y\tilde{w}(\mathbf{y})e^{-in\theta}\, d\theta = ik\tilde{w}(\mathbf{x}_m)e^{-in\psi}L_n^{01}(\alpha^{(m)}) \tag{A.4}$$

and

$$\int_{\theta_1^{(m)}}^{\theta_2^{(m)}} \tilde{w}(\mathbf{y})e^{-in\theta}\, d\theta = \tilde{w}(\mathbf{x}_m)e^{-in\psi}L_n^{00}(\alpha^{(m)}) \tag{A.5}$$

Next note that $\tilde{\phi}_N(\mathbf{y}) = \mathbf{n}\cdot\nabla_y\tilde{w}(\mathbf{y})$
and so from (A.4)

$$\int_{\theta_1^{(m)}}^{\theta_2^{(m)}} \tilde{\phi}_N(\mathbf{y})e^{-in\theta}\, d\theta = ik\tilde{w}(\mathbf{x}_m)e^{-in\psi}L_n^{01}(\alpha^{(m)}) \tag{A.6}$$

Furthermore we can determine

$$\begin{aligned}\tilde{\phi}_T(\mathbf{y}) &= \mathbf{t}\cdot\nabla_y\tilde{w}(\mathbf{y}) \\ &= -ik\tilde{w}(\mathbf{x}_m)\sin(\theta-\psi)e^{i\alpha^{(m)}\cos(\theta-\psi)}\end{aligned} \tag{A.7}$$

and thus

$$\int_{\theta_1^{(m)}}^{\theta_2^{(m)}} \tilde{\phi}_T(\mathbf{y})e^{-in\theta}\,d\theta = -ik\tilde{w}(\mathbf{x}_m)e^{-in\psi}L_n^{10}(\alpha^{(m)}) \tag{A.8}$$

Moving onto moments, we have

$$\tilde{m}_N(\mathbf{y}) = \tilde{m}_{ij}(\mathbf{y})n_in_j = -D[(1-\nu)\tilde{w}_{,ij}(\mathbf{y})n_in_j + \nu\nabla_y^2\tilde{w}(\mathbf{y})] \tag{A.9}$$

and using $\nabla^2\tilde{w} = -k^2\tilde{w}$ we obtain

$$\tilde{m}_N(\mathbf{y}) = Dk^2\tilde{w}(\mathbf{x}_m)[(1-\nu)\cos^2(\theta-\psi)+\nu]e^{i\alpha^{(m)}\cos(\theta-\psi)} \tag{A.10}$$

so that

$$\int_{\theta_1^{(m)}}^{\theta_2^{(m)}} \tilde{m}_N(\mathbf{y})e^{-in\theta}\,d\theta = Dk^2\tilde{w}(\mathbf{x}_m)e^{-in\psi}((1-\nu)L_n^{02}(\alpha^{(m)})+\nu L_n^{00}(\alpha^{(m)})). \tag{A.11}$$

Finally,

$$\tilde{m}_T(\mathbf{y}) = m_{,ij}(\mathbf{y})n_it_j = -D[(1-\nu)\tilde{w}_{,ij}(\mathbf{y})n_it_j] \tag{A.12}$$

so that

$$\tilde{m}_T(\mathbf{y}) = -Dk^2(1-\nu)\tilde{w}(\mathbf{x}_m)\sin(\theta-\psi)\cos(\theta-\psi)e^{i\alpha^{(m)}\cos(\theta-\psi)} \tag{A.13}$$

and thus

$$\int_{\theta_1^{(m)}}^{\theta_2^{(m)}} \tilde{m}_T(\mathbf{y})e^{-in\theta}\,d\theta = -Dk^2(1-\nu)\tilde{w}(\mathbf{x}_m)e^{-in\psi}L_n^{11}(\alpha^{(m)}). \tag{A.14}$$

The expressions for the source coefficients thus become

$$\begin{aligned}\{B_{m,n}^S,\mathcal{B}_{m,n}^S\} = \gamma k^2 D\alpha^{(m)}e^{-in\psi}\tilde{w}(\mathbf{x}_m)\Big[&i\{J_n(\alpha^{(m)}),I_n(\alpha^{(m)})\}L_n^{01}(\alpha^{(m)})+ \\ &\{-J_n'(\alpha^{(m)}),I_n'(\alpha^{(m)})\}L_n^{00}(\alpha^{(m)})\Big]\end{aligned} \tag{A.15}$$

$$\begin{aligned}\{B_{m,n}^T,\mathcal{B}_{m,n}^T\} = -\gamma k^2 D(1-\nu)in\tilde{w}(\mathbf{x}_m)e^{-in\psi} \\ \Big(\{J_n'(\alpha^{(m)})-\frac{1}{a^{(m)}}J_n(\alpha^{(m)}),I_n'(\alpha^{(m)})-\frac{1}{a^{(m)}}I_n(\alpha^{(m)})\}iL_n^{10}(\alpha^{(m)}) \\ +\{J_n(\alpha^{(m)}),I_n(\alpha^{(m)})\}L_n^{11}(\alpha^{(m)})\Big).\end{aligned} \tag{A.16}$$

$$\{B^N_{m,n}, \mathcal{B}^N_{m,n}\} = \gamma k^2 D\alpha^{(m)} \tilde{w}(\mathbf{x}_m) e^{-in\psi} \Bigg[\Big\{ (1-\nu) J_n''(\alpha^{(m)}) - \nu J_n(\alpha^{(m)}), I_n''(\alpha^{(m)}) + \nu I_n(\alpha^{(m)}) \Big\} i L_n^{01}(\alpha^{(m}$$
$$+ \{ J_n'(\alpha^{(m)}), I_n'(\alpha^{(m)}) \} \Big((1-\nu) L_n^{02}(\alpha^{(m)}) + \nu L_n^{20}(\alpha^{(m)}) \Big) \Bigg]$$

As in Norris et al. (2012) we can use the Jacobi-Anger identity to show that

$$L_n^{00}(\alpha) = G(\alpha) = \sum_{\ell=-\infty}^{\infty} J_\ell(\alpha) i^{\ell+1} \frac{e^{i(\ell+n)\psi}}{\ell+n} [e^{-i(\ell+n)\theta_2^{(m)}} - e^{-i(\ell+n)\theta_1^{(m)}}]$$
$$= \sum_{\ell=-\infty}^{\infty} J_\ell(\alpha) F_{\ell n}(\psi, \theta_1^{(m)}, \theta_2^{(m)}) \tag{A.17}$$

Noticing that $\dfrac{\partial^j L_n^{00}(\alpha}{\partial \alpha^j} = i^j L_n^{0j}(\alpha)$ we thus have:

$$L_n^{0j}(\alpha) = (-i)^j G^{(j)}(\alpha)$$
$$= (-i)^j \sum_{\ell=-\infty}^{\infty} J_\ell^{(j)}(\alpha) F_{\ell n}(\psi, \theta_1^{(m)}, \theta_2^{(m)}) \tag{A.18}$$

Next, using integration by parts

$$L_n^{10}(\alpha) = \int_{\theta_1^{(m)}-\psi}^{\theta_2^{(m)}-\psi} \sin\Theta e^{i\alpha^{(m)}\cos\Theta - in\Theta}\, d\Theta \tag{A.19}$$
$$= \left[\frac{i}{\alpha} e^{i\alpha\cos\Theta - in\Theta} \right]_{\theta_1^{(m)}-\psi}^{\theta_2^{(m)}-\psi} - \frac{n}{\alpha} L_n^{00}(\alpha) \tag{A.20}$$

and

$$L_n^{11}(\alpha) = \int_{\theta_1^{(m)}-\psi}^{\theta_2^{(m)}-\psi} \sin\Theta\cos\Theta e^{i\alpha^{(m)}\cos\Theta - in\Theta}\, d\Theta \tag{A.21}$$
$$= \frac{i}{\alpha} \left[\cos\Theta e^{i\alpha\cos\Theta - in\Theta} \right]_{\theta_1^{(m)}-\psi}^{\theta_2^{(m)}-\psi} + \frac{i}{\alpha} L_n^{10}(\alpha) - \frac{n}{\alpha} L_n^{01}(\alpha) \tag{A.22}$$

Also we can easy deduce that

$$L_n^{20}(\alpha) = \int_{\theta_1^{(m)}-\psi}^{\theta_2^{(m)}-\psi} \sin^2\Theta e^{i\alpha^{(m)}\cos\Theta - in\Theta}\, d\Theta \tag{A.23}$$
$$= L_n^{00}(\alpha) - L_n^{02}(\alpha) \tag{A.24}$$
$$= \sum_{\ell=-\infty}^{\infty} (J_\ell(\alpha) + J_\ell^{(2)}(\alpha)) F_{\ell n}(\psi, \theta_1^{(m)}, \theta_2^{(m)}) \tag{A.25}$$

Appendix B

Calculation of chapter 4

B.1 Calculation for Eq.4.13

Form Eq.4.11, the $\nabla \cdot \sigma$ refers to the calculation of three terms. The first is:

$$\nabla \cdot ((\nabla \cdot \mathbf{u})\mathbf{I}) = \left(\partial_i(\nabla \cdot \mathbf{u})\ \delta^{ji}\right)\mathbf{e_j} + (\nabla \cdot \mathbf{u})\,(K \cdot \mathbf{I})\,.$$

Because $\nabla \cdot \mathbf{u}$ is a scalar function, its partial derivative is exactly its covariant derivative:

$$\partial_i(\nabla \cdot \mathbf{u})\ \delta^{ji}\mathbf{e_j} = \partial_j(\nabla \cdot \mathbf{u})\mathbf{e_j} = \nabla(\nabla \cdot \mathbf{u}).$$

Then:

$$\nabla \cdot ((\nabla \cdot \mathbf{u})\mathbf{I}) = \nabla(\nabla \cdot \mathbf{u}) + (K \cdot \mathbf{I})\,.$$

The second is $\nabla \cdot (\nabla \mathbf{u})$:

$$\nabla \cdot (\nabla \mathbf{u}) = \nabla \cdot (g^{jk}\nabla_k u^i \mathbf{e_i} \otimes \mathbf{e_j}) = g^{jk}\nabla_j \nabla_k u^i \mathbf{e_i} = \Delta \mathbf{u},$$

where metricity ($\nabla g = \mathbf{0}$) has been used. For the third term:

$$\nabla \cdot (\nabla \mathbf{u})^t = \nabla \cdot (g^{ki}\nabla_k u^j \mathbf{e_i} \otimes \mathbf{e_j}) = g^{ki}\nabla_j \nabla_k u^j \mathbf{e_i}.$$

Interverting the two covariant derivative is possible, using:

$$\nabla_j \nabla_k u^j = \nabla_k \nabla_j u^j + R_{l\cdot jk}^{\cdot j} u^l - S_{jk}^l \nabla_l u^j.$$

We recognise

$$g^{ki}\nabla_k \nabla_j u^j \mathbf{e_i} = \nabla(\nabla \cdot \mathbf{u})$$

and $R_{lk} = R_{l\cdot jk}^{\cdot j}$ are the covariant component of the Ricci tensor. Finally:

$$\nabla \cdot (\nabla \mathbf{u})^t = \nabla(\nabla \cdot \mathbf{u}) + g^{ki}\left(R_{lk}u^l - S_{jk}^l \nabla_l u^j\right)\mathbf{e_i}.$$

After collecting all terms:

$$\nabla \cdot \sigma = (\lambda + \mu)\nabla(\nabla \cdot \mathbf{u}) + \mu\Delta\mathbf{u} + \mathbf{t}^{\mathrm{mat}} \qquad \text{with}$$
$$\mathbf{t}^{\mathrm{mat}} = \lambda(\nabla \cdot \mathbf{u})\,(K \cdot \mathbf{I}) + \mu g^{kj}\left(R_{lk}u^l - S_{ik}^l \nabla_l u^i\right)\mathbf{e_j}.$$

B.2 Example with the material strain

Begin with Eq.4.13. Because $\nabla \cdot \mathbf{u}$ is a scalar function, its partial derivative is exactly its covariant derivative:

$$\nabla\big(\nabla \cdot \mathbf{u}\big) = \big(\partial_k \partial_i u^i + K^i_{ij} \partial_k u^j\big)\, \mathbf{e_k} = \partial_k \partial_i u^i \mathbf{e_k}.$$

The best way to compute $\mathbf{\Delta u}$ is to use the definition $\mathbf{\Delta u} = \nabla \cdot (\nabla \mathbf{u})$ and to apply the relation Eq.4.8 keeping in mind that K is constant. After rearrangement:

$$\begin{aligned} \mathbf{\Delta U} &= \Big(\partial_i \partial_i u^k + 2K^k_{il} \partial_i u^l + K^i_{il} \partial_l u^k + (K^i_{il} K^k_{ln} + K^k_{il} K^l_{in}) u^n\Big)\, \mathbf{e_k} \\ &= \Big(\partial_i \partial_i u^k + 2K^k_{il} \partial_i u^l + K^k_{il} K^l_{in} u^n\Big)\, \mathbf{e_k}. \end{aligned}$$

$$\begin{aligned} \text{For } k=1 \ : \quad & 2K^1_{il} \partial_i u^l = 2\left(K^1_{23} \partial_2 u^3 + K^1_{32} \partial_3 u^2\right) = S\big(\partial_2 u^3 - \partial_3 u^2\big) \\ & K^1_{il} K^l_{in} u^n = (K^1_{23} K^3_{21} + K^1_{32} K^2_{31}) u^1 = -\frac{S^2}{2} u^1. \\ \text{For } k=2 \ : \quad & 2K^2_{il} \partial_i u^l = 2\left(K^2_{13} \partial_1 u^3 + K^2_{31} \partial_3 u^1\right) = S\big(\partial_1 u^3 + \partial_3 u^1\big) \\ & K^2_{il} K^l_{in} u^n = (K^2_{13} K^3_{12} + K^2_{31} K^1_{32}) u^2 = -\frac{S^2}{2} u^2. \\ \text{For } k=3 \ : \quad & 2K^3_{il} \partial_i u^l = 2\left(K^3_{12} \partial_1 u^2 + K^3_{21} \partial_2 u^1\right) = -S\big(\partial_1 u^2 + \partial_2 u^1\big) \\ & K^3_{il} K^l_{in} u^n = (K^3_{12} K^2_{13} + K^3_{21} K^1_{23}) u^3 = -\frac{S^2}{2} u^3. \end{aligned}$$

It is straightforward to observe:

$$K \cdot \mathbf{I} = \Big(K^l_{lj} \delta^{kj} + K^k_{lj} \delta^{jl}\Big)\, \mathbf{e_k} = \mathbf{0}.$$

Then $\mathbf{t}^{\mathrm{mat}}$ is reduced to:

$$\mathbf{t}^{\mathrm{mat}} = \mu \Big(R_{lj} u^l - S^l_{ij} \nabla_l u^i\Big)\, \mathbf{e_j},$$

where $R_{lj} u^l \mathbf{e_j} = S^2/2 u^1 \mathbf{e_1}$. The last term is

$$-S^l_{ij} \nabla_l u^i \mathbf{e_j} = S^l_{ji} \Big(\partial_l u^i + K^i_{lk} u^k\Big)\, \mathbf{e_j}.$$

$$\begin{aligned} \text{For } j=1 \ : \quad S^l_{1i} \Big(\partial_l u^i + K^i_{lk} u^k\Big) &= 0. \\ \text{For } j=2 \ : \quad S^l_{2i} \Big(\partial_l u^i + K^i_{lk} u^k\Big) &= S^1_{23} \left(\partial_1 u^3 + K^3_{12} u^2\right) + S^3_{21} \left(\partial_3 u^1 + K^1_{32} u^2\right) \\ &= S\left(\partial_1 u^3 - \frac{S}{2} u^2\right). \\ \text{For } j=3 \ : \quad S^l_{3i} \Big(\partial_l u^i + K^i_{lk} u^k\Big) &= S^1_{32} \left(\partial_1 u^2 + K^2_{13} u^3\right) + S^2_{31} \left(\partial_2 u^1 + K^1_{23} u^3\right) \\ &= -S\left(\partial_1 u^2 + \frac{S}{2} u^3\right). \end{aligned}$$

By collecting each contribution we obtain:

$$\begin{aligned}\nabla\cdot\sigma &= \left[(\lambda+\mu)\partial_1\partial_i u^i + \mu\partial_i\partial_i u^1 + \mu S\left(\partial_2 u^3 - \partial_3 u^2\right)\right]\mathbf{e_1} + \\ &\quad \left[(\lambda+\mu)\partial_2\partial_i u^i + \mu\partial_i\partial_i u^2 + \mu S\left(\partial_3 u^1 + 2\partial_1 u^3 - S u^2\right)\right]\mathbf{e_2} + \\ &\quad \left[(\lambda+\mu)\partial_3\partial_i u^i + \mu\partial_i\partial_i u^3 - \mu S\left(2\partial_1 u^2 + \partial_2 u^1 + S u^3\right)\right]\mathbf{e_3}\end{aligned}$$

B.3 Example with the spatial strain

In the special case studied in the last section, $\mathbf{f}^{\mathrm{sp}}$ is reduced to $2\mu K\cdot\varepsilon$. Because $K^i_{ij}=0$,

$$\mathbf{f}^{\mathrm{sp}} = 2\mu\ K^k_{ij}\varepsilon^{ji}\ \mathbf{e_k}.$$

Details along each directions follow

$$\text{For } k=1\ :\quad K^1_{lj}\varepsilon^{jl} = K^1_{23}\varepsilon^{32} + K^1_{32}\varepsilon^{23} = 0.$$

$$\text{For } k=2\ :\quad K^2_{lj}\varepsilon^{jl} = K^2_{13}\bar{\varepsilon}^{31} + K^2_{31}\varepsilon^{13} = \frac{S}{2}\left(\partial_1 u^3 + \partial_3 u^1\right).$$

$$\text{For } k=3\ :\quad K^3_{lj}\varepsilon^{jl} = K^3_{21}\varepsilon^{12} + K^3_{12}\varepsilon^{21} = -\frac{S}{2}\left(\partial_1 u^2 + \partial_2 u^1\right).$$

Finally, by collecting all contributions we obtain:

$$\begin{aligned}\nabla\cdot\sigma &= \left[(\lambda+\mu)\partial_1\partial_i u^i + \mu\partial_i\partial_i u^1\right]\mathbf{e_1} + \\ &\quad \left[(\lambda+\mu)\partial_2\partial_i u^i + \mu\partial_i\partial_i u^2 + \mu S\left(\partial_1 u^3 + \partial_3 u^1\right)\right]\mathbf{e_2} + \\ &\quad \left[(\lambda+\mu)\partial_3\partial_i u^i + \mu\partial_i\partial_i u^3 - \mu S\left(\partial_1 u^2 + \partial_2 u^1\right)\right]\mathbf{e_3}.\end{aligned}$$

Bibliography

[Ana07] G. Ananthakrishna. Current theoretical approaches to collective behavior of dislocations. *Physics Reports*, 440(4-6):113 – 259, 2007.

[BBS55] B. A. Bilby, R. Bullough, and E. Smith. Continuous distributions of dislocations: a new application of the method of non-riemannian geometry. *Proc. R. Soc. Lond. A*, 231:263–273, 1955.

[BGS57] B. A. Bilby, L. R. T. Gardner, and A. N. Stroh. Continuous distribution of dislocations and the theory of plasticity. *Actes du Xième Congrès International de Mécanique Appliquée, volume III*, pages 35–44, 1957.

[Bur39] J. M. Burgers. Some considerations of the field of stress connected with dislocations in a regular crystal lattice: Part i. *Proceedings Kon. Neder. Akad. Wetensch.*, 42:293–325, 1939.

[Car86] E. Cartan. *On Manifolds with an Affine Connection and the Theory of General Relativity (English translation of the French original by A. Magnon and A. Ashtekar)*. 1986.

[CC09] E. Cosserat and F. Cosserat. *Théorie des Corps Déformables*. Librairie Scientifique A. Hermann et fils, Paris. ISBN 978-1429704847, reprinted by Cornell University Library, 1909.

[CMA+09] M. Chekroun, L. Le Marrec, O. Abraham, O. Durand, and G. Villain. Analysis of coherent surface wave dispersion and attenuation for non-destructive testing of concrete. *Ultrasonics*, 49, 2009.

[CML+09] M. Chekroun, L. Le Marrec, B. Lombard, J. Piraux, and O. Abraham. *Ultrasonic wave propagation in non homogeneous media, Comparison between a multiple scattering method and direct numerical simulations for elastic wave propagation in concrete*. 2009.

[CMLP12] M. Chekroun, L. Le Marrec, B. Lombard, and J. Piraux. Time-domain numerical simulations of multiple scattering to extract elastic effective wavenumbers. *Waves in Random and Complex Media*, 22, 2012.

[CN10] J. M. Conoir and A. N. Norris. Effective wave numbers and reflection coefficients for an elastic medium containing random configurations of cylindrical scatterer. *Wave Motion*, 47:183–197, 2010.

[d'A47] Jean Le Rond d'Alembert. Recherches sur la courbe que forme une corde tendue mise en vibration. *Histoire de l'Académie des Sciences et Belles-Lettres de Berlin*, 1747.

[Dev92] R. Devever. *Elie Cartan and Albert Einstein: Letters on Absolute Parallelism*. 1992.

[dMP12] F. dell'Isola, A. Madeo, and L. Placidi. Linear plane wave propagation and normal transmission and reflection at discontinuity surfaces in second gradient 3d continua. *ZAMM*, pages 52–71, 2012.

[EC64] Eringen and A. Cemal. Mechanics of micromorphic materials. Technical report, DTIC Document, 1964.

[EL88] D. G. B. Edelen and D. C. Lagoudas. *Gauge theory and defects in solids*. 1988.

[FH97] N. A. Fleck and J. W. Hutchinson. Strain gradient plasticity. *Advances in Applied Mechanics*, 33:295–361, 1997.

[Fol45] L. L. Foldy. The multiple scattering of waves. i. general theory of isotropic scattering by randomly distributed scatterers. *Phys. Rev.*, 67:107–119, 1945.

[Ger73] P. Germain. The method of virtual power in continuum mechanics. part 2: Microstructure. *SIAM J. Appl. Math.*, pages 556–575, 1973.

[GHNH99] H. Gao, Y. Huang, W. D. Nix, and J. W. Hutchinson. Mechanism-based strain gradient plasticity i. theory. *J. Mech. Phys. Solids*, 47:1239–1263, 1999.

[Ham02] R. T. Hammond. Torsion gravity. *Reports on Progress in Physics*, 65(5):599, 2002.

[HO07] F.W. Hehl and Obukhov. élie cartan's torsion in geometry and in field theory, an essay. *Annales de la Fondation Louis de Broglie*, 32, 2007.

[Ies]

[KE83] A. Kádic and D. G. B. Edelen. A gauge theory of dislocations and disclinations. volume 174 of *Lecture Notes in Physics*. Springer, 1983.

[Kit85] Kitahara. *Boundary integral equation methods in eigenvalue problems of elastodynamics and thin plates*. Elsevier, 1985.

[Kle08] H. Kleinert. *Multivalued fields: in condensed matter, electromagnetism and gravitation*. World Scientific, Singapour, 2008.

[Kon55] K. Kondo. Non-riemannian geometry of imperfect crystals from a macroscopic viewpoint. *Memoirs of the unifying study of basic problems in engineering and physical science by means of geometry*, 1, 1955.

[Kro60] E. Kroner. General continuum theory of dislocations and proper stresses. *Arch. Rat. Mech. Anal.*, pages 273–334, 1960.

[Kro80] E. Kroner. Continuum theory of defects. *Physics of defects*, pages 215–315, 1980.

[Kro86] E. Kroner. On gauge theory in defect mechanics. In K. Kirchgssner E. Krner, editor, *Trends in Applications of Pure Mathematics to Mechanics*, volume 249 of *Lecture Notes in Physics*, pages 281–294. Springer Berlin Heidelberg, 1986.

[Kro01] E. Kroner. Benefits and shortcomings of the continuous theory of dislocations. *Int. J. of Solid and Strucutres*, pages 1115–1134, 2001.

[KV92] M. O. Katanaev and I. V. Volovich. Theory of defects in solids and three-dimensional gravity. *Annals of Physics*, 216(1), 1992.

[Lax52] M. Lax. Multiple scattering of waves. ii. the effective field in dense systems. *Phys. Rev.*, 85:621–629, 1952.

[Laz00] M. Lazar. Dislocation theory as a 3-dimensional translation gauge theory. *Annalen der Physik*, 512:461–473, 2000.

[Laz02] M. Lazar. An elastoplastic theory of dislocations as a physical field with torsion. *J.Phys. A: Math. Gen.*, 35(8):1983–2004, 2002.

[Laz11] M. Lazar. On the elastic fields produced by nonuniformly moving dislocations: a revisit. *Philosophical Magazine*, 2011.

[LB67] P. Lloyd and M. V. Berry. Wave propagation through an assembly of spheres. IV. Relation between different scattering theories. *Proc. Phys. Soc. London*, 91:678–688, 1967.

[LH10] M. Lazar and F. W. Hehl. Cartans spiral staircase in physics and, in particular, in the gauge theory of dislocations. *Foundations of Physics*, 40(9-10):1298–1325, 2010.

[LHD+13] D. Liu, Y. He, D. J. Dunstan, B. Zhang, Z. Gan, P. Hu, and H. Ding. Toward a further understanding of size effects in the torsion of thin metal wires: an experimental and theoretical assessment. *Int. J. of Plasticity*, 41:30–52, 2013.

[LM05] C. M. Linton and P. A. Martin. Multiple scattering by random configurations of circular cylinders: Second-order corrections for the effective wavenumber. *J. Acoust. Soc. Am.*, 117(6):3413–3423, 2005.

[LM06] C. M. Linton and P. A. Martin. Multiple scattering by multiple spheres: A new proof of the Lloyd-Berry formula for the effective wavenumber. *SIAM J. Appl. Math.*, 66(5):1649–1668, 2006.

[Lom10] B. Lombard. Modélisation numérique de la propagation et de la diffraction d'ondes mécaniques, hdr thesis, aix-marseille 2. 2010.

[LP04] B. Lombard and J. Piraux. Numerical treatment of two-dimensional interfaces for acoustic and elastic waves. *J. Comput. Phys.*, 195, 2004.

[LP08] J. Li and J. B. Pendry. Hiding under the carpet: A new strategy for cloaking. *Phys. Rev. Lett.*, 101(20), 2008.

[LS96] K. C. Le and H. Stumpf. On the determination of the crystal reference in nonlinear continuum theory of dislocations. 1996.

[Lun88] F. Lund. Response of a stringlike dislocation loop to an external stress. *J. Mater. Res.*, 3 (2), 1988.

[Mar] P. A. Martin. Multiple scattering by random configurations of circular cylinders: Reflection, transmission, and effective interface conditions. *jasa*, 129:1685–1695.

[Mar83] *Mathematical foundations of elasticity*. 1983.

[Mar06] P. A. Martin. *Multiple Scattering: Interaction of Time-harmonic Waves with N Obstacles*. Cambridge University Press, New York, 2006.

[Mau10] G. A. Maugin. *Configurational forces: thermomechanics, physics, mathematics, and numerics*. Taylor & Francis, 2010.

[Mau13a] G. Maugin. *Continuum Mechanics Through the Twentieth Century : A concise Historical Perspective*. Solid Mechanics and Its Applications. Springer Verlag - Dordrecht, 2013.

[Mau13b] G. A. Maugin. *Continuum Mechanics Through the Twentieth Century : A concise Historical Perspective (2013), Solid Mechanics and Its Applications*. Springer Verlag - Dordrecht, 2013.

[MCE+12] N. Mujic, M. T. Cerda, R. Espinoza, J. Lisoni, and F. Lund. Ultrasound as a probe of dislocation density in aluminum. *Acta Materialia*, 60(16):5828 – 5837, 2012.

[MHR88] T. A. Mokhtar, R. B. Herrmann, and D. R. Russel. Seismic velocity and q model for the shallow structure of the arabian shield from short-period rayleigh waves. Geophysics, 1988.

[Mil01] G. W. Milton. *The Theory of Composites*. Cambridge University Press, 1st edition, 2001.

[Mil06] D. A. Miller. On perfect cloaking. *Opt. Express*, 14(25):12457–12466, December 2006.

[Mil12] W. Miller. *Symmetry and Separation of Variables*. Encyclopedia of Mathematics and its Applications. Cambridge University Press, 2012.

[Min64] R. D. Mindlin. Micro-structure in linear elasticity. *Archive for Rational Mechanics and Analysis*, 16(1):51–78, 1964.

[MM08] P. A. Martin and A. Maurel. Multiple scattering by random configurations of circular cylinders: Weak scattering without closure assumptions. *Wave Motion*, 45:865–880, 2008.

[MML] A. Maurel, J-F. Mercier, and F. Lund.

[MML04] A. Maurel, J-F. Mercier, and F. Lund. Elastic wave propagation through a random array of dislocations. *Phys. Rev. B*, 2004.

[MMW63] A. A. Maradudin, E. W. Montroll, and G. H. Weiss. *Theory of lattice dynamics in the harmonic approximation*. Academic, New York, 1963.

[Mur63] T. Mura. Continuous distribution of moving dislocations. *Philos. Mag.*, 8 (89), 1963.

[MY81] G. A. McMechan and M. J. Yedlin. Analysis of dispersive waves by wave field transformation. *Geophysics*, 46, 1981.

[Nak96] M. Nakahara. *Geometry, Topology and Physics*. Graduate Student Series Physics, 1996.

[NAP12] A. N. Norris, F. A. Amirkulova, and W. J. Parnell. Source amplitudes for active exterior cloaking. *submitted*, 1:1, 2012.

[Nol67] W. Noll. Materially uniform simple bodies with inhomogeneities. *Arch. Rat. Mech. Anal.*, 27:1–32, 1967.

[NS11] A. N. Norris and A. L. Shuvalov. Elastic cloaking theory. *Wave Motion*, 49:525–538, 2011.

[Nye53] J. F. Nye. Some geometrical relations in dislocated crystals. *Acta Metallurgica*, 1:153 – 162, 1953.

[Olv00] P. J. Olver. *Applications of Lie Groups to Differential Equations*. Graduate texts in mathematics. Springer, 2000.

[OoSU10] F. W. J. Olver, National Institute of Standards, and Technology (U.S.). *NIST Handbook of Mathematical Functions*. Cambridge University Press, 2010.

[PRGM13] L. Placidi, G. Rosi, I. Giorgio, and A. Madeo. Reflection and transmission of plane waves at surfaces carrying material properties and embedded in second-gradient materials. *Mathematics and Mechanics of Solids*, 2013.

[PSS06] J. B. Pendry, D. Schurig, and D. R. Smith. Controlling electromagnetic fields. *Science*, 312(5781), 2006.

[Rak97] L.R. Rakotomanana. Contribution a la modélisation géométrique et thermodynamique d'une classe de milieux faiblement continus. *Arch. Rat. Mech. Anal.*, 141:199–236, 1997.

[Rak09] L. R. Rakotomanana. *Éléments de dynamique des solides et structures déformables*. presses polytechniques et universitaires romandes, 2009.

[RMG13] G. Rosi, A. Madeo, and J.-L. Guyader. Switch between fast and slow biot compression waves induced by "second gradient microstructure" at material discontinuity surfaces in porous media. *Int. J. Solids. Struct.*, 2013.

[SG05] P. Sharma and S. Gati. Gauge-field-theory solution of the elastic state of a screw dislocation in a dispersive (non-local) crystalline solid. *Proc. R. Soc. Lond. A*, 4611:1081– 1095, 2005.

[TBR11] N. A. Tamarasselvame, M. Buisson, and L.R. Rakotomanana. Wave propagation within some non-homogeneous continua. *C. R. Mécanique*, 339:779–788, 2011.

[Twe67] V. Twersky. *On multiple scattering of waves,Publications of the National Bureau of Standards*. U.S. Government Printing Office, 1967.

[Vas]

[VMO11] F. G. Vasquez, G. W. Milton, and D. Onofrei. Exterior cloaking with active sources in two dimensional acoustics. *Wave Motion*, 49:515–524, 2011.

[VMOS12] F. G. Vasquez, G. W. Milton, D. Onofrei, and P. Seppecher. Transformation elastodynamics and active exterior acoustic cloaking. In S. Guenneau and R. Craster, editors, *Acoustic Metamaterials: Negative Refraction, Imaging, Lensing and Cloaking*. Canopus Academic Publishing and Springer SBM, 2012.

[WJP11] P. A. Marin W. J. Parnell. Multiple scattering of flexural waves by random configurations of inclusions in thin plates. *Wave Motion*, 48(2):161 – 175, 2011.

[WT61] P. C. Waterman and R. Truell. Multiple scattering of waves. *Journal of Mathematical Physics*, 2(4):512–537, 1961.

[YDH98] G. Yang, Y. Duan, and Y. Huang. Topological invariant in riemann-cartan manifold and space-time defects. *Int. Journal of Theoretical Physics*, 37(12):2953–2964, 1998.

List of Figures

Résumé

Dans la première partie, on s'intéresse à la multi-diffusion d'une onde acoustique avec une matrice homogène 2D contenant N inclusions. Dans le cas particulier de deux inclusions, on met alors en évidence l'importance du contraste matrice/inclusion dans les termes d'interactions entre inclusions. Le cas général de la multi-diffusion, pour distribution aléatoire de N inclusions, est ensuite développé dans l'esprit de Foldy-Lax basé sur des moyennes d'ensembles. Ainsi on cherche à déterminer le nombre d'onde effectif de l'onde effective, définie comme la moyenne du champ total, dans le cas d'une onde incidente émise par un point source. La deuxième partie est consacrée au *cloaking* actif dans une plaque. On détermine ainsi les amplitudes modales des sources multipolaires afin d'éteindre une onde plane ou émise par un point source, dans une région donnée. En outre, cette méthode peut s'appliquer pour éteindre l'onde diffractée par un défaut. Enfin dans la dernière partie, on se propose d'étudier la propagation d'onde au sein d'un milieu comportant des dislocations. On utilise la géométrie de Riemann-Cartan afin de modéliser ce milieu continu. Afin d'illustrer les différences que peuvent induire deux définitions possibles de la déformation (spatiale et matérielle), nous étudions la propagation d'ondes 3D dans l'exemple simple d'un milieu continu avec une densité uniforme et stationnaire de défauts. L'anisotropie et l'atténuation sont présentes dans les deux modèles mais sous forme différente. Enfin la déformation matérielle induit des modes de respiration et, en régime haute fréquence, des ondes transverses qui suivent l'escalier en spirale de Cartan.

Abstract

In the first part, we investigate the multiple scattering of an acoustic wave within an homogeneous matrix containing N obstacles. In the particular case with 2 obstacles, we show the importance of the contrast matrix/obstacle in the coupling terms between inclusions. The general case of multiple scattering by N obstacles randomly distributed is then developed following the Foldy-Lax theory based on ensemble averaging. We aim to evaluate the effective wavenumber of the effective wave, defined as the average of the total field, in the case where the incoming wave is emitted by a point-like source. The second part is dedicated to the active cloaking in a thin plate. Hence we determine the modal amplitudes of the sources in order to extinct an incoming wave in a given region. This method can be applied to extinct the wave scattered by an obstacle. Finally, in the last part, the Riemann-Cartan geometry is used to model continuum with dislocations. In order to illustrate the differences induced by two possible definitions for the strain (spatial or material) in this framework, propagation of 3D waves is studied for a simple example of infinite continuum with uniform and stationary defects density. Anisotropy and attenuation are caught by both models even if these effects are quite different. Furthermore the material strain uniform breathing modes and, in the high frequency regime, transverse waves which follow the Cartan's spiral staircase.